INTERNATIONAL JOURNAL

of

COMPUTERS COMMUNICATIONS & CONTROL

ISSN 1841-9836

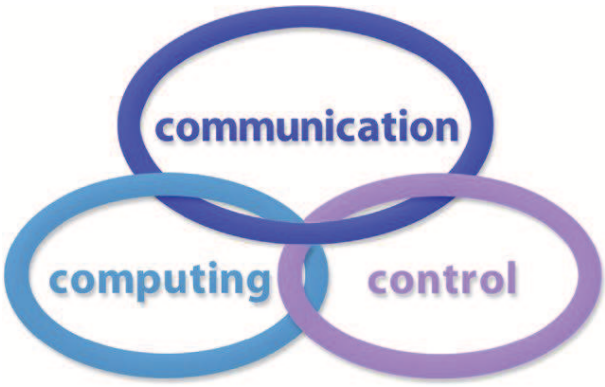

A Bimonthly Journal
With Emphasis on the Integration of Three Technologies

Year: 2016 Volume: 11 Issue: 5 Month: October

This journal is a member of, and subscribes to the principles of, the Committee on Publication Ethics (COPE).

CCC Publications - Agora University

CCC Publications

http://univagora.ro/jour/index.php/ijccc/

BRIEF DESCRIPTION OF JOURNAL

Publication Name: International Journal of Computers Communications & Control.
Acronym: IJCCC; **Starting year of IJCCC:** 2006.
ISO: Int. J. Comput. Commun. Control; **JCR Abbrev:** INT J COMPUT COMMUN.
International Standard Serial Number: ISSN 1841-9836.
Publisher: CCC Publications - Agora University of Oradea.
Publication frequency: Bimonthly: Issue 1 (February); Issue 2 (April); Issue 3 (June); Issue 4 (August); Issue 5 (October); Issue 6 (December).
Founders of IJCCC: Ioan DZITAC, Florin Gheorghe FILIP and Misu-Jan MANOLESCU.
Logo:

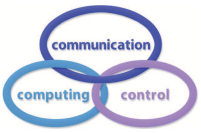

Indexing/Coverage:

- Since 2006, Vol. 1 (S), IJCCC is covered by Thomson Reuters and is indexed in ISI Web of Science/Knowledge: Science Citation Index Expanded.

  2016 Journal Citation Reports® Science Edition (Thomson Reuters, 2016):
  Subject Category: (1) Automation & Control Systems: Q4(2009,2011,2012,2013,2014,2015), Q3(2010); (2) Computer Science, Information Systems: Q4(2009,2010,2011,2012,2015), Q3(2013,2014).

  Impact Factor/3 years in JCR: 0.373(2009), 0.650 (2010), 0.438(2011); 0.441(2012), 0.694(2013), 0.746(2014), 0.627(2015).
  Impact Factor/5 years in JCR: 0.436(2012), 0.622(2013), 0.739(2014), 0.635(2015).

- Since 2008 IJCCC is indexed by Scopus (SNIP2014= 1.029):
  Subject Category: (1) Computational Theory and Mathematics: Q4(2009,2010,2012,2015), Q3(2011,2013,2014); (2) Computer Networks and Communications: Q4(2009), Q3(2010, 2012, 2013, 2015), Q2(2011, 2014); (3) Computer Science Applications: Q4(2009), Q3(2010, 2011, 2012, 2013, 2014, 2015).

  SJR: 0.178(2009), 0.339(2010), 0.369(2011), 0.292(2012), 0.378(2013), 0.420(2014), 0.319(2015).

- Since 2007, 2(1), IJCCC is indexed in EBSCO.

Focus & Scope: International Journal of Computers Communications & Control is directed to the international communities of scientific researchers in computer and control from the universities, research units and industry.

To differentiate from other similar journals, the editorial policy of IJCCC encourages the submission of original scientific papers that focus on the integration of the 3 "C" (Computing, Communication, Control).

In particular the following topics are expected to be addressed by authors: (1) Integrated solutions in computer-based control and communications; (2) Computational intelligence methods (with particular emphasis on fuzzy logic-based methods, ANN, evolutionary computing, collective/swarm intelligence); (3) Advanced decision support systems (with particular emphasis on the usage of combined solvers and/or web technologies).

Editorial Address:
Agora University/ R&D Agora Ltd. / S.C. Cercetare Dezvoltare Agora S.R.L.
Piata Tineretului 8, Oradea, jud. Bihor, Romania, Zip Code 410526
Tel./ Fax: +40 359101032
E-mail: ijccc@univagora.ro, rd.agora@univagora.ro, ccc.journal@gmail.com
Journal website: http://univagora.ro/jour/index.php/ijccc/

Gheorghe Păun
Institute of Math. of Romanian Academy
Bucharest, PO Box 1-764, Romania
gpaun@us.es

Mario de J. Pérez Jiménez
Dept. of CS and Artificial Intelligence
University of Seville, Sevilla,
Avda. Reina Mercedes s/n, 41012, Spain
marper@us.es

Dana Petcu
Computer Science Department
Western University of Timisoara
V.Parvan 4, 300223 Timisoara, Romania
petcu@info.uvt.ro

Radu Popescu-Zeletin
Fraunhofer Institute for Open
Communication Systems
Technical University Berlin, Germany
rpz@cs.tu-berlin.de

Imre J. Rudas
Óbuda University
Budapest, Hungary
rudas@bmf.hu

Yong Shi
School of Management
Chinese Academy of Sciences
Beijing 100190, China &
University of Nebraska at Omaha
Omaha, NE 68182, U.S.A.
yshi@gucas.ac.cn, yshi@unomaha.edu

Athanasios D. Styliadis
University of Kavala
Institute of Technology
65404 Kavala, Greece
styliadis@teikav.edu.gr

Gheorghe Tecuci
Learning Agents Center
George Mason University
U.S.A.
University Drive 4440, Fairfax VA
tecuci@gmu.edu

Horia-Nicolai Teodorescu
Faculty of Electronics and
Telecommunications
Technical University "Gh. Asachi" Iasi
Iasi, Bd. Carol I 11, 700506, Romania
hteodor@etc.tuiasi.ro

Dan Tufiş
Research Institute for Artificial Intelligence
of the Romanian Academy
Bucharest, "13 Septembrie" 13, 050711,
Romania
tufis@racai.ro

Lotfi A. Zadeh
Director,
Berkeley Initiative in Soft Computing (BISC)
Computer Science Division
University of California Berkeley,
Berkeley, CA 94720-1776
U.S.A.
zadeh@eecs.berkeley.edu

DATA FOR SUBSCRIBERS
Supplier: Cercetare Dezvoltare Agora Srl (Research & Development Agora Ltd.)
Fiscal code: 24747462
Headquarter: Oradea, Piata Tineretului Nr.8, Bihor, Romania, Zip code 410526
Bank: BANCA COMERCIALA FEROVIARA S.A. ORADEA
Bank address: P-ta Unirii Nr. 8, Oradea, Bihor, România
IBAN Account for EURO: RO50BFER248000014038EU01
SWIFT CODE (eq.BIC): BFER RO BU

INTERNATIONAL JOURNAL OF COMPUTERS COMMUNICATIONS & CONTROL
ISSN 1841-9836, Volume 11, Issue 5, October, 2016.

Contents

INTERNATIONAL JOURNAL OF COMPUTERS COMMUNICATIONS & CONTROL
ISSN 1841-9836, 11(5):602-612, October 2016.

Language Processes and Related Statistics in the Posts Associated to Disasters on Social Networks

S.C. Bolea

Speranţa Cecilia Bolea
Institute of Computer Science of the Romanian Academy - Iasi Branch
Romania, Iasi, Carol I, 8
cecilia.bolea@iit.academiaromana-is.ro

Abstract: This paper provides a detailed and long-period statistics of the use of synonyms in posts related to specific events on social networks (SNs), an extended analysis of the correlations of the flows of the synonyms in such posts, a study of the applicability of Zipf's law to posts related to specific events on SNs, and an analysis of the dynamics of the fluxes of synonyms in the posts. The paper also introduces the study of the distances in the phase space for the characterization of the dynamics of the word fluxes on social networks. This article is a partial report on recent research performed for a deeper analysis of social networks and of processes developing on social networks, including used lexicon, dynamics of messages related to a specific type of topic, and relationships of the processes on SNs with external events.
Keywords: social networks, disaster, analytics, language statistics, correlative analysis, Zipf's law, dynamics.

1 Introduction

Analytics aimed to social networks have explosively developed during the last few years, with some of them focusing on the rescue from disasters [3], [5], others proposing means for disaster management [6], [10], [26] and others on disaster prevention and mitigation [1,2], [11], [15], [22], [27].

The main purpose of this paper is fact-finding about the language of the social networks and related posts, for messages connected to dramatic events such (fires and earthquakes). In subsidiary, we are interested in the distributions of the most used words and of the synonyms. A hypothesis we made in connection with the word probability distribution is that it departs from the typical distribution of the language, which is a Zipf's distribution.

This article is a partial report on recent research related to the deeper analysis of social networks and of processes developing on SNs; the analysis refers to the lexicon used, dynamics of messages related to a specific type of topic, and the relationships of the processes on SNs with external events. The general lexicon was studied in [24], and issues related to the use of synonyms in tweets were discussed in [4], [20], and [24].

The main contributions of this paper include the detailed and long-period statistics of the use of synonyms in posts related to specific events on SNs, the extended analysis of the correlations of the flows of the synonyms [29] in those posts, a study of the applicability of Zipf's law to posts related to specific events on SNs, and the detailed analysis of the dynamics of the fluxes of synonyms in the posts. The research was performed in the frame of a larger project, being a part of it (see Acknowledgments).

We advance the study of correlation between time series of the number of words occurrences especially of synonyms in messages related to disasters effects on SNs, and compare the SNs from this point of view. Also, we apply a recently proposed nonlinear technique of analysis of time series for better characterizing, and differentiating specificities of SNs.

One of the purposes of this article is to present a full year data statistics for synonyms usage in posts related to two types of potentially disastrous events, namely earthquakes and fires, and to analyze in detail the dynamics of the words most used in such posts. The utility of this study is multifold and includes the optimization of searches in software applications for disaster monitoring and management, and better understanding the language use under and in relation with such events [18]. The results may also be of interest to psycho-linguistics, beyond descriptive linguistics. A special emphasis is placed on the correlative study of the dynamics of the flows of synonyms in the posts.

This research associates with other analyses of the language used in SNs reported recently in the literature, for example with the vast literature on sentiment analysis on SNs [7], [12], including the time of disaster events [16], [17].

Both the mentioned project and this study relates to previous interests of our research group in computational linguistics and speech technology. The research in the project and partly in this study also reflects the interest in detecting attitudes in messages and to a standing interest in detecting emotions in speech and texts as in the studies [9], [13], [25], [28].

2 Data collection and processing method

The data collection process was described in [24]; data comprises all posts, including articles and blogs pointed to by messages on Twitter and Google+, during the period March 2015 and March 2016, as detected with queries using the keywords *(cutremur OR seism) AND Vrancea*, respectively *incendiu OR foc*.

An important difference between the dataset we used and the data in other papers is that we have not restricted ourselves only to the messages, but we also downloaded the media articles or blogs having addresses in the collected messages. Therefore, the most or at least a large part of the text analyzed comes from the media, not from the respective social network (SN) messages. Thus, a larger lexicon was included in the database. Yet, the most frequent words found beyond stop words have been those intimately related to the search condition, which is an interesting and somewhat unexpected fact. The text was lemmatized before performing the statistics. In doing so, words with various grammatical forms were reduced to their main representative. We used the free lemmatizer for the Romanian language from RACAI Institute, available at [30]. The statistic of words in this study actually represents the statistic of lemmas in the dataset.

The dataset was conventionally split by SN and by months and is reported as such in the paper, for example in the correlative analysis of synonyms and in the analysis of their dynamics of occurrences. The descriptive statistics, including Zipf's law detection, refers to the whole database, on each SN, thus extending the results in [24].

The dataset includes 3.715 posts for the *earthquake* type of event (database named *CutremurDB*) and 1.106 for *fire* type (database named *FocDB*). We reiterate that the only events of interest here are the earthquakes and the fires. The total number of posts, words (without stopwords), and the number of characters (with spaces) are given in Table 1 for the two classes of posts. The stopwords are the words such as "0 retweets 0 likes", "0 retweets 2 like", "view summary" and "newline", and their form depends on the type of browser used (Google Chrome, Mozilla Firefox).

The *FocDB* database is larger than *CutremurDB* because fires are much more frequent events, thus produce more posts on SNs. Interestingly, the posts related to earthquakes have a small number of lemmas (Table 1). The average number of words per post are: 126 words for Google+ and 124 words for Twitter in *CutremurDB*, and 317 words for Google+ and 131 words for Twitter in *FocDB*.

Table 1: The number of posts and lemmas

	Posts	Lemma	No. of lemmas	Char with spaces
Google+(*CutremurDB*)	318	6.872	40.196	174.030
Twitter(*CutremurDB*)	941	12.229	116.667	632.979
Google+(*FocDB*)	245	15.041	77.909	466.618
Twitter(*FocDB*)	279	10.396	36.665	231.293

Both databases, *CutremurDB* and *FocDB* have the same structure and contain the fields: *year*, *month*, *posts* (number of posts from the month), *lemma* (number of lemmas), *no. of lemmas* (number of lemmas occurrences), *char with spaces* (number of characters including spaces) and $lemma_1, lemma_2, \cdots, lemma_n$, where $lemma_i, i \in \{1, n\}$ represents the significant words referring earthquake and fire (nouns, verbs, adjectives, adverbs). The other words such as pronouns, prepositions, conjunctions, numerals and punctuations have no relevance in our study, and they do not appear in our databases.

3 Main findings

3.1 Descriptive statistics of synonyms used in relation to specific events

This study contributes to the descriptive statistics of the SN language by determining the probabilities of the most frequent words and synonyms in posts related to earthquakes and fires on social networks, on extended periods. The main results are summarized in Table 2, where *lemma* denotes the number of lemmas and *No. of lemmas* the number of lemma's occurrences.

Table 2: The probabilities of the most important lemmas for CutremurDB and FocDB

CutremurDB	cutremur	seism	seismic	magnitudine	Richter	Vrancea	epicentru	adâncime	produce
p for Google+	0,0310	0,0123	0,0069	0,0158	0,0149	0,0244	0,0041	0,0079	0,0133
p for Twitter	0,0311	0,0130	0,0064	0,0165	0,0137	0,0244	0,0054	0,0085	0,0153
FocDB	incendiu	foc	izbucni	pompier	suferi	stinge	flacără	pericol	arde
p for Google+	0,0092	0,0069	0,0018	0,0027	0,0003	0,0006	0,0012	0,0002	0,0012
p for Twitter	0,0260	0,0164	0,0055	0,0098	0,0005	0,0024	0,0047	0,0007	0,0027

The best correlation found (in CutremurDB) is for the lemmas: *cutremur* - *Vrancea* and *cutremur* - *produce* (see Table 3). This is because the messages about earthquakes found on SNs have a very similar "Un cutremur cu magnitudinea de 3, 5 grade pe scara Richter s-a produs luni seara în zona seismică Vrancea...", "An earthquake with a magnitude of 3.5 on the Richter scale occurred Monday evening in Vrancea seismic zone...". The correlations between *cutremur* and *seism* synonyms is a little smaller than the above. The synonyms *incendiu* and *foc* have a higher value of correlation than other pairs of words (see Table 3).

It was shown in [19], [23] that there is a strong correlation between the number of posts related to potentially or actually disastrous events and the intensity of the event. Precisely, in the cited papers it was found that the peak of the number of posts per day (post flux) related to the event correlates with the number of victims in several types of disasters; when the event is only potentially disastrous, such as a small seism, the peak of the post flux was found to correlate with the magnitude of the earthquakes. In addition, it was shown in [19], [23] that the flux of posts related to such events is well represented by a pulse with exponential growth and decay, in the form

Table 3: Examples of correlations in the use of words: correlations of the time series of the monthly number of occurrences of the lemmas

Word pairs CutremurDB	**Correlation value**		**Word pairs FocDB**	**Correlation value**	
	Google+	**Twitter**		**Google+**	**Twitter**
cutremur - seism	0,87	0,96	incendiu - foc	0,99	0,95
cutremur - seismic	0,78	0,90	incendiu - izbucni	0,90	0,66
cutremur - magnitudine	0,89	0,96	incendiu - pompier	0,69	0,92
cutremur - Richter	0,86	0,93	incendiu - suferi	0,77	0,69
cutremur - Vrancea	0,97	0,97	incendiu - stinge	0,82	0,26
cutremur - epicentru	0,81	0,86	incendiu - flacără	0,87	0,36
cutremur - adâncime	0,82	0,99	incendiu - pericol	0,61	0,37
cutremur - produce	0,96	0,98	incendiu - arde	0,83	0,75
cutremur - grad	0,87	0,98	incendiu - distruge	0,79	0,08
cutremur - intensitate	0,61	0,85	incendiu - răni	0,93	0,04
cutremur - România	0,83	0,92	incendiu - România	0,81	0,80

$$n(t) = \{ \begin{array}{c} Ae^{\lambda(t-t_0)} \\ Ae^{\lambda(t_m-t_0)}e^{-\kappa(t-t_m)} \end{array} \quad (1)$$

Above, t is time, $n(t)$ is the number of posts per day (flux) at time t, t_0 is the moment of the event, t_m is the moment when the peak occurs, and λ and κ are coefficients. A similar evolution was verified for the words *cutremur* and *foc* in our database, see Figure 1.

Notice that during the months of autumn and winter the number of fires increases compared with the other months of the year. Yet the summer heat may cause vegetation fires. These facts are mirrored by the number of related messages on SNs, see *foc* in Figure 1.

3.2 Zipf's law and the lexicons of posts on SNs

Recall that Zipf's law [14] states that the logarithm of the probability of a word in a language is related to the rank of the word,

$$log(p(w)) = \alpha \times rank(w) + \beta \quad (2)$$

Zipf-like laws, that is, power laws, are well known in statistical linguistics, see for example [14], and in many other domains such as populations of cities, economy, and biology. Explained in more detail, this law says that, when ordering the words of any language, including Romanian, according to their frequency of apparition in a large corpus, the logarithm of their apparition probability decreases linearly with their rank. This means that selecting at random words in a specified language, the law should not apply. We have been interested, see [24], to find if Zipf's law is relevant to the database related to disasters. Our initial hypothesis was that the law would not be valid because of the very restrictive set of words used in such posts, their low rank in the language, and their supposedly almost random choice from the lexicon of the global lexicon of the language.

Yet, our hypothesis was overturned [24], in that at least the most frequently used words obeyed Zipf's law, while words with higher rank confirmed the hypothesis. The results of log-lin representation of the probabilities of the most frequent 8 words, topic *seism* for Google+ (3), and Twitter (4) are:

$$Y = -0,1969X - 3,3642; R^2 = 0,9555 \quad (3)$$

$$Y = -0,1592X - 3,0524; R^2 = 0,9494 \quad (4)$$

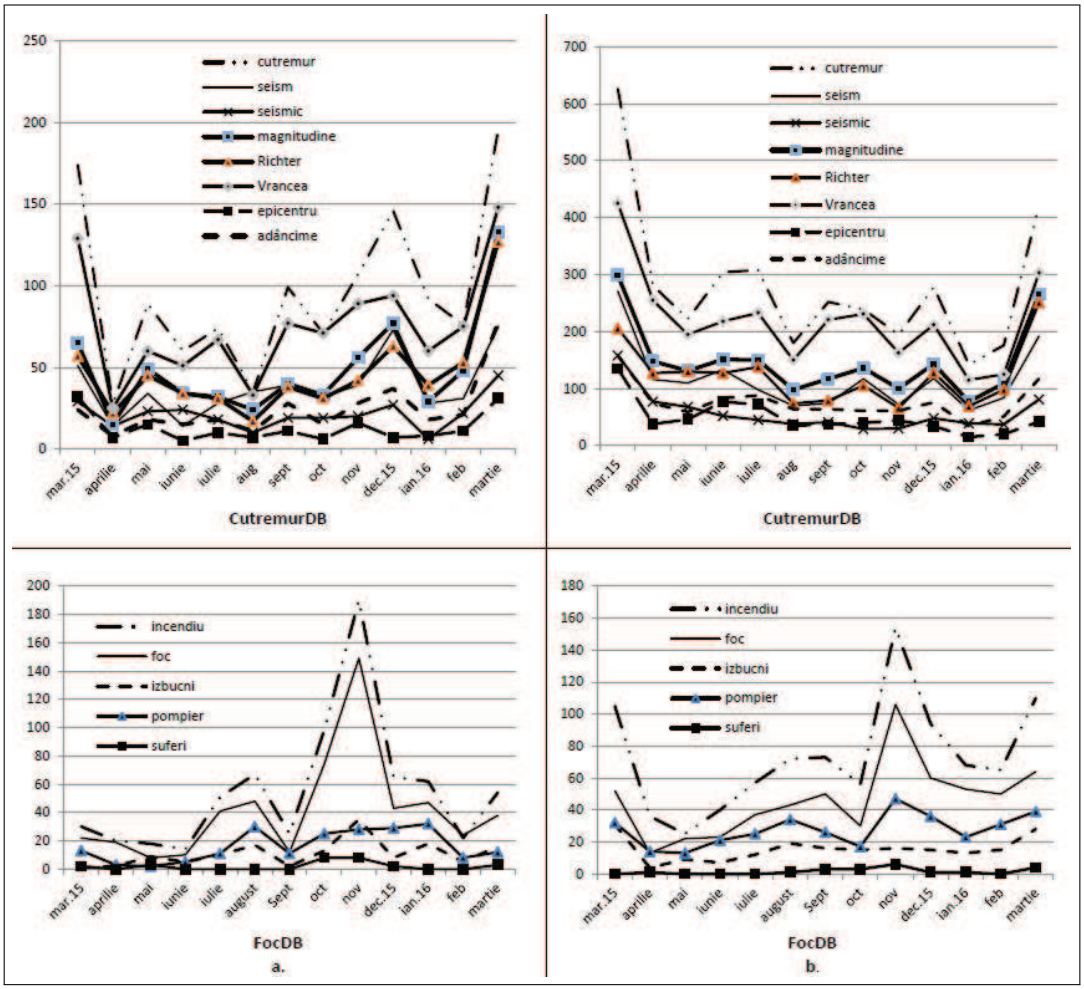

Figure 1: Time series of keywords occurrences: a. Google+, b. Twitter

The main results are shown in Fig. 2, indicating a good agreement ($R^2 > 0.7$) with Zipf's law. Notice that on Google+ the slope slightly differs from that on Twitter, indicating a lexicon-based personality of the two SNs. Additional results are given on the SRoL website described in [9].

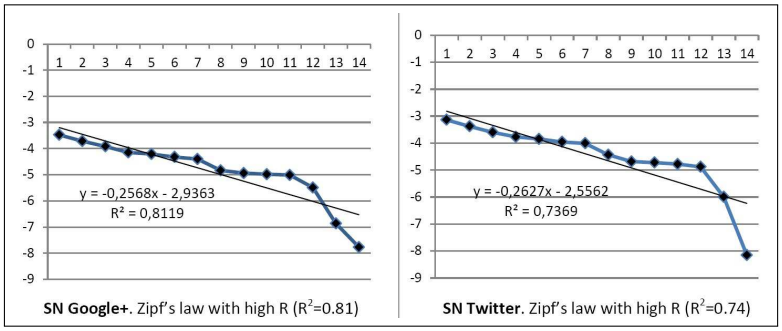

Figure 2: Log-lin representation of the probabilities of the most frequent 14 words, topic *seism*

Analyzing the equations 3, 4 and Figure 2, the first ranked words (up to 8) obey the Zipfs law. In case of *FocDB*, the first ranked words(up to 8 or 14) obey Zipf's law (see (5), (6) and Figure 3).

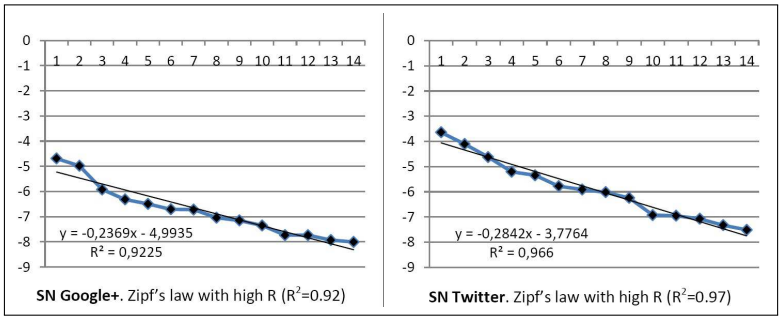

Figure 3: Log-lin representation of the probabilities of the most frequent 14 words, topic *incendiu*

$$Y = -0,33X - 4,6241; R^2 = 0,8933; in\ Google+\ SN \tag{5}$$

$$Y = -0,3481X - 3,5163; R^2 = 0,9489; in\ Twitter\ SN \tag{6}$$

3.3 Dynamics of the fluxes of synonyms

The notion of dynamics of SNs originates from the papers [19], [23], where it was shown that the flow of messages streaming from an event on SNs is predictable and has a dynamics that has characteristics of nonlinearity. It was shown that the time series of the number of messages related to events correlate with the level of seismic activity [19], [23].

One of the issues only slightly addressed in [24] is that of the dynamics of the use of keywords and synonyms. In many respects, this dynamics resembles with the dynamics of the number of messages addressing a certain disaster event, as dealt in [19], [23]. The interest in the dynamics is multifold and includes the expectation of correlation of the query based on keywords and the number of returned messages related to a specified event (probability of finding messages related to an event when the search uses a given keyword), and the dynamics of the joint use of synonyms in messages. On the other hand, the study [24] proved that, while the time series of the number

of occurrences of the words "cutremur" and "seism" are strongly correlated, they have dynamics that are clearly differentiated in the phase space.

In this sub-section, we study the difference in the dynamics of synonyms, continuing [24], by generating the phase-space plots (maps) of the time series of the synonyms and then by applying the method of *windows* in the time space, as proposed in [21]. That method is essentially an approximate way of determining the probability that the attractor of the time series has a point in a specified rectangular region of the phase space. Four windows were defined in the rectangular coverage of the attractors, as suggested in [24], and the counts for the respective four windows was performed, producing a vector with four components for each time series. Then, the distance between the vectors was determined (method due to HN Teodorescu). We found that the Euclidean distance is low only for the pair of synonyms *cutremur* and *seism* on the Twitter SN and for Google+ SN, this distance is a little larger.

The phase space, in a simplified case of the phase plane for the dynamics $x(t)$, is simply defined as the plane $(x, \dot{x})$, $\dfrac{dx}{dt} = \dot{x}$, with the corresponding graphical representation. The characterization method introduced in [21], consists in determining the frequency of a point in the phase space that lies in the 2D interval (rectangle) $[a_1, a_2] \times [b_1, b_2]$, for a set of non-overlapping rectangles defined in the phase space. Let us consider the attractor of the time series of the flux of a specified word, $n_w(t_k)$, for a given time duration $t_1, \cdots, t_p$ framed in the rectangle $[min_{j\in\{1,p\}} n_w(t_k), max_{j\in\{1,p\}} n_w(t_k)] \times [min_{j\in\{1,p\}} dn_w(t_k), max_{j\in\{1,p\}} dn_w(t_k)]$, where $dn_w(t_k) = n_w(t_k) - n_w(t_{k-1})$. Divide this rectangular subspace of the phase space into four equal rectangles, overlapping only on one of their edges,

$$R_1 = [min_{j\in\{1,p\}} n_w, \frac{min_j n_w + max_j n_w)}{2} \times [min_j dn_w, \frac{min_j dn_w + max_j dn_w}{2}] \tag{7}$$

where everywhere above *min* and *max* are for $j \in \{1, p\}$; similarly one defines R_2, R_3, R_4, see Fig. 4. Denote the number of points that fall in these rectangles by $n_1(w_1)$, $\cdots$, $n_4(w_1)$. Form the vector $\overrightarrow{\omega_1} = (n_1(w_1), n_2(w_1), n_3(w_1), n_4(w_1))$. Perform the same operations for the specified word, w_2, whose dynamics we wish to compare with $\overrightarrow{\omega_1}$, and find $\overrightarrow{\omega_2}$. Then, the distance $d(\overrightarrow{\omega_1}, \overrightarrow{\omega_2})$ between the two dynamics is the distance between $\overrightarrow{\omega_1}$ and $\overrightarrow{\omega_2}$ (personal communication HNT):

$$d(\overrightarrow{\omega_1}, \overrightarrow{\omega_2}) = \sum_{k=1-4} |n_k(w_1) - n_k(w_2)|,$$

or the Euclidean distance would be $d(w_1, w_2) = \sqrt{\sum_{k=1-4}(n_k(w_1) - n_k(w_2))^2}$. A further improvement is to use relative frequencies in the distances, dividing by the total number of points in the phase diagrams, $\nu_k = n_k/p$, where $p = \sum_k n_k$.

The distances between the attractors in the phase plane provides a quantitative, simple characterization of the similarity of the dynamics of the two time series compared, supplementing the information given by the correlation. The phase diagrams for four of the most frequent words found on *Google+* are shown in Figure 4; the corresponding Euclidean distances between the dynamics are given in Table 4, which stands for the matrix $[d_{12}]$, where d_{12} denotes the distance between words.

The results presented in Table 4 show that the larger Euclidean distance is between the dynamics of the words *magnitudine* and *Vrancea*, and the smallest distance is between *seism* and *Vrancea* respectively *cutremur* and *magnitudine*, on Google + (both distances 1.41). Comparatively, the time series for the word pair *cutremur* and *magnitude* have the third higher correlation (see Table 3), only slightly higher than the correlation for the pair *cutremur* - *seism*. Even less favorably compares the value of the distance between the dynamics of *cutremur* and *Vrancea* $d = 3.75$, the third largest, with the correlation of their time series, which is the highest,

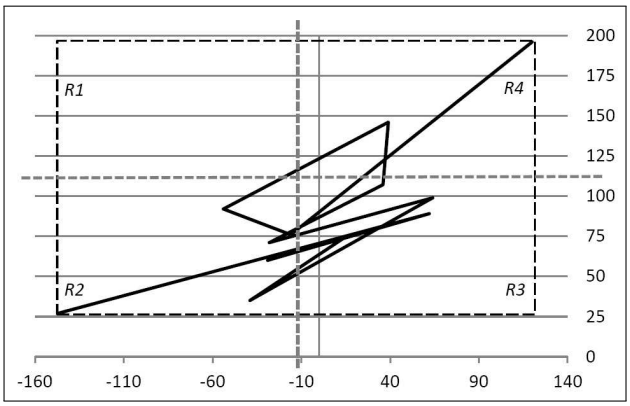

Figure 4: Example of dynamics in the phase plane of the series for *cutremur*

Table 4: Euclidean distances between the dynamics of the words *cutremur*, *seism*, *Vrancea*, and *magnitudine* (relative frequencies)

Words	cutremur	seism	Vrancea	magnitudine
cutremur	0	2,83	3,75	1,41
seism		0	1,41	4,24
Vrancea			0	5,10
magnitudine				0

$C = 0.97$. This shows that distances between the dynamics and the value of the correlation of the respective time series carry at least partly different information and help differentiate between the processes represented by the time series.

4 Discussion

The use of synonyms has also a psycho-linguistic background [24]; as such, it relates to emotions and attitudes expressed in the posts. It would be interesting to follow this study by a research of the uttering of the synonyms on voice-enabled SNs in view of detecting their emotional charge using various methods of characterization, such as those in [8], [9], [13], [28] that report on emotion recognition tools specifically for the Romanian language.

Not all messages posted on SNs contain diacritics. This can present a problem in recognizing lemmas. In this study, all the words with and without diacritics were taken into account.

There is a difference between the same messages on different browsers and SNs. So, the stopwords for TwitterSN are (in Google Chrome): "*no* retweets *no* likes", "Reply", "Retweet", "More", "Like" "newline", and in case of Mozilla's browser the stopwords are "*no* retweets *no* likes" and "newline", where *no* is a number. The stopwords in Google+SN are: "Adauga un comentariu...", "newline". This posts were saved first in .DOCX, than transformed in .TXT.

The earthquake's posts contain information about the earthquake from a specific day. In almost all messages there are dates about the biggest earthquake from that year, or the previous years. This is the reason for the *CutremurDB* contain a small numbers of words than *FocDB*. The data bases include only the following words: nouns, verbs, adjectives, adverbs; we deleted the conjunctions, prepositions, numerals.

5 Conclusions

One of the interesting findings first detected in the preliminary study [24] and confirmed by this ampler database is that Zipf's law is still valid for the most important most frequent 6-7 words used in the posts related to disaster. This is surprising because the words are not among the most used in a language, that is, they are among the rare words in common language; moreover, they are not selected in any specific way preserving the distribution in the common language, so there is no reason that these words still obey a Zipf-type law. However, the law breaks down when we try to expand the set of the most frequent words beyond the number of eight. These facts may indicate that the word selection mechanism in the common language scales down to the lexicon used when dealing specific topics. This scaling property of language statistics (Zipf's law) was never been pointed out before [24], according to our knowledge.

Social networks have their own specificity, with features that could be likened to the personality of humans; the specific use of synonyms is one of that. The parameters in Zipf's law for the lexicons used in posts related to various types of events may help to automatically identify the SN from a set of posts, only knowing the related type of event eliciting the messages.

The posts which have been studied for one year are mostly messages sent by newspapers and TV's and have an informal structure of mass-media type.

Acknowledgments

This work was supported in part by the SPS NATO Program under Grant G4877 /SfP 984877. The author acknowledges the help of Horia-Nicolai Teodorescu (HNT), who, as the PI of the cited grant, established the principles and methods of this research, proposed the main ideas, proposed the structure of this paper and suggested some of the text. This paper reports detailed and complete results complementing [24], where the research was largely done by HNT.

Bibliography

[1] Abbasi, M.A. et al. (2012), Lessons Learned in Using Social Media for Disaster Relief - ASU Crisis Response Game, *Social Computing, Behavioral - Cultural Modeling and Prediction*, Springer, LNCS 7227:282-289.

[2] Acar, A.; Muraki, Y.(2011); Twitter for Crisis Communication: Lessons Learned from Japan's Tsunami Disaster, *Int. J. Web Based Communities*, 7(3): 392-402.

[3] Anderson, K.M.; Schram, A. (2011); Design and Implementation of a Data Analytics Infrastructure in Support of Crisis Informatics Research (NIER Track), *The 33rd Int. Conf. Software Engineering, ICSE'11*, Waikiki, Honolulu, USA, May 21-28, ACM, 844-847.

[4] Bolea, S.C. (2015); Vocabulary, Synonyms and Sentiments of Hazard-Related Posts on Social Networks, *8th IEEE Int. Conf. on Speech Technology and Human-Computer Dialogue, SPED*, Bucharest, Romania, October 14-17.

[5] Boulos, M.N.K. et al. (2010), Social Web Mining and Exploitation for Serious Alications: Technosocial Predictive Analytics and Related Technologies for Public Health, Environmental and National Security Surveillance, *Computer Methods and Programs in Biomedicine*, 100(1): 16-23.

[6] Bruns, A.; Burgess, J.E. (2012); Local and Global Responses to Disaster: #eqnz and the Christchurch Earthquake, *Disaster and Emergency Management Conf., Proc., AST Management Pty Ltd*, pp. 86-103.

[7] Cambria, E. et al. (2013), New Avenues in Opinion Mining and Sentiment Analysis, *IEEE Intelligent Systems*, doi:10.1109/MIS.2013.30, 28(2): 15-21.

[8] Ciobanu, A. et al. (2014), Automatic Fury Recognition in Audio Records, *Proc. 12th Int. Conference on Development and Application Systems (DAS)*, Suceava, Romania, May 15-17, 176-179.

[9] Feraru, S.M. et al. (2010), SRoL - Web-Based Resources for Languages and Language Technology e-Learning, *International Journal Computers Communications & Control*, 5(3): 301-313.

[10] Kryvasheyeu, Y. et al. (2016), Rapid Assessment of Disaster Damage Using Social Media Activity, *Science Advances*, DOI: 10.1126/sciadv.1500779, 2(3):e1500779.

[11] Merchant, R.M. et al. (2011), Integrating Social Media into Emergency-Preparedness Efforts, *The New England Journal of Medicine*, 365:289-291.

[12] Nakov, P. et al. (2013), SemEval-2013 Task 2: Sentiment Analysis in Twitter, *2nd Joint Conf. Lexical and Computational Semantics (*SEM), 7th Int. Workshop SemEval*,Atlanta, June 14-15, 2:312-320.

[13] Pavaloi, I. et al. (2013), Acoustic Analysis Methodology on Romanian Language Vowels for Different Emotional States, *Proc. Int. Symposium on Signals, Circuits and Systems (ISSCS)*, Iasi, Romania, July 11-12.

[14] Piantadosi, S. T. (2014); Zipf's Word Frequency Law in Natural Language: A Critical Review and Future Directions, *Psychon Bull Rev.*, DOI: 10.3758/s13423-014-0585-6, 5:1112-1130.

[15] Pirnau, M. (2015); Tool for Monitoring Web Sites for Emergency-Related Posts and Post Analysis, *8th IEEE Int. Conf. on Speech Technology and Human-Computer Dialogue, SPED*, Bucharest, Romania, October 14-17.

[16] Saharia, N. (2015); Detecting Emotion from Short Messages on Nepal Earthquake, *Proceedings of the 8th International Conference on Speech Technology and Human-Computer Dialogue, SPED*, Bucharest, Romania, October 14-17.

[17] Saif, H. et al.(2012), Semantic Sentiment Analysis of Twitter, *Proceedings of the 11th Int. Conference The Semantic Web, Part I*, Boston, USA, November 11-15, pp. 508-524.

[18] Temnikova, E. et al. (2015), EMterms 1.0: A teminological Resource for Crisis Tweets, *Proceedings ISCRAM 2015 Conference*, Kristiansand, Norway, May 24-27.

[19] Teodorescu, H.N.L. (2015); On the Responses of Social Networks to External Events, *Proc. ECAI 2015 7th IEEE Int. Conf. on Electronics, Computers and Artificial Intelligence*, Bucharest, Romania, June 25-27, DOI: 10.1109/ECAI.2015.7301138, 13-18.

[20] Teodorescu, H.N.; Bolea S. C. (2016); Analysis of Probabilities of Specified Words' Occurrences in SN Messages related to Catastrophes, *18-th Int. Conf. System Analysis and Information Technology, SAIT*, Kyiv, Ukraine, May 30-June 2.

[21] Teodorescu, H.N. (2012); Characterization of Nonlinear Dynamic Systems for Engineering Purposes - A partial Review, *International Journal of General Systems*, 41(8):805-825.

[22] Teodorescu, H.N. (2013); SN Voice and Text Analysis as a Tool for Disaster Effects Estimation - A Preliminary Exploration, *Proceedings 7th IEEE Conference on Speech Technology and Human - Computer Dialogue*, Cluj Napoca, Romania, October 16-19.

[23] Teodorescu, H.N. (2016); Emergency-Related, Social Network Time Series: Description and Analysis, *Time Series Analysis and Forecasting, Contributions to Statistics*, Springer International Publishing Switzerland, pp.205-215.

[24] Teodorescu, H.N.L.; Bolea S.C. (2016); On the Algorithmic Role of Synonyms and Keywords in Analytics for Catastrophic Events, *Proceedings ECAI-2016, 8th International Conference on Electronics, Computers and Artificial Intelligence*, Ploiesti, Romania, June 30-July 2.

[25] Teodorescu, H.N.; Feraru, S.M. (2007); A Study on Speech with Manifest Emotions, *Lecture Notes In Artificial Intelligence*, Springer Berlin Heidelberg, 4629: 254-261.

[26] Verma, S. et al. (2011), Natural Language Processing to the Rescue?: Extracting Situational Awareness Tweets During Mass Emergency, *Proc. Fifth Int. AAAI Conf. on Weblogs and Social Media*, North America, July, 385-392.

[27] Yang M. et al. (2011), Social Media Analytics for Radical Opinion Mining in Hate Group Web Forums, *J. Homeland Security and Emergency Management*, August 11, 8(1), DOI: 10.2202/1547-7355.1801.

[28] Zbancioc, M.; Feraru, M. (2012); Emotion Recognition of the SROL Romanian Database Using Fuzzy KNN Algorithm, *Int. Symposium on Electronics and Telecommunications IEEE-ISETC 2012 Tenth Edition*, Timisoara, Romania, 347-350.

[29] http://www.dictionardesinonime.ro/.

[30] http://www.racai.ro/en/tools/text/

INTERNATIONAL JOURNAL OF COMPUTERS COMMUNICATIONS & CONTROL
ISSN 1841-9836, 11(5):613-630, October 2016.

Efficient Historical Query in HBase for Spatio-Temporal Decision Support

X.Y. Chen, C. Zhang, B. Ge, W.D. Xiao

Xiao-Ying Chen, Chong Zhang*, Bin Ge, Wei-Dong Xiao
Science and Technology on Information Systems Engineering Laboratory
National University of Defense Technology
Changsha 410073, P.R.China
chenxiaoying1991@yahoo.com, leocheung8286@yahoo.com
gebin1978@gmail.com, wilsonshaw@vip.sina.com
*Corresponding author: leocheung8286@yahoo.com

Abstract: Comparing to last decade, technologies to gather spatio-temporal data are more and more developed and easy to use or deploy, thus tens of billions, even trillions of sensed data are accumulated, which poses a challenge to spatio-temporal Decision Support System (stDSS). Traditional database hardly supports such huge volume, and tends to bring performance bottleneck to the analysis platform. Hence in this paper, we argue to use NoSQL database, HBase, to replace traditional back-end storage system. Under such context, the well-studied spatio-temporal querying techniques in traditional database should be shifted to HBase system parallel. However, this problem is not solved well in HBase, as many previous works tackle the problem only by designing schema, i.e., designing row key and column key formation for HBase, which we don't believe is an effective solution. In this paper, we address this problem from nature level of HBase, and propose an index structure as a built-in component for HBase. STEHIX (Spatio-TEmporal Hbase IndeX) is adapted to two-level architecture of HBase and suitable for HBase to process spatio-temporal queries. It is composed of index in the meta table (the first level) and *region index* (the second level) for indexing inner structure of HBase regions. Base on this structure, three queries, range query, kNN query and GNN query are solved by proposing algorithms, respectively. For achieving load balancing and scalable kNN query, two optimizations are also presented. We implement STEHIX and conduct experiments on real dataset, and the results show our design outperforms a previous work in many aspects.
Keywords: spatio-temporal query, HBase, range query, kNN query, GNN query, load balancing.

1 Introduction

Nowadays, either organizations or common users need sophisticated spatio-temporal Decision Support System (stDSS) [1] for countless geospatial applications, such as urban planning, emergency response, military intelligence, simulator training, and serious gaming. Meanwhile, with the development of positioning technology (such as GPS) and other related applications, huge of spatio-temporal data are collected, of which volume increases to PB or even EB. Consequently, this necessarily poses a challenge to stDSS applications. Traditionally, these data are stored in relational database, however, since the database can't resist such a huge volume, such architecture would bring performance bottleneck to the whole analysis task. Hence, the new structural storage system should back up stDSS. In this paper, we argue that HBase [2] is capable to accomplish such task, since HBase is a key-value, NoSQL storage system, which can support large-scale data operations efficiently.

On the other hand, from system point of view, an ideal geospatial application designed to formulate and evaluate decision-making questions for stDSS should contain efficient presentation

of a basic set of spatio-temporal queries, such as: find doctors who can carry out rescue in a certain area, recently, find 5 flower shops nearest to Tony, a group of friends spreading over different places want to find nearest restaurant to them, aggregately, i.e., the sum of distances to them is minimum. These operations are supported well in relational database, however, they are not supported by HBase in a straightforward way. The main reason is that HBase do not natively support multi-attribute index, which limits the rich query applications.

Hence in this paper, we explore processing for basic spatio-temporal queries in HBase for stDSS. From a variety of applications, we mainly address three common and useful spatio-temporal queries as follows:

- **range query**: querying data in specific spatial and temporal range. For instance, in real-time monitoring and early warning of population, query the number of people in different time intervals within a specific area.
- **kNN query (k-Nearest Neighbor)**: querying data to obtain k nearest objects to a specific location during a certain period. For instance, in the past week, find 5 nearest Uber taxis to a given shopping mall.
- **GNN query (Group Nearest Neighbor)**: querying data to obtain k nearest objects aggregately (measured by sum of distances) to a group of specific locations during a certain period. For instance, during last month, find the nearest ship to the given three docks.

As an example, Figure 1 shows the spatial distribution of users during two time interval [1, 6] and [7, 14]. For range query, find the users who are in the spatial range marked by the dashed line rectangle within time period [1, 6], apparently, $\{u_1, u_3\}$ is the result. For 1NN query, if we want to find the users who are nearest to p_1 during time period [1, 6] and [7, 14], respectively, the result is u_2 for [1, 6] and u_1 for [7, 14]. For GNN query, if we want to find the user who are nearest to p_1 and p_2 by summing the distances during time period [1, 6], the result is u_2.

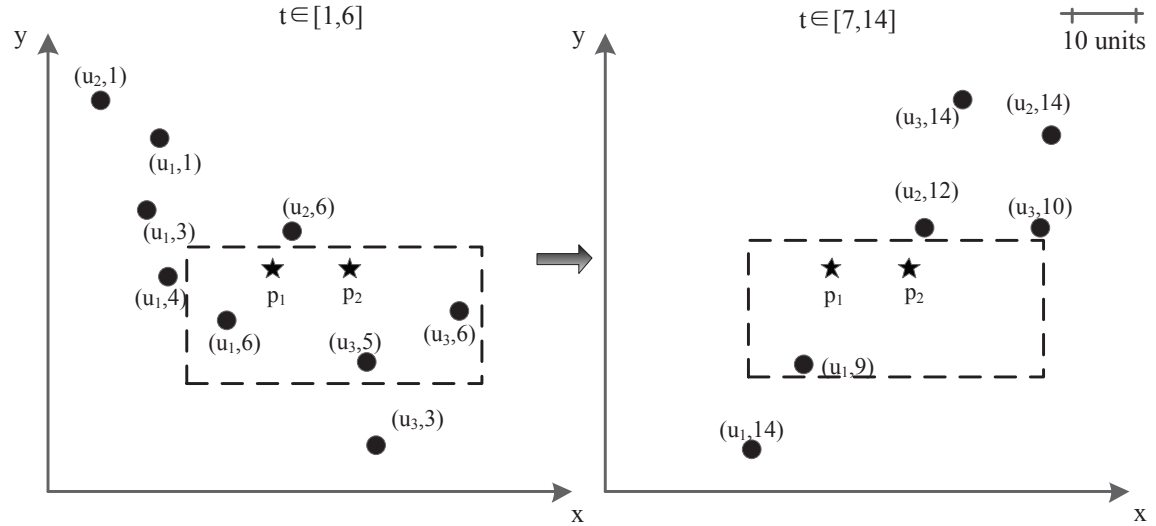

	$(u_2,6)$	$(u_1,6)$	$(u_1,4)$	$(u_3,5)$	$(u_1,3)$	$(u_1,1)$	$(u_3,6)$	$(u_3,3)$	$(u_2,1)$
$\|p_1,u_i\|$	9	16	23	28	30	38	42	44	53
$\|p_2,u_i\|$	14	27	37	20	43	48	27	39	63
sum	23	43	60	48	73	86	69	83	116

	$(u_1,9)$	$(u_2,12)$	$(u_1,14)$	$(u_3,10)$	$(u_3,14)$	$(u_2,14)$
$\|p_1,u_i\|$	21	22	42. 5	45	47	52
$\|p_2,u_i\|$	30	10	52	32	38	42. 5
sum	51	32	94. 5	77	85	94. 5

Figure 1: An example for range, kNN and GNN query

1.1 Motivation

Our motivation is to adapt HBase to efficiently process spatio-temporal queries as basic operations for spatio-temporal decision support system. Although some previous works propose distributed index on HBase, but these works only consider spatial dimension, more critically, most of these works only concern how to design schema for spatial data, which do not tackle the problem from the nature level of HBase, except one, MD-HBase [5] is designed to add index structure into the meta table, however, it doesn't provide index to efficiently retrieve the inner data of HBase regions. Our solution, STEHIX (Spatio-TEmporal Hbase IndeX), is built on two-level lookup mechanism, which is based on the retrieval mechanism of HBase. First, we use Hilbert curve to linearize geo-locations and store the converted one-dimensional data in the meta table, and for each region, we build a *region index* indexing the *StoreFile*s in HBase regions. We focus on range query, kNN query and GNN query for such environment in this paper.

1.2 Contributions and paper organization

We address how to efficiently answer range query, k nearest neighbor (kNN) query and GNN query on spatio-temporal data in HBase. Our solution is called STEHIX (Spatio-TEmporal Hbase IndeX), which fully takes inner structure of HBase into consideration. The previous works focus on building index based on the traditional index, such as R-tree, B-tree, while our method constructs index based on HBase itself, thus, our index structure is more suitable for HBase retrieval. In other way, STEHIX considers not only spatial dimension, but also temporal one, which is more in line with user demand.

We use Hilbert curve to partition space as the initial resolution, the encoded value of which is used in the meta table to index HBase regions, then we use quad-tree to partition Hilbert cells as the finer resolution, based on this, we design *region index* structure for each region, which contains the finer encoded values for indexing spatial dimension and time segments for indexing temporal dimension. And later, we show such two-level index structure, meta table + *region index*, is more suitable for HBase to process query in the experiment. Based on our index structure, algorithms for range query, kNN query and GNN query are devised, and load balancing policy and optimization to kNN query are also presented to raise STEHIX performance. We compare STEHIX with MD-HBase on real dataset, and the results show our design philosophies make STEHIX to be more excellent than the counterpart. In summary, we make the following contributions:

- We propose STEHIX structure which fully follow inner mechanism of HBase and is a new attempt on building index for spatio-temporal data in HBase platform.
- We propose efficient algorithms for processing range query, kNN query and GNN query in HBase.
- We carry out comprehensive experiments to verify the efficiency and scalability of STEHIX.

The rest of this paper is organized as follows. Section 2 reviews related works. Section 3 formally defines the problem and prerequisites. Section 4 presents STEHIX structure. In section 5, algorithms for range query kNN query and GNN query are presented. Section 6 reports the optimizations to the index. And we experimentally evaluate STEHIX in section 7. Finally, section 8 concludes the paper with directions for future works.

2 Related Works

To overcome the drawbacks of traditional RDBMS, as an attractive alternative for large-scale data processing, Cloud storage system currently adopts a hash-like approach to retrieve data that only support simple keyword-based queries, but lacks various forms of information search. For data processing operations, several cloud data managements (CDMs), such as HBase, are developed. HBase, as NoSQL databases, is capable to handle large scale storage and high insertion rate, however, it does not offer much support for rich index functions. Many works focus on this point and propose various approaches.

Nishimura et al. [5] address multidimensional queries for PaaS by proposing MD-HBase. It uses k-d-trees and quad-trees to partition space and adopts Z-curve to convert multidimensional data to a single dimension, and supports multi-dimensional range and nearest neighbor queries, which leverages a multi-dimensional index structure layered over HBase. However, MD-HBase builds index in the meta table, which does not index inner structure of regions, so that scan operations are carried out to find results, which reduces its efficiency.

Hsu et al. [6] propose a novel Key formulation scheme based on R^+-tree, called KR^+-tree, and based on it, spatial query algorithm of kNN query and range query are designed. Moreover, the proposed key formulation schemes are implemented on HBase and Cassandra. With the experiment on real spatial data, it demonstrates that KR^+-tree outperforms MD-HBase. KR^+-tree is able to balance the number of false-positive and the number of sub-queries so that it improves the efficiency of range query and kNN query a lot. This work designs the index according to the features found in experiments on HBase and Cassandra. However, it still does not consider the inner structure of HBase.

Zhou et al. [7] propose an efficient distributed multi-dimensional index (EDMI), which contains two layers: the global layer divides the space into many subspaces adopting k-d-tree, and in the local layer, each subspace is associated to a Z-order prefix R-tree (ZPR-tree). ZPR-tree can avoid the overlap of MBRs and obtain better query performance than other Packed R-trees and R^*-tree. This paper experimentally evaluates EDMI based on HBase for point, range and kNN query, which verifies its superiority. Compared with MD-HBase, EDMI uses ZPR-tree in the bottom layer, while MD-HBase employs scan operation, so that EDMI provides a better performance.

Han et al. [8] propose HGrid data model for HBase. HGrid data model is based on a hybrid index structure, combining a quad-tree and a regular grid as primary and secondary indices, supports efficient performance for range and kNN queries. This paper also formulates a set of guidelines on how to organize data for geo-spatial applications in HBase. This model does not outperform all its competitors in terms of query response time. However, it requires less space than the corresponding quad-tree and regular-grid indices.

HBaseSpatial, a scalable spatial data storage based on HBase, proposed by Zhang et al. [9]. Compared with MongoDB and MySQL , experimental results show it can effectively enhance the query efficiency of big spatial data and provide a good solution for storage. But this model does not compare with other distributed index method.

All the previous works we have mentioned above only consider the spatial query. For moving objects, a certain type of geo-spatial applications, requires high update rate and efficient real-time query on multi-attributes such as time-period and arbitrary spatial dimension. Du et al. [10] present hybrid index structure based on HBase, using R-tree for indexing space and applying Hilbert curve for traversing approaching space. It supports efficient multi-dimensional range queries and kNN queries, especially it is adept at skewing data compared with MD-HBase and KR^+-tree. As this work focus on moving objects, it is different for our goal, and it also does not take the inner structure of HBase into account.

To address the shortcoming which have mentioned above, the STEHIX structure which fully follow inner mechanism of HBase and is a new attempt on building index for spatio-temporal data in HBase platform is proposed.

3 Problem Definition and Prerequisites

In this section, we first formally describe spatio-temporal data, and then present the structure of HBase storage. For simplicity, only two-dimensional space is considered in this paper, however, our method can be directly extended into higher dimensional space.

A record r of spatio-temporal data can be denoted as $\langle x, y, t, \mathcal{A}\rangle$, where (x, y) means the geo-location of the record, t means the valid time when the data is produced, $\mathcal{A}$ represents other attributes, such as user-id, object's shape, descriptions, and etc. We give the descriptions for structure of storage and index in HBase [11], [12], for simplicity, some unrelated components, such as *HLog* and version, are omitted. Usually, an HBase cluster is composed of at least one administrative server, called *Master*, and several other servers holding data, called *RegionServer*s.

Logically, a table in HBase is similar to a grid, where a cell can be located by the given row identifier and column identifier. Row identifiers are implemented by row keys (rk), and the column identifier is represented by column family (cf) + column qualifier (cq), where a column family consists of several column qualifiers. The value in a cell can be referred to as the format (rk, cf:cq). Table 1 shows a logical view of a table in HBase. For instance, value v_1 can be referred to as (rk_1, cf_1:cq_1).

Table 1: Logical View for HBase Table

	cf_1			cf_2	
	cq_1	cq_2	cq_3	cq_a	cq_b
rk_1	v_1	v_2	v_3	v_4	v_5
rk_2	v_6	v_7	v_8	v_9	v_{10}

Physically, a table in HBase is horizontally partitioned along rows into several regions, each of which is maintained by exactly one *RegionServer*. The client directly interacts with the respective *RegionServer* when executing read or write operations. When the data, formally as $\langle rk$, cf:cq, $value\rangle$ (we alternatively use term key-value data in rest of the paper), are written into a region, the *RegionServer* first keeps the data in a list-like memory structure called *MemStore*, where each entry is pre-configured with the same fixed size (usually 64KB) and the size of a certain number of entries is equal to that of the block of the underlying storage system, such as HDFS. When the size of *MemStore* exceeds a pre-configured number, the whole *MemStore* is written into the underlying system as a *StoreFile*, the structure of which is similar to that of *MemStore*. Further, when the number of *StoreFile*s exceeds a certain number, the *RegionServer* will execute the compaction operation to merge *StoreFile*s into a new large one. HBase provides a two-level lookup mechanism to locate the *value* corresponding to the key (rk, cf:cq). The catalog table *meta* stores the relation {[table name]:[start row key]:[region id]:[region server]}, thus given a row key, the corresponding *RegionServer* can be found, and then the *RegionServer* searches the *value* locally according to the given key (rk, cf:cq). Figure 2 shows an example of HBase two-level lookup structure.

From above descriptions, we can see that HBase only provides a simple hierarchical index structure based on the meta table, and the corresponding *RegionServer* must do scan work to refine the results, which would be inefficient to handle spatio-temporal queries.

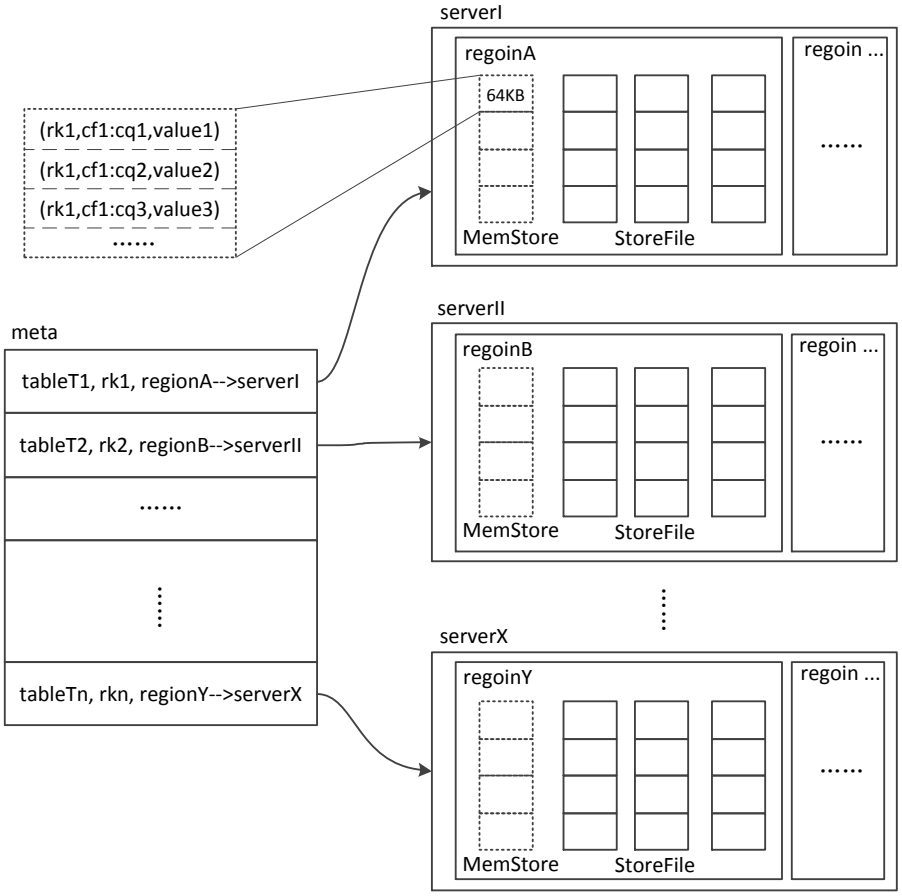

Figure 2: HBase Two-Level Lookup

4 STEHIX Structure

In this section, we present the structure of our index, STEHIX (Spatio-TEmporal Hbase IndeX). The following philosophies are considered during index design, 1) for applications, it is not necessary for users to dedicatedly to design schema for query spatio-temporal data, i.e., our index should add no restriction on schema design, but a inner structure associated with HBase, 2) the index should be in accordance with the architecture of HBase as identical as possible, 3) the index should be adaptive to data distribution.

For design rule 1), we don't care the schema design and generalize each record to be a key-value data in *StoreFile*(*MemStore*), formally $(rk,\ cf{:}cq,\ r)$, where $r{=}\langle x,\ y,\ t,\ \mathcal{A}\rangle$.

For design rule 2), our index is built on the two-level lookup mechanism. In particular, we use Hilbert curve to linearize geo-locations and store the converted one-dimensional data in the meta table, and for each region, we build a *region index* to index the *StoreFile*s. Figure 3 shows an overview of STEHIX architecture.

4.1 Meta Table Organization

We use Hilbert curve to partition the whole space as the initial granularity. According to the design rationale of HBase, the prefix of row key should be different so that the overhead of inserting data could be distributed over *RegionServer*s. And such design is able to satisfy this demand.

Hilbert curve is a kind of space filling curve which maps multi-dimensional space into one-dimensional space. In particular, the whole space is partitioned into equal-size cells and then

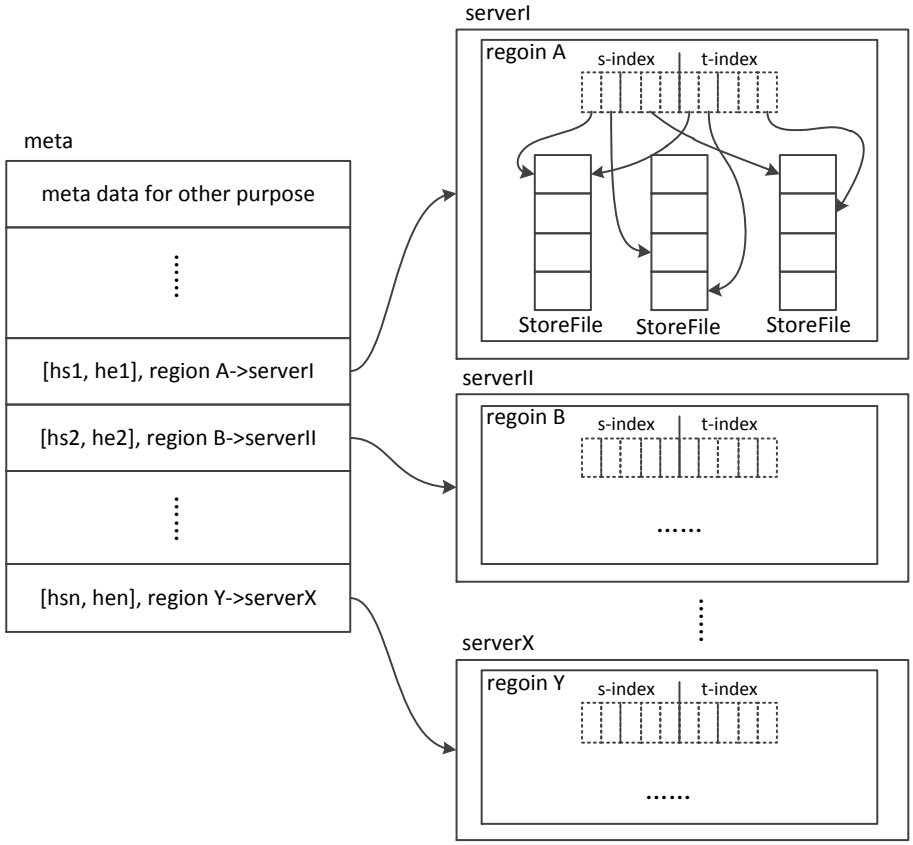

Figure 3: Overview of STEHIX

a curve is passed through each cell for only once in term of some sequence, so that every cell is assigned a sequence number. Different space filling curves are distinguished by different sequencing methods. Due to information loss in the transformation, different space filling curves are evaluated by the criteria, locality preservation, meaning that how much the change of proximities is from original space to one-dimensional space. Hilbert curve is proved to be the best locality preserved space filling curve [13]. With Hilbert curve, any object in the original space is transformed into $[0, 2^{2\lambda} - 1]$ space, where λ is called the order of Hilbert curve. Figure 4 shows four Hilbert curves in two-dimensional space with λ=1, 2, 3 and 4.

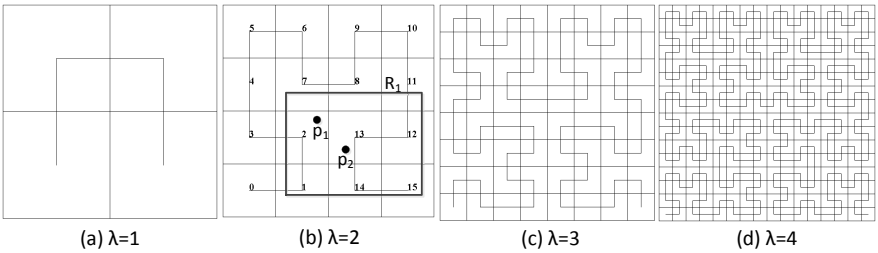

Figure 4: Hilbert Curves

We describe three functions for Hilbert curve, first one is mapping a point in the original space to a value in one-dimensional space, the second is mapping a range window to a series of intervals, and the third is retrieving proximity cells of a point. Specifically, for a Hilbert curve with order=λ,

- $coorToCell(p)$. Given a point p=(x_1, x_2, …, x_n) in n-dimensional space $\mathbb{S}$, $coorToCell(p)$ returns a cell number (between 0 and $2^{2\lambda} - 1$) referring the cell where p lies within $\mathbb{S}$.

- $rectToIntervals(R)$. Given a range window R=(x_1^l, x_2^l, ..., x_n^l, x_1^u, x_2^u, ..., x_n^u) in n-dimensional space $\mathbb{S}$, where x_i^l and x_i^u ($1 \leq i \leq n$) are the lower and upper bound of the ith-dimension, respectively, $rectToIntervals(R)$ returns a series of intervals representing the cells intersecting with R in $\mathbb{S}$.
- $getNeighborCells(p)$. Given a point p=(x_1, x_2, ..., x_n) in n-dimensional space $\mathbb{S}$, $getNeighborCells(p)$ returns a list of cell numbers referring the cells which are neighbors of the cell $coorToCell(p)$.

For instance, in Figure 4 (b), $coorToCell(p_1) = 2$, $coorToCell(p_2) = 13$, $rectToIntervals(R_1)$ = {[1,2], [7,8], [11,15]}, and $getNeighborCells(p_2)$={1, 2, 7, 8, 11, 12, 15, 14}.

Based on above descriptions, we use Hilbert cell value as row key in the meta table to index spatio-temporal data as first level, thus, each record can be placed into the corresponding region according to Hilbert value of spatial part of the record. In particular, the following mapping structure is built in the meta table (for simplicity, table name is omitted): {[start Hilbert cell, end Hilbert cell]:[region id]:[region server]}. Initially, assuming there are N regions across M *RegionServer*s, we can uniformly assign Hilbert cells to these regions, for instance, the first entry could be $\{[0, ((2^{2\lambda} - 1)/N) - 1] : regionA : serverI\}$, and the second $\{[((2^{2\lambda} - 1)/N), (2 * (2^{2\lambda} - 1)/N) - 1] : regionB : serverII\}$.

4.2 Region Index Structure

For retrieving local data efficiently, we design the *region index* which is kept in memory like *MemStore*. Considering *MemStore* is always kept in memory, *region index* is only to index *StoreFile*, however, for answering a query, *MemStore* must be scanned to guarantee the completeness of results.

Region index is a list-like in-memory structure, each entry of which points to a list of addresses referring to key-value data in the *StoreFile*. The *region index* consists of two parts, one is called *s-index* indexing spatial component of data, the other is called *t-index* indexing the temporal part, and such design is able to benefit query efficiency as we will see in next section.

For constructing *s-index*, the space is further partitioned at a finer granularity, i.e., each Hilbert cell is recursively divided by quad-tree and the resulting tiles are encoded with binary Z-Order. Such consideration is able to deal with the skewed data, i.e., when a hotspot is detected, quad-tree can be used recursively until the hotspot is eliminated. Later, we will use this idea to design an adaptive load balancing policy. After partitioning the Hilbert cell, each tile is corresponding to an entry in the *s-index*, i.e., the entry points to the key-value data whose geo-locations lie in that tile. For instance, Figure 5 shows an example of meta table and region index, where in the meta table, Hilbert cells [0, 1] indexes $regionA : serverI$ and [2, 3] for $regionB : serverII$, respectively. For $regionA$, Hilbert cells 0 and 1 are divided using quad-tree into 11 tiles, 7 of which are 2-bit tiles and 4 are 4-bit tiles, and for each entry in *s-index*, the identifier is a combination of Hilbert value and binary Z-Order value, for instance, entry 0-10, where 0 is the number of Hilbert cell 0 and 10 is the code of lower-right tile in Hilbert cell 0, points to a list containing two addresses referring to two key-value records in *StoreFile*.

For building *t-index*, we use a period T to bound the length of the list of *t-index*, and such consideration is based on the fact that there may be some cycle for the spatial change of objects. The period T is divided into several segments, each of which is corresponding to an entry in *t-index*. Each entry points to a list of addresses referring to key-value data in *StoreFile*, whose temporal component modulo T lies in the segment. Continuing the example, Figure 5 shows the structure of *t-index*. Let T=24, which means a period of 24 hours is a cycle, and let each segment = 3 hours, which means T is divided into 8 segments, and entry [3, 6) points to 8 key-value data whose temporal value modulo 24 between 3 and 6.

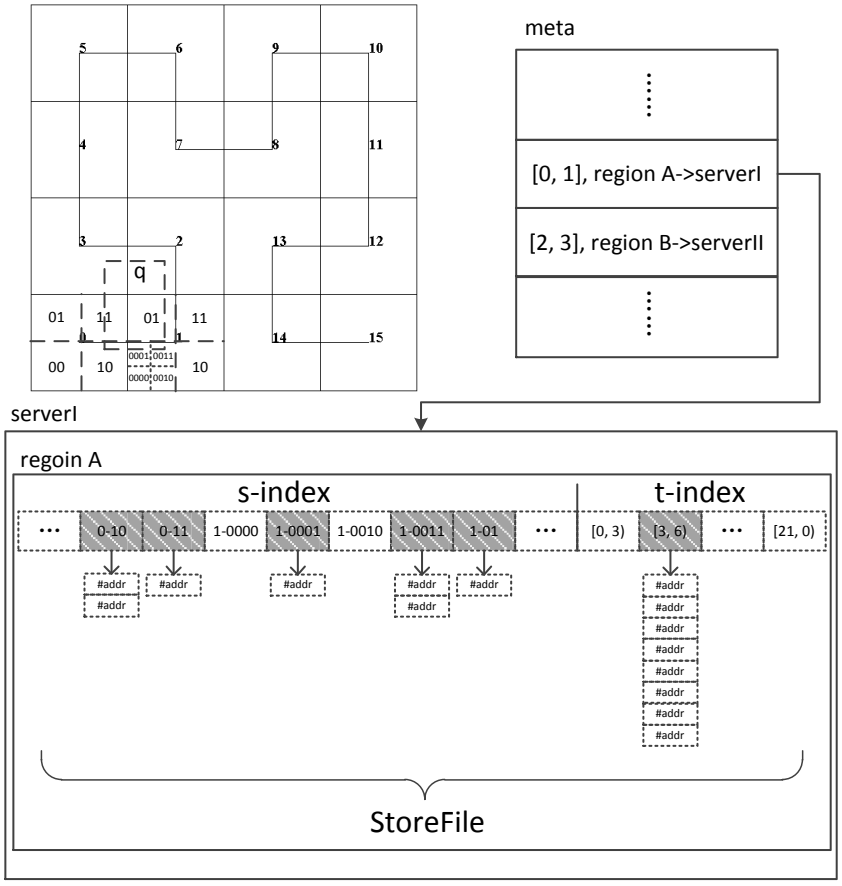

Figure 5: Region Index Structure

5 Query Processing

In this section, the processing algorithms for range query, kNN query and GNN query are presented.

5.1 Range Query

A range query q=(x_l, y_l, x_u, y_u, t_s, t_e), aims to find all the records, whose geo-locations lie in the range (x_l, y_l, x_u, y_u) during time [t_s, t_e].

The basic work flow for processing a range query q is described as follows, first, using Hilbert curve, spatial predicate (x_l, y_l, x_u, y_u) is converted into a set of one-dimensional intervals I_q, then according to mapping relation in the meta table, the involved *RegionServer*s are informed to search the corresponding regions locally, utilized by *region index*. Here we propose a query optimization, i.e., using *s-index* and *t-index* to calculate selectivity, which is helpful to choose the high-selectivity to filter more unrelated data, in particular, the spatial predicate is recursively divided by quad-tree, the results of which are intersected with the entries in *s-index*, and then the number of addresses to key-value data can be calculated, say sn, similarly, using *t-index* can also calculate a number, tn, then if sn is less than tn, *s-index* is followed to retrieve results, other wise *t-index* is used.

Algorithm 1 describes the range query processing for STEHIX. In line 1, the spatial predicate is converted into one-dimensional intervals I_q, and the temporal predicate is converted into [0, T] interval in line 2. In line 3, function $findRegions()$ finds the involved regions which intersect with I_q. From line 4 to 11, each corresponding *region index* is inspected to retrieve results, in

particular, *s-index* and *t-index* is used to calculate selectivity for the query, which is implemented by function $getCard()$, and the index with the lower cardinality is chosen to retrieve the results.

Algorithm 1 Range Query Processing

Require:
q=$(x_l, y_l, x_u, y_u, t_s, t_e)$
Ensure:
$Qlist$ //result list
1: $I_q = rectToIntervals(x_l, y_l, x_u, y_u)$
2: $key_s = t_s \ mod \ T$, $key_e = t_e \ mod \ T$
3: $Regions$=$findRegions(I_q)$
/*the following processing is executed separately in each *region*/
4: **for** each $region \in Regions$ **do**
5: sn=$region.s\text{-}index.getCard(x_l, y_l, x_u, y_u)$
6: tn=$region.t\text{-}index.getCard(key_s, key_e)$
7: **if** $sn \leq tn$ **then**
8: $Qlist$←$region.s\text{-}index.seachIndex(q)$
9: **else**
10: $Qlist$←$region.t\text{-}index.seachIndex(q)$
11: **end if**
12: **end for**
13: **return** $Qlist$

Figure 5 shows an example for range query processing in STEHIX. The spatial bound of q is depicted with dashed line and we assume that temporal predicate of q is [3, 6]. Then Hilbert cells 0 and 1 are intersected with q, thus, two entries in the meta table are examined, namely, $\{[0, 1] : regionA : serverI\}$ and $\{[2, 3] : regionB : serverII\}$. For instance, in $regionA$, the entries in *s-index* are intersected with spatial predicare of q, resulting 0-10, 0-11, 1-0001, 1-0011, 1-01 these 5 entries, which refer to totally 7 addresses to key-value data, and similarly, entry [3, 6) of *t-index* refers to 8 addresses, consequently *s-index* is followed to retrieve the results.

5.2 kNN Query

A kNN query could be formally defined as: given a set $\mathcal{R}$ of spatio-temporal data records, a kNN query q=(x_q, y_q, t_s, t_e, k), aims to find a set $\mathcal{R}(q) \subseteq \mathcal{R}$, such that $|\mathcal{R}(q)|$=k, and $d(o, (x_q, y_q)) \leq d(o\prime, (x_q, y_q))$, $\forall o \in \mathcal{R}(q)$, $o\prime \in \mathcal{R} \setminus \mathcal{R}(q)$, and $o.t$, $o\prime.t \in [t_s, t_e]$, where $d()$ is the Euclidean distance function.

We don't want to use n range queries to accomplish the kNN query, which means continuously enlarging spatial range of the query until k records are obtained [14], because we believe such a method would cause heavy querying overhead. We propose an approach utilized by incremental retrieval idea [15]. The basic work flow is, proximity objects of point (x_q, y_q) are constantly, incrementally retrieved until k results are found. In particular, first, Hilbert cell h containing point (x_q, y_q) is located, then the corresponding *region index* is utilized to retrieve all records lie in h, meanwhile, neighbor cells of h are also retrieved, and these records and Hilbert cells are all enqueued into a priority queue where priority metric is the distance from (x_q, y_q) to record or Hilbert cell. Then top element is constantly dequeued and processed, either being added to result list or being followed to retrieve neighbor cells to be enqueued, until k results are found.

Algorithm 2 presents kNN query processing. The first line initializes a priority queue PQ where each element is ordered by the distance from (x_q, y_q) to the element. The element can be Hilbert cell or record, and if it is a Hilbert cell, the distance is $MINDIST$ [16], other wise, the distance is the Euclidean distance from (x_q, y_q) to geo-location of the record. In line 2, the Hilbert cell containing (x_q, y_q) is gained, and is enqueued in line 3. From line 4, the procedure constantly retrieves top element e from PQ (line 5) and processes it, in particular, if e is a Hilbert cell (line 6), find the corresponding region rg from the meta table (line 7), and then the corresponding *region index* is searched to retrieve all the records satisfying temporal predicate (line 8), which are enqueued into PQ (line 9 to 11), after that, the neighbor cells of e are obtained and enqueued into PQ (line 12 to 15); other wise, i.e., if e is a record (line 16), which means e is a result, e is added into $Qlist$ (line 17), and the above procedure is looped until the size of

Algorithm 2 kNN Query Processing

Require:
q=(x_q, y_q, t_s, t_e, k)
Ensure:
$Qlist$ //result list
1: PQ=$null$ //initial a priority queue
2: h=$coorToCell(x_q, y_q)$
3: $PQ.enqueue(h, MINDIST((x_q, y_q), h))$
4: **while** $PQ \neq \phi$ **do**
5: e=$PQ.dequeue()$
6: **if** e is typeof cell **then**
7: rg=$findRegions(e)$
8: RS=$rg.findRecords(e, (t_s, t_e))$
9: **for** each $record \in RS$ **do**
10: $PQ.enqueue(record, dist((x_q, y_q), record))$
11: **end for**
12: $CellSet$=$getNeighborCells(e.center)$
13: **for** each $cell \in CellSet$ **do**
14: $PQ.enqueue(cell, MINDIST((x_q, y_q), cell))$
15: **end for**
16: **else if** e is typeof record **then**
17: $Qlist \leftarrow e$
18: **if** $Qlist.size()$=k **then**
19: **return** $Qlist$
20: **end if**
21: **end if**
22: **end while**

$Qlist$ reaches k (line 18 to 20).

5.3 GNN Query

A GNN query in our work could be formally defined as: given a set $\mathcal{R}$ of spatio-temporal data records and a set of location point(s) P, a GNN query q=(P, t_s, t_e, k), aims to find a set $\mathcal{R}(q) \subseteq \mathcal{R}$, such that $|\mathcal{R}(q)|$=k, and the point(s) of $\mathcal{R}(q)$ with smallest sum of distances to all points in P ($|P|$=n), i.e. $\sum_{i=1}^{N} d(o,(x_i,y_i)) \leq \sum_{i=1}^{n} d(o\prime,(x_i,y_i))$, $\forall o \in \mathcal{R}(q)$, $o\prime \in \mathcal{R} \setminus \mathcal{R}(q)$, and $o.t$, $o\prime.t$ $\in$[t_s, t_e], where $d()$ is the Euclidean distance function.

Different from kNN query, GNN query aims to finds a group of point(s) that nearest to a set of points. In kNN query processing, firstly Hilbert cell h containing point (x_q, y_q) is located, while in GNN processing, we firstly find the ideal nearest neighbor p, which could not exist in the dataset $\mathcal{R}$. This approach is that the nearest neighbor is the point(s) "near" p. Let (x,y) be the coordinates of ideal 1NN point p and (x_i,y_i) be the coordinates of point $p_i \in P$, p minimizes the sum of distance function:

$$sum_{dist}(p,P) = \sum_{i=1}^{n} \sqrt{(x-x_i)^2 + (y-y_i)^2} \tag{1}$$

Partially calculate the derivation of function $sum_{dist}(p,P)$ with respect to variables x and y, let them equal to zero, we have:

$$\begin{cases} \dfrac{\partial sum_{dist}(p,P)}{\partial x} = \displaystyle\sum_{i=1}^{n} \frac{x-x_i}{\sqrt{(x-x_i)^2+(y-y_i)^2}} = 0 \\ \dfrac{\partial sum_{dist}(p,P)}{\partial y} = \displaystyle\sum_{i=1}^{n} \frac{y-y_i}{\sqrt{(x-x_i)^2+(y-y_i)^2}} = 0 \end{cases} \tag{2}$$

However, this equations can not be solved when $n > 2$. According to the method in [18], we start with the arbitrary initial coordinates $x = \frac{\sum_{i=1}^{n} x_i}{n}$, $y = \frac{\sum_{i=1}^{n} y_i}{n}$, then modifies as follows:

$$x = x - \eta \frac{\partial sum_{dist}(p,P)}{\partial x}, y = y - \eta \frac{\partial sum_{dist}(p,P)}{\partial y} \tag{3}$$

where η is a step size. The process is repeated until the distance function $sum_{dist}(p,P)$ converges to a minimum value. We call this processing $p = getNearest(P)$. The range around p in which we should look for points of $\mathcal{R}(q)$.

The basic work flow is similar to kNN query processing which introduce above. Algorithm 3 presents GNN query processing. In particular, first, Hilbert cell h containing point p (x, y) is located, then the corresponding *region index* is utilized to retrieve all records lie in h, meanwhile, neighbor cells of h are also retrieved, and these records and Hilbert cells are all enqueued into a priority queue where priority metric is the sum of distance from P to record or Hilbert cell. Then top element is constantly dequeued and processed, either being added to result list or being followed to retrieve neighbor cells to be enqueued, until k results are found.

Algorithm 3 GNN Query Processing

Require:
q=(P, t_s, t_e, k)
Ensure:
$Qlist$ //result list
1: PQ=*null* //initial a priority queue
2: $p = getNearest(P)$
3: h=$coorToCell(p)$
4: $PQ.enqueue(h, sum_{MINDIST}((P), h))$
5: **while** $PQ \neq \phi$ **do**
6: e=$PQ.dequeue()$
7: **if** e is typeof cell **then**
8: rg=$findRegions(e)$
9: RS=$rg.findRecords(e, (t_s, t_e))$
10: **for** each $record \in RS$ **do**
11: $PQ.enqueue(record, sum_{dist}((P), record))$
12: **end for**
13: $CellSet$=$getNeighborCells(e.center)$
14: **for** each $cell \in CellSet$ **do**
15: $PQ.enqueue(cell, sum_{MINDIST}((x_q, y_q), cell))$
16: **end for**
17: **else if** e is typeof record **then**
18: $Qlist \leftarrow e$
19: **if** $Qlist.size()=k$ **then**
20: **return** $Qlist$
21: **end if**
22: **end if**
23: **end while**

6 Optimizations

In this section, we propose two methods for raising performance of STEHIX from the aspects of load balancing and query optimization.

6.1 Adaptive Load Balancing

For achieving design rule 3), adaptive load balancing is considered. Our spatial partition procedure contains two phases, first is Hilbert curve, and the second is quad-tree. And load balancing is based on the second phase and region split, in particular, when the volume of a region exceeds a limit due to the hotspot in spatial dimension, the procedure detects which Hilbert cell is the hotspot, and uses a quad-tree to divide it into four subspaces, thus the original region is split into five regions, i.e., four corresponds to the four subspaces and one corresponds to the undivided Hilbert cell(s). After that, the meta table is also updated to renew the mapping information as well as the *region index*. Figure 6 shows an example of region split. We can see when a hotspot is generated in Hilbert cell 0, the cell is divided into four subspaces by quad-tree, and the corresponding region is split into five, namely, 0-00, 0-01, 0-10, 0-11 and 1, and the meta table and new regions are updated accordingly.

6.2 Optimization for kNN Query

From kNN algorithm we can see, each time for retrieving the records of a Hilbert cell, the meta table must be searched to locate the corresponding region, which would increase overhead of the query. To deal with such a problem, we add modifications to *region index*, in particular, each *region index ri* is connected to the regions whose Hilbert cells are the neighbors of *ri*'s

region's Hilbert cells. Thus, when *getNeighborCells*() method is invoked, the current region is able to retrieve records from proximity regions, however, not all the records can be retrieved, and for this case, the meta table should be searched. Nevertheless, this optimization would reduce the overhead of querying the meta table.

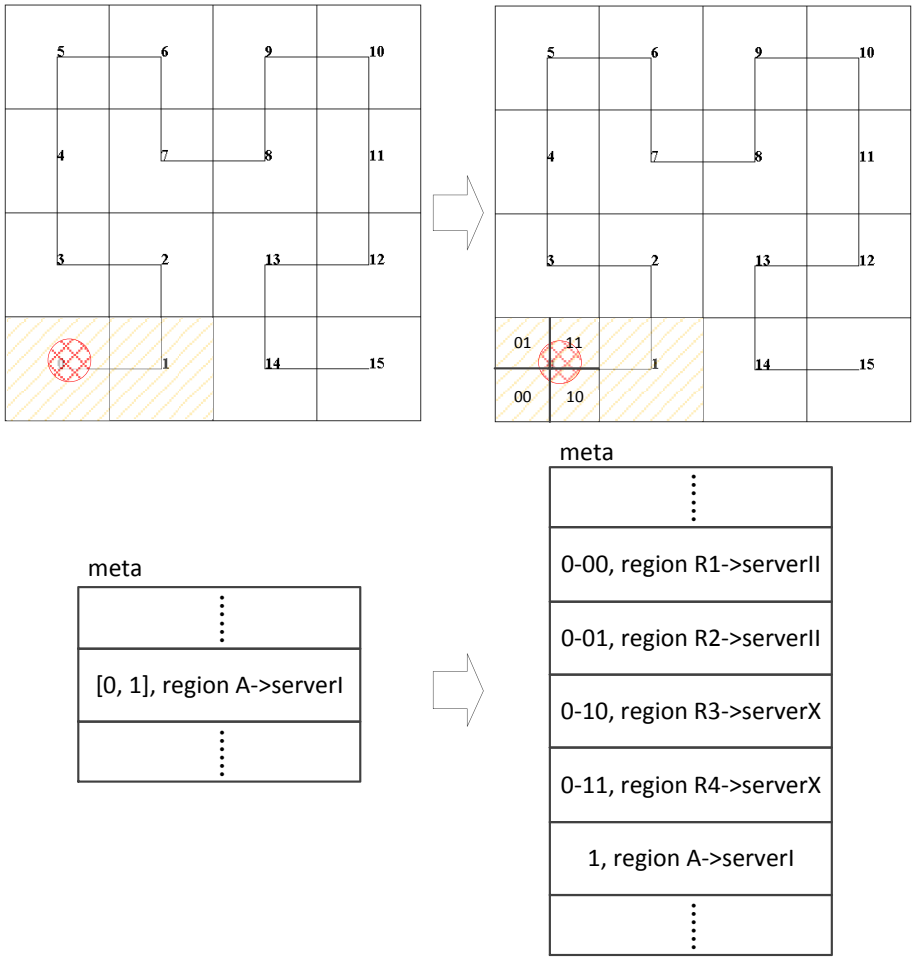

Figure 6: Load Balancing

7 Experimental Evaluation

We evaluate our algorithms on real dataset, which contains trajectories of taxis in Beijing[1]. In particular, the dataset contains about 100 million records, and temporal range is from Nov. 1st to 3rd, and each record in the dataset contains vehicle ID, geo-location, recording time stamp, etc.

Our algorithms are implemented in Hadoop 2.5.1 and HBase 0.98.6, and run on a cluster with size varied from 5 to 33, in which each node is equipped with Intel(R) Core(TM) i3 CPU @ 3.40GHz, 4GB main memory (for *Master* 16GB), and 500GB storage, and operating system is CentOS release 6.5 64bit, and network bandwidth is 10Mbps. For comparison, we choose MD-HBase due to the similar function.

[1]http://activity.datatang.com/20130830/description

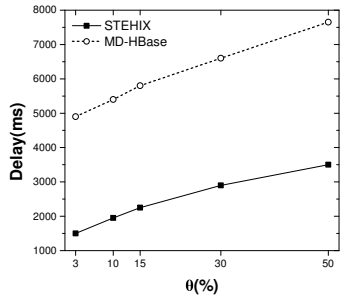

(a) Effect of selectivity

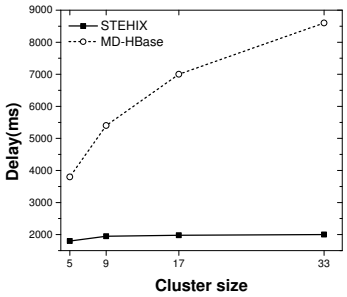

(b) Effect of cluster size

Figure 7: Experimental Results for Range Queries

7.1 Range Queries

First, we evaluate the algorithm for range queries. And we introduce two parameters to test the algorithm under various conditions. One is selectivity θ defined as:

$$\theta = \frac{L_{(t_s,t_e)}}{L_t} \cdot \frac{A_{R_q}}{A_{\mathbb{S}}}$$

where $L_{(t_s,t_e)}$ means the length of query temporal range (t_s, t_e), L_t means the length of temporal extent of the dataset, A_{R_q} means the area of query spatial range R_q, and $A_{\mathbb{S}}$ means the area of the whole space. Selectivity specifies the size of the query range, and the larger θ is, the more spatio-temporal records are involved. In this experiment, the default values of θ and cluster size are 10% and 9, respectively. For each value of θ or size, we issue 10 queries with different temporal ranges and spatial ranges, and collect the average response time as the measurement of performance.

First, we vary θ from 3% to 50% and Figure 7(a) shows the results. We can see that response time increases with θ for both methods. This is because a larger selectivity would access more records to be retrieved and examined, which increases the processing time. However, we can see STEHIX outperforms MD-HBase, which can be explained by the design of *region index*. Although MD-HBase builds index in the meta table, it doesn't index inner structure of regions, thus, scan operations are carried out to find results, which cost heavily. Our STEHIX is adapted to the two-level architecture of HBase, and is able to use *region index* to efficiently search each region, which highly improve performances.

Next, we vary cluster size from 5 to 33, and Figure 7(b) shows the results. It is apparent that STEHIX is excellent due to its nearly horizontal response time and good scalability. When the number of cluster size is increased, more *RegionServer*s take part in the processing and use their *region index*es parallel. However, due to lack of indexing *StoreFile*s, the scalability of MD-HBase is not good.

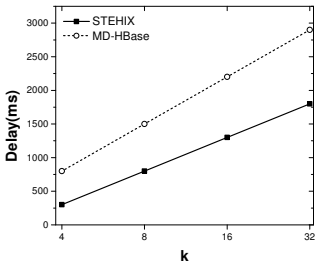

(a) Effect of k

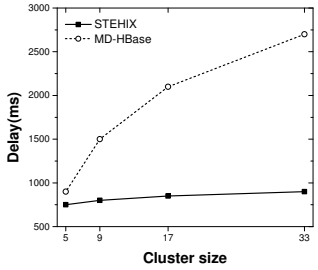

(b) Effect of cluster size

Figure 8: Experimental Results for kNN Queries

7.2 kNN Queries

In this experiment, the default values of k and cluster size are 8 and 9, respectively. First, we vary k from 4 to 32, and Figure 8(a) shows that STEHIX outperforms MD-HBase. When k is increased, both methods need more time to process queries. STEHIX uses less time to retrieve k results, which can be explained by the same reason, i.e., the *region index* embedded in HBase region. And then cluster size is varied from 5 to 33, still, STEHIX is better than MD-HBase, Figure 8(b) shows the fact.

7.3 GNN Queries

In this experiment, we vary the size of location set P and cluster to measure performance of STEHIX. Note that MD-HBase does not study GNN query, so we just simply use our virtual centroid method to apply to it. We vary n (size of P) from 3 to 9, and Figure 9(a) shows the results. We can see with increasing of n, the response time is also increased, this is because a larger size of P would cause more time to calculate the virtual centroid, however, we can the delay time does not increase very steeply, due to the fact that computing the virtual centroid only cost CPU time. Similarly, our STEHIX still outperforms MD-HBase in both varying n and cluster size.

7.4 Effect of Optimizations

We examine the effect of optimizations to STEHIX in this experiment, and Figure 10 show the results. First, we use maximum imbalance load ratio [17] as metric, and test our adaptive load balancing policy, the results of comparison with non-load balancing are plotted in Figure 10 (a). We can see with cluster size increased, both ratios are raised, this is because the more nodes participate in the cluster, the more difficult is to distribute load uniformly, however, we can see our load balancing method indeed takes effect, i.e., when load balancing policy is used, the ratio is averagely around 6, while the counterpart shows the performance about 38 to 70. Next, we test the effect of kNN optimization, from Figure 10 (b), we can see the connections among *region index*es give chances to reduce querying overhead.

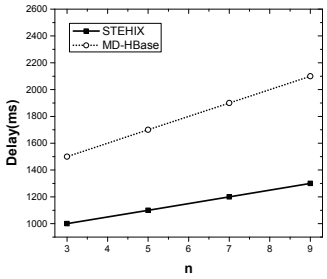

(a) Effect of size of P

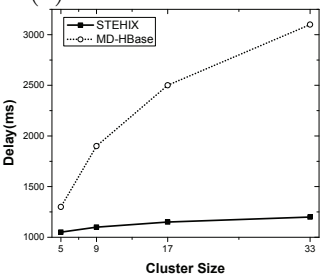

(b) Effect of cluster size

Figure 9: Experimental Results for GNN Queries

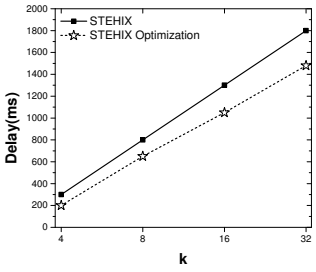

(a) Effect of k

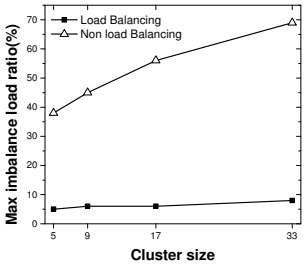

(b) Effect of cluster size

Figure 10: Experimental Results for Optimizations

8 Conclusion and Future Works

With development of positioning technology, more and more spatio-temporal data need to be processed. To equip HBase with efficient and scalable spatio-temporal querying capability will benefit the whole spatio-temporal decision support system. In this paper, we argue that many previous works fail to tackle this problem due to lack of deep design for HBase, while we address the problem by proposing a novel index structure adapted to two-level architecture of HBase, which is suitable for HBase to process queries. Algorithms for range query, kNN query and GNN query are designed, what's more, the optimizations for load balancing and kNN query are also proposed. We carry out extensive experimental studies for verifying our index, and the results show that our approach for HBase is more efficient and scalable than the previous work.

In the future, we plan to utilize this idea to efficiently store and retrieve graph data and apply to social networks.

Acknowledgment

This work is supported by NSF of China grant 61303062 and 71331008. We would like to thank Peijun He for helping with the implementation.

Bibliography

[1] Van Orshoven et al. (2011), Upgrading geographic information systems to spatio-temporal decision support systems, *Mathematical and Computational Forestry & Natural Resource Sciences*, 3(1): 36-41.

[2] Wiki, H. HBase: bigtable-like structured storage for Hadoop HDFS. 2012-02-23)[2012-04-17]. http://wiki. apache, org/hadoop/Hbase.

[3] Ralph Kimball, Margy Ross (1996), *The data warehouse toolkit*, Wiley.

[4] Ralph Kimball, Margy Ross (2012), *The Data Warehouse Toolkit: The Complete Guide to Dimensional Modeling*, 2nd Edition, Wiley.

[5] Nishimura, S., Das, S., Agrawal, D., Abbadi, A. E. (2011, June). MD-HBase: A scalable multi-dimensional data infrastructure for location aware services. *In Mobile Data Management (MDM), 2011 12th IEEE International Conference on*, 1: 7-16.

[6] Hsu, Y. T., Pan, Y. C., Wei, L. Y., Peng, W. C., Lee, W. C. (2012), Key formulation schemes for spatial index in cloud data managements. *In Mobile Data Management (MDM), 2012 IEEE 13th International Conference on*, 21-26.

[7] Zhou, X., Zhang, X., Wang, Y., Li, R., Wang, S. (2013), Efficient distributed multi-dimensional index for big data management. *In Web-Age Information Management*, Springer Berlin Heidelberg, 130-141.

[8] Han, D., & Stroulia, E. (2013), Hgrid: A data model for large geospatial data sets in hbase. *In Cloud Computing (CLOUD), 2013 IEEE Sixth International Conference on*, 910-917.

[9] Zhang, N., Zheng, G., Chen, H., Chen, J., Chen, X. (2014). Hbasespatial: A scalable spatial data storage based on hbase. *In Trust, Security and Privacy in Computing and Communications (TrustCom), 2014 IEEE 13th International Conference on*, 644-651.

[10] Du, N., Zhan, J., Zhao, M., Xiao, D., & Xie, Y. (2015), Spatio-Temporal Data Index Model of Moving Objects on Fixed Networks Using HBase, *In Computational Intelligence & Communication Technology (CICT), 2015 IEEE International Conference on*, 247-251.

[11] HBase, A. (2012), Apache hbase reference guide. Webpage available at http://wiki. apache. org/hadoop/Hbase/HbaseArchitecture. Webpage visited, 04-04.

[12] George, L. (2011). HBase: the definitive guide, O'Reilly Media, Inc.

[13] Faloutsos, C., Roseman, S. (1989), Fractals for secondary key retrieval, *Proceedings of the eighth ACM SIGACT-SIGMOD-SIGART symposium on Principles of database systems*, 247-252.

[14] Wang, J., Wu, S., Gao, H., Li, J., Ooi, B. C. (2010), Indexing multi-dimensional data in a cloud system. *Proceedings of the 2010 ACM SIGMOD International Conference on Management of data*, 591-602.

[15] Hjaltason, G. R., Samet, H. (1999), Distance browsing in spatial databases, *ACM Transactions on Database Systems (TODS)*, 24(2): 265-318.

[16] Roussopoulos, N., Kelley, S., Vincent, F. (1995). Nearest neighbor queries. *In ACM sigmod record*, 24(2):71-79.

[17] Vu, Q. H., Ooi, B. C., Rinard, M., Tan, K. L. (2009), Histogram-based global load balancing in structured peer-to-peer systems, *Knowledge and Data Engineering, IEEE Transactions on*, 21(4): 595-608.

[18] Hochreiter, S., Younger, A. S., Conwell, P. R. (2001), Learning to Learn Using Gradient Descent. *Artificial Neural Networks-ICANN 2001*, Springer Berlin Heidelberg.

INTERNATIONAL JOURNAL OF COMPUTERS COMMUNICATIONS & CONTROL
ISSN 1841-9836, 11(5):631-644, October 2016.

Extended Collaborative Filtering Technique for Mitigating the Sparsity Problem

K. Choi, Y. Suh, D. Yoo

Keunho Choi
Korea Workers' Compensation and Welfare Service
8, Beodeunaru-ro 2-gil, Yeongdeungpo-gu, Seoul, Republic of Korea
ckh0515@hanmail.net

Yongmoo Suh
Korea University Business School
Anam-Ro 145, Seongbuk-Gu, Seoul, Republic of Korea
ymsuh@korea.ac.kr

Donghee Yoo*
Department of Management Information Systems, Gyeongsang National University, BERI
501 Jinju-daero, Jinju, Republic of Korea
*Corresponding author: dhyoo@gnu.ac.kr

Abstract: Many online shopping malls have implemented personalized recommendation systems to improve customer retention in the age of high competition and information overload. Sellers make use of these recommendation systems to survive high competition and buyers utilize them to find proper product information for their own needs. However, transaction data of most online shopping malls prevent us from using collaborative filtering (CF) technique to recommend products, for the following two reasons: 1) explicit rating information is rarely available in the transaction data; 2) the sparsity problem usually occurs in the data, which makes it difficult to identify reliable neighbors, resulting in less effective recommendations. Therefore, this paper first suggests a means to derive implicit rating information from the transaction data of an online shopping mall and then proposes a new user similarity function to mitigate the sparsity problem. The new user similarity function computes the user similarity of two users if they rated similar items, while the user similarity function of traditional CF technique computes it only if they rated common items. Results from several experiments using an online shopping mall dataset in Korea demonstrate that our approach significantly outperforms the traditional CF technique.
Keywords: recommendation system, collaborative filtering, sparsity problem, similarity function.

1 Introduction

In the age of information overload, information about products and services on the Internet is growing explosively; consequently, people have difficulty in processing the overwhelming amount of information that is available. To address this problem, a number of personalized recommendation techniques have been introduced by many studies, so that sellers of online shopping malls can survive high competition and buyers can locate the best product information for their own needs [1–3]. Personalized recommendations are usually seen as a specific kind of information filtering that enables people to filter out unnecessary and uninteresting information [4]. Among the many recommendation techniques that have been suggested, collaborative filtering (CF) has been widely adopted in many practical applications due to its simplicity and effectiveness and has proven to be useful [2].

However, it is still not easy for most online shopping malls to make use of the collaborative filtering technique for recommendation, because explicit rating information required by the technique is rarely available in online shopping malls and/or because there is a high chance of sparsity in the transaction data of online shopping malls. Thus, there is a need to devise a way to derive implicit rating information that can play the role of explicit rating information and extend the collaborative filtering technique so that it can be used effectively even when there is a sparsity problem in the transaction data of online shopping malls.

It is known that personalized recommendation and improved customer retention forms a virtuous cycle in which good quality of recommendation leads to improved customer retention which in turn leads to the better quality of recommendation through more customer input into the recommendation system [2]. As such, the recommendation system that we propose in this paper will contribute to the higher level of customer retention of online shopping malls, which will help them to survive today's high competition.

In this paper, therefore, we first suggest a means to derive implicit rating information from the transaction data available on an online shopping mall. We assumed that the number of purchasing the same item represents the preference toward the item and thus can be used as implicit rating information on the item. Then we propose a new user similarity function that can mitigate the sparsity problem. The traditional collaborative filtering technique calculates the user similarity of two users only when they have rated common items. In that case, we come across bad recommendation quality due to the sparsity problem. Instead, our new user similarity function computes user similarity if they rated similar items which include common items. So, we define an item similarity function as a function that computes the item similarity of all pairs of items purchased by two users whose similarity is to be computed and use the item similarity to define the user similarity function.

We have implemented both a recommendation system which uses the extended collaborative filtering technique with our new user similarity function and a benchmark system which adopts the traditional collaborative filtering technique. Results from a series of experiments using the transaction data of an online shopping mall in Korea clearly demonstrate that our approach significantly improves the quality of recommendation systems, compared with those obtained from a benchmark system.

The rest of this paper is organized as follows. Section 2 reviews the previous studies on recommendation systems, especially those which have attempted to solve the sparsity problem of the collaborative filtering technique. Section 3 describes our proposed similarity function in detail, and Section 4 provides the details of the several experiments conducted to verify our approach and the results from those experiments. The last section concludes our paper with summary, implications, and limitations.

2 Previous works

This section reviews general recommendation techniques with a focus on the collaborative filtering technique related to our study.

2.1 General recommendation techniques

The techniques used in most recent recommendation systems can generally be classified into one of the following four types: *Content-based filtering* (CBF); *Collaborative filtering* (CF); *Rule-based approach*; *Hybrid approach*.

CBF typically 1) constructs a content-based *item profile* by extracting a set of features from each item in the item set; 2) builds a content-based *user profile* from a set of features of the

items that each user purchased; 3) calculates the similarity between the user profiles and the item profiles; and 4) recommends the top n items with the highest similarity scores. In other words, CBF mainly recommends items based on the similarity between items to recommend and items already purchased [5, 6]. However, CBF has several limitations: 1) it is not easy to obtain a sufficient number of features for item profiles and user profiles (*insufficient features problem*) [7]; 2) items that can be recommended are limited to those similar to the items that a target user previously purchased (*over-specialization problem*) [8]; and 3) new users who have not yet purchased items cannot get appropriate recommendations (*new user problem*) [9].

CF typically 1) builds a rating-based user profile from the rating information of each user on items; 2) identifies neighbors (also called like-minded users) who rated items similarly as the target user; 3) predicts ratings of the target user on target items purchased not by the target user, but by the neighbors; and 4) recommends the top n items with the highest predicted ratings. However, CF also has some limitations: 1) it is difficult to recommend items for users who have not yet rated items (*new user problem*) [10, 11]; 2) it is difficult to recommend items that have never been rated by users before (*new item problem*) [5, 12]; and 3) it makes poor recommendations when rating information is insufficient (*sparsity problem*) [4, 13].

Rule-based approach typically derives rules among items in the item set from a large transaction dataset collected over time, using data mining techniques. The rules could be either *association rules* among items purchased together [14] or *sequential patterns* among items purchased in sequence over time [15, 16]. However, the rule-based approach to recommending items has limitations in that it is difficult to recommend items that do not appear in association rules or sequential patterns; moreover, it does not take into account users' preference (or rating information) on items.

Hybrid approach has been developed to overcome – or at least reduce – the weaknesses of CBF, CF, and the rule-based approach [4, 5]. In general, the hybrid approach makes recommendations by combining results from each recommendation technique, selecting one of recommendation techniques to be applied according to specific criteria, or embedding one or more recommendation techniques in applying other recommendation techniques.

2.2 Collaborative filtering

Thus far, many recommendation systems using the CF technique have been developed and used in many practical applications, such as Tapestry for recommending news articles [17], GroupLens for net news [18], and Ringo for music [7]. The CF technique utilizes users' rating information on items to represent their preference on corresponding items and predicts a target user's ratings of items based on the user's similarity in ratings [19, 20].

The CF technique can be further classified into *model-based* and *memory-based* CF techniques. In the model-based CF technique, a model such as a probabilistic model or a machine learning model is built from a large collection of ratings in order to predict a target user's ratings on target items [21–23]. Koren [23] suggested the new neighbor model, in which neighbor relations were modeled by minimizing the regularized squared error function. In addition, he extended the model to utilize both explicit (i.e., rating information) and implicit feedback (i.e., binary information [rated vs. not rated]) from users. Salakhutdinov and Srebro [24] introduced a weighted version of trace-norm regularization. The trace-norm regularization is a popular method for completing the user-item rating matrix in CF. However, the method does not perform well when entries of the user-item rating matrix are sampled non-uniformly. In order to solve the problem, they proposed a trace-norm weighted by the frequency of users and items as a regularizer.

In the memory-based CF technique, items are recommended mainly based on the similarity

between users as described in Section 2.1 [25,26]. Balabanovic and Shoham [5] developed the Fab system, which combines CF with CBF to improve the accuracy of recommendation systems by mitigating new item, insufficient features, and over-specialization problems inherent to CF and CBF. In the Fab system, items are recommended to a target user if and only if each item is highly similar to the target user's profile and each item is rated by the neighbors of the target user. Yang et al. [27] attempted to propose a new similarity function to be used in CF techniques in order to deal with the weaknesses of CF technique, namely, 1) CF is sometimes overly confident, 2) CF tends to discard some useful information in user profiles, and 3) CF often derives some untrustworthy inferences when making a prediction. To this end, they took into account the similarity between a target item and each of the co-rated items in order to determine whether the two items belong to the same genre of interest or not. In addition, they calculated the similarity between two users by giving different weights to the co-rated items classified into three classes according to the differences between the ratings of the two users on the items.

In order to alleviate the sparsity problem, Liu et al. [28] proposed a hybrid recommendation system. They first filled a blank in the user-item rating matrix with a weighted average rating of items already rated by the user, where the weights of the rated items were calculated by the similarity between an unrated item and the rated items based on feature values. CF is then applied to the user-item rating matrix. Our approach is different from their approach in that our approach uses only users' ratings on items to mitigate the sparsity problem, whereas their approach needs additional information about features of items, which may cause additional problems (e.g., insufficient features), thereby reducing the application area. Shambour and Lu [13] proposed a hybrid trust-enhanced CF recommendation approach (TeCF), which integrates both an implicit trust-filtering recommendation approach and an enhanced user-based CF recommendation approach. By incorporating trust propagation, they attempted to relax the sparsity problem. Although this approach can extend the number of potential neighbors, the reliability of the similarity between potential neighbors still needs to be improved. Our study focuses primarily on improving the reliability of the similarity between users in order to mitigate the sparsity problem in a memory-based CF. Formoso et al. [10] proposed an approach called *profile expansion* based on the query expansion techniques used in information retrieval to mitigate the new user problem which can cause the sparsity problem. In their study, the size of a user's original profile increased by adding a set of item-rating pairs to the profile based on item-global, item-local, or user-global profile expansion technique. Item-global profile expansion technique finds items similar to the items already exist in the user profile and adds the found items to the user profile, while item-local profile expansion technique finds items to be added to the user profile based on the items recommended to the user. User-local profile expansion technique finds the user's neighbors and adds items rated by them to the user profile. The difference between their approach and our approach is that they calculate a user similarity between two users based on the expanded user profile, while we compute the user similarity by taking into account item similarity of all pairs of items rated by these users without expanding the user profile.

3 Proposed approach

This section provides the explanation on the notations used in the equations that define a new similarity function and explains how we extended ratings on only commonly rated items to ratings on all pairs of items to mitigate the sparsity problem using the new user similarity function.

Table 1: Notations

Notations	Descriptions
U	The number of total users
I	The number of total items
$AP(A,i)$	Absolute preference of user A on item i
$RP(A,i)$	Relative preference of user A on item i
$R_{A,i}$	Rating of user A on item i
m	The number of items commonly rated by both users
U_{ij}	The number of users who rated both items i and j
$Cosine(A,B)$	Cosine similarity between users A and B
$P_{A,i}^{Predicted}$	The predicted preference of target user A on target item i
$ISIM(i,j)$	The similarity between items i and j
$USIM(A,B)$	The similarity between users A and B
k	The number of neighbors selected
n	The number of items recommended

3.1 Notations

Table 1 shows the description of notations used in the equations that define a new user similarity function. However, the equations will be provided in Section 3.2, Section 3.3, and Section 3.4 again with explanation on each notation for the better readability of the paper.

3.2 Deriving implicit ratings of users on items

In many online shopping malls, it is usually difficult to obtain explicit rating information on items. In order to apply the CF technique to such circumstance, this study derived implicit ratings of users on items from transaction data as an alternative to explicit ratings.

First, the absolute preference of user A on item i, $AP(A,i)$, is calculated from following equation.

$$AP(A,i) = \ln\left(\frac{\text{The number of transactions of user } A \text{ including item } i}{\text{The number of transactions of user } A} + 1\right) \quad (1)$$

Since it only takes into account the frequency of purchase, the absolute preference of user A on item i increases as the number of transactions of user A including that item increases. This value, however, may not represent the preference of user A on item i exactly because the frequency of purchase is quite different depending on the item price, item lifetime, and so on. For instance, since expensive items or items with long lifespan are usually purchased infrequently, the preferences of users on them cannot be higher than those on cheap items or on items with short lifespan. Thus, it is necessary to define relative preference which is comparable among items using the absolute preferences of other users on item i. The relative preference of user A on item i, $RP(A,i)$ is thus defined as in equation (2).

$$RP(A,i) = \frac{AP(A,i)}{\text{Max.}AP(u,i)} \quad (2)$$

, where u denotes every user who purchased item i. The reason for using Max function as a denominator in equation (2) is to make $RP(A,i)$ range from 0.0 to 1.0 (i.e., normalization).

Finally, $RP(A,i)$ is multiplied by 5 and rounded up so that *implicit rating* ranges from 1 to 5, as is mostly used in current recommendation systems, which is explained by equation (3).

Table 2: Example of user-item implicit rating matrix

User	Item 1	Item 2	Item 3	Item 4	Item 5
A	-	4	2	3	-
B	3	-	4	-	5
C	2	2	-	3	-
D	-	3	-	3	3
E	5	-	-	3	2

$$Implicit\ rating\,(A,i) = Round\ up\ \ (5\ \times\ \ RP\,(A,i)) \tag{3}$$

3.3 New user similarity function for mitigating the sparsity problem

With the implicit ratings of users on items derived in Section 3.2, the similarity between a target user and every other user is calculated. As mentioned earlier, traditional CF-based recommendation systems have calculated the similarity between two users from the rating information of co-rated items by both users, as shown in equation (4). The similarity function defined in equation (4) is *cosine similarity* which is one of widely used similarity functions in CF.

$$Cosine\,(A,B) = \frac{\sum_{i=1}^{m}(R_{A,i})\,(R_{B,i})}{\sqrt{\sum_{i=1}^{m}(R_{A,i})^2}\sqrt{\sum_{i=1}^{m}(R_{B,i})^2}} \tag{4}$$

, where $R_{A,i}$ and $R_{B,i}$ denote the ratings of users A and B on item i, respectively and m denotes the number of items commonly rated by both users. For example, in traditional CF approach, the similarity between users A and B is calculated from the rating information of item 3 which is commonly rated by both users (see Table 2). However, this may result in untrustworthy inference in calculating the similarity between them since insufficient rating information (i.e., rating information of users A and B only on item 3) is used to calculate the similarity, which is known as the *sparsity problem*. In addition, some potentially useful information (i.e., rating information of user A on items 2 and 4, and those of B on items 1 and 5) may be discarded in traditional CF approach.

In order to mitigate the above problems, this paper adapted the cosine similarity as equation (5) by assuming that two items i and j can be regarded as *commonly rated* by two users A and B if they are similar to each other and rated by user A or user B. Using the equation (5), we can calculate the user similarity between users A and B based on the item similarity, computed by considering rating information of all pairs of *commonly rated items* (i.e., $N_{I_A} \times N_{I_B}$, where N_{I_A} and N_{I_B} denote the number of items rated by users A and B, respectively). In the example of table 2, item similarity is defined to include all pairs of *commonly rated items* by users A and B when the user similarity between users A and B is to be computed (i.e., nine item pairs: (item 2, item 1), (item 2, item 3), (item 2, item 5), (item 3, item 1), (item 3, item 3), (item 3, item 5), (item 4, item 1), (item 4, item 3), and (item 4, item 5)). Our approach, therefore, improves the reliability of the similarity between two users by utilizing rating information of all similar item pairs, thereby mitigating the sparsity problem caused by insufficient rating information. User similarity between two users A and B is defined as follows:

$$USIM\,(A,B) = \frac{\sum_{i\in I_A}\sum_{j\in I_B}\left\{ISIM\,(i,j)^2 \times (R_{A,i}) \times (R_{B,j})\right\}}{\sqrt{\sum_{i\in I_A}\sum_{j\in I_B}\left\{ISIM\,(i,j) \times (R_{A,i})\right\}^2} \times \sqrt{\sum_{i\in I_A}\sum_{j\in I_B}\left\{ISIM\,(i,j) \times (R_{B,j})\right\}^2}} \tag{5}$$

, where I_A and I_B denote a set of items rated by user A and user B, respectively, and $ISIM(i, j)$, the similarity between item i and item j, is calculated similarly to $USIM(A, B)$[1], using the cosine similarity (i.e., equation (4)), as defined in equation (6).

$$ISIM(i,j) = \frac{\sum_{A=1}^{U_{ij}} (R_{A,i}) \times (R_{A,j})}{\sqrt{\sum_{A=1}^{U_{ij}} (R_{A,i})^2} \times \sqrt{\sum_{A=1}^{U_{ij}} (R_{A,j})^2}} \tag{6}$$

, where U_{ij} denotes the number of users who rated both items i and j.

3.4 Predicting preference of a target user on target items

After calculating the user similarity between a target user and every other user, the top k users with the highest similarity are selected as neighbors of the target user. Then, rating information of the neighbors is used to predict the preference of the target user on target items, as shown in equation (7).

$$P_{A,i}^{Predicted} = \frac{1}{\sum_{B=1}^{k} |USIM(A,B)|} \times \sum_{B=1}^{k} USIM(A,B) \times R_{B,i} \tag{7}$$

, where $P_{A,i}^{Predicted}$ denotes the predicted preference of target user A on item i, k the number of user A's neighbors, and $USIM(A,B)$ the similarity between the target user A and A's neighbor user B calculated using equation (5).

Finally, the top n items with the highest preference are recommended for the target user, where items already purchased by the target user may be included in recommendation list since this study assumes that users may repurchase the same item, differently from usual recommendation systems.

4 Experiments

This section describes the experimental design for evaluating the effect of our ideas proposed in Section 3 on the accuracy of recommendation, and explains the implication of the results from the experiments.

4.1 Experimental design

The data used in our experiment were provided by one of the biggest online shopping malls in Korea from August 16, 2008 to August 15, 2009 (12 months), which consists of 15,860 transactions of 234 users on 1,097 items[2], and shows high sparsity rate of 98.59%[3]. Prior to conducting our experiments, we divided our dataset into four parts, as shown in Fig 1. Firstly, it was divided by time into Part A and B, and secondly by random sampling of users into Part C and D. Part A consists of transaction data collected during the first 6 months and Part B during the second 6 months. Part C consists of transaction data from 70% of the users, randomly chosen, and Part D the transaction data of the remaining users.

[1] $USIM(A, B)$ takes a value between 0 and 1.

[2] Since it is difficult to recommend items to users who have purchased a small number of transactions as in most recommendation systems (i.e., new user problem), this study focused on the users who are involved in more than 30 transactions among total 1,000 users.

[3] 3,626 distinct transactions among 256,698 ($= 234 \times 1,097$) possible transactions.

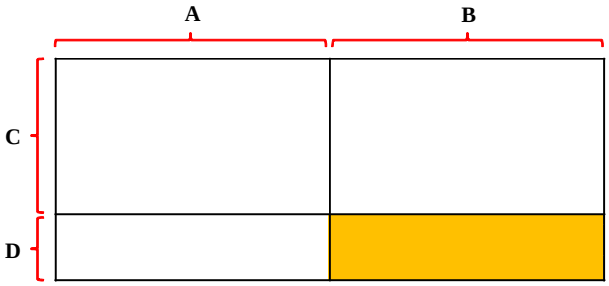

Figure 1: Four parts of our dataset

When making recommendations, we used Part A*(C+D) in order to calculate the similarity between each target user and every other user, and recommended items for the target users in Part B*D. In our experiment, as a means to measure the quality of recommendation, we also used precision, recall, and F1, as used elsewhere to evaluate and compare the quality of recommendations. F1 is the harmonic average of precision and recall.

In order to ensure that our proposed approach actually improves the quality of recommendation system, we implemented both our recommendation system and a benchmark system using Transact-SQL on Microsoft SQL Server 2008.

4.2 Experimental results and analysis

In order to compare our proposed recommendation system with the benchmark system (i.e., traditional CF approach which calculates the similarity between users using equation (4)), we conducted several experiments. In the first experiment, we evaluated the effects of both the number of recommendations and the number of neighbors on the accuracy of the benchmark system. As shown in Fig. 2 (a), when the number of neighbors was low (i.e., $k \leq 40$), the precision of benchmark system tends to increase as the number of recommendations increases. On the contrary, however, when the number of neighbors was high (i.e., $k \geq 60$), the precision of benchmark system tends to increase as the number of recommendations decreases. The best precision was achieved when the number of neighbors was 120 and the number of recommendations was 10. Generally, as shown in Fig. 2 (b) and (c), the recall and F1 of benchmark system tend to increase as the number of recommendations increases, regardless of the number of neighbors. However, as the number of neighbors increases, the effects of the number of recommendations on the recall and F1 of benchmark system decrease. The best recall was achieved when the number of neighbors was 10 and the number of recommendations was 50, and the best F1 when the number of neighbors was 40 and the number of recommendations was 50.

Similar experiment was conducted to evaluate the effects of both the number of recommendations and the number of neighbors on the accuracy of our proposed system. As shown in Fig. 3 (a), when the number of neighbors was low (i.e., $k \leq 20$), the precision of proposed system tends to increase as the number of recommendations decreases. In addition, when the number of neighbors was high (i.e., $k \geq 60$), the precision of proposed system also tends to increase as the number of recommendations decreases. The best precision was achieved when both the number of neighbors and the number of recommendations were 10. Generally, as shown in Fig. 3 (b) and (c), the recall and F1 of proposed system tend to increase as the number of recommendations increases, regardless of the number of neighbors. However, as the number of neighbors increases, the effects of the number of recommendations on the recall and F1 of proposed system decrease. The best recall was achieved when the number of neighbors was 10 and the number of recommendations was 50, and the F1 when the number of neighbors 10 and the number of recommendations was 30.

In the final experiment, we compared the best precision, recall, and F1 of benchmark system

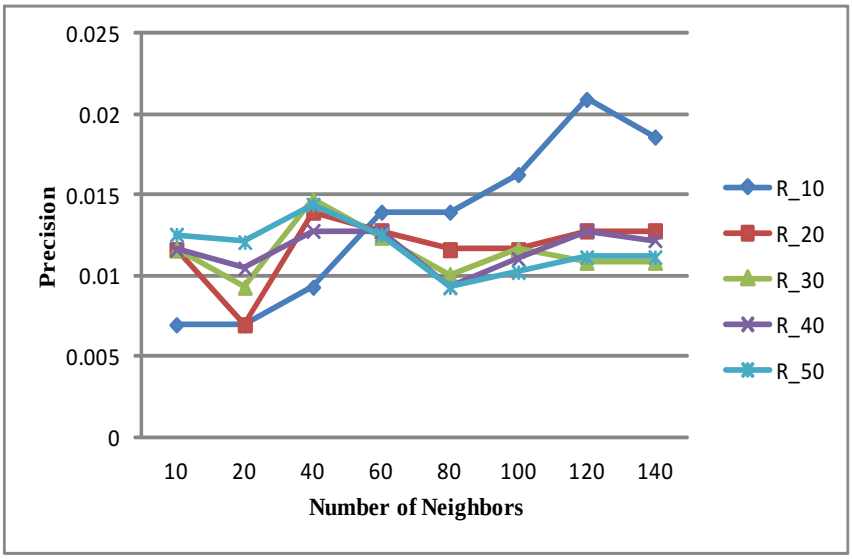

(a) Precision

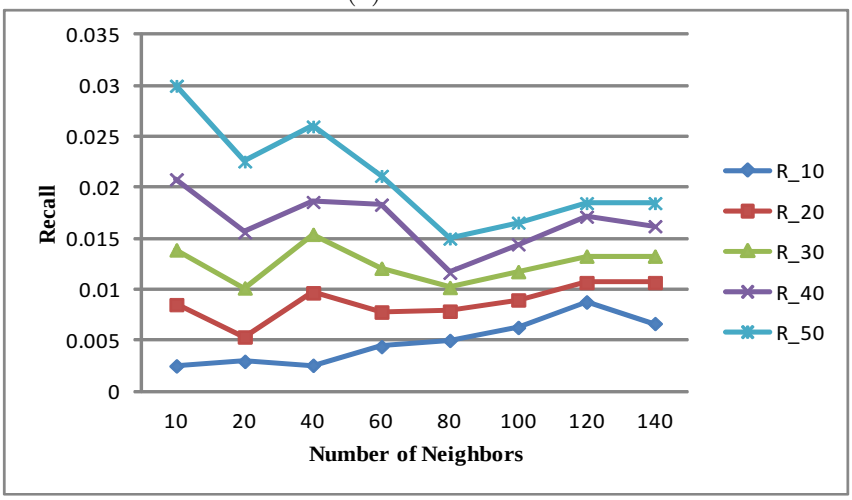

(b) Recall

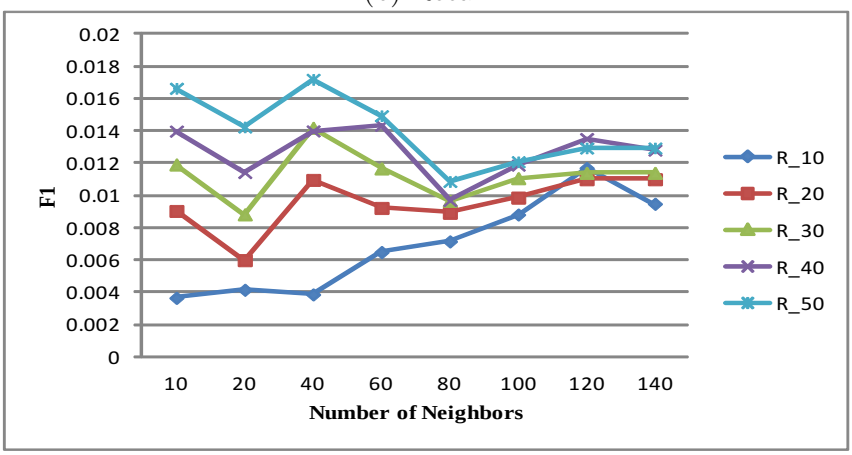

(c) F1

Figure 2: The effect of both the number of recommendations and the number of neighbors on the accuracy of benchmark system (N in R_N represents the number of recommendations)

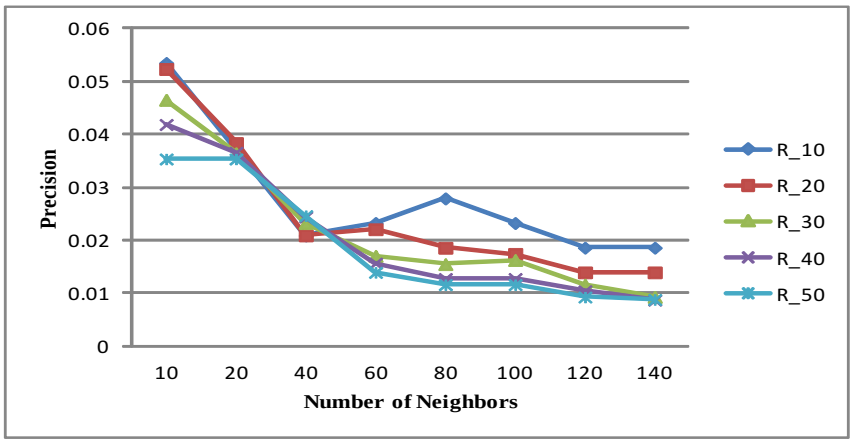

(a) Precision

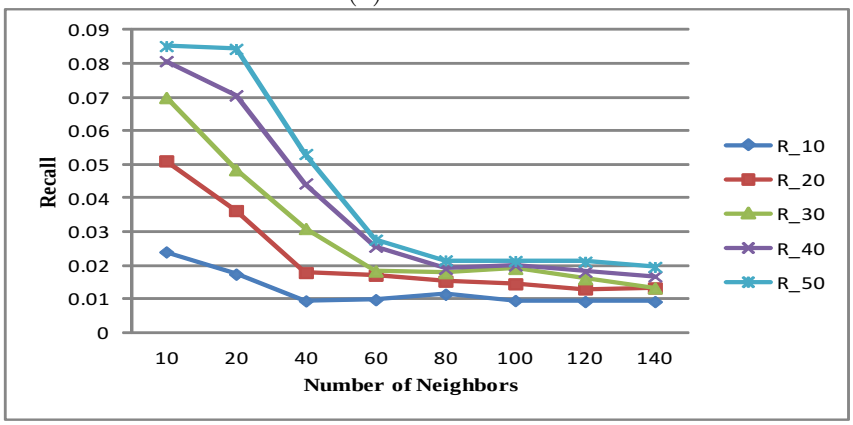

(b) Recall

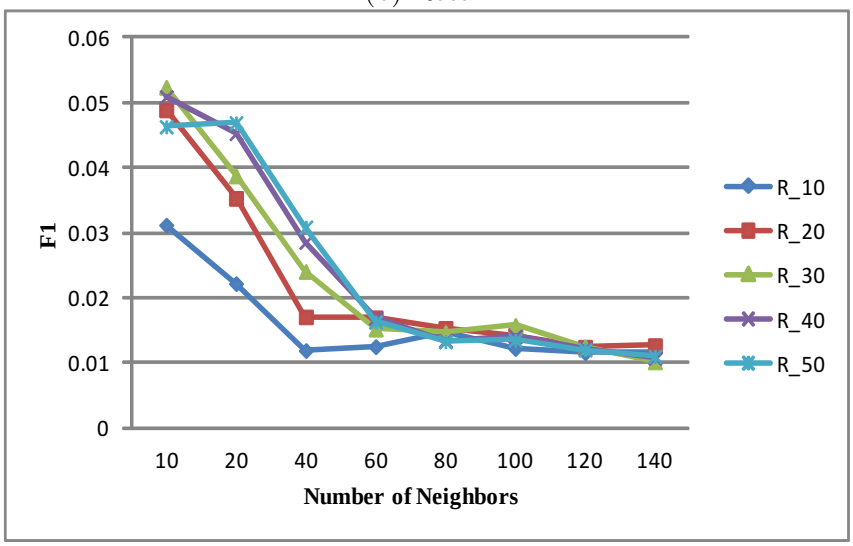

(c) F1

Figure 3: The effect of both the number of recommendations and the number of neighbors on the accuracy of proposed system

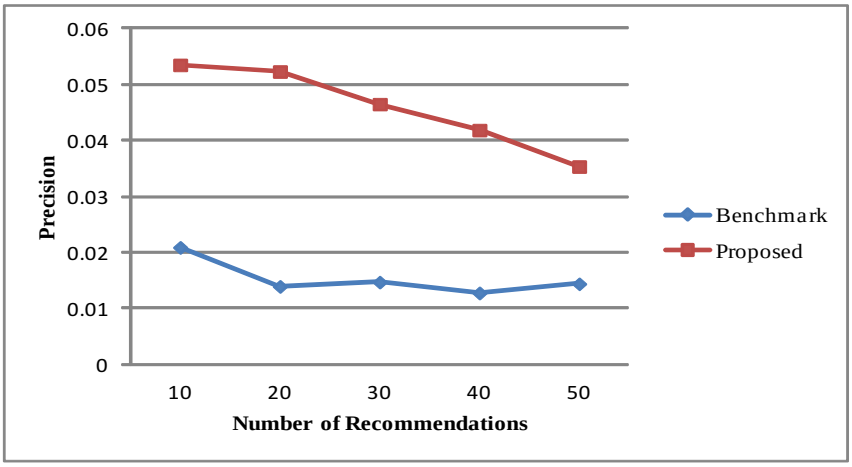

(a) Precision

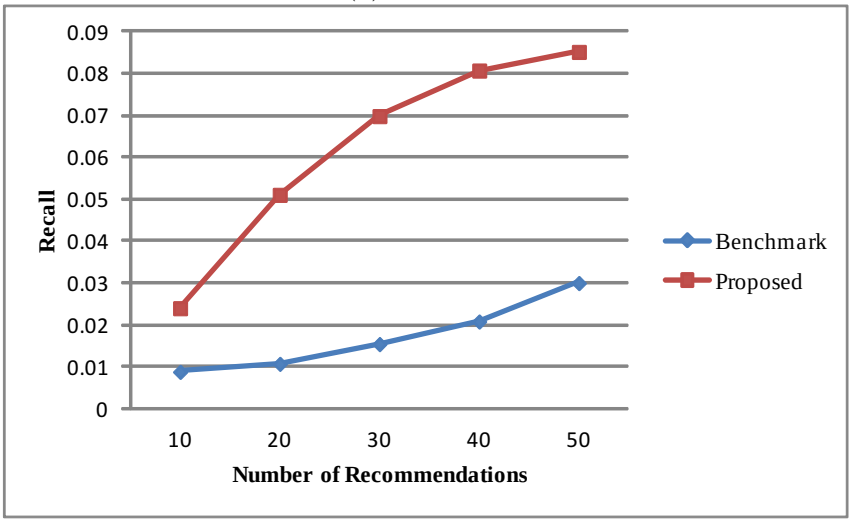

(b) Recall

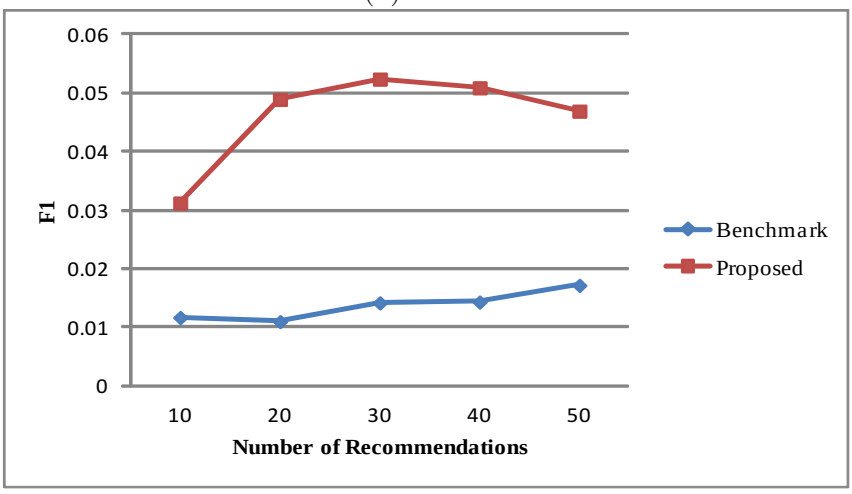

(c) F1

Figure 4: A comparison between the benchmark system and the proposed system

(i.e., precision at $k = 120$ ($n = 10$) and 40 ($n = 20$, 30, 40, and 50), recall at $k = 120$ ($n =$ 10 and 20), 40 ($n = 30$), and 10 ($n = 40$, 50), and F1 at $k =$120 ($n = 10$, 20), 40 ($n = 30$ and 50), and 60 ($n = 40$)) with those of our proposed system (i.e., precision at $k = 10$ ($n =$ 10, 20, 30, 40) and 20 ($n = 50$), recall at $k = 10$ ($n = 10$, 20, 30, 40, and 50), and F1 at k $= 10$ ($n = 10$, 20, 30, and 40) and 20 ($n = 50$)). As shown in Fig. 4 (a), (b), and (c), our proposed system considerably outperformed the benchmark system in precision, recall, and F1, regardless of the number of recommendations. The results from our experiments proved that our approach to extending collaborative filtering technique to consider all pairs of similar items when computing the user similarity is effective on mitigating the sparsity problem, thereby enhancing the accuracy of recommendation systems.

5 Conclusions

The collaborative filtering technique has been suggested as one of the best methods for making recommendations and has proven to be useful in many applications, but that technique is not easy to use for recommendations in online shopping malls, because explicit rating information is rarely available. In addition, one of the problems of the technique, the sparsity problem, occurs due to the low level of customer input into the recommendation system in online shopping malls. Therefore, online shopping malls which have to survive high competition must resolve these two problems to be able to make effective recommendations which in turn improve their customer retention rate.

With an objective to provide online shopping malls with a way to make better recommendations this paper first explains how to derive implicit rating information from the transaction data that will replace the explicit rating information. It then defines a new user similarity function which computes a user similarity between two users by taking into account item similarity of all pairs of similar items, rated by these users.

In order to compare our proposed recommendation system with a traditional recommendation system, we implemented both systems and conducted several experiments. The results obtained from these experiments indicate that our approach considerably outperformed the traditional collaborative filtering approach in precision, recall, and F1. This study, however, leaves something to be desired. More reliable and interesting results could be obtained if we have used bigger datasets from more than one online shopping mall over a longer period of time.

Bibliography

[1] M. Pazzani, D. Billsus (1997); Learning and Revising User Profile: The Identification of Interesting Web Sites, *Machine Learning*, 27(3): 313-331.

[2] T. Zhang, R. Agarwal, H.C. Lucas (2011); The Value of IT-Enabled Retailer Learning: Personalized Product Recommendations and Customer Store Loyalty in Electronic Markets, *MIS Quarterly*, 35(4): 859-881.

[3] Y. Jing, H. Liu (2013); A Model for Collaborative Filtering Recommendation in E-Commerce Environment, *International Journal of Computers Communications and Control*, 8(4): 560-570.

[4] D.R. Liu, C.H. Lai, W.J. Lee (2009); A Hybrid of Sequential Rules and Collaborative Filtering for Product Recommendation, *Information Sciences*, 179(20): 3505-3519.

[5] M. Balabanovic, Y. Shoham (1998); Content-Based, Collaborative Recommendation, *Communications of the ACM*, 40(3): 66-72.

[6] K. Lang (1995); NewsWeeder: Learning to Filter Netnews, *Pro. of the 12th Int. Conference on Machine Learning.*

[7] U. Shardanand, P. Maes (1995); Social Information Filtering Algorithms for Automating "Word of Mouth", *Pro. of the SIGCHI Conference on Human Factors in Computing Systems.*

[8] G. Adomavicius, A. Tuzhilin (2005); Towards the Next Generation of Recommender Systems: A Survey of the State-of-the-Art and Possible Extensions, *IEEE Transactions on Knowledge and Data Engineering*, 17(6): 734-749.

[9] D. Billsus, M.J. Pazzani (1998); Learning Collaborative Information Filters, *Pro. of the 15th Int. Conference on Machine Learning.*

[10] V. Formoso, D. Fernandez, F. Cacheda, V. Carneiro (2012); Using Profile Expansion Techniques to Alleviate the New User Problem, *Information Processing and Management*, 49(3): 659-672.

[11] H.N. Kim, A.T. Ji, I. Ha, G.S. Jo (2010); Collaborative Filtering based on Collaborative Tagging for Enhancing the Quality of Recommendation, *Electronic Commerce Research and Applications*, 9(1): 73-83.

[12] T.Q. Lee, Y. Park, Y.T. Park (2008); A Time-based Approach to Effective Recommender Systems Using Implicit Feedback, *Expert Systems with Applications*, 34(4): 3055-3062.

[13] Q. Shambour, J. Lu (2011); A Hybrid Trust-Enhanced Collaborative Filtering Recommendation Approach for Personalized Government-to-Business e-Services, *International Journal of Intelligent Systems*, 26(9): 814-843.

[14] C.C. Aggarwal, C. Procopiuc, P.S. Yu (2002); Finding Localized Associations in Market Basket Data. *IEEE Transactions on Knowledge and Data Engineering*, 14(1): 51-62.

[15] C.L. Huang, W.L. Huang (2009); Handling Sequential Pattern Decay: Developing a Two-Stage Collaborative Recommendation System, *Electronic Commerce Research and Applications*, 8(3): 117-129.

[16] Y. Wang, W. Dai, Y. Yuan (2008); Website Browsing Aid: A Navigation Graph-based Recommendation System, *Decision Support Systems*, 45(3): 387-400.

[17] D. Goldberg, D. Nichols, B.M. Oki, D. Terry (1992); Using Collaborative Filtering to Weave an Information Tapestry, *Communications of the ACM*, 35(12): 61-70.

[18] P. Resnick, N. Iacovou, M. Suchak, P. Bergstrom, J. Riedl (1994); GroupLens: An Open Architecture for Collaborative Filtering of Netnews. *Pro. of the 1994 ACM Conference on Computer Supported Cooperative Work.*

[19] G. Adomavicius, Y. Kwon (2007); New Recommendation Techniques for Multicriteria Rating Systems, *IEEE Intelligent Systems*, 22(3): 48-55.

[20] I.S. Altingovde, O.N. Subakan, O. Ulusoy (2012); Cluster Searching Strategies for Collaborative Recommendation Systems, *Information Processing and Management*, 49(3): 688-697.

[21] K.W. Cheung, J.T. Kwok, M.H. Law, K.C. Tsui (2003); Mining Customer Product Ratings for Personalized Marketing, *Decision Support Systems*, 35(2): 231-243.

[22] K. Goldberg, T. Roeder, D. Gupta, C. Perkins (2001); Eigentaste: A Constant Time Collaborative Filtering Algorithm, *Information Retrieval*, 4(2): 133-151.

[23] Y. Koren (2010); Factor in the Neighbors: Scalable and Accurate Collaborative Filtering, *ACM Transactions on Knowledge Discovery from Data*, 4(1): 1-24.

[24] R. Salakhutdinov, N. Srebro (2010); Collaborative Filtering in a Non-Uniform World: Learning with the Weighted Trace Norm, arXiv:1002.2780v1, 1-9.

[25] D. Joaquin, I. Naohiro (1999); Memory-based Weighted-Majority Prediction. *Pro. of ACM SIGIR' 99 Workshop on Recommender Systems: Algorithms and Evaluation.*

[26] J. Lee, S. Lee, H. Kim (2011); An Probabilistic Approach to Semantic Collaborative Filtering Using World Knowledge, *Journal of Information Science*, 37(1): 49-66.

[27] J.M. Yang, K.F. Li, D.F. Zhang (2009); Recommendation based on Rational Inferences in Collaborative Filtering, *Knowledge-Based Systems*, 22(1): 105-114.

[28] Z. Liu, W. Qu, H. Li, C. Xie (2010); A Hybrid Collaborative Filtering Recommendation Mechanism for P2P Networks, *Future Generation Computer Systems*, 26(8): 1409-1417.

INTERNATIONAL JOURNAL OF COMPUTERS COMMUNICATIONS & CONTROL
ISSN 1841-9836, 11(5):645-656, October 2016.

Statistical Automaton for Verifying Temporal Properties and Computing Information on Traces

A. Ferlin, V. Wiels, P. Bon

Antoine Ferlin*
1. IFSTTAR, 20 rue Élisée Reclus,
BP 70317, 59666 Villeneuve d'Ascq Cedex, France
2. ONERA/DTIM, 2 avenue E. Belin
BP74025, 31055 Toulouse, France
3. AIRBUS OPERATIONS S.A.S.,
316 route de Bayonne, 31060 Toulouse Cedex 09, France
*Corresponding author: antoine.ferlin@ifsttar.fr

Virginie Wiels
ONERA/DTIM, 2 avenue E. Belin
BP74025, 31055 Toulouse, France
virginie.wiels@onera.fr

Philippe Bon
IFSTTAR, 20 rue Élisée Reclus,
BP 70317, 59666 Villeneuve d'Ascq Cedex, France
philippe.bon@ifsttar.fr

Abstract: Verification is decisive for embedded software. The goal of this work is to verify temporal properties on industrial applications, with the help of formal dynamic analysis. The approach presented in this paper is composed of three steps: formalization of temporal properties using an adequate language, generation of execution traces from a given property and verification of this property on execution traces. This paper focuses on the verification step. Use of a new kind of Büchi automaton has been proposed to provide an efficient verification taking into account the industrial needs and constraints. A prototype has been developed and used to carry out experiments on different anonymous real industrial applications.
Keywords: Statistical Büchi Automaton, Information Computation, Runtime Verification, Dynamic analysis, Linear Temporal Logic.

1 Introduction

Development of critical software is constrained by certification standards. More precisely, DO-178 concerns avionics software. It defines objectives for each step of the software development process and, in particular, for the verification phase. AIRBUS has investigated the use of several kinds of verification methods. These methods can be classified using two criteria: formal or not, static or dynamic. Classic verification means are typically not formal: test is dynamic, review is static. Formal techniques are typically static, but there has been a lot of work recently on run-time verification which can be classified as formal and dynamic.

The origin of this work is the verification of temporal properties in an industrial context. These properties cannot easily be verified using the current AIRBUS verification framework based on static analysis [18]. Another way consists in using dynamic analysis to perform the verification of temporal properties. Testing can be difficult for properties involving timing aspects. Simulation, which consists in testing a software on a simulated hardware, has been experimented

and allows the analysis of the program at each step of its execution. However, even if commandability and observations are easier with simulation than with testing, considered executions are very long and manual verification of a property is difficult and costly.

This paper presents a dynamic analysis approach to formally verify temporal properties on execution traces generated by simulation. The context of the industrial process restricts the dynamic analysis approach to off-line analysis techniques, i.e. a posteriori verification on execution traces. Constraints also exist on the generation of traces: values of variables at given instants are obtained by positioning explicit observation points in the program, and the number of such observation points must be minimized for efficiency reasons. Execution traces are generated using existing test cases. Test strategy is not considered in this paper. It is focused on the use of patterns of temporal properties to compute statistical information. The aim is double. The first goal is to conciliate the temporal properties which classically have a semantics on infinite traces, with finite traces. Secondly, when a property is violated, this method can provide additional information to the client instead of the basic "Ok/Failure" response. When bugs occurs, this method limits the necessary investigations, hence reduces the debugging cost.

An overview of the proposed approach is detailed in section 2. Section 3 positions our work according to related work. Section 4 recalls classic definitions and details the verification phase using automata that compute statistical information. Section 5 provides experiment results in terms of verification time and statistical information use. Finally, we conclude about our work and provide future work elements in Conclusions.

2 Overview of the approach

We are working within the Airbus simulation framework. This framework simulates hardware of the program to be verified. The simulated hardware is instrumented, so the program executed on this framework is the embedded software. Extraction of execution data consists in generating a trace with the help of observation points. They can only be defined using a debuggin interface. Our goal is to verify a temporal property on an execution trace of a given program. The first step consists in defining an adapted language to formalize a temporal property. The second step is trace generation. Verification of the property on the trace is the last step (Figure 1). In this paper, we focus on the last step. However, we give some essential elements of the first two steps hereafter.

The first step consists in identifying properties to be verified. Currently, the industrial methodology verifies temporal properties using non-formal static analysis. In other words, the verification phase is done by engineers using code review. Hence, the goal of this approach is typically focused on industrial needs. Actually, verification cost and time have to be reduced as much as possible and safety has to be at least identical with the present verification approach. In addition, the new equipped approach must be as simple as possible for operators.

Formalisation of temporal properties consists of four steps. Firstly, some properties are gathered from critical software. Secondly, properties are classified. Then, a dedicated language is defined from gathered classified properties. This language is based on a combination between a subset of LTL and regular expressions. Some operators on variables had been defined in order to have access to some information such as the time of the last modification of a variable. The language definition is not the purpose of this article and can be found in [9]. Use of a dedicated language is a consequence of the desire for simplification for operators. Finally, the properties studied are formalized using our dedicated language.

One issue with a posteriori dynamic analysis is gathering traces. Indeed, trace size quickly increases with execution time and with the number of collected variables. We use two ways to minimize traces. Firstly, we only collect, at each step of the program (a step is a C instruction),

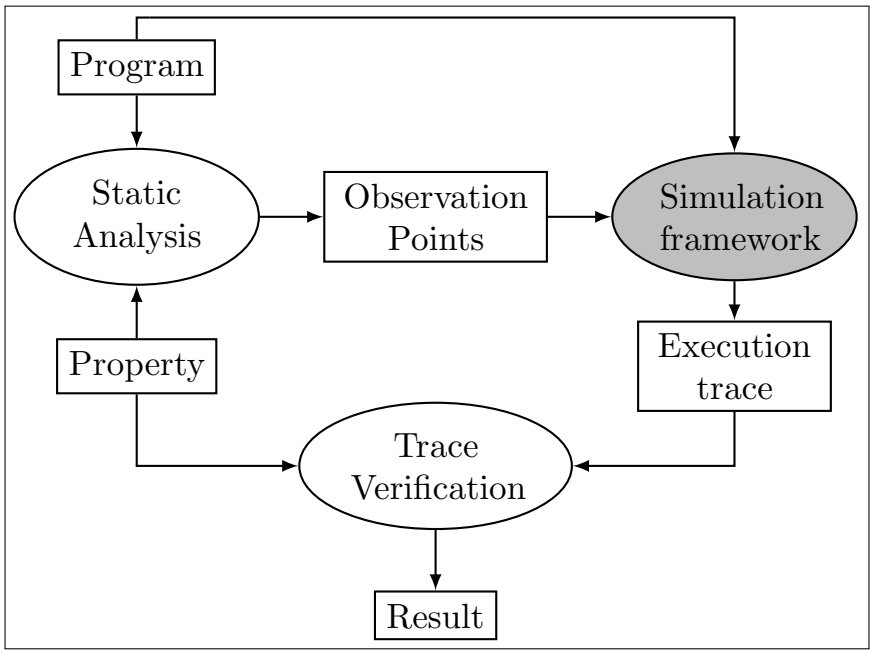

Figure 1: Overview of the approach

variables which are necessary to verify a given property. Secondly, we only collect these variables if their value changes. More details on trace generation can be found in [8].

This last step consists in verifying a formalized property on an execution trace. This step needs as input an execution trace given by the previous steps. Properties are formalized using language defined in the first steps and are then transformed into a Büchi automaton which is executed on the trace to be verified.

3 Related Work

Existing work on run-time verification [1] can be classified in two categories: on-line or a posteriori. An "on-line" approach means that the verification is done during the execution of the programme, whereas an "a posteriori" approach is done on execution traces. On-line verification consists either in adding assertions to the programme to express the properties to be monitored during the execution, or in executing, parallel to the programme, an automaton representing the property and taking as inputs data from the programme execution. A lot of work exists for on-line verification, especially for Java programmes and in the aspect-oriented programming community [7,12,13,16,19]. We work on C programmes which are either sequential hard-realtime programmes, or multitask realtime programmes (ARINC 653, POSIX platforms) and for certification reasons, we are restricted to an "a posteriori" verification. Existing works are fewer and differentiated by the following criteria.

The first criterion is the nature of the considered execution traces. In several existing works, complete execution traces can be obtained by listening to all the variables of the programme [3, 17]. This is not the case in our context: traces are obtained by positioning observation points in given places of the programme and we use static analysis to compute a minimized number of observation points. Indeed, the bigger the number of observation points, the bigger the size of the execution trace.

The second issue is the implementation of an efficient verification technique on the traces obtained that can be very large. Existing works are based on rewriting techniques [12] or specific techniques, such as translation of LTL formula into state machines [11] [6]. We use an existing

tool for LTL properties and propose specific techniques for regular expressions and parametric properties.

The last criterion is the way to handle finite traces. Classic models in temporal logic are infinite, while we want to verify properties on finite traces. Existing work proposes different solutions to this problem. [2] proposes an adaptation of the temporal language semantics. [15] and [4] propose a multi-valued logic to handle the cases where it is not possible to conclude on the satisfaction of a formula. In particular, [4] needs to generate two Büchi automata (one for the LTL_3 property ϕ and one for $\neg\phi$). This method requires time when the property depth is high. [15] also gives an interesting account of different work dealing with the finite trace issue and especially work that explores means to decide whether all possible infinite completion of a finite trace verifies a given property. A simple solution can also be to loop on the last state in order to render a finite trace infinite, but it modifies the satisfiability of some formulae [13]. We propose a simple pragmatic approach to this problem in section 4.2.

4 Verification of properties on execution traces

The last step of our approach consists in verifying a formalised property on an execution trace. This step needs as input the formalised property and a corresponding trace. The property is formalized and the trace is generated according to the method proposed in 2. The temporal property is translated into a Büchi automaton using *Ltl2ba* [10]. Hence, it is executed on the trace to perform the evaluation of the mapping formula.

In order to explain our approach, let us recall the definition of a Büchi automaton, which is based on the definition of the classic automaton.

4.1 Definitions

[14] defines an automaton as follows:

Definition 1 (Automaton)**.** An automaton is a 5-uplet $A = (Q, \Sigma, \rightarrow, q_0, F$ such that:

- Q is a set of states
- Σ is an alphabet
- $\rightarrow \in Q \times \Sigma \times Q$ is a transition relation
- q_0 is an initial state
- $F \subseteq Q$ a set of final states.

Definition 2 (Accepting condition)**.** A word $w \in \Sigma^*$ n length sized is a word of $\mathcal{L}(A)$ [14] where A is an automaton, if and only if there is a sequence $(q)_{i,i\in[\![0,n]\!]}$ which begins at q_0, such that $\forall i \in [\![0, n-1]\!]$, $(q_i, w_i, q_{i+1}) \in \rightarrow$ and $q - n \in F$.

An automaton A recognises the regular language $\mathcal{L}(A)$ defined on the Σ alphabet. All words of $\mathcal{L}(A)$ are finites words.

The Büchi automaton definition can now be expressed using the automaton definition [5]:

Definition 3 (Büchi Automaton)**.** A Büchi automaton is an automaton such that the accepting condition of a word is modified, in order to accept infinite words.

Definition 4 (Accepting condition)**.** A word $w \in \Sigma^\omega$ is a word of $\mathcal{L}(B)$, where B is a Büchi automaton, if and only if there is a sequence $(q)_{i,i\in\mathbb{N}}$ which begins at q_0 and such that $\forall i \in [\![0, n-1]\!]$, $(q_i, w_i, q_{i+1}) \in \rightarrow$ and $\forall j \in \mathbb{N}, \exists k \in \mathbb{N}, k > j$ and $q_k \in F$.

After the recall of these definitions, the next step consists in handling finite trace with a Büchi automaton which only accepts infinite words or traces.

4.2 The finite trace problem

Let us assume that ϕ is a temporal property and σ_∞ an infinite trace. The property is transformed into a Büchi automaton $\mathcal{B}_\phi$. Hence, $\sigma_\infty \vDash \phi$ if and only if σ_∞ is recognized by $\mathcal{B}_\phi$.

We deal with finite trace, whereas the semantics of LTL is on infinite ones. A classic solution consists in transforming the finite trace into an infinite one by looping over the last element. But this solution introduces border effects which have to be controlled. Hence, if we have a result on the trace σ_∞, what will we able to conclude about the finite trace σ which derives from σ_∞? This is how we propose to respond to this question.

A specific algorithm has then been defined to handle the execution of the Büchi automaton at the end of the trace. This algorithm answers the following question: is there an infinitely often accessible final state? This algorithm performs:

1. Computing the strongly connected components of the Büchi automaton, by only taking into account transitions where the formula is true.
2. Defining a direct acyclic graph (dag), equivalent to the Büchi automaton, from the strongly connected components computation.
3. Browsing the direct acyclic graph for each element of the current state.
4. Determining for each state of the dag accessed from an element of the current state if it is a final state of the Büchi automaton.

We have thus implemented a verification algorithm for the property on the trace. But the transformation of a finite trace into an infinite one modifies the satisfiability of some formulae.

The satisfiability of a property may change according to the nature of a trace, as presented in the following instances.

Example 5. *The formula $\Diamond(\Box A \vee \Box\neg A)$ (which means: eventually we always have A or we always have not A) is true with a finite trace which loops at the end, because the last state is A or non-A (Figure 2,b)). With an infinite trace, this formula may be false (Figure 2,a)). For instance, if the trace alternates A and non-A at each state, the formula will be false.*

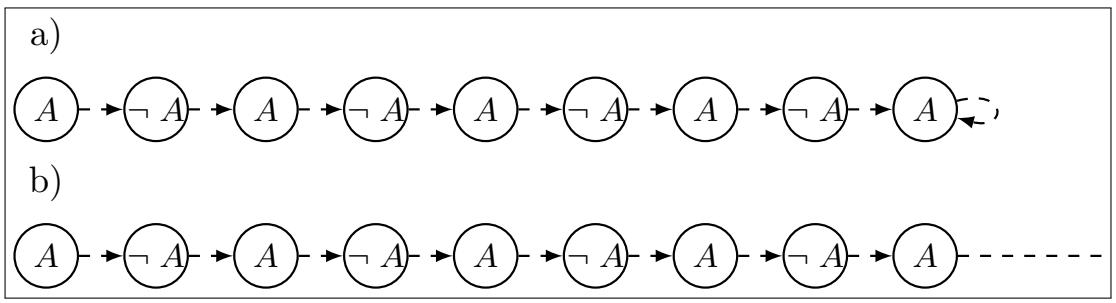

Figure 2: Two traces

In the considered context, the satisfaction of a formula may depend on the place where the execution is stopped in the program.

Example 6. *In the following example, the first trace is a theoretical trace corresponding to an infinite execution of the program. The other two traces are prefixes of the infinite trace where execution has been stopped at different execution times. The property $\Box(P \Rightarrow \Diamond Q)$ is false on the first prefix, but the same property is true on the second prefix.*

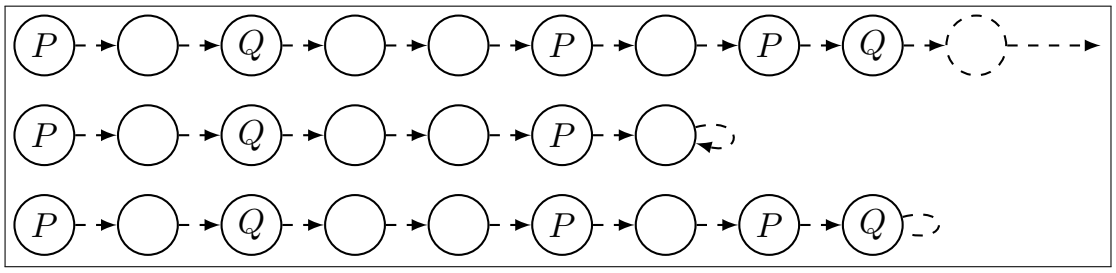

Figure 3: Satisfiability depends on the end of trace

In order to evaluate the interpretation of a property, we propose the following algorithmic method. ϕ is a property to be verified on an execution trace σ. $\mathcal{A}_\phi$ refers to the Büchi automaton associated to ϕ. σ_i is a trace state which is not the last trace state. Hence, there are two possible cases:

- if the set of reachable states of $\mathcal{A}_\phi$ is the empty set, then the property will be violated;
- When the last state of σ is reached, there is a loop over this one. $\mathcal{A}_\phi$ is then considered as a graph. Transitions with the formula evaluated to false are deleted. The mapping direct acyclic graph is computed and is browsed in order to determine if an accepting state is reachable infinitely often. Two sub-cases are possible:
  - An accepting state of $\mathcal{A}_\phi$ is reachable infinitely often. Hence the property is satisfied until the end of trace. However, it could be violated after this point of the programme execution. This is the case of safety and liveness properties.
  - Any accepting state of $\mathcal{A}_\phi$ is infinitely often reachable. The property is not satisfied. However, it would be satisfied after this point of the programme execution. This is the case of liveness property.

4.3 Statistical Büchi automaton, a pragmatic approach

We propose a pragmatic approach to handle "end of trace". We provide the user with statistical information on the satisfaction of the property. Two kinds of information are provided:

- Additional information for all properties which have not been verified. When the property is not verified, the last state where the property is true is provided. This information helps targeting where the potential problem is inside the code.
- Additional information for properties which comply with a pattern. This second aspect allows the giving of a set of information which is richer than the other one, because information is given even if the property is evaluated to true.

Statistical information depends on the pattern and is computed using an automaton which is executed instead of the Büchi automaton.

The definition of the statistical Büchi automaton is split into two parts hereafter. The first part consists of the statistical counters. The second part consists of their integration into a classic Büchi automaton.

Definition 7. $\mathcal{C}$ is a set of integer variables called counters. $\Lambda_\mathcal{C} : (\mathcal{C} \to \mathbb{Z}) \to (\mathcal{C} \to \mathbb{Z})$ is a set of actions on $\mathcal{C}$, depending on current value of all variables. Operations are characterized by the following grammar:

$\langle$ operations $\rangle$ ::=
| $\langle$ operations $\rangle$ $\langle$ operation $\rangle$

This rule defines a list of operations. The list can be empty or not.

⟨ operation ⟩ ::= ⟨ counter ⟩ = ⟨ expression ⟩

This rule defines an operation. An operation always modifies a counter.

⟨ expression ⟩ ::= ⟨ ZConst ⟩
| ⟨ counter ⟩
| ⟨ expression ⟩ + ⟨ expression ⟩
| - ⟨ expression ⟩
| ⟨ expression ⟩ × ⟨ expression ⟩
| ⟨ expression ⟩ ÷ ⟨ expression ⟩
| ⟨ expression ⟩ % ⟨ expression ⟩
| Min(⟨ expressions ⟩)
| Max(⟨ expressions ⟩)

This rule defines an expression. Integer constants (*ZConst*) and *counter* can be used inside operations. Authorized operations are addition, opposite, *plication, euclidean division, modulo, minimum and maximum.

⟨ expressions ⟩ ::= ⟨ expression ⟩,⟨ expression ⟩
| ⟨ expression ⟩,⟨ expressions ⟩

This rule is used for Min and Max operations. The list has at least two expressions.

Hence, a statistical Büchi automaton is :

Definition 8. A statistical automaton is a five-uplet $\mathcal{A} = (Q, \Sigma, \rightarrow, q_0, F, \mathcal{C}_0)$ where:

- Q is a set of states
- Σ an alphabet
- $\rightarrow \subseteq Q \times \Sigma \times \Lambda_{\mathcal{C}} \times Q$ a transition relation
- $q_0 \in Q$ is the initial state;
- $F \subseteq Q$ a set of accepting states;
- $\mathcal{C}_0 : \mathcal{C} \rightarrow \mathbb{Z}^{\iota}$, is a function which returns the initial value of each element of $\mathcal{C}$

Statistical information depends on the pattern and is computed using an automaton which is executed in parallel with the Büchi automaton.

Example 9. *The automaton of the pattern $\Box\Diamond p$ allows the computing of the number of states where p is true (Figure 4). Each time p is true, the nb_p counter is incremented. At the end of trace execution, we know how many times p was true.*

In this pragmatic approach, the statistical automaton replaces the classic Büchi automaton. Each time a transition is true, the mapping list of operations is applied to the counters. Currently, three patterns are recognized (these patterns have often been encountered in the studied industrial applications). The past version of each pattern is recognized to

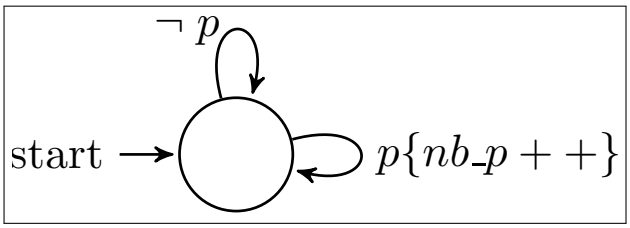

Figure 4: Automaton of the pattern $\Box\Diamond p$

- $\Box\Diamond p$
- $\Box(p \Rightarrow q)$
- $\Box(p \Rightarrow \Diamond q)$

Adding a new pattern with this approach is facilitated. Actually, each pattern is described inside a file (formula, statistical automaton, printing system of statistical information). Hence, if an agent wants to collect additional information for a new pattern, he can define the automaton attached to that pattern to compute his own information.

The next step of this work consists in testing our approach on real industrial cases.

5 Implementation and Experiments

In this section, we detail some elements of the implementation of the prototype *AnTarES*, and propose experiments on real industrial cases. Let us recall, *AnTarES* is an industrial proprietary prototype.

5.1 *AnTarES*, a tools for Analyse of Trace of Execution of Software

AnTarES implements our approach from the transformation of the temporal property into a Büchi automaton to the verification of this property on an execution trace. *AnTarES* uses *Ltl2ba* for the transformation. The major steps are summarized in figure 1

AnTarES is written in OCaml with around 16,300 lines of code. The verifier is split into three applications:

- a reader module, which reads the trace. This task can be done by several readers dispatched on several networked computers. This fact allows the distribution of the calculus load on available resources. In addition, two trace formats are currently handled by the tool: the standard VCD format (Value Change Dump - ASCII based format for dump files), and a data base format. Because these trace formats are transformed into a generic format which is used for verification, adding a new format is easy. The stored trace σ is a sequence of states σ_j. A state is a list of pairs (variable, value);
- a central server module, which will be able to ask the appropriate reader module, if the reading task is dispatched on several computers;
- a client module, which does the verification.

In order to evaluate our prototype, experiments have been done on traces which come from different avionics software. The goal of these experiments was to check that identified requirements can be formalized using our specification language and to assess the efficiency of our approach, for all kinds of properties. As a reminder, verification of temporal properties with non-formal static analysis (code reviewing) needs several days. We aim to decrease the verification time.

Our approach has been tested on programs in order to evaluate the different aspects of this one. The first program is an embedded software, whereas the last one is a hardware model of the dynamic-analysis framework we use to generate execution trace for the first program. The experiments conditions are identical for all experiments : the used machine is an octo-core machine with a 2Ghz-and-512ko-cache processor.

5.2 Experiments on a first software

This experiment evaluates three aspects of our approach: reverse reading, parametric properties, and computation of additional information for a specific pattern. This software is based on the Arinc 653 standard. The verified part of this software is around 550 lines of C code. The Arinc 653 library is around 2,600 lines of C code. It is a multi-task software which is stopped after a finite number of loops. The software communicates with other applications using dynamically created ports. The property consists in ensuring that each port has been initialised before being used. The size of the trace is relatively small (about 129 states). The property is verified for all possible values of *used_port* which are 1,2, and 5 in the trace. The formalized properties are the shape of $\boxdot(used\_port = x \Rightarrow \diamondsuit(created\_port = x))$, where $x \in \{1, 2, 5\}$. The recognized pattern is $\boxdot(P \Rightarrow \diamondsuit Q)$. Then, the mapping statistical automaton computes the number of occurrences of P ($used\_port = 1$ for example) before Q occurs ($created\_port = 1$).

Table 1: Additional information: Occurrence of used port

Port	Occurrence
1	107
2	2
5	20

Table 2: Computation time

Module	Time (s)
Reader	0.015
Server	0.024
Client	0.07

Execution times of each module are displayed in Table 2. Because of the small size of the trace, only one reader module is used here. This is in charge of the trace reading, the server makes the link between the reader and the client, and the client is responsible for the verification itself. Verification time of the client includes transformation of the LTL formula into a Büchi automaton, duplication of the Büchi automaton and verification of the formula. Verification of this property on a trace with 129 states is efficient, considering that four properties are simultaneously verified: one for each value of *used_port*.

According to table 1, which gather the results of the verification of the properties on the trace, we can see the usage of each port. Relative to the number of elements, port 1 is used for $82,9\%$ of the cases, whereas port 2 is used for $1,6\%$ of the cases.

This experiment shows that statistical information can be used to check orthogonal properties, such as the number of uses of a port. Indeed, with this statistical information, the used port and their frequency of use are known.

5.3 Experiments on a second software

This experiment has been done on a model of the AIRBUS simulation framework. This model consists of a processor, an interruption control system, an EEPROM, an emitter, and a watchdog. This model represents 675 lines of C. This is a mono-task software which loops infinitely. The aim of this study consists in verifying the behaviour of the watchdog. It checks time between two writing actions on the EEPROM. If the difference between the two writing actions is more than T_0, then an interruption signal is sent to the calculator and the emitter.

In this experiment, we want to verify that a variable must be written in the EPPROM at lest every T_0 seconds. If time is more than T_0, a watchdog raises a signal to the controller, otherwise

nothing happens.

The property can be split into two sub-properties which are:

- $\square((\tau - last\_write\_time > T_0) \Rightarrow signal)$, means when the delta between the last write time and the current time (τ) is upper than T_0, then *signal* will be raised (overflow case).
- $\square((\tau - last\_write\_time \leqslant T_0) \Rightarrow \neg(signal))$ means when the delta is lower or equal to T_0, then *signal* will not be raised (nominal case) .

The properties have been verified on a trace with $1,848,633$ states. In addition, the equations follow the pattern $\square(p \Rightarrow q)$. Hence, we have information about how much the overflow case and the nominal case happen. We cut trace reading in 5 reader modules.

Table 3: Second software, time results

Module	Nominal Time(s)	overflow Time(s)
Reader(min-max)	9.21-10.09	9.21-10.09
Server	3.04	3.04
Client	25.84	35.84

Pattern information says that the nominal case happens $1,848,629$ times (more than $99,99\%$ of the cases) and overflow case happens only 4 times ($2.16 \times 10^{-4}\%$). This information is essential, because it shows that overflow is not frequent. If overflow appears more frequently, then the software will probably have a bug. The acceptable maximal level of appearance of this second property depends on the size of the trace and on the software. This kind of problem could not be detected without statistical information.

Finally, this experiment shows that verification of temporal properties on big traces including computation of statistical information is efficient (less than 50 seconds, trace reading included). In addition, use of patterns can help to detect bugs which are complex to find.

5.4 Discussions around the experiments

The experiments have been processed on embedded avionics software and on models of the dynamic-analysis framework. It shows that the defined approach is efficient on big traces. Indeed, the order of magnitude of time verification is several hundred seconds in comparison with several days with a non-formal verification method (code reviewing). Use of patterns to compute statistical information is useful to help decide if a property is true or false when the entire trace has been analysed. In addition, this statistical information allows the treatment of orthogonal properties such as "how much time a port has been used?" (first software).

Conclusions

This paper has presented an approach for the verification of temporal properties on execution traces of avionics software. This approach was needed because these kinds of properties are difficult to verify using existing techniques. The definition of the solution was guided by industrial needs and constraints. This approach proceeds in three steps: definition of a dedicated property language, generation of trace executions using static analysis, and verification of the property on the trace. The verification step is built in order to handle finite traces, whereas temporal properties have a semantics on infinite traces. To do this, additional statistical information about the trace are provided to help the verifier to conclude about the verification result. This statistical information depends on the property pattern. Frequently encountered patterns are implemented in *AnTarES*. Other patterns can easily be added with the definition of a new statistical automaton.

A prototype *AnTarES* has been developed (18,500 lines of OCaml code) and integrated into the AIRBUS simulation framework. Experiments conducted on industrial applications allowed us to assess the efficiency of our approach on different kinds of properties and different sizes of trace. An industrial deployment of the tool would require adding a graphical user interface to display results and to provide user-friendly ways to write properties. In addition, in order to simply the specification of properties we aim to improve the language with parametric variable handling. We hope to improve the handling of past formulae by reverse reading the trace during the automaton execution. These are parts of future work.

This approach is a contribution to the overall industrial strategy, which consists in reducing the part of testing in the verification process of avionics software by developing and integrating static and dynamic analyses techniques [18]. Future work will target means to better combine static and dynamic analysis.

Acknowledgment

The work is funded by the French national research agency (ANR) in the context of the PERFECT and RE(H)STRAIN Projects.

Bibliography

[1] Runtime verification, 2001-2009.

[2] H. Barringer, A. Goldberg, K. Havelund, and K. Sen (2004); Rule-based runtime verification. In B. Steffen and G. Levi, eds., *Verification, Model Checking, and Abstract Interpretation*, vol. 2937 of *LNCS*. Springer.

[3] Howard Barringer, Allen Goldberg, Klaus Havelund, and Koushik Sen (2003); Eagle does space efficient ltl monitoring. Technical report, Nasa.

[4] Andreas Bauer, Martin Leucker, and Christian Schallhart (2011); Runtime verification for ltl and tltl. *ACM Trans. Softw. Eng. Methodol.*, 20(4):14:1–14:64.

[5] J.Richard Büchi (1990); On a decision method in restricted second order arithmetic. In Saunders Mac Lane and Dirk Siefkes, editors, *The Collected Works of J. Richard Büchi*, Springer New York., 425–435.

[6] Marcelo d'Amorim and Grigore Rosu (2005); Efficient monitoring of omega-languages. In *CAV'05*, 364–378.

[7] Doron Drusinsky. The temporal rover and the atg rover. In K. Havelund, J. Penix, and W. Visser, editors, *SPIN Model Checking and Software Verification*, volume 1885 of *Lecture Notes in Computer Science*. Springer, 2000.

[8] A. Ferlin and V. Wiels (2012); Combination of static and dynamic analyses for the certification of avionics software. In *Software Reliability Engineering Workshops (ISSREW), 2012 IEEE 23rd International Symposium on*, 331–336.

[9] Antoine Ferlin (2013); *Verification de propriétés temporelles sur des logiciels avioniques par analyse dynamique formelle*. PhD thesis, Thèe de doctorat dirigée par Wiels, Virginie Sureté de logiciel et calcul de haute performance Toulouse, ISAE 2013.

[10] P. Gastin and D. Oddoux. Fast LTL to Büchi automata translation. In *Proceedings of the 13th International Conference on Computer Aided Verification (CAV'01)*, vol. 2102 of *LNCS*. Springer, 2001.

[11] D. Giannakopoulou and K. Havelund. Automata-based verification of temporal properties on running programs. In *Automated Software Engineering*, 2001.

[12] K. Havelund and G. Rosu (2001), Monitoring programs using rewriting. In *Automated Software Engineering*, 135 – 143.

[13] Klaus Havelund, Grigore Rosu (2002), A rewriting-based approach to trace analysis. *Automated Software Engineering*, 1-21.

[14] S C Kleene (1956), Representation of events in nerve nets and finite automata. In *In Automata Studies*. Princeton University Press: Princeton.

[15] Martin Leucker, Christian Schallhart (2009), A brief account of runtime verification. *The Journal of Logic and Algebraic Programming*, 78(5):293 – 303, The 1st Workshop on Formal Languages and Analysis of Contract-Oriented Software (FLACOS07).

[16] Patrick O'Neil Meredith, Dongyun Jin, Dennis Griffith, Feng Chen, Grigore Rosu (2012), An overview of the mop runtime verification framework. *International Journal on Software Tools for Technology Transfer*, 14:249–289.

[17] A. Pnueli, A. Zaks (2006), Psl model checking and run-time verification via testers. In *FM 2006: Formal Methods*, vol. 4085 of *LNCS*. Springer.

[18] Jean Souyris, Virginie Wiels, David Delmas, Hervé Delseny (2009), Formal verification of avionics software products. In *Formal Methods, Lecture Notes in Computer Science*, 5850: 32-546.

[19] Volker Stolz and Eric Bodden (2006), Temporal assertions using aspectJ, Proceedings of the Fifth Workshop on Runtime Verification (RV 2005), *Electronic Notes in Theoretical Computer Science*, 144(4):109 –124.

INTERNATIONAL JOURNAL OF COMPUTERS COMMUNICATIONS & CONTROL
ISSN 1841-9836, 11(5):657-666, October 2016.

Robust Face Recognition Against Soft-errors Using a Cross-layer Approach

G.-M. Jeong, C.-W. Park, S.-I. Choi, K. Lee, N. Dutt

Gu-Min Jeong, Chang-Woo Park
Department Electrical Engineering
Kookmin University
Jeongeung-dong, Songbuk-gu
Seoul, 136-702, Korea
gm1004@kookmin.ac.kr, high1117@nate.com

Sang-Il Choi*
Department Applied Computer Engineering
Dankook University
Jukjeon-dong, Suji-gu, Yongin-si
Gyeonggi-do, 448-701, Korea
*Corresponding author: choisi@dankook.ac.kr

Kyoungwoo Lee
Department Computer Science
Yonsei University
Sinchon-dong, Seodaemun-gu
Seoul, 120-749, Korea
kyoungwoo.lee@gmail.com

Nikil Dutt
Department Computer Science
University of California, Irvine
Irvine, CA 92697, USA
dutt@ics.uci.edu

Abstract: Recently, soft-errors, temporary bit toggles in memory systems, have become increasingly important. Although soft-errors are not critical to the stability of recognition systems or multimedia systems, they can significantly degrade the system performance. Considering these facts, in this paper, we propose a novel method for robust face recognition against soft-errors using a cross layer approach. To attenuate the effect of soft-errors in the face recognition system, they are detected in the embedded system layer by using a parity bit checker and compensated in the application layer by using a mean face. We present the soft-error detection module for face recognition and the compensation module based on the mean face of the facial images. Simulation results show that the proposed system effectively compensates for the performance degradation due to soft errors and improves the performance by 2.11 % in case of the Yale database and by 10.43 % in case of the ORL database on average as compared to that with the soft-errors induced.
Keywords: Soft-error, Face recognition, Cross-layer approach, Mean face.

1 Introduction

Nowadays, memory errors due to various causes have become a critical threat for the performance and stability of numerous systems. In particular, soft-errors, which are transient bit toggles in memory systems, have become increasingly important factors for the performance

degradation of various applications. Soft-errors denote the phenomenon that changes the memory bit value temporarily from 1 to 0 and vice versa due to abnormal conditions such as high radiation, high pressure or high temperature [1].

Although the soft-errors are not permanent and nondestructive, there have been several reports on the damages due to soft-errors. SUN and Hewlett Packard announced the loss due to soft-errors in their server systems [2, 3]. Further, soft errors brought a billion-dollar automotive factory to halt every month [4].

Until now, there have been several researches on the protection of soft-errors [5–9]. Especially, for multimedia systems, cross-layer based approaches have been introduced to compensate for the negative effects of soft-errors. Since soft-errors are not critical to the system stability, cooperation across system abstraction layers can help to build a cost-efficient system against soft-errors from a hardware layer to an application layer in mobile embedded systems [10].

In this paper, we propose a robust and cost-effective system for face recognition against soft-errors by using a cross layer approach. First, we analyze the effect of soft-errors for face recognition systems and show that the soft-errors induced in the JPEG image can degrade the performance of the recognition system [11, 12]. Next, we propose a cross-layer compensation module consisting of a detector in the hardware layer and a corresponding compensator in the application layer. To attenuate the negative impact of soft-errors in face recognition systems, they are detected in the embedded system layer by using a parity bit checker. When they are detected, the mean face method is used for compensating for the negative impact on the performance at the application layer. The classification experiments are performed for the Yale [13] and ORL databases [14]. The features for classification are extracted by using the RLDA (Regularized Linear Discriminant Analysis) method [12]. The experimental results demonstrate the effectiveness of the proposed method. Further, the proposed cross-layer based compensation method can improve the system performance by 2.11 % and by 10.43 % on average in case of YALE and ORL databases, respectively, as compared to the performance with soft-errors in the face recognition system.

The remainder of this paper is organized as follows. In Section 2, we introduce an exemplary face recognition system for the simulation and the effect of soft-errors in JPEG images. Then, in Section 2, we describe an analysis of the effect of soft-errors on the face recognition system. In Section 4, we present the proposed cross-layer approaches and experimental results. The conclusion follows in Section 5.

2 Exemplary face recognition system and effect of soft-errors in JPEG images

2.1 Exemplary face recognition system

Figure 1 shows the exemplary face recognition system considered in this study. As shown in figure 1, after a JPEG image is captured using a camera, it is transmitted to the classification part and decoded in the BMP format. Then, after preprocessing, it is classified using various classification methods [12, 15–17]. For the analysis of the soft-error impacts, we assume that the soft-error occurs inside the JPEG file. Hence, we assume that the soft-error can occur in the memory when storing or decoding the JPEG file.

2.2 Effect of soft-errors in JPEG file

The JPEG file is a compressed image file format. The effects of soft-errors depend on where they occur. For example, the effects are different between the soft-errors in the header information

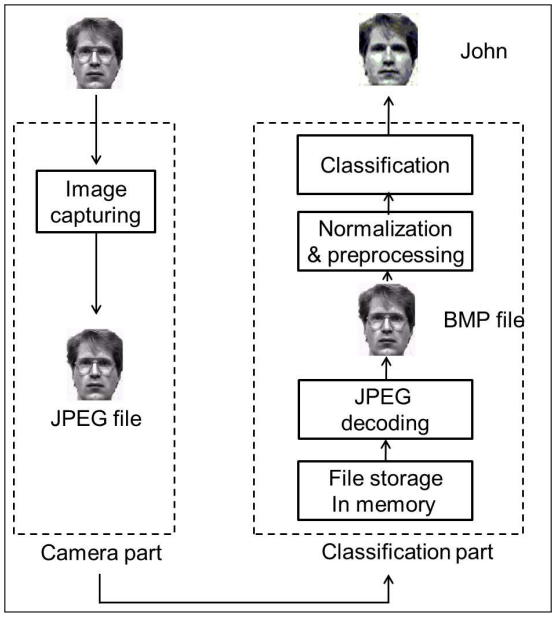

Figure 1: An exemplary face recognition system

Figure 2: Effect of soft-errors for the decoding of JPEG files. (a) Decoded image without soft-errors (b) Examples of decoded images with bit-errors

parts and those in the compressed 8×8 blocks. Figure 2 shows various examples of decoded images when soft-errors occur in the JPEG file. Note that the decoded results may differ according to the implemented decoder. If the exceptions are not handled appropriately, the decoder can even be stopped. When soft-errors occur in the critical data of the header such as errors in the length of the file or the length of the block data, the decoder can lose all its information afterwards. In the case of a soft-error in block data, the block can be decoded inappropriately, causing a significant degradation of the quality.

3 Effect of soft-errors on the face recognition system

In this section, we discuss the effects of soft-errors on face recognition systems. We build a model of the soft-errors in the face recognition system and analyze the performance degradation for the recognition rate when these errors are induced.

3.1 Modeling of soft-errors and system setting

To conduct a quantitative analysis of soft-errors, we make the following assumptions of soft-errors for a face recognition system:
Assumptions of the soft-errors

- A1) A single-bit soft-error occurs for one facial image, particularly in the test set.
- A2) A soft-error occurs only for the block data part.

On the basis of A1) and A2), we can conclude that only one block is affected by a single-bit soft-error. Further, for the system setting, a soft-error is detected using a parity bit checker in the memory and it is notified to the JPEG decoder. When the JPEG decoder receives the information of the soft-error occurrence, it passes over the decoding of the corresponding block. Hence, the corresponding 8×8 block of the soft-error is filled with 0's instead of the real decoded data. Figure 3 shows the overall processing based on the system setting in our study.

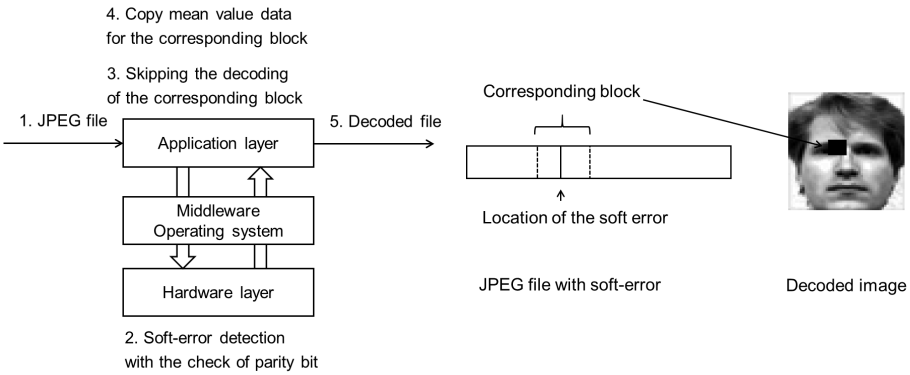

Figure 3: Decoding procedure for the JPEG file with a soft error. a) Decoding procedure considering a soft-error in the block data. b) Decoded image based on the considered system setting

3.2 Classification experiment for the soft-errors

We apply the proposed method to the Yale database in order to observe the effect of soft-error on the recognition rate. The Yale database contains 165 gray images of 15 individuals, having

different facial expressions, with or without glasses, and under different lighting conditions. Each face image is cropped and re-scaled so that the center of each eye is placed at a fixed point in an image of 60×50 pixels. On the basis of assumption A1), we consider that a soft-error occurs in all the images for the test set, while no error occurs for the training set. There exist 42 blocks (size: 8×8) in a 60×50 image as shown in figure 4(a). Hence, we conduct 42 times an 11-fold cross validation [17] according to the location of the soft-error, as depicted in figure 4(b).

In these 11-fold cross validations, one image from each subject is randomly selected for testing while the remaining images are used for training. In other words, we consider 150 images in the training set and 15 images for the probing. For the selected 15 images for the test, we assume that there occur a soft-error, as shown in figure 4(b).

For the classification, the R-LDA method [12] is used as a feature extraction method and the one nearest neighbor rule is applied as a classifier with the L2 distance metric. It is noted that the R-LDA method is well known but is not necessarily the best one.

In Table 1, the first and second columns show the recognition rates without a soft-error and with a soft-error, respectively. As summarized in Table 1, we can observe the average performance degradation of 2.45 % in terms of the recognition rate in the case with the soft-errors as compared to that in the case without the soft-error. As shown in figure 7(a), there is a significant degradation (up to approximately 10 %) according to the block numbers, and we can see that there is a significant performance degradation due to the single-bit soft-errors.

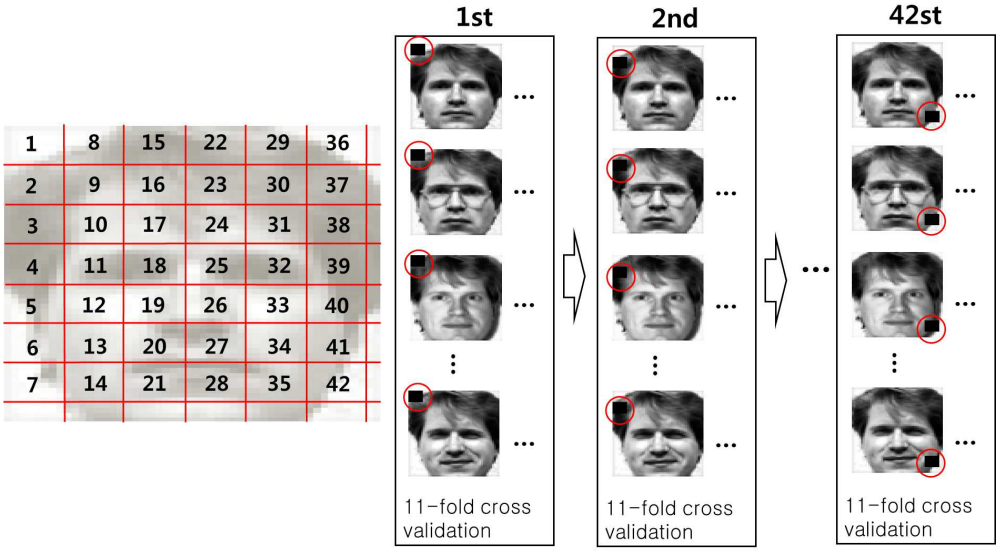

Figure 4: Classification experiment for the soft-errors. a) 42 blocks inside the 60 × 50 image. b) 42 times 11-fold cross validation.

4 Cross-layer approach for compensation of soft-errors in the face recognition system

4.1 Overall structure of the proposed method

Considering the performance degradation of the soft-errors, we propose a cost- and performance-effective compensation method for the face recognition system. Figure 5 shows the overall structure of the proposed compensation method in a cross-layered manner. As shown in figure 5, when the occurrence of the soft-error is notified from the hardware layer to the application layer, the proposed method can compensate the corresponding block for the performance degradation with

the mean value data from the database. By this compensation, we can enhance the performance of the recognition system in a cost-effective manner.

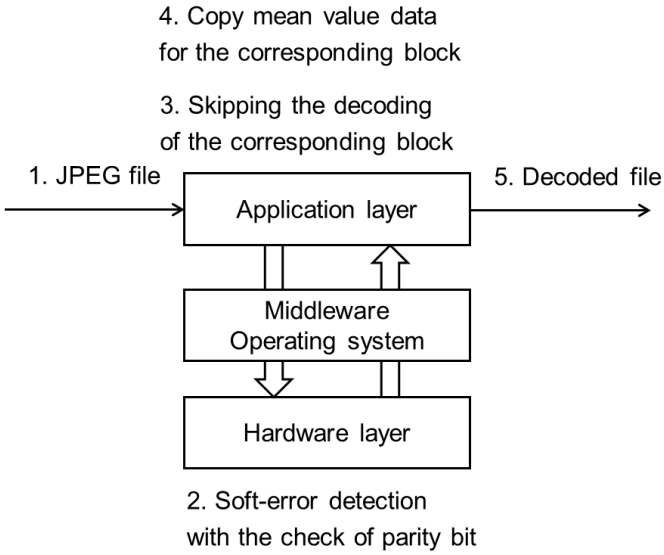

Figure 5: Overall structure of the proposed compensation method

In the proposed cross-layered approach, we detect the soft-error by using parity bit checkers cost-effectively rather than by using ECC (Error Correction Codes) modules. Indeed, the real compensation for the soft-errors is achieved in the application layer. In the application layer, we should mitigate the impact of soft-errors on the performance in the data block, which is filled with 0's by skipping the decoding.

In the face recognition method, the mean face is effectively used for the illumination compensation and other applications [18, 19]. Likewise, if we use a mean face for the training data, we can improve the system performance. In this paper, we use the corresponding mean block from the mean face of the training set. Figure 6 shows an example of a mean face for the Yale database.

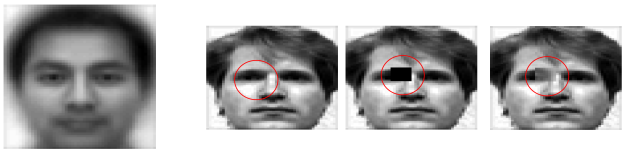

Figure 6: Compensation using mean face. a) Example of a mean face for the Yale database. b) Facial images without a soft-error, with a soft-error and with the compensation.

4.2 Experimental results and analysis

Table 1 shows the recognition rate for the cases with a soft-error, without a soft-error, and with the compensation for the soft-error, respectively in the Yale database. As shown in table 1, the proposed compensation method can enhance the performance by 2.11 % as compared to that in the case with soft-errors. In the comparison between the cases with no soft-error and compensation, there is a performance difference of only 0.34%. Figure 7(a) shows the recognition rate according to the blocks in the Yale database.

Further, Table 2 and Figure 7(b) show the experimental results for the ORL database. The images are resized into 56×46 pixels in this experiment. As shown in Table 2 and Figure 7(b),

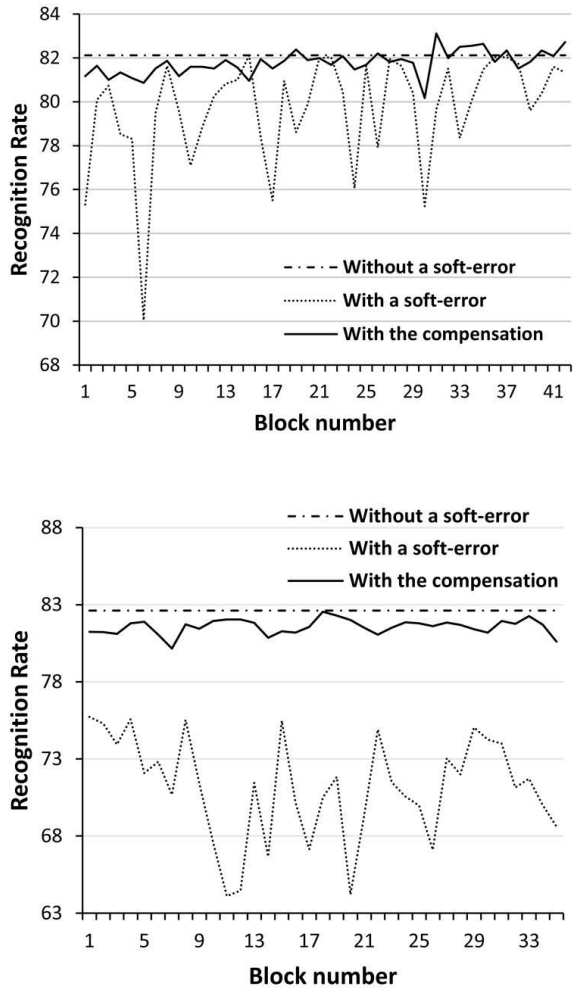

Figure 7: Recognition rate according to the block numbers for the Yale and ORL databases. a) Yale database. b) ORL database.

Table 1: Comparison of the recognition rate for the soft error in the Yale database(%)

No. of features	No error	Soft-error	Compensation
1	35.15	26.16	29.12
2	54.55	49.62	55.90
3	73.94	68.40	73.61
4	82.42	76.64	80.52
5	83.03	81.52	83.52
6	83.64	83.52	84.49
7	86.67	86.25	87.76
8	89.70	88.86	90.17
9	92.73	91.44	92.81
10	93.33	91.75	92.94
11	93.33	92.44	93.19
12	93.94	92.83	93.67
13	93.94	93.29	93.78
14	93.33	92.73	93.41
Average	82.12	79.67	81.78

a soft-error can degrade the performance by approximately 11.48 %. However, the proposed compensation method can achieve a performance improvement of approximately 10.43 % as compared to the case with the soft-error while it incurs a 1.05 % performance degradation as compared to the case without the soft-errors.

From these experiments, we can conclude that the proposed method can mitigate the impact of soft-errors on the system performance effectively.

Table 2: Comparison of the recognition rate for the soft error in the ORL database(%)

No. of features	No error	Soft-error	Compensation
1	6.75	5.92	7.46
2	13.50	10.86	15.32
3	27.50	17.01	25.58
4	41.75	22.69	38.09
5	48.00	27.58	45.10
6	56.25	33.60	52.59
7	62.75	38.80	59.81
8	69.00	44.29	65.58
9	74.75	49.59	70.98
10	79.00	54.16	76.16
15	87.50	70.49	86.37
20	95.75	82.61	94.73
25	97.25	90.64	96.88
30	98.50	93.14	98.06
35	98.00	94.70	97.90
Average	82.62	71.14	81.57

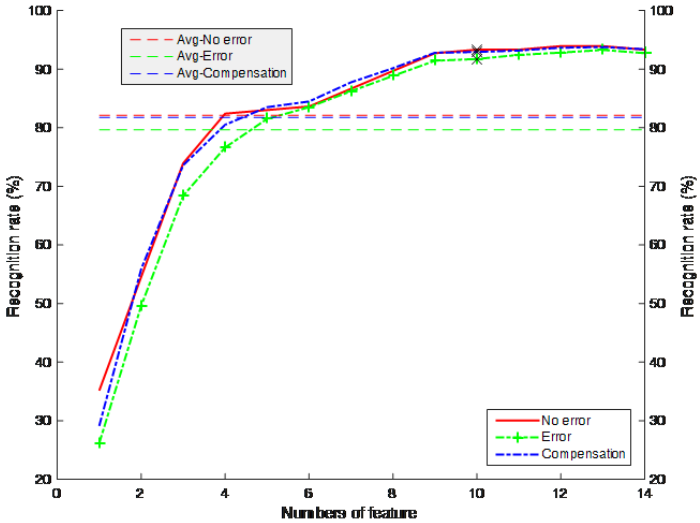

Figure 8: Recognition rate according to the numbers of feature of for the Yale database.

The recognition rate versus the numbers of feature of Yale database is shown in Figure 8 for three cases: non-error, error and compensation. It is obvious that the recognition rates increase with small numbers of feature, from one feature to eight features, and after that, the recognition rates would be almost saturated even if the numbers of feature increase how much. Therefore, we will select the minimum numbers of feature that the higher rates can be achieved.

Table 3: Average recognition rates of two selection method RLDA and LBP for Yale and ORL database(%)

Selection Method	Yale			ORL		
	No error	Error	Compensation	No error	Error	Compensation
RLDA	83.11	73.57	82.27	80.04	72.67	78.96
LBP	87	86.79	86.86	89.12	88.58	88.92

We have also applied Local Binary Pattern (LBP) as a feature selection method for both

databases by measuring Chi-square distances, and the result is shown in Table 3. These data in the table show the average recognition rates of forty-two blocks for three cases: non-error, error and compensation. From this table, there is no doubt that the recognition rates obtained from LBP is higher than from RLDA. The reason is that LBP uses all blocks as features, whereas RLDA only extracts some important features, hence, LBP can achieve higher result. However, LBP's running-time is also longer than RLDA.

5 Conclusion

In this paper, we have proposed a robust face recognition method for soft-errors by using a cross-layer approach. First, we have analyzed the effect of soft-error on a face recognition system. For the soft-errors in the images of the training set, the performance is degraded. Next, we have presented a novel face recognition method for the robust system against soft-errors by using a cross-layer approach. In the proposed method, the soft-errors are detected using a parity bit checker in the hardware layer and compensated in the application layer using a mean face. Simulation results have revealed that the proposed system have effectively compensated for the performance degradation due to soft errors.

A more systematic compensation method such as the compensation for the occluded images can be considered with the proposed method. It remains as a future work.

Acknowledgment

This research was supported by the Basic Science Research Program through the National Research Foundation of Korea (NRF) funded by the Ministry of Education (NRF-2015R1D1A1A01060917) and the Basic Science Research Program (No. 2015R1A1A1A05001065) through the National Research Foundation of Korea (NRF) funded by the Ministry of Science ICT and Future Planning, and also supported by the Human Resources Program in Energy Technology of the Korea Institute of Energy Technology Evaluation and Planning (KETEP) granted financial resource from the Ministry of Trade Industry and Energy, Republic of Korea (No. 20154030200830).

Bibliography

[1] Baumann, Robert (2005); Soft errors in advanced computer systems, *Design & Test of Computers*, ISSN 0740-7475, 22(3): 258-266.

[2] Lyons, D. (2000), *Sun Screen: Soft Error Issue in Sun Enterprise Servers*, www.members.forbes.com/global/2000/11130323026a.html.

[3] Sarah E. Michalak et al. (2005); Predicting the number of fatal soft errors in los alamos national laboratory's ASC Q supercomputer. *IEEE Transactions on Device and Materials Reliability*, ISSN 1530-4388 5(3): 329-335.

[4] Marc Tremblay, Yuval Tami. (1989); Support for fault tolerance in VLSI processors, *IEEE International Symposium on Circuits and Systems*, 1: 388-392.

[5] Borodin, Demid, Ben HH Juurlink. (2010); Instruction precomputation with memoization for fault detection, *Proceedings of the Conference on Design, Automation and Test in Europe*, ISBN 978-3-9810801-6-2, 1665-1668.

[6] Lee, Kyoungwoo, et al. (2006) Mitigating soft error failures for multimedia applications by selective data protection. *Proceedings of the 2006 international conference on Compilers, architecture and synthesis for embedded systems*, ISBN: 1-59593-543-6, 411-420.

[7] Nakka, Nithin, Karthik Pattabiraman, and Ravishankar Iyer. (2007); Processor-Level Selective Replication. *Proceedings of the 37th Annual IEEE/IFIP International Conference on Dependable Systems and Networks*, ISBN 0-7695-2855-4, 544-553.

[8] Lee, Kyoungwoo, et al. (2007); Partially protected caches to reduce failures due to soft errors in multimedia applications. *IEEE Transactions on Very Large Scale Integration (VLSI) Systems*, ISSN 1063-8210, 17(9): 1343-1347.

[9] Vera, Xavier, et al. (2009); Selective replication: A lightweight technique for soft errors. *ACM Transactions on Computer Systems*, ISSN 0734-2071, 27(4), DOI: 10.1145/1658357.1658359.

[10] Lee, Kyoungwoo, et al. (2008); Mitigating the impact of hardware defects on multimedia applications: a cross-layer approach. *Proceedings of the 16th ACM international conference on Multimedia*, ISBN: 978-1-60558-303-7, 319-328.

[11] Lu, Juwei et al. (2003); Regularized discriminant analysis for the small sample size problem in face recognition. *Pattern Recognition Letters*, ISSN 0167-8655, 24(16): 3079 - 3087.

[12] Lu, Juwei, Konstantinos N. Plataniotis, and Anastasios N. (2005); Regularization studies of linear discriminant analysis in small sample size scenarios with application to face recognition. *Pattern Recognition Letters*, ISSN 0167-8655, 26(2): 181-191.

[13] Center for Computational Vision and Control, Yale University, The Yale Face Database, http://cvc.yale.edu/projects/yalefaces/yalefaces.html.

[14] AT&T Laboratories Cambridge. The ORL database of faces, http://www.uk.research.att.com/facedatabase.html.

[15] Lu, Juwei, Kostantinos N. Plataniotis, and Anastasios N. (2003); Face recognition using LDA-based algorithms, *Neural Networks*, ISSN 1045-9227, 14(1): 195 - 200.

[16] Turk, Matthew, and Alex Pentland. (1991); Eigenfaces for recognition, *Journal of cognitive neuroscience*, ISSN 0898-929X, 3(1): 71-86.

[17] Andrew R. Webb (eds.)(2002); *Statistical Pattern Recognition, 2ndnd ed*, Wiley, ISBN: 978-0-470-85478-5.

[18] Choi, Sang-Il, Chong-Ho Choi, and Nojun Kwak. (2011); Face recognition based on 2D images under illumination and pose variations, *Pattern Recognition Letters*, ISSN 0167-8655, 32(4): 561-571.

[19] Choi, Sang-Il, and Gu-Min Jeong. (2011); Shadow compensation using fourier analysis with application to face recognition, *IEEE Signal Processing Letters*, ISSN 1070-9908, 18(1): 23-26.

INTERNATIONAL JOURNAL OF COMPUTERS COMMUNICATIONS & CONTROL
ISSN 1841-9836, 11(5):667-684, October 2016.

Degree of Project Utility and Investment Value Assessments

A. Kaklauskas

Arturas Kaklauskas
Vilnius Gediminas Technical University,
Vilnius, Lithuania
arturas.kaklauskas@vgtu.lt

Abstract: This article recommends a new INVAR Method for a multiple criteria analysis (Degree of Project Utility and Investment Value Assessments along with Recommendation Provisions). Its use can be for a sustainable building assessment. The INVAR Method can additionally assist in determining the investment value of a project under deliberation and provide digital recommendations for improving projects. Furthermore, the INVAR Method can optimize the selected criterion seeking that the project under deliberation would be equally competitive in the market, as compared to the other projects under comparison. The INVAR Method is additionally able to calculate the value that the project under deliberation should be for this project to become the best among those under deliberation. The case studies presented in this research are for demonstrating this developed method.
Keywords: COPRAS, DUMA and INVAR Methods, Multiple criteria analysis, Investment value, Utility degree, Recommendations.

1 Introduction

The increased awareness about building energy consumption and sustainability has resulted in the development of various means for predicting performance and rating sustainability. The Building Research Establishment Environmental Assessment Method (BREEAM) and Leadership in Energy and Environmental Design (LEED) are the most commonly used Performance Rating Systems [1]. According to Lee [2], statistical analysis reveals a moderate degree of agreement amongst the five schemes (BREEAM, LEED, CASBEE, BEAM Plus and the Chinese ESGB) on weights and ranks of weights allocated to five key assessment aspects. Ferreira [3] compare the criteria weighting process of four sustainable construction assessment tools (LiderA, SB ToolPT, Code for Sustainable Homes and LEED for Homes 2012) and show that the four different weighting sets are robust and generally similar.

A discussion on BREEAM and multiple criteria decision making follows as an example.

The hierarchical structures of key criteria and features of BREEAM Offices are by levels of Issues, Categories and Criteria. The top level contains ten distinct issues (the maximum number of obtainable credits appears in parentheses): Management (22), Health & Well-being (14), Energy (30), Transport (9), Water (9), Materials (12), Waste (7), Land Use & Ecology (12), Pollution (13), Innovation (10). The second level includes 69 categories and the third level – 114 criteria. Expert opinion determines the total number of credits for each category [4]. The use of the BREEAM credits scoring system is for determining the overall assessment grade, which may be Pass ($\geq 30\%$), Good ($\geq 45\%$), Very Good ($\geq 55\%$), Excellent ($\geq 70\%$) and Outstanding ($\geq 85\%$). No weightings are applied to credits awarded under different categories, as the number of obtainable credits assigned to each category already reflects the weight assigned to a category of assessment relative to other categories (as per [2]). For example, BREEAM (Code for Sustainable Homes) divides into nine categories, which subdivide into 34 issues (criteria). The award for each issue according to its performance can be a maximum number of credits. Then, for each category, the percentage of the total credits awarded for all its issues is determined. That percentage is

multiplied by its weight [5, 6]. In the end, the weighted values of all those nine categories are added up to obtain one of the six possible certification classes. Thus there is maintenance of the weighting structure with natural adjustments to market needs [3].

Multiple criteria decision making (MCDM) comprises a finite set of alternatives, which decision makers must select, evaluate or rank according to the weights of a finite set of criteria. The multiple criteria nature of the problem regarding energy performance assessment of buildings makes the MCDM Method ideal for coping with the complexity of the problem [7]. Berardi [8] emphasizes sustainability assessments in a built environment using multiple criteria rating systems. Other scientists [9–15] have also done multiple criteria and multi-aspect analysis of green buildings. COPRAS method [9, 10] was found to be an effective method for the green buildings assessment.

COPRAS (**Co**mplex **Pr**oportional **As**sessment Method) method was developed by E. Zavadskas and A. Kaklauskas [16]. The COPRAS method consists of five stages. Later, this method has been supplemented with a new "Method of **D**efining the **U**tility and **Ma**rket Value of a Property" (DUMA) developed by Kaklauskas [14], see [17]. The degrees of utility of the property considered as well as the market value of a property being valuated is determined in seven DUMA method stages.

The newly developed INVAR (Degree of Project Utility and Investment Value Assessments along with Recommendations) method by Kaklauskas integrates the philosophy of COPRAS and DUMA methods and offers the new opportunities. These new opportunities are as follows: defining the investment value of a project; providing digital tips for improving projects; optimizing a selected criterion; calculating the value of the project, which would permit it to be best among others under deliberation. Determining the priorities and utility degree of projects applying Stages 1-5 of the INVAR method are identical to COPRAS method. Other INVAR method 6-11 stages are different from the COPRAS and DUMA methods.

According to the International Valuation Standards [18], investment value is the value of an asset to the owner or a prospective owner for individual investment or operational objectives. As stated in Business Dictionary, investment value reflects the value of an asset to its owner, depending on his or her expectations and requirements. Schmidt [19] believes that investment value refers to the value to a specific investor, based on requirements of that investor, tax rate, and financing. The INVAR Method for an analysis of sustainable buildings (see case studies) use the same initial data as the BREEAM Method uses.

The INVAR Method was applied in research in various EU projects (INTELLITIES, IDES-EDU, Brita in Pubs); the author took part in the research. The results of these projects were discussed in a number of publications by the author in conjunction with colleagues [20–25].

The structure of this paper is as follows: after this introduction, Section 2 describes the INVAR Method. Section 3 follows with Case Studies. Finally the discussion and conclusions appear in Section 4.

2 INVAR Method

Assessing utility degree and the value of a project under investigation along with the establishment of priorities for this project's implementation is not especially difficulty. However, this first requires obtaining the numerical values and weights of criteria and applying multiple criteria decision making methods. The presentation of the analysis of projects under comparison is in the form of a grouped decision making matrix, where columns contain n alternative projects under consideration. Meanwhile the rows represent all the pertinent quantitative and conceptual information (see Table 1) [14].

Table 1: Grouped decision making matrix of the multiple criteria analysis of projects under comparison

Criteria describing the alternatives	*	Weights	Measurement units	Projects under comparison					
				a_1	a_2	...	a_j	...	a_n
X_1	z_1	q_1	m_1	x_{11}	x_{12}	...	x_{1j}	...	x_{1n}
X_2	z_2	q_2	m_2	x_{21}	x_{22}	...	x_{2j}	...	x_{2n}
X_3	z_3	q_3	m_3	x_{31}	x_{32}	...	x_{3j}	...	x_{3n}
...	...	...	...	...	...	...	...	...	...
X_i	z_i	q_i	m_i	x_{i1}	x_{i2}	...	x_{ij}	...	x_{in}
...	...	...	...	...	...	...	...	...	...
X_m	z_m	q_m	m_m	x_{m1}	x_{m2}	...	x_{mj}	...	x_{mn}
Conceptual information pertinent to projects (i.e., texts, drawings, graphics, video tapes and virtual and augmented realities)									

* – The sign $z_i(+(-))$ indicates that a greater (lesser) criterion value corresponds to greater (lesser) significance for stakeholders.

The INVAR method [14] assumes direct and proportional dependence of significance and a priority of investigated versions in a system of criteria that adequately describe the alternatives and on the values and weights of those criteria. Significance, priority, utility degree and investment value of alternatives, presentation of quantitative recommendations and optimization of different criteria are determined in 11 stages.

INVAR method stages 1-5 are identical as COPRAS method [9, 10, 14].

Stage 1. First, form a weighted, normalized decision making matrix D. The purpose of this stage is to receive dimensionless, weighted values from the comparative indices. Upon establishing the dimensionless values of the indices, all criteria, originally having different dimensions, become comparable. The following formula for this purpose is:

$$d_{ij} = \frac{x_{ij} \cdot q_i}{\sum_{j=1}^{n} x_{ij}}, \quad i = \overline{1,\ \mathrm{m}}; \quad j = \overline{1,\ \mathrm{n}}, \tag{1}$$

where x_{ij} is the value of the i-th criterion in the j-th alternative of a solution, m – the number of criteria, n – the number of the alternatives compared and q_i – the weight of the i-th criterion.

The sum of dimensionless, weighted index values d_{ij} of each criterion x_i is always equal to the weight q_i of this criterion:

$$q_i = \sum_{j=1}^{n} d_{ij}, \quad i = \overline{1,\ \mathrm{m}}; \quad j = \overline{1,\ \mathrm{n}}. \tag{2}$$

In other words, the value of the weight q_i of the investigated criterion proportionally distributes over all the alternative versions a_j according to their values x_{ij}.

Stage 2. The sums of weighted, normalized indices describing the j-th version are calculated. The minimizing of index S_{-j} and maximizing of index S_{+j} describe the versions. The lower value of minimizing indices is better (investment). The greater value of maximizing indices is better (management, health & wellbeing, energy, transport, water, materials, waste, land use & ecology,

pollution, innovation). The formula for calculating the sums is:

$$S_{+j} = \sum_{i=1}^{m} d_{+ij}; \quad S_{-j} = \sum_{i=1}^{m} d_{-ij}, \quad i = \overline{1,\ \mathrm{m}}; \quad j = \overline{1,\mathrm{n}}. \tag{3}$$

In this case, the values S_{+j} (the greater the project "pluses" of this value, the greater the satisfaction of interested parties) and S_{-j} (the lower the project "minuses" of this value, the better the goal attainments by interested parties) express the degree of goals attained by interested parties pertinent to each alternative project. In any case, the sum of the "pluses" S_{+j} and the "minuses" S_{-j} of all alternative projects is always respectively equal to all the sums of the weights of the maximizing and minimizing criteria:

$$\begin{aligned} S_+ &= \sum_{j=1}^{n} S_{+j} = \sum_{i=1}^{m}\sum_{j=1}^{n} d_{+ij}, \\ S_- &= \sum_{j=1}^{n} S_{-j} = \sum_{i=1}^{m}\sum_{j=1}^{n} d_{-ij}, \quad i = \overline{1,\ \mathrm{m}}, \quad j = \overline{1,\ \mathrm{n}}. \end{aligned} \tag{4}$$

This way the calculations performed may be additionally checked.

Stage 3. The basis pertinent to determining the significance (efficiency) of the versions under comparison constitutes the descriptions of the features pertinent to positive project "pluses" and to negative project "minuses". The formula for finding the relative significance Q_j of each project a_j is:

$$Q_j = S_{+j} + \frac{S_{-min} \cdot \sum\limits_{j=1}^{n} S_{-j}}{S_{-j} \cdot \sum\limits_{j=1}^{n} \frac{S_{-min}}{S_{-j}}}, \quad j = \overline{1,\ \mathrm{n}}, \tag{5}$$

where S_{-min} is the least value of the S_{-j}.

Stage 4. Determining the priorities of projects pertains to the axiom that the greater the Q_j the higher the efficiency (priority) of the project. The analysis of the method presented allows stating that it may be easily applied for evaluating projects and selecting the most efficient of them, while fully aware of the physical meaning of the process. Moreover, it allows formulating a reduced criterion Q_j directly proportional to the relative effect of the compared criteria values d_{ij} and weights q_i on the end result (see Table 2). Determining the utility degrees of the project under consideration as well as the investment value of a project under valuation occurs in seven stages.

Stage 5. The formula used for the calculation pertinent to project a_j utility degree N_j is:

$$N_j = (Q_j \div Q_{max}) \cdot 100\% \tag{6}$$

Here Q_j and Q_{max} are the significances of the project obtained from Equation 5.

The utility degree N_j of project a_j indicates the satisfaction level of the interested parties. The more goals achieved and the more important they are, the higher is the degree of project utility.

Stage 6. Calculating the investment value $x_{1j\ cycle\ e}$ of the project under deliberation a_j can be by means of e approximation. The problem may be stated as follows: What investment value $x_{1j\ cycle\ e}$ of the assessed project a_j will make it equally competitive on the market with the projects under comparison $(a_1 - a_n)$ (see Table 3)? The measurement of the value $x_{1j\ cycle\ e}$ is by price (Euro, British pounds, U.S. dollar or others) per square meter.

Table 2: Alternative results of a multiple criteria analysis

Criteria describing the alternatives	*	Weights	Measurement units	Projects under comparison					
				a_1	a_2	...	a_j	...	a_n
X_1	z_1	q_1	m_1	d_{11}	d_{12}	...	d_{1j}	...	d_{1n}
X_2	z_2	q_2	m_2	d_{21}	d_{22}	...	d_{2j}	...	d_{2n}
X_3	z_3	q_3	m_3	d_{31}	d_{32}	...	d_{3j}	...	d_{3n}
...	...	...	...	...	...	...	...	...	...
X_i	z_i	q_i	m_i	d_{i1}	d_{i2}	...	d_{ij}	...	d_{in}
...	...	...	...	...	...	...	...	...	...
X_m	z_m	q_m	m_m	d_{m1}	d_{m2}	...	d_{mj}	...	d_{mn}
Sums of weighted, normalized, maximizing indices (project "pluses") of the project				S_{+1}	S_{+2}	...	S_{+j}	...	S_{+n}
Sums of weighted, normalized, minimizing indices (project "minuses") of the project				S_{-1}	S_{-2}	...	S_{-j}	...	S_{-n}
Significance of the project				Q_1	Q_2	...	Q_j	...	Q_n
Priority of the project				P_1	P_2	...	P_j	...	P_n
Utility degree of the project (%)				N_1	N_2	...	N_j	...	N_n

* – The sign $z_i(+(-))$ indicates that a greater (lesser) criterion value corresponds to greater (lesser) significance for stakeholders.

Assuming $N_{je} > \sum_{j=1}^{n} N_j \div n$, then continue increasing the value $x_{1j\ cycle\ e}$ of this project a_j (see Table 3) by 1 unit costs per square meter (e.g., 1 Euro/m^2) and performing calculations as per Stages 1-6 with the gained decision making matrix until arriving at Inequality $N_{je} < \sum_{j=1}^{n} N_j \div n$ during e approximations. Then the final value $x_{1j\ cycle\ e}$ (while $N_{je} > \sum_{j=1}^{n} N_j \div n$) equals the investment value:

$$x_{1j\ iv} = x_{1j\ cycle\ e} \tag{7}$$

Assuming $N_{je} < \sum_{j=1}^{n} N_j \div n$, then continue reducing the value $x_{1j\ cycle\ e}$ of this project a_j (see Table 3) by 1 unit costs per square meter (e.g., 1 Euro/m^2) and performing calculations as per Stages 1-6 with the gained decision making matrix until arriving at Inequality $N_{je} > \sum_{j=1}^{n} N_j \div n$ during e approximations. Then the final value $x_{1j\ cycle\ e}$ (while $N_{je} < \sum_{j=1}^{n} N_j \div n$) equals the investment value (see Formula 7).

Stage 7. Performing the optimization of value x_{ij} is possible for any criterion during e approximations. It is necessary to determine, what the optimized value $x_{ij\ cycle\ e}$ should be for alternative a_j to be equally competitive in the market with the other alternatives under comparison $(a_1 - a_n)$ (see Table 3).

The optimization of value x_{ij} for any criterion pertinent to the project under deliberation a_j may be determined by performing complex analyses of the benefits and drawbacks of these projects. Development of a grouped, decision making matrix for the multiple criteria analysis of a project transpires by calculating the optimization of value x_{ij} during e approximations of a

Table 3: Grouped decision making matrix for the investment value assessment of project a_j (optimization of value x_{ij} for any criterion)

Criteria describing the alternatives	*	Weights	Measurement units	Project under valuation and projects under comparison					
				a_1	a_2	...	a_j	...	a_n
X_1	z_1	q_1	m_1	x_{11}	x_{12}	...	$\boldsymbol{x_{1j\ cycle\ e}}$	...	x_{1n}
X_2	z_2	q_2	m_2	x_{21}	x_{22}	...	x_{2j}	...	x_{2n}
X_3	z_3	q_3	m_3	x_{31}	x_{32}	...	x_{3j}	...	x_{3n}
...	...	...	...	...	...	...	...	...	...
X_i	z_i	q_i	m_i	x_{i1}	x_{i2}	...	$\boldsymbol{x_{ij\ cycle\ e}}$	...	x_{in}
...	...	...	...	...	...	...	...	...	...
X_m	z_m	q_m	m_m	x_{m1}	x_{m2}	...	x_{mj}	...	x_{mn}
N_{je}				N_{1e}	N_{2e}	...	$\boldsymbol{N_{je}}$	...	N_{ne}
Conceptual information pertinent to projects (i.e., texts, drawings, graphics, video tapes and virtual and augmented realities)									

* – The sign $z_i(+(-))$ indicates that a greater (lesser) criterion value corresponds to greater (lesser) significance for stakeholders.

project under valuation by the block-diagram, as presented in Figure 1. Use of Stages 1-5 and 7 accomplishes a set assessment of all the positive and negative features of a project (criteria, its values and weights). Perform calculations by using a grouped decision making matrix (see Table 3) and Stages 1-5 and 7.

The calculation for the corrected optimization of value $x_{ij\ cycle\ e}$ for any criterion a_j is by formula:

$$Assuming\ N_{je} > \sum_{j=1}^{n} N_j \div n\ and\ X_i\ is\ X_{i-},\ then\ x_{ij\ cycle\ e} = x_{ij\ cycle\ 0} \times (1 + e \times r), \quad e = \overline{1,\ \mathrm{r}}$$

$$Assuming\ N_{je} > \sum_{j=1}^{n} N_j \div n\ and\ X_i\ is,\ X_{i+},\ then\ x_{ij\ cycle\ e} = x_{ij\ cycle\ 0} \times (1 - e \times r), \quad e = \overline{1,\ \mathrm{r}} \tag{8a}$$

$$Assuming\ N_{je} < \sum_{j=1}^{n} N_j \div n\ and\ X_i\ is\ X_{i-},\ then\ x_{ij\ cycle\ e} = x_{ij\ cycle\ 0} \times (1 - e \times r), \quad e = \overline{1,\ \mathrm{r}}$$

$$Assuming\ N_{je} < \sum_{j=1}^{n} N_j \div n\ and\ X_i\ is\ X_{i+},\ then\ x_{ij\ cycle\ e} = x_{ij\ cycle\ 0} \times (1 + e \times r), \quad e = \overline{1,\ \mathrm{r}} \tag{8b}$$

where e is the number of cycles during which optimization value $x_{ij\ cycle\ e}$ can be determined by means of e approximation of the project under deliberation a_j. Meanwhile r is the amount by which the optimization value $x_{ij\ cycle\ e}$ of the project under deliberation a_j increases (decreeses) by means of cycling, to satisfy Inequality 9. $X_{i+}(X_{i-})$ – indicates that a greater (lesser) criterion value corresponds to a greater (lesser) significance for stakeholders.

Assuming the utility degree N_{je} of the project under deliberation a_j is greater than the average utility degree (Formula 8a) of the projects under comparison, it means project a_j is more beneficial on average than the projects under comparison are. For the project under deliberation

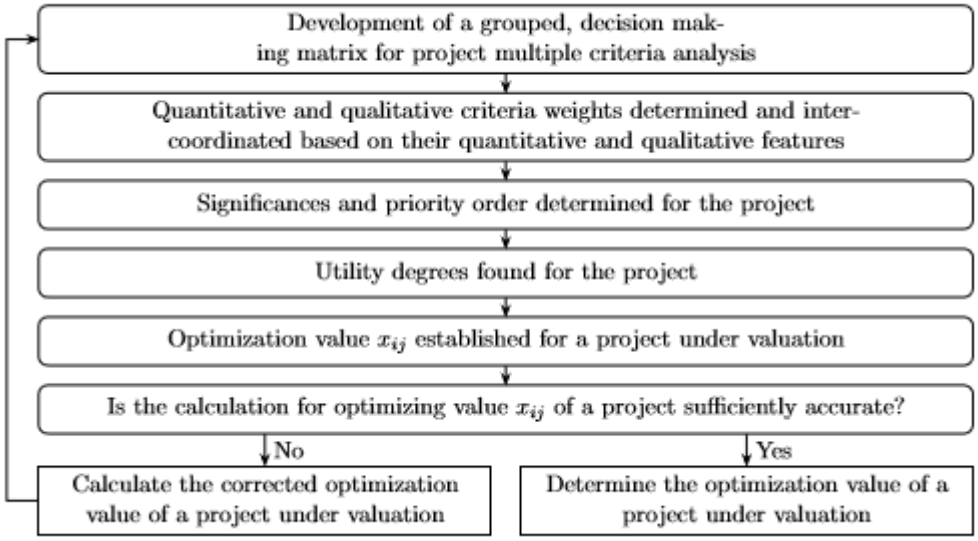

Figure 1: Block-diagram for a project's optimization value assessment

to be equally competitive on the market with the projects under comparison $(a_2 - a_n)$, reduce (increase) the value $x_{ij\ cycle\ e}$ of its criterion (see formula 8a) under deliberation by an r amount over e cycles, until satisfying the next inequality:

$$| N_{je} - \sum_{j=1}^{n} N_{je} \div n| < s \tag{9}$$

where s is the accuracy, by percentage, to be achieved by calculating the value $x_{ij\ cycle\ e}$ of the criterion under deliberation of project a_j. For example, given that $s = 0.5\%$, the number of calculation approximations will be lower than it is at $s = 0.1\%$.

The decision maker selects the r and s amounts depending on the accuracy needed for the calculations.

Assuming the utility degree N_{je} of the project under deliberation a_x is lower than the utility degree (Formula 8b) is on average of the projects under comparison, it means project a_j is less beneficial on average than the projects under comparison are. For the project under deliberation to be equally competitive on the market with comparison projects $(a_1 - a_n)$, increase (reduce) the value $x_{ij\ cycle\ e}$ of its criterion (see formula 8b) under deliberation by an r amount over e cycles, until satisfying Inequality 9.

Assuming Inequality 9 is not satisfied, it means the calculation of the value $x_{ij\ cycle\ e}$ of the criterion under deliberation of the project under valuation a_j is not sufficiently accurate, and it is necessary to repeat the approximation cycle. Thereby the corrected revision of value $x_{ij\ cycle\ e}$ of the project under valuation substitutes into a grouped decision making matrix of a project's multiple criteria analysis. Recalculate Formulae 1-8 until satisfying Inequality 9.

There is a determination of the optimization value $x_{ij\ cycle\ e}$ for any criterion of the project under valuation a_j. Upon satisfaction of Inequality 9, the application of the next, Formula 10 is to determine the optimization value $x_{ij\ cycle\ e}$ for any criterion of project a_j:

$$x_{ij\ opt\ value} = x_{ij\ cycle\ e} \tag{10}$$

Stage 9. Presenting indicator x_{ij} of the quantitative recommendation i_{ij} showing the percentage of a possible improvement in the value of indicator x_{ij} for it to become equal to the best value

$x_{i\,max}$ of criterion X_i is by the formula (see Tables 4 and 8):

$$i_{ij} = |x_{ij} - x_{i\,max}| \div x_{ij} \times 100\% \tag{11}$$

where i_{ij} is the quantitative recommendation i_{ij} of indicator x_{ij} showing the percentage of a possible improvement in the value of indicator x_{ij} for it to become equal to the best value $x_{i\,max}$ of criterion X_i. Meanwhile $x_{i\,max}$ is the value of the indicator of the best criterion X_i of the variants under comparison.

Stage 10. Indicator x_{ij} of quantitative recommendation r_{ij} showing the percentage of possible improvement of utility degree N_j of alternative a_j upon presentation of $x_{ij} = x_{i\,max}$. In other words, r_{ij} shows the percentage of possible improvement in the utility degree N_j of alternative a_j, assuming the value of indicator x_{ij} can be improved up to the best value $x_{i\,max}$ of the indicator of criterion X_i. The calculation is by formula:

$$r_{ij} = (q_i \times x_{i\,max}) \div (S_{-j} + S_{+j}) \times 100\% \tag{12}$$

where r_{ij} is the indicator x_{ij} of the quantitative recommendation r_{ij} showing the percentage of possible improvement in the utility degree N_j of alternative a_j, when $x_{ij} = x_{i\,max}$.

The submission of the quantitative recommendations i_{ij} and r_{ij} of value x_{ij} is in a matrix form (see Table 4).

Stage 11. This stage involves calculation by approximation e cycle to determine, what the value $x_{1j\,cycle\,e}$ should be for the project under deliberation a_j to become the best among those under deliberation. The problem may be stated as follows: What investment value $x_{1j\,cycle\,e}$ of the project under valuation a_j will make it the best on the market, as per the projects under comparison $(a_1 - a_n)$ (see Table 3)? The measurement of value $x_{1j\,cycl\,e}$ is by price (Euro, British pounds, U.S. dollar or others) per square meter. The reduction in the price of this project per 1 square meter unit (e.g., 1 Euro/m^2) continues until utility degree $N_{j\,e}$ of the project under deliberation a_j equals 100%.

3 Case Studies: Describing the sustainability of buildings assessed by the INVAR Method

3.1 Case Study 1: Calculations of the IKEA shopping center utility degree

A specific example appears next to demonstrate the INVAR method more clearly. Five buildings for retail operations a_1 – a_5 are under analysis for this case study. All the data come from the BREEAM pre-assessment reports and other sources pertinent to IKEA shopping center a_1 [26,27], Orchard Park District Centre a_2 [28], Friargate Court & Retail Units a_3 [29], Dorking Store a_4 [30] and Retail Foodstore a_5 [31]. Table 5 shows this data. Table 5 consists of criteria (BREEAM Sections and investment), their values (BREEAM Section scores and prices per square meter) and weights. The sum of the weights of all the BREEAM criteria (BREEAM Sections) is equal to one, because the calculation of the section score section has assessed the weighting. The weight of the Investment criterion is compared to the sum of the weights from all the other criteria (BREEAM Sections). This associates with the requirement that the price of these projects must equal the achieved results.

The basis for performing an assessment of the sustainability of retail buildings consists of the 11 INVAR method stages. These calculations appear in brief below.

Stage 1: The weighted normalized decision making matrix D is formed (see Formula 1, Table 5 and 9). The first formula for this purpose is:

Table 4: Quantitative recommendations submitted in a matrix form

Criteria describing the alternatives	*	Weights	Measurement units	Compared projects					
				a_1	a_2	...	a_j	...	a_n
X_1	z_1	q_1	m_1	x_{11}	x_{12}	...	x_{1j}	...	x_{1n}
Possible improvement of the value of indicator x_{1j} for it to become equal to the best value $x_{1\,max}$ of criterion X_1			%	i_{11}	i_{12}	...	i_{1j}	...	i_{1n}
Possible improvement of the utility degree N_j of alternative a_j upon presentation of $x_{1j} = x_{1\,max}$			%	r_{11}	r_{12}	...	r_{1j}	...	r_{1n}
X_2	z_2	q_2	m_2	x_{21}	x_{22}	...	x_{2j}	...	x_{2n}
Possible improvement in the value of indicator x_{2j} for it to become equal to the best value $x_{2\,max}$ of criterion X_2			%	i_{21}	i_{22}	...	i_{2j}	...	i_{2n}
Possible improvement of utility degree N_j of alternative a_j upon presentation of $x_{2j} = x_{2\,max}$			%	r_{21}	r_{22}	...	r_{2j}	...	r_{2n}
...	...	...	...	...	...	...	...	...	...
X_i	z_i	q_i	m_i	x_{i1}	x_{i2}	...	x_{ij}	...	x_{in}
Possible improvement in the value of indicator x_{ij} for it to be equal to the best value $x_{i\,max}$ of criterion X_i			%	i_{i1}	i_{i2}	...	i_{ij}	...	i_{in}
Possible improvement in utility degree N_j of alternative a_j upon presentation of $x_{ij} = x_{i\,max}$			%	r_{i1}	r_{i2}	...	r_{ij}	...	r_{in}
...	...	...	...	...	...	...	...	...	...
X_m	z_m	q_m	m_m	x_{m1}	x_{m2}	...	x_{mj}	...	x_{mn}
Possible improvement in the value of indicator x_{mj} for it to be equal to the best value $x_{m\,max}$ of criterion X_m			%	i_{m1}	i_{m2}	...	i_{mj}	...	i_{mn}
Possible improvement of utility degree N_j of alternative a_j upon presentation of $x_{mj} = x_{m\,max}$			%	r_{m1}	r_{m2}	...	r_{mj}	...	r_{mn}

$d_{11} = 10 \times 1774 \div (1774 + 1953.8 + 2370 + 1890 + 2045) = 1.7682$

$d_{12} = 1.1 \times 1953.8 \div (1774 + 1953.8 + 2370 + 1890 + 2045) = 1.9474$

$d_{13} = 1.1 \times 2370 \div (1774 + 1953.8 + 2370 + 1890 + 2045) = 2.3623$

The value of weight q_i of the investigated criterion distributes proportionally among retail buildings under analysis a_j according to their values x_{ij} (see Table 6). For example:

$q_2 = 0.1068 + 0.2403 + 0.1942 + 0.2403 + 0.2185 = 1.0$

$q_4 = 0.2709 + 0.1996 + 0.0925 + 0.1913 + 0.2457 = 1.0$

Stage 2: The sums of weighted normalized indices describing the j-th version are calculated. Formula 3 calculates the sums:

$S_{+1} = 0.1068 + 0.2293 + 0.2709 + 0.2056 + 0.0957 + 0.1186 + 0.13 + 0.1944 + 0.2557 + 0.0 = 1.607$

$S_{-1} = 1.7682\ etc.$

In any case, the sums of the "pluses" S_{+j} and "minuses" S_{-j} of all alternative projects are always, respectively, equal to all sums of the weights of maximizing and minimizing criteria (see Formula 4):

$S_+ = 1.607 + 1.7515 + 2.2967 + 1.6557 + 2.689 = 10.0$

$S_- = 1.7682 + 1.9474 + 2.3623 + 1.8838 + 2.0383 = 10.0$

Table 5: Initial data for INVAR method calculations (see [32])

Quantitative and qualitative information pertinent to retail buildings								
Criteria describing the retail buidlings	*	Measurement units	Weight	Compared retail buidlings				
				a_1	a_2	a_3	a_4	a_5
Investment	-	Euro/m^2	10	**1774**	1953.8	2370	1890	2045
Management	+	Points	1	4.8	10.8	8.73	10.8	9.82
Health & Wellbeing	+	Points	1	10.65	10	7.5	8.3	10
Energy	+	Points	1	14.44	10.64	**4.93**	10.2	13.1
Transport	+	Points	1	5.6	4.92	7.11	2.5	7.11
Water	+	Points	1	1.98	5.33	4	4.7	4.67
Materials	+	Points	1	4.12	5.77	9.62	4.8	10.42
Waste	+	Points	1	3.22	4.69	3.75	5.6	7.5
Land Use & Ecology	+	Points	1	7	6	7	7	9
Pollution	+	Points	1	5.8	3.08	6.15	3.8	3.85
Innovation	+	Points	1	0	0	2	0	2

* – The sign "+/-" indicates that a greater (lesser) criterion value corresponds to greater (lesser) significance for a user (stakeholder).

Stage 3: Formula 5 finds the relative significance Q_j of each project a_j (see Table 6):

$$Q_1 = 1.607 + \frac{1.7682 \times (1.7682 + 1.9474 + 2.3623 + 1.8838 + 2.0383)}{1.7682 \times (1.7682 \div 1.7682 + 1.7682 \div 1.9474 + 1.7682 \div 2.3623 + \\ + 1.7682 \div 1.8838 + 1.7682 \div 2.0383)} = 3.8478$$

$$Q_2 = 1.7515 + \frac{1.7682 \times (1.7682 + 1.9474 + 2.3623 + 1.8838 + 2.0383)}{1.9474 \times (1.7682 \div 1.7682 + 1.7682 \div 1.9474 + 1.7682 \div 2.3623 + \\ + 1.7682 \div 1.8838 + 1.7682 \div 2.0383)} = 3.7861$$

Stage 4: The greater the Q_j, the higher is the efficiency (priority) of the retail buildings: $Q_5 > Q_3 > Q_1 > Q_2 > Q_4$ (see Table 6: $4.6329 > 3.974 > 3.8478 > 3.7861 > 3.759$).

Stage 5: Formula 6 is used for calculating utility degree N_j:

$N_1 = (3.8478 \div 4.6329) \times 100\% = 83.05\%$
$N_2 = (3.7861 \div 4.6329) \times 100\% = 81.72\%$
$N_3 = (3.974 \div 4.6329) \times 100\% = 85.78\%$
$N_4 = (3.759 \div 4.6329) \times 100\% = 81.14\%$
$N_5 = (4.6329 \div 4.6329) \times 100\% = 100\%$

The results of a multiple criteria evaluation of the sustainable retail buildings under analysis appear in Table 6. Table 6 shows that the fifth version a_5 is the best by utility degree equaling $N_5 = 100\%$. The third version a_3 was second according to priority, and its utility degree was equal to $N_3 = 85.78\%$.

3.2 Case Study 2: Calculations of the IKEA shopping center investment value

The calculations of the investment value of the IKEA shopping center under valuation are according to data from Table 5 and Stages 1-6. Construction of the IKEA shopping center for furniture and home furnishings was in several stages. First, there was selection of a lot and then, the detailed planning for merging two lots. Upon approval of the detailed plan, there were

Table 6: INVAR method calculation results

Quantitative and qualitative information pertinent to retail buildings								
Criteria describing retail buidlings	*	Measurement units	Weight	Retail buidings under comparison				
				a_1	a_2	a_3	a_4	a_5
Investment	-	Euro/m^2	10	1.7682	1.9474	2.3623	1.8838	2.0383
Management	+	Points	1	0.1068	0.2403	0.1942	0.2403	0.2185
Health & Wellbeing	+	Points	1	0.2293	0.2153	0.1615	031787	0.2153
Energy	+	Points	1	0.2709	0.1996	0.0925	0.1913	0.2457
Transport	+	Points	1	0.2056	0.1806	0.261	0.0918	0.261
Water	+	Points	1	0.0957	0.2577	0.1934	0.2273	0.2258
Materials	+	Points	1	0.1186	0.1661	0.277	0.1382	0.3
Waste	+	Points	1	0.13	0.1894	0.1515	0.2262	0.3029
Land Use & Ecology	+	Points	1	0.1944	0.1667	0.1944	0.1944	0.25
Pollution	+	Points	1	0.2557	0.1358	0.2712	0.1675	0.1698
Innovation	+	Points	1	0	0	0.5	0	0.5
Sums of weighted, normalized maximizing indices (project "pluses") of the retail buildings				1.607	1.7515	2.2967	1.6557	2.689
Sums of weighted, normalized minimizing (projects "minuses") indices of the retail buildings				1.7682	1.9474	2.3623	1.8838	2.0383
Significance of the retail buildings				3.8478	3.7861	3.974	3.759	4.6329
Priority of the retail buildings				3	4	2	5	1
Utility degree of the retail buildings (%)				83.05%	81.72%	85.78%	81.14%	100%

* – The sign "+/-" indicates that a greater (lesser) criterion value corresponds to greater (lesser) significance for a user (stakeholder).

ecological tests conducted on the lot, followed by the design and then the arrangement of the lot. Some 2,400 units of garages and their foundations were demolished. The partial use of processed construction materials was for new construction, and the remaining materials, for transferring to other waste handlers. The amount of contaminated soil removed was 1,000 tons (see Figure 2). The retail buildings designed a parking lot for 953 automobiles of which 37 are for the disabled and 36 for families with children. The unused areas of the lot have planted greenery. The water supply of the city provides the water for the building. Centralized sewage networks of the city handle the captured wastewater from the facilities and rainwater that then flow into appropriate piping. The facility contains an installed, autonomous water heating system using solar energy. Air conditioning installations consist of efficient heat pumps and the ventilation – of productive recovery systems. The centralized heating network supplies heat. The design and construction of the building were according to customer specifications and were in consideration of permissible noise level maintenance. The project blueprint stipulates an external enclosure that insulates noise to no less than 32 dB. The main indicators of the project are total building area – 25,359 m^2, main area – 21,533 m^2, building height – 15.84 m, drinking water supply pipeline – 3,300 m, wastewater pipeline – 1,900 m and rainwater pipeline – 2,358 m. Air conditioning and ventilation systems are installed in the retail buildings for assuring hygienic stipulations for the facilities and the required, stable air temperature and moisture stipulations for the administrative facilities of the work environment. The lighting for the building divides into zones that are all independently controlled. Only certified materials having the least impact on the environment over the life of the building were used for the building's internal and external systems. The insulation materials used were those having the least impact on the environment but containing the best thermal insulation properties. The investment of the IKEA shopping center was 47.2 mln. Euro.

The aim was to establish, what the investment value $x_{11\,cycle\,e}$ (see the bold-faced numbers

Figure 2: IKEA shopping center for furniture and home furnishings: a) IKEA lot under arrangement and b) operating IKEA shopping center

in Tables 5 and 7) of the investment should be for a_1 to be equally competitive in the market against the other retail buildings under comparison (a_2 – a_5). Applications of INVAR Stages 1-6 serve to accomplish a set assessment of the positive and negative features of all these retail buildings.

As Table 7 shows, the most beneficial retail building during the 124^{th} cycle of approximation ($e = 124$), according to its designation for use, is a_5 ($N_{5\,124} = 100\%$). The second under comparison that is most beneficial is a_1 ($N_{1\,124} = 86.43\%$) and the third under comparison – a_3 ($N_{3\,124} = 85.77\%$). The calculated utility degrees of the sustainable retail buildings under comparison make it apparent that the cost $x_{11\,124} = 1650$ (Euro/m^2) for IKEA shopping center under valuation a_1 is still too high. Therefore this retail buildings a_1 is not equally competitive in the market, as compared to the sustainable retail buildings under comparison, once the assessment of their sets of specific positive and negative features is complete. Stage 6 also affirms the same fact: the calculation of the investment value for retail building a_1 during the 124^{th} cycle of approximation was not sufficiently accurate (see column 9 in Table 7). Table 7 shows that Inequality (see column 9 in Table 7) was unsatisfactory for the first 144 cycles. The determination of the investment value of a_1 under valuation with respect to the other retail buildings under comparison appears in the final, 145^{th} approximation cycle – $N_{1\,145cycle} = 87.04\%$ ($N_{2\,145cycle} = 81.53\%$, $N_{3\,145cycle} = 85.77\%$, $N_{4\,145cycle} = 80.91\%$ and $N_{5\,145cycle} = 100\%$). In the 144^{th} approximation cycle, the utility degree of project under comparison a_1 calculates at $N_1 = 87.02\%$. The degrees of utility for the retail buildings under analysis show that a_1 under valuation in the 145^{th} approximation cycle is more beneficial than is the second retail building under comparison a_2 by 5.51% and more beneficial than retail building under comparison a_4 by 6.13%. There was a revision of the investment value x_{11} in every cycle (from $x_{11\,cycle\,0} = 1774$ Euro/m^2), each by 1 Euro/m^2 by size until Inequality (see column 9 in Table 7) was satisfied ($x_{11\,cycle\,145} = 1629$ Euro/m^2). Thus investment value $x_{11\,cycle\,e}$ (respectively, 1774, ..., 1629) is checked for accuracy pertinent to retail building a_1 by placing them into the bold cell of the decision making matrix (see Table 5). All calculations were repeated according to Stages 1-6 until Inequality (see column 9 in Table 7) was satisfied in the 145^{th} cycle. Table 7 shows that the calculations of investment value $x_{11\,cycle\,e}$ become more and more accurate with each, next e approximation cycle for retail building a_1 under analysis.

3.3 Case Study 3: Provision of recommendations

The results of the provision of recommendations by applying Stages 1-5, 9 and 10 of the INVAR method for the retail buildings appear in Table 8. Initial data for the calculations are presented in Table 5. Meanwhile, the recommendations for bettering the criteria for these retail buildings under comparison appear in Table 8. Recommendations arrive in a matrix (see Table

Table 7: Revised changes in value and investment value determinations for IKEA shopping center under valuation a_1

Approximation cycle	*	Utility degree change in retail buildings under deliberation by rationalizing the corrected value $x_{11\,cycle\,e}$ of building a_1					**	***
		Utility degree N_{1e}	Utility degree N_{2e}	Utility degree N_{3e}	Utility degree N_{4e}	Utility degree N_{5e}		
1	2	3	4	5	6	7	8	9
0	**1774**	83.05%	81.72%	85.78%	81.14%	100%	86.34%	$\lvert -4.11\%\rvert < 0.02\%$
...	**...**	...	...	...	...	...	...	...
124	**1650**	86.43%	81.56%	85.77%	80.95%	100%	86.94%	$\lvert -0.64\%\rvert < 0.02\%$
...	**...**	...	...	...	...	...	...	...
134	**1640**	86.72%	81.55%	85.77%	80.93%	100%	87.00%	$\lvert -0.34\%\rvert < 0.02\%$
...	**...**	...	...	...	...	...	...	...
144	**1630**	87.02%	81.53%	85.77%	80.91%	100%	87.05%	$\lvert -0.03\%\rvert < 0.02\%$
145	$\boldsymbol{x_{1j\,iv}}$ = **1629**	87.04%	81.53%	85.77%	80.91%	100%	87.05%	$\lvert -0.01\,\%\rvert < 0.02\,\%$

* - revised changes in value and investment value $x_{11\,cycle\,e}$ (Euro/m^2) of IKEA shopping center under valuation a_1.

** $(N_{1e} + N_{2e} + N_{3e} + N_{4e} + N_{5e}) \div 5$

*** Inequality to determine, whether the calculation of revised value $x_{11\,cycle\,e}$ of IKEA shopping center under valuation a_1 is sufficiently accurate.

8) by using Formulae 10 and 11 during Stages 9 and 10. Every window in Table 8 describing Alternative a_j consists of three parts: x_{ij} – the value of the i-th criterion (X_i) in the j-th alternative; quantitative recommendation i_{ij} showing the percentage of a possible improvement in the value of indicator x_{ij} for it to become equal to the best value $x_{i\,max}$ of criterion X_i ($x_{ij} = x_{i\,max}$); and quantitative recommendation r_{ij} showing the percentage of possible improvement of utility degree N_j of alternative a_j upon presentation of $x_{ij} = x_{i\,max}$. If, for example, it would be possible to improve the assessment of the Health & Wellbeing criterion for building a_3 ($i_{33} = 42\%$) from the $x_{33} = 7.5$ value achieved up to the best value for a_1 ($x_{34} = 10.65$), then the utility degree N_3 for building a_3 would increase by $r_{33} = 2.1\%$. Analogically, if the assessment of the Energy criterion for building a_3 ($x_{43} = 5.1$) could be improved up to the amount of the best assessment for building a_1 ($x_{41} = 14.44$), then the effectiveness of the criterion Energy for building a_3 would increase by $i_{43} = 183.14\%$, and the utility degree N_3 would increase by $r_{43} = 9.1569\%$ (see Table 8).

3.4 Case Study 4: Optimization of the value

This example, based on Stages 1-5 and 7, will determine, what the value $x_{43\,cycle\,e}$ of the BREEAM Energy Section (see the number in bold in Table 5) must be for project a_3 to be equally competitive on the market, as compared to the other retail buildings under comparison (a_1, a_2, a_4, a_5) by a set assessment of all their positive and negative features. It is possible to optimize any one of the criteria or their composite parts by the new INVAR method, which deliberates the sustainability of retail buildings under analysis in an integrated manner by using Pre-assessment Reports. The optimization of the score of the Energy Section of BREEAM, which appears next, will serve as an example (see Table 5).

The determination of the optimized score $x_{43\,cycle\,e}$ for the project under valuation a_3 appears

Table 8: Quantitative recommendations submitted in a matrix form

Quantitative and qualitative information pertinent to alternatives								
Criteria describing the alternatives	*	Measurement units	Weight	Alternatives				
				a_1	a_2	a_3	a_4	a_5
Health & Wellbeing	+	Points	1	$\boldsymbol{x_{31}} = 10.65$ (0%) (0%)	10 (6.5%) (0.325%)	$\boldsymbol{x_{33}} = 7.5$ ($\boldsymbol{i_{33}} = 42\%$) ($\boldsymbol{r_{33}} = 2.1\%$)	8.3 (28.31%) (1.4157%)	10 (6.5%) (0.325%)
Energy	+	Points	1	$\boldsymbol{x_{41}} = 14.44$ (0%) (0%)	10.64 (35.71%) (1.7857%)	$\boldsymbol{x_{43}} = 5.1$ ($\boldsymbol{i_{43}} = 183.14\%$) ($\boldsymbol{r_{43}} = 9.1569\%$)	10.2 (41.57%) (2.0784%)	13.1 (10.23%) (0.5115%)

*- The sign "+/-" indicates that a greater (lesser) criterion value corresponds to a greater (lesser) significance for a user (stakeholder).

in Table 9. The formulation of this task is the following: determine, what the optimized score $x_{43\,cycle\,e}$ should be for building under valuation a_3 for it to be equally competitive in the market, as compared with the sustainable retail buildings (a_1, a_2, a_4, a_5) after a complex assessment of their positive and negative features. The decision making matrix (see Table 5), the amalgamated block diagram submitted in Figure 1 and the calculations performed by Stages 1-5 and 7 serve as the basis for these calculations. The results of the e approximation cycles of these calculations appear in Table 9. The aim was to establish, what the score $x_{43\,cycle\,e}$ should be (see the numbers

Table 9: What score $x_{43\,cycle\,e}$ should be for building a_3 to be equally competitive in the market with other retail buildings under comparison (a_1, a_2, a_4, a_5)

Approximation cycle	Score $x_{43\,cycle\,e}$	Utility degree N_{1e}	Utility degree N_{2e}	Utility degree N_{3e}	Utility degree N_{4e}	Utility degree N_{5e}	*	**
0	**4.93**	83.05%	81.72%	85.78%	81.14%	100%	86.34%	$\lvert -0.7\%\rvert > 0.1\%$
...	**...**	...	...	...	...			...
7	**5**	83.05%	81.72%	85.81%	81.14%	100%	86.34%	$\lvert -0.67\%\rvert > 0.1\%$
...	**...**	...	...	...	...			...
57	**5.5**	83.04%	81.72%	86.03%	81.14%	100%	86.39%	$\lvert -0.45\%\rvert > 0.1\%$
...	**...**	...	...	...	...			...
107	**6**	83.02%	81.72%	86.25%	81.14%	100%	86.43%	$\lvert -0.19\%\rvert > 0.1\%$
...	**...**	...	...	...	...			...
157	**6.5**	83.01%	81.72%	86.47%	81.14%	100%	86.47%	$\lvert 0\%\rvert < 0.1\%$

* $(N_{1e} + N_{2e} + N_{3e} + N_{4e} + N_{5e}) \div 5$

** Inequality 9 to determine, whether the calculation of revised value $x_{43\,cycle\,e}$ of under valuation a_3 is sufficiently accurate.

in bold in Tables 5 and 9) for building a_3 to be equally competitive in the market with other retail buildings under comparison (a_1, a_2, a_4, a_5). Applications of INVAR Stages 1-5 and 7 serve to accomplish a set assessment of the positive and negative features of all these retail buildings. Table 9 shows that Inequality 9 was unsatisfactory for the first 156 cycles. The score x_{43} was increased in every cycle (from $x_{43\,cycle\,0} = 4.93$) by an amount of 0.01 until Inequality 9 was satisfied ($x_{43\,cycle\,157} = 6.5$). Then scores $x_{43\,cycle\,e}$ (respectively, 4.94, ... and 6.5) are checked for accuracy pertinent to building a_3 by placing these results into the bold cell of the decision making matrix (see Tables 5 and 9). All the calculations were repeated according to Formulae Stages 1-5 and 7 until Inequality 9 was satisfied in the 157^{th} cycle. Table 9 shows the

Table 10: What should the value $x_{11\,cycle\,e}$ of IKEA shopping center be for this project to become the best among those under deliberation?

Approxi-mation cycle	Investment value $x_{11\,cycle\,e}$ (Euro/m^2)	Utility degree				
		N_{1e}	N_{2e}	N_{3e}	N_{4e}	N_{5e}
0	1774	83.05%	81.72%	85.78%	81.14%	100%
124	1650	86.43%	81.56%	85.77%	80.95%	100%
134	1640	86.72%	81.55%	85.77%	80.93%	100%
174	1600	87.92%	81.49%	85.77%	80.86%	100%
274	1500	91.14%	81.34%	85.77%	80.68%	100%
424	1350	96.73%	81.07%	85.76%	80.37%	100%
474	1300	98.84%	80.97%	85.76%	80.25%	100%
484	1290	99.27%	80.95%	85.76%	80.23%	100%
494	1280	99.72%	80.93%	85.76%	80.20%	100%
499	1275	99.94%	80.92%	85.76%	80.19%	100%
504	1270	100%	80.78%	85.62%	80.04%	99.84%

calculations of score $x_{43\,cycle\,e}$ becoming more and more accurate with each, next approximation cycle for building under analysis a_3.

3.5 Case Study 5: What should the value of the IKEA shopping center be for this project to be the best among those under deliberation?

The calculations in this example are by approximation e cycle to determine, what the value $x_{11\,cycle\,e}$ of IKEA shopping center a_1 should be for this project to become best among those under deliberation a_1-a_5. The price of this project continues being reduced by 1 Euro/m^2 until N_{1e} becomes equal to 100% (Stages 1-5 and 11).

Table 10 shows that $N_{1e} = 100\%$ had not been satisfied over 503 cycles. That is the reason the investment value $x_{11\,cycle\,e}$ of the project under valuation a_1, which had been revised 504 times, was entered into the decision making matrix (Table 5) for the multiple criteria analysis of retail building. Table 10 shows that, in each following approximation cycle, the calculation of the revised investment value $x_{11\,cycle\,e}$ of building under valuation a_1 became more and more accurate.

All the calculations by Stages 1-5 and 11 were repeated, until $N_{1e} = 100\%$ was satisfied in the 504^{th} cycle. It can be stated that this project can become the most effective among the projects under comparison, once the value $x_{11\,cycle\,e}$ of the IKEA shopping center = 1270 Euro/m^2.

4 Conclusion

This article recommends a new multiple criteria analysis, the INVAR method (Degree of project Utility and investment value Assessments along with recommendation provisions). INVAR method stages 1-5 are identical as COPRAS method [9, 10, 14]. It generates conditions to assess management, health & wellbeing, energy, transport, water, materials, waste, land use

& ecology, pollution, innovation, comfort, quality of life and aesthetics as well as its technical, economic, legal/regulatory, educational, social, cultural, ethical, psychological, emotional, religious and ethnic aspects in conformity with requirements and opportunities for clients, designers, contractors, users and other stakeholders. The systems and the values and weights of the quantitative and qualitative criteria express these requirements. The INVAR method allows determining the strongest and weakest aspects of each project pertinent to a sustainable building and its constituent parts. Performance of the analyses is to learn by what degree one alternative is better than is another. Furthermore, this discloses the details, why this is so. The practical case studies presented in this research validate this developed method. An analysis of the results reached by the INVAR method permits making the following claims:

- The INVAR method can determine the utility degree and investment values of the projects under deliberation.
- The INVAR method can provide digital tips for improving projects.
- The INVAR method can define, what the value of a selected criterion needs to be for the project under deliberation to be equally competitive in the market, as compared with others under comparison after a set assessment of all their positive and negative features.
- The INVAR method can calculate, what the value of the project under deliberation should be for this project to become the best among others under deliberation.

Acknowledgment

The author thanks Ms. Vijole Arbas for her help in translating to English and editing this article.

Bibliography

[1] Schwartz, Y., Raslan, R. (2013), Variations in results of building energy simulation tools, and their impact on BREEAM and LEED ratings: A case study, *Energy and Buildings*, 62: 350-359.

[2] Lee, W.L. (2013), A comprehensive review of metrics of building environmental assessment schemes, *Energy and Buildings* 62: 403-413.

[3] Ferreira, J., Pinheiro, M. D., de Brito, J. (2014), Portuguese sustainable construction assessment tools benchmarked with BREEAM and LEED: An energy analysis, *Energy and Buildings*, 69: 451-463.

[4] Howard, N. (2005), Building environmental assessment methods: in practice, *The 2005 World Sustainable Building Conference, Tokyo*, 27-29.

[5] Communities and Local Government, Code for Sustainable Homes – *Technical Guide, Communities and Local Government Publications*, London, United Kingdom, 2010, 292 p.

[6] Forbes, D., Smith, S., Horner, R. (2008), Investigating the weighting mechanism in BREEAM Ecohomes, *CIB W055 – W065 Joint International Symposium: Transformations through Construction*, Dubai, United Arabic Emirates.

[7] Kabak, M., Kose, E., KÄąrÄąlmaz, O., Burmaoglu, S. (2014), A fuzzy multi-criteria decision making approach to assess building energy performance, *Energy and Buildings*, 72: 382-389.

[8] Berardi, U. (2015), Chapter 15 – Sustainability assessments of buildings, communities, and cities, *Assessing and Measuring Environmental Impact and Sustainability*, 497-545.

[9] Mulliner, E., Smallbone, K., Maliene, V. (2013), An assessment of sustainable housing affordability using a multiple criteria decision making method, *Omega*, 41 (2): 270-279.

[10] Mulliner, E., Malys, N., Maliene, V.(2016), Comparative analysis of MCDM methods for the assessment of sustainable housing affordability, *Omega*, 59 (Part B) , 146-156.

[11] Banaitiene, N., Banaitis, A., Kaklauskas, A., Zavadskas, E. K. (2008), Evaluating the life cycle of a building: A multivariant and multiple criteria approach, *Omega*, 36(3): 429-441.

[12] Li, Y., Yu, W., Li, B., Yao, R. (2016), A multidimensional model for green building assessment: A case study of a highest-rated project in Chongqing,*Energy and Buildings*, 125(1): 231-243.

[13] Balaban, O., de Oliveira, J. A. P. (2016), Sustainable buildings for healthier cities: assessing the co-benefits of green buildings in Japan, *Journal of Cleaner Productionl*, In Press, Corrected Proof 2016.

[14] Kaklauskas, A. (1999), *Multiple criteria decision support of building life cycle*, Research report presented for habilitation (DrSc): Technological sciences, civil engineering (02T), Vilnius Gediminas Technical University, Vilnius: Technika, 1999, 118 p.

[15] Kaklauskas, A. (2015), Biometric and Intelligent Decision Making Support. *Series: Intelligent Systems Reference Library, XII*. Springer-Verlag, Berlin, 81 , 228 p.

[16] Zavadskas, E. K., Kaklauskas, A., V. Sarka (1994), The new method of multicriteria complex proportional assessment of projects. *Technological and economic development of economy*, 3: 131-139.

[17] Method of Defining the Utility and Market Value of a Property, https://www.researchgate.net/publication/301771443

[18] International Valuation Standards, International Valuation Standards Council, 2011, 128 p.

[19] Schmidt, R. Difference between Market Value and Investment Value in Commercial Real Estate, *Property Metrics*, 2014.

[20] Kaklauskas, A., Zavadskas, E. K., Raslanas, S.(2005), Multivariant design and multiple criteria analysis of building refurbishments, *Energy and Buildings*, 37(4): 361-372.

[21] Kaklauskas, A., Zavadskas, E. K., Raslanas, S., Ginevicius, R., Komka, A., Malinauskas, P. (2006), Selection of low-e windows in retrofit of public buildings by applying multiple criteria method COPRAS: a Lithuanian case, *Energy and Buildings*, 38(5):454-462.

[22] Kaklauskas, A., Kelpsiene, L., Zavadskas, E. K., Bardauskiene, D., Kaklauskas, G., Urbonas, M., Sorakas, V. (2011), Crisis management in construction and real estate: Conceptual modeling at the micro-, meso- and macro-levels. *Land Use Policy*, 28(1): 280-293.

[23] Kaklauskas, A., Rute, J., Zavadskas, E. K., Daniunas, A., Pruskus, V., Bivainis, J., Gudauskas, R., Plakys, V. (2012), Passive house model for quantitative and qualitative analyses and its intelligent system, *Energy and Buildings*, 50: 7-18.

[24] Kanapeckiene, L., Kaklauskas, A., Zavadskas, E. K., Raslanas, S. (2011), Method and system for Multi-Attribute Market Value Assessment in analysis of construction and retrofit projects. *Expert Systems with Applications*, 38(11): 14196-14207.

[25] Kaklauskas, A., Zavadskas, E. (2007), Decision support system for innovation with a special emphasis on pollution, *International Journal of Environment and Pollution*, 30(3-4): 518-528.

[26] Jurgaitis, J. (2014), Building environmental impact assessment methods application in Lithuania. Master thesis, Construction Technology and Management study program. Supervisor: A. Kaklauskas, 98 p.

[27] Kajauskaite, E. (2013), Moderniu inzineriniu sprendimu ir darnios statybos pavyzdys, *Structum*, 46-54.

[28] Gifford (2010), Orchard Park District Centre, Hull. BREEAM pre-assessment summary. Report No. 17318-SU001, 30 p.

[29] Scott Hughes Design (2013), Friargate Court & Retail Units, Preston. Stage B, BREEAM Strategy & Pre-Assessment Report. Project number: 2604, 102 p.

[30] Morrisons (2011), Dorking Store. BREEAM pre-assessment, 14 p.

[31] S. R. Fall (2013), New Retail Foodstore. BREEAM pre-assessment report, 47 p.

[32] Calculations with INVAR method. `http://iti.vgtu.lt/ilearning/simpletable.aspx?sistemid=675`

INTERNATIONAL JOURNAL OF COMPUTERS COMMUNICATIONS & CONTROL
ISSN 1841-9836, 11(5):685-696, October 2016.

Application of Visual Servo Control in Autonomous Mobile Rescue Robots

H. Lang, M.T. Khan, K.-K. Tan, C.W. de Silva

Haoxiang Lang
Department of Mechanical Engineering,
University of Ontario Institute of Technology.
haoxiang.lang@uoit.ca

Muhammad Tahir Khan*
Institute of Mechatronics,
University of Engineering and Technology, Peshawar, Pakistan.
Corresponding author: tahir@uetpeshawar.edu.pk

Kok-Kiong Tan
Department of Electrical and Computer Engineering,
National University of Singapore.
Address: 4 Engineering Drive 3 Singapore 117576, Singapore.
eletankk@nus.edu.sg

Clarence W. de Silva
Department of Mechanical Engineering,
University of British Columbia.
desilva@mech.ubc.ca

Abstract: Mobile robots that integrate visual servo control for facilitating autonomous grasping and manipulation are the focus of this paper. In view of mobility, they have wider application than traditional fixed-based robots with visual servoing. Visual servoing is widely used in mobile robot navigation. However, there are not so many report for applying it to mobile manipulation. In this paper, challenges and limitations of applying visual servoing in mobile manipulation are discussed. Next, two classical approaches (image-based visual servoing (IBVS) and position-based visual servoing (PBVS)) are introduced aloing with their advantages and disadvantages. Simulations in Matlab are carried out using the two methods, there advantages and drawbacks are illustrated and discussed. On this basis, a suggested system in mobile manipulation is proposed including an IBVS with an eye-in-hand camera configuration system. Simulations and experimentations are carried with this robot configuration in a search and rescue scenario, which show good performance.
Keywords: Mobile Robots, Visual Servoing, Robot Control, Search and Rescue.

1 Introduction

Research and applications of mobile robots have drawn much attention in the robotics community because the emphasis of robotic research appears to have shifted from structured industrial environments to dynamic and partially-known natural environments (e.g., homes, cities, planet surfaces and deep sea). Mobile robots can be implemented in homecare, surveillance, exploration, search and rescue tasks where the working environments may be too hazardous for human workers. In such scenarios, robots are expected to have extensive autonomous ability and human capabilities, yet not suitable or impractical for human presence.

Examples for the necessity of applying autonomous search and rescue robots in practical applications were highlighted in the destruction of the World Trade Center in 2001 due to terrorist

attack in New York City and the damage caused by earthquake and tsunami in Sendai, Japan in 2012. In both incidents, not only did large numbers of victims lose their life, but significant number of rescues scarified their life in rescuing work. They were mainly caused by the search and rescue activities after those incidents because of dangerous environments and lacking of heavy-duty tools. Generally speaking, in any incidents, rescuers have about forty-eight hours to save humans in incident sciences. However, most of these time is wasted due to lacking of necessary resources or heavy-duty equipment for accessing damaged or contagious areas that are not suitable for humans. In this scenario, search and rescue robots have the advantages of being deployed instantaneously, and operating in any given working environments without human engagement.

An autonomous robot that is able to operate in unknown and dynamic workspace will have significant benefits in the above mentioned two cases in the areas of search and rescue. However, there is no such robot available in the market yet because of existing challenges in developing such systems in terms of both hardware and software. This paper focus on the control software of such system and emphasis on examining two traditional visual servoing methodologies along with their challenges in applying them in autonomous mobile manipulation applications. Two traditional methods of visual servo control are presented and examined through simulations; and comparative evaluation of these two methods are discussed, respectively. In the application of visual servoing, a suitable method for autonomous mobile rescue robots is suggested. Simulations and experimentations are carried out and demonstrated the effectiveness of the system and the methodologies.

2 Two Traditional Visual Servoing Methods

Vision-based mobile manipulation systems typically utilize camera with image processing and computer vision algorithms as its main sensory feedback in the control loop of mobile bases and their manipulators. This approach is called a visual servo control system or visual servoing, which involves many related research areas including image processing, computer vision, dynamic system modeling of robots and nonlinear control theory [1].

Vision sensors, usually cameras, are powerful sensors because they mimic human sense of vision and provide non-contact measurement of workspace. Furthermore, they can provide various types of sensed data such as pose, distance and objects in camera scenes. Because of these advantages of vision sensory, researchers have paid great attention to implement it in practical applications, especially in robotics ares. However, the image capturing hardware and processing software took seconds in producing image and doing analysis that makes real-time control impossible to apply in robotic applications [2]. Originally, Sanderson and Weiss invented a hierarchical Dynamic Look-an-Move structure to overcome the inefficiency of the vision system [3] where vision was utilized to provide control inputs to the joint-level controller. Then, the sub-control system utilized the joint feedback to internally stabilize the robot.

Nowadays, computer vision has benefited from the rapid development of computer technologies and image sensing hardware (CCD and CMOS) in terms of the processing time. Therefore, it makes possible for so called direct visual servoing where it heavily relies on the speed of vision processing for computing joint inputs [4] in robot control. Since 1990s, the term "visual servoing" (more appropriately, visual servo control) has accepted as a generic description of robotic system that has a visual feedback control loop. The subject has been studied in various forms for over twenty years now, with applications ranging from initially simple pick-and-place tasks to complex, real-time and autonomous mobile manipulation applications.

Visual servo control of mobile robots has drawn more attentions recently. When compared to the traditional fixed-base manipulators, one advantage of mobile robots is their ability to

navigate in a large workspace because of its mobility. A mobile manipulation system has better maneuverability and larger coverage of the workspace, which make it more widely applicable than a traditional fixed-based manipulator.

Autonomous navigation control of mobile robots employs the application of visual servo control. There is limited activity in this context possibly because mobile manipulation requires more accurate positioning performance and hence it is rather challenging. Some examples of visual servo application in mobile navigation are indicated in [5, 6]. The research and physical demonstration of visual servoing in mobile manipulation have been mostly limited two degrees of freedom DOF [7] and simplified robot models [8].

3 Developments in Visual Servoing Systems

In general, traditional visual servoing can be categorized into image-based and position-based approaches based on how the vision information is utilized [2]. The two traditional approaches can share similar control block diagrams with difference in reference of the control system and the processed information acquired from camera (Figure 1).

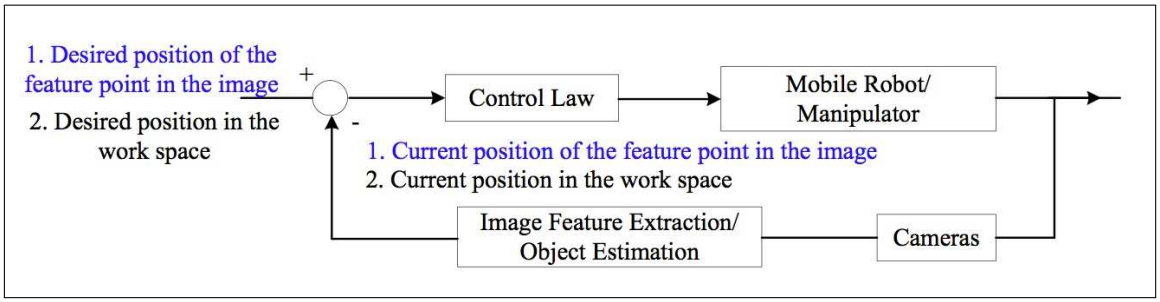

Figure 1: Block diagram of difference between position-based and Image-based visual servoing.

The objective of the controller is to minimize either the position error of the image or the position error of the object in the 3D space for two different methods respectively by controlling the motion of the robot joints. The error can be defined as follows:

$$e(t) = s(i(t), c) - s_r \tag{1}$$

where $e(t)$ is is the error between desired and measured positions; s is the measurement from the image or pose estimation using computer vision; $i(t)$ is the image data from the camera; c is mathematic model of the camera; and s_r is the reference of the control system. $s(i(t), c)$ and s_r can be decided in detail depending on the type of visual servoing that is utilized. Once they are decided, a velocity controller of robot joints can be designed by

$$\dot{s} = L\xi_c^c \tag{2}$$

where $\dot{s}$ is the velocity of the target objects (targets in the image from the camera in IBVS approach and 3D pose of the camera through 3D reconstruction in PBVS approach); L is the interaction matrix; and ξ_c^c is the velocity vector of the camera with respect to its own coordinate frame. Combining equations (1) and (2), the error dynamic equation can be written below:

$$\dot{e}(t) = L\xi_c^c \tag{3}$$

where $\dot{e}(t)$ is the time variation of the error. The square-of-error norm can be utilized to generate the control law as a candidate Lyapunov function:

$$\dot{s} = L^{-1}(-ke) \tag{4}$$

3.1 Image-based Visual Servoing Approach

The objective of image-based visual servoing (IBVS) is to decrease position errors of target objects in images acquired from the camera by moving each joint of the robot. The controller will continuously adjust the speeds of the robot joints based on controller outputs so that the trajectories of the target objects (u_i, v_i) navigate toward the desired positions (u_{di}, v_{di}) on camera sciences. The error vector of the target objects in the image plane is given by

$$e = \begin{bmatrix} u - u_d \\ v - v_d \end{bmatrix} = \begin{bmatrix} -s_x(r - r_d) \\ -s_y(c - c_d) \end{bmatrix} \tag{5}$$

where s_x and s_y represent the physical dimensions of image pixels of the camera sensor; and r, c are pixel coordinates. The velocity of the target objects can be expressed as

$$\dot{e} = \begin{bmatrix} \frac{d(u-u_d)}{dt} \\ \frac{d(v-v_d)}{dt} \end{bmatrix} = \begin{bmatrix} \dot{u} \\ \dot{v} \end{bmatrix} \tag{6}$$

Substituting equation (6) into (3), we can acquire the following equation:

$$\begin{bmatrix} \dot{u} \\ \dot{v} \end{bmatrix} = L\xi_c^c \tag{7}$$

Assuming that the error dynamics obeys $\dot{e} = -ke$, a proportional controller based on the Lyapunov method can be designed accordingly:

$$\xi_c^c = L^{-1}(-ke) \tag{8}$$

where k is the proportional gain (a scalar), with $k > 0$. Therefore, the control law can be obtained by substituting equation (5) into (8), as

$$\xi_c^c = -kL^{-1} \begin{bmatrix} -s_x(r - r_d) \\ -s_y(c - c_d) \end{bmatrix} \tag{9}$$

In equation (9), r and c represent the pixel coordinate in the captured image by the camera. The desired velocities of the camera in the 3D space can be computed from the image measurements. Moreover, the developed controller guarantees asymptotic stability in the closed-loop system.

The image Jacobian (L) in the model of IBVS [9], which is also named as interaction matrix, describes the motion relationship between the target objects in the image and camera in 3D space in terms of their velocities, respectively. The detailed formulation of the interaction matrix is shown below:

$$\begin{bmatrix} \dot{u} \\ \dot{v} \end{bmatrix} = L\xi_c^c = \begin{bmatrix} -\frac{\lambda}{z^c} & 0 & \frac{u}{z^c} & \frac{uv}{\lambda} & -\frac{\lambda^2+u^2}{\lambda} & v \\ 0 & -\frac{\lambda}{z^c} & \frac{v}{z^c} & \frac{\lambda^2+u^2}{\lambda} & -\frac{uv}{\lambda} & -u \end{bmatrix} \xi_c^c \tag{10}$$

where λ is focal length; and z^c is the distance between the object of interest and the camera coordinate frame in the 3D workspace. The distance must be either measured or approximated for completing the interaction matrix. In many applications, multiple objects of interest are usually measured for the purpose of estimating the distance information if there is no direct way of measuring it. Moreover, if it is a typical robotics arm with six degree-of-freedom (DOF), at least three objects of interest are required. In practical applications, four objects of interest are usually utilized so that the system can overcome both singularity of the interaction matrix and local minima [1–4].

3.2 Position Based Visual Servoing

In Position-based Visual Servoing (PBVS) approach [10] [11], features of the object of interest are extracted from images from one or more cameras. Both camera model and a geometric model of the target object are utilized to mathematically estimate the pose of the camera with respect to the target object in a 3D space. It involves three coordinate frames for designing a control system. They are current frame f_c, desired frame f_d, and reference frame f_r. In the workspace, the reference frame is typically attached to the target object. In the robot workspace, the function of the controller is to calculate and provide outputs for moving the robot with the ultimate goal of reducing the error between the current measured pose and the desired reference pose. The approach is also named 3D visual servoing because the control scheme is defined in the Cartesian space. However, the IBVS is usually called 2D visual servoing because it doesn't need to consider the pose of the robot in its workspace. Instead, it only considers target objects in provided image from cameras, which is a 2D workspace. The features in PBVS can be defined below:

$$s = (T, \theta U) \tag{11}$$

where T is a translation vector and θU is an orientation vector, respectively. The error dynamic equation for the controller can be written by

$$e = (T_r^c - T_d, \theta U) \tag{12}$$

The interaction matrix can be written as:

$$L = \begin{bmatrix} -I_3 & [T_r^c]_x \\ 0 & L_{\theta U} \end{bmatrix} \tag{13}$$

where $L_{\theta U}$ can be described by [18]:

$$L_{\theta U} = I_3 - \frac{\theta}{2}[U]_x + \left(1 - \frac{sinc\theta}{sinc^2\frac{\theta}{2}}\right)[U]_x^2 \tag{14}$$

where $sincx$ is the sine cardinal, which is defined by $xsincx = \sin x$ and $sinc0 = 1$. Therefore, the velocity control scheme can be generated as follows:

$$v_c = -kL^{-1}e \tag{15}$$

4 Visual Servoing Simulations

Figure 2 shows a typical image-based visual servoing system in Matlab simulation. In the simulation results, the control system detects the current position of the objects (they are four marks "o" in this case) which locate in the right bottom corner. By comparing the current locations of the objects with the desired locations which are marked by "*", a position error vector will be generated and fed into the image-based visual servoing controller for calculating the velocity commands for each joint of the robot. The robot applied the velocity commands for its joints; and move in the 3D workspace. Figure 2(a) shows the trajectory of the objects from the initial locations to the goal locations during the servoing. Figure 2(b) shows the convergence of the position error during servoing. Since the IBVS scheme decides the 3D motion of the robot based on 2D feedback information, it simplifies the control problem. However, it losses the control of the pose and trajectory of the robot in the 3D workspace. Therefore, obstacle

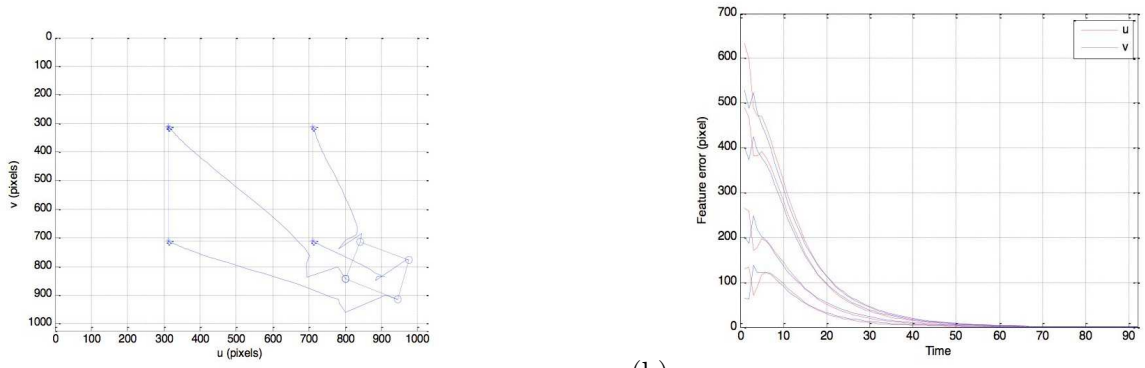

(a) (b)

Figure 2: IBVS in Matlab simulation: (a) trajectories of objects of interest in camera scenes; (b) error convergence of the positions of the objects.

avoidance and other psychical constraints during the servoing cannot be considered. Moreover, if large displace of the camera is required for moving from the current pose to the desired pose, the control system may easily fail because a large change of image scene can be caused by a small displacement of the camera in Cartesian space. Furthermore, the interaction matrix in the model of the IBVS introduce non-linear and time-varying terms, which are challenges of designing controllers.

Figure 3 demonstrates a typical position-based visual servoing in Matlab simulation. In this given example, the pose of the camera is controlled by eliminating the pose error between the current pose of the camera and the desired pose of the camera in 3D workspace. Figure 3(a) demonstrates the initial pose of the camera in the 3D workspace and the desired pose of the camera, respectively. Figure 3(b) records the velocity commands that are sent from the controller to each joint of the robot. Figure 3(c) shows the trajectory of the camera pose during servoing. Comparing the IBVS showed in above section, one of the most significant advantages of this approach is that it controls the pose and trajectory of the camera in the Cartesian space directly. Obstacles and other physical constraints can be easily considered and integrated into the system during servoing. However, there is a disadvantage in this approach. There is absolutely no control of the image, which will result in losing objects of interest in the camera scene. Eventually, it will cause the failure of the whole control system because there will no data and information from the feedback loop in the control system. Moreover, 3D models of objects of interest have to be completely available. Moreover, 3D reconstruction is a challenge because multiple feature points are required from camera in order to calculate poses, which may not be the case during the servoing. Camera calibration result will be another issue for successful PBVS system.

5 Application of Visual Servoing in Autonomous Mobile Robots

Figure 4(a) shows a robotic search and rescue scenario, in a future city. It presents an emergency situation where a group of general-purpose robots identify injured humans and remove them from the dangerous region. In applications of autonomous search and rescue robots, the workspace is usually large, and sometimes unknown and dynamic; the base frame of the robot has ability to move around in a large area; and the objects of interest are not predefined well, which depend on different applications. Therefore, 3D models of target objects are unavailable in most of the time. In this situation, position-based visual servoing will fail and image-based visual servoing has the advantages over the position-based visual serving of reducing the computational burden by avoiding unnecessary image interpretations. Also, it eliminates the calibration errors of camera parameters. Furthermore, the eye-in-hand camera configuration has more advantages

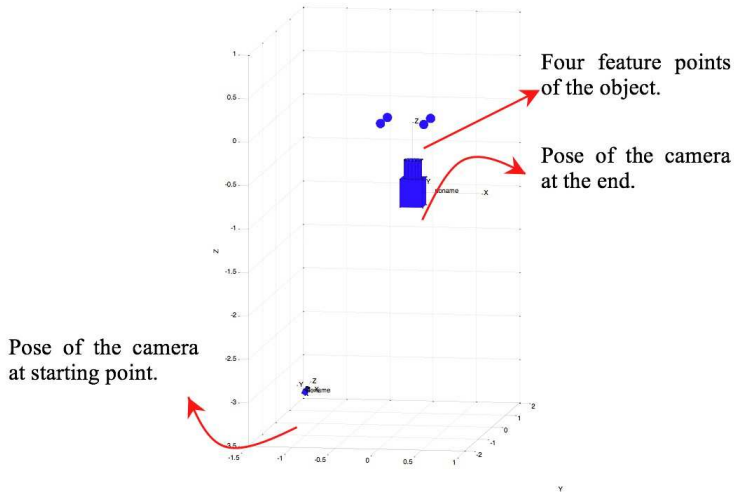

(a)

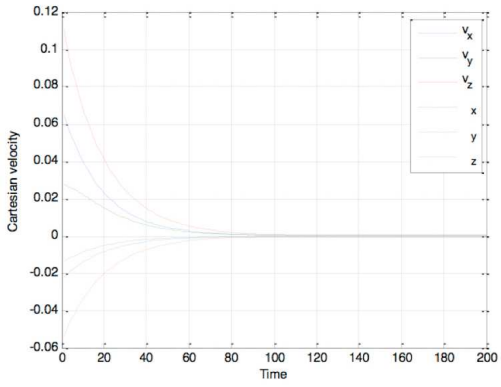

(b)

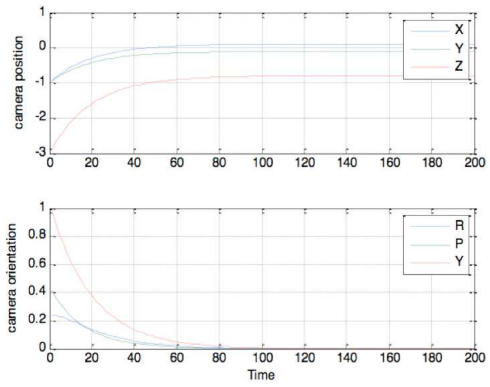

(c)

Figure 3: PBVS simulation in Matlab: (a) current and desired pose of the camera Cartesian space; (b) controller output; (c) trajectory of the camera pose in Cartesian space.

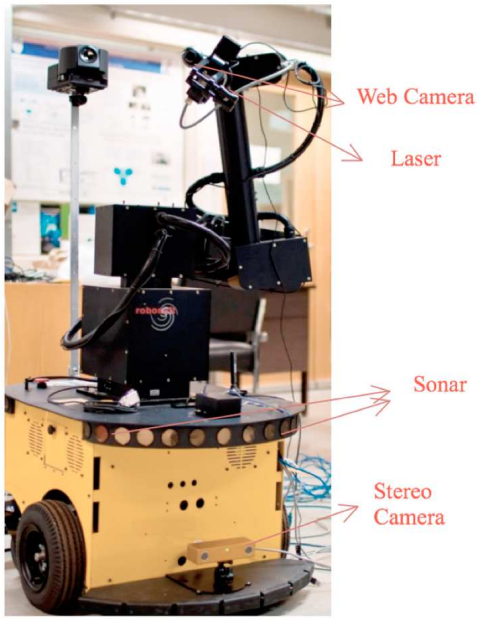

(a)

(b)

Figure 4: (a) Robot search and rescue scenario; (b) Physical configuration of the test bed.

than the eye-to-hand one in mobile robot applications. The suggested system for autonomous mobile rescue application is illustrated in Figure 4(b).

The given system contains a mobile base (pioneer powerbot), a manipulator (robuarm), and different types of sensors (a web camera, laser, sonar, and stereo camera). Both two cameras are configured as eye-in-hand configuration. The nonlinear terms in the IBVS model is linearized by updating the position of the feature points in each iteration. The time-varying term (the distance between object and camera) is also updated in each iteration by using the measurement results from the laser distance finder and sonar sensors. Therefore, there is no need for distance estimation in the proposed approach. Figure 4(b) describes an application of the proposed system where there are general-purpose robots in a future city (e.g., surveillance). If an incident or emergency situation occurs in the city, these robots are able to quickly response and change their roles to involve emergency cases such as search and rescue work.

The control law of traditional IBVS is discussed and shown in (9), which describes the relationship between the velocities of the camera and of the feature points in the image. Now, the relationship between velocity of the camera with respect to its own coordinate frame and speeds of each joints will be formulated, which is the mathematic model of IBVS of the robot. In order to generate the model, one should first consider the mathematic relationship between the velocity of the end effector with respect to the robot base frame and the velocity of each joint

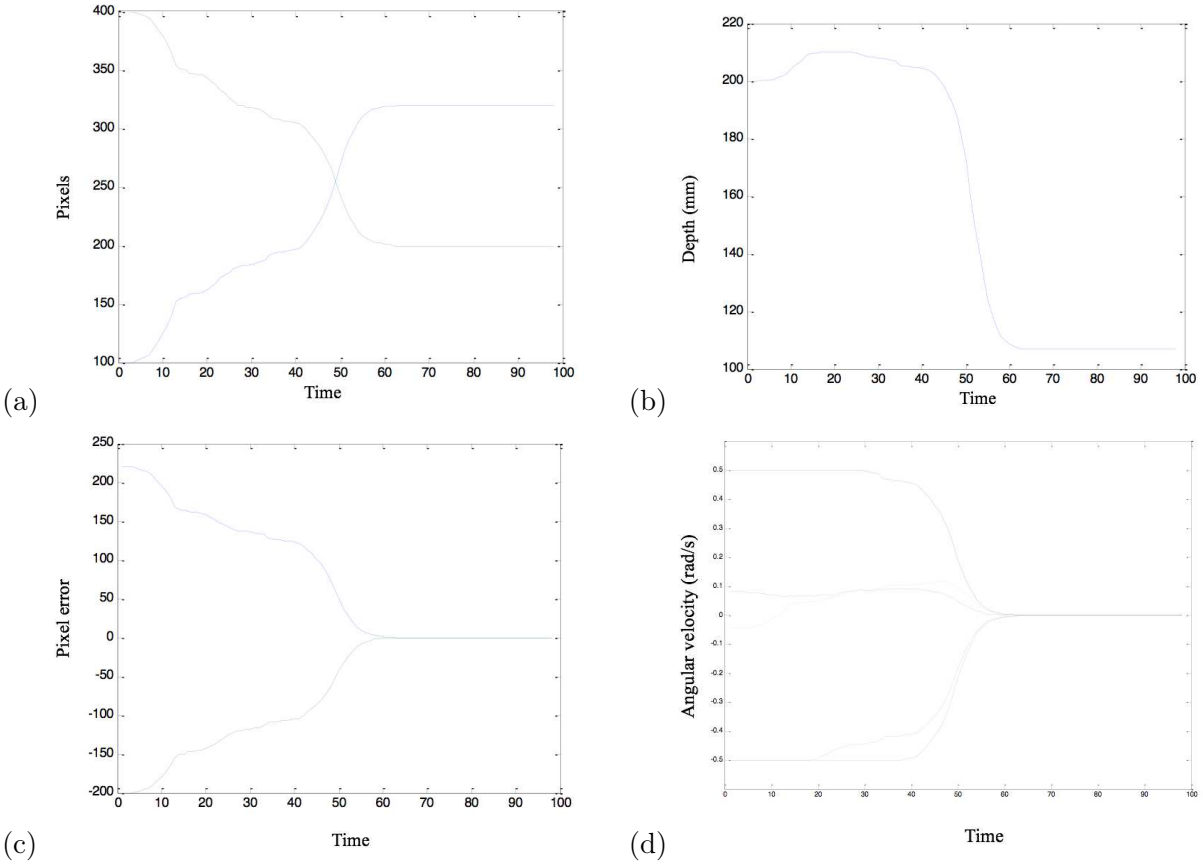

Figure 5: (a) the performance of the system in terms of the trajectory of the feature point; (b) distance information measured by laser distance finder; (c) error convergence of the system; (d) velocities commands from the controller.

as:

$$\xi_t^r = J_1 \dot{q} \tag{16}$$

where J_1 is the Jacobian matrix, and $\dot{q}$ is the velocity vector of the robot joints. The velocity of the end effector with respect to its own coordinate frame is derived by

$$\xi_t^t = G^{-1} \xi_t^r \tag{17}$$

where $G = \begin{bmatrix} R_t^r & 0_{3\times3} \\ 0_{3\times3} & R_t^r \end{bmatrix}$. Since the camera is rigidly attached to the end effector, the camera frame and the end effector frame have a constant relationship of homogeneous transformation. Therefore, the relationship between camera velocity and the robot end-effector velocity may be written as:

$$\xi_t^t = J_2 \xi_c^c \tag{18}$$

where $J2 = \begin{bmatrix} R_c^t & s(d_c^t) R_c^t \\ 0_{3\times3} & R_c^t \end{bmatrix}$.

Finally, by combining equations 9, 20, 21, 22, the mathematical representation of the relationship between object velocities on camera scenes and joint velocities of the robot can be written as:

$$\dot{s} = L J^{-} 1_2 G^{-1} J_1 \dot{q} \tag{19}$$

Denoting the terms $LJ^{-}1_2G^{-1}J_1$ by M , equation (19) can be simplified as:

$$\dot{s} = M\dot{q} \tag{20}$$

The square of the error norm can be utilized to derive the control law as a candidate Lyapunov function:

$$\dot{q} = M^{-1}(-ke) \tag{21}$$

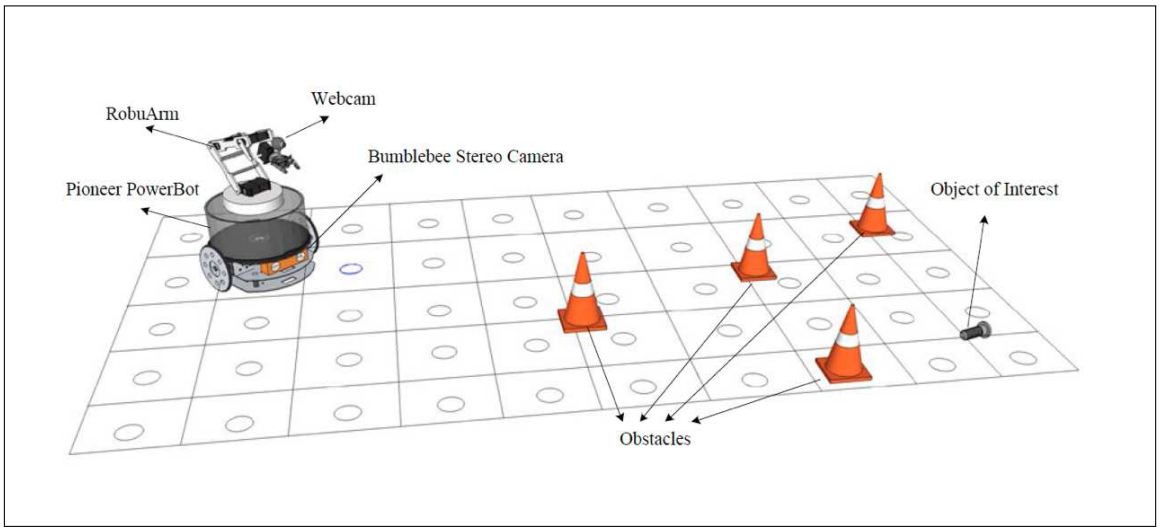

Figure 6: Experimental setup in the laboratory.

There are nonlinear and time varying terms in this model which can cause challenges in designing and implementing controller. In order to eliminate the nonlinear and time-varying terms, an adaptive parameter updating mechanism is introduced in the system to linearize and nonlinear terms and update the time varying terms so that the system can be considered a linear system. The time varying term in the model is the distance between camera and objects. A laser distance finder is utilized to update the modeling by using the depth measurement from the laser distance finder. The non-linear terms are about the position of the objects in the image plane in the interaction matrix. To eliminate those nonlinear terms, the position of the objects in the interaction matrix are updated in each iteration of the controller. Figure 5 shows the performance of the suggested IBVS system in Matlab simulation. The trajectory of the object on images is shown in Figure 5(a). The distance measurements between camera and object by the laser distance finder is illustrated in Figure 5(b). Figure 5(c) shows the performance of the controller, showing the error convergence. Figure 5(d) shows the velocity history of each joint of the robot during the servoing.

Figure 6 shows the experimental setup in our laboratory. The purpose of the mobile robot is to find the object of interest in the workspace, navigate to it and finally approach and grasp the object using image-based visual seroving. In this paper, only the visual servoing aspect is considered. During the final operation, the stereo camera mounted on the mobile base will detect the object of interest in the scene and guide the robot to move toward to the object by using visual servo control. The mobile robot approaches the object until the object is inside the workspace of the manipulator. Next, the visual servoing of the manipulator is activated to grasp the object.

Figure 7 presents an experimental result of the proposed system. Figure 7(a) shows the desired camera view, and Figure 7(b) shows the current camera view when the robot starts to servo. As discussed in the previous session, the purpose of the IBVS is to eliminate the image error between the current camera view and the desired camera view, by controlling the motion

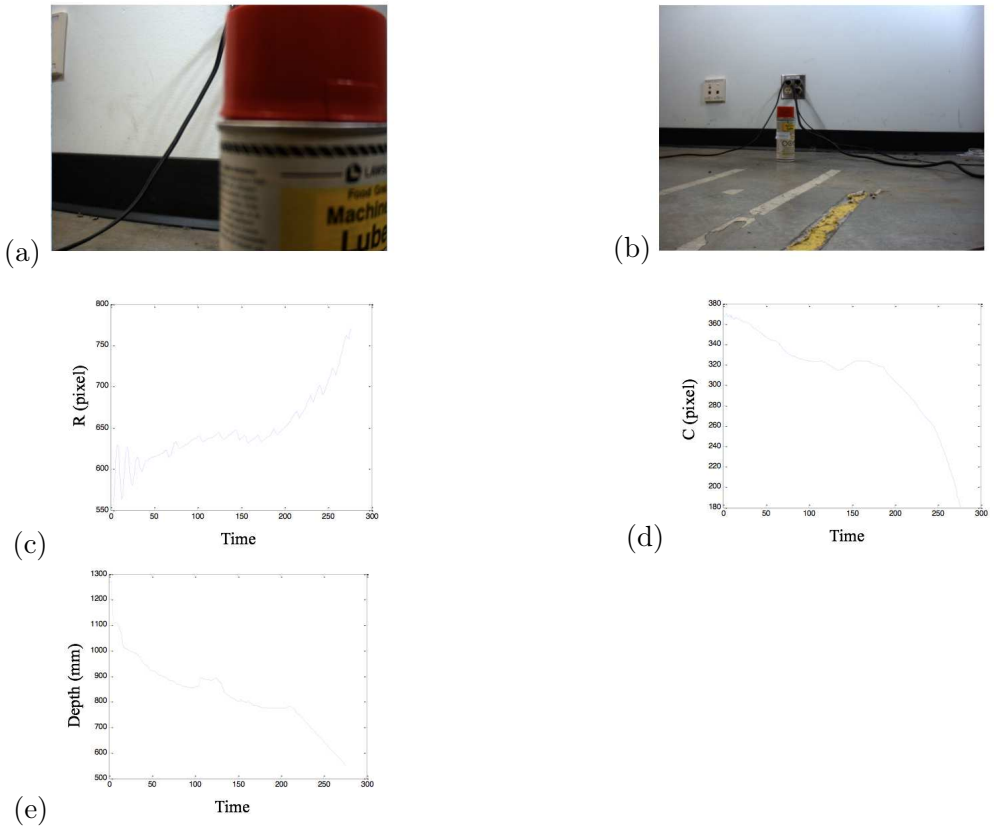

Figure 7: (a) Desired camera view; (b) current camera view; (c) trajectory of the object in in R; (d) trajectory of the object in C; (e) distance between the camera and the target object.

of the robot. Specifically, the system controls the robot motion by eliminating the position error of the object in the camera view. Figure 7(a) gives the trajectory of the object in the camera view in the row (R) axis; and Figure 7(b) gives the trajectory of the object in the camera view in the column (C) axis. Figure 7(d) gives the distance between the camera and object.

6 Conclusions

This paper introduced and described two basic methods of vision servoing for mobile robots. The detailed formulation of these two methods were discussed along with their advantages and disadvantages in applying in mobile robots. A suggested method including selection of visual servoing method and hardware configuration was proposed for applications of autonomous mobile manipulation. Both simulation and experimentation were carried out with the proposed system. The results showed the effectiveness and good performance of the methodology in a mobile robotic application.

Bibliography

[1] Chaumette, F. ; Hutchinson, S. (2006); Visual servo control part 1: basic approaches, *IEEE Robotics and Automation Magazine*, 13(4): 82-90.

[2] Agin, G. J. (1979); Real time control of a robot with a mobile camera, *SRI International, Menlo Park, Technical Note 179.*

[3] Sanderson, A. C. ; Weiss, L. E. (1980), Image-based visual servo control using relational graph error signals, *in Proc. IEEE*,:1074-1077.

[4] Hutchinson, S. ; Hager, G.D. ; Corke, P. I. (1996), A tutorial on visual servo control, *IEEE Transaction On Robotics and Automation*, , 12(5): 651-670.

[5] Ma, Y. ; Kosecka, J. ; Sastry, S. S. (1999), Vision guided navigation for a nonholonomic mobile robot, *IEEE Transactions on Robotics and Automation*, 15(3): 521-536.

[6] Fang, Y.; Dixon, W. E. ; Dawson, D. M. ; Chawda, P. (2005), Homography-based visual servo regulation of mobile robots, *IEEE Transactions on Systems, Man and Cybernetics - Part B*, 35(5): 1041-1050.

[7] Wang, Y. ; Lang, H. ; de Silva, C. W. (2010), A hybrid visual servoing controller for robust manipulation using mobile robots, *IEEE/ASME Transactions on Mechatronics*, 15(5): 757-769.

[8] Gangloff, J. ; de Mathelin, M. (2002), Visual servoing of a 6-DOF manipulator for unknown 3-D profile following, *IEEE Transactions on Robotics and Automation*, 18(4): 511-519.

[9] Spong, M. W. ; Hutchinson S. ; Vidyasagar M. (2005); Robot Modeling and Control, *Wiley.*

[10] Malis, E. ; Chaumette, F. ; Boudet, S. (1999), 1-1/2-D Visual Servoing, *IEEE Transactions on Robotics and Automation*, 15(2): 238-250.

[11] Wilson, W. J. ; Hulls, C. C. W. ; Bell, G. S. (1996), Relative end-effector control using Cartesian position-based visual servoing, *IEEE Transactions on Robotics and Automation*, 12(5): 684-696.

INTERNATIONAL JOURNAL OF COMPUTERS COMMUNICATIONS & CONTROL
ISSN 1841-9836, 11(5):697-708, October 2016.

NVP: A Network Virtualization Proxy for Software Defined Networking

B. Pinheiro, E. Cerqueira, A. Abelem

Billy Pinheiro*, Eduardo Cerqueira, Antonio Abelem
Federal University of Para
Brazil, Para, Belem
*Corresponding author: billy@ufpa.br
cerqueira@ufpa.br, abelem@ufpa.br

Abstract: The combination of Network Function Virtualization (NFV) and Software Defined Networking (SDN) can improve the control and utilization of network resources. However, this issue still requires proper solutions to virtualize large-scale networks, which would allow the use of SDN and Virtualization in real environments. Thus, this paper proposes a virtualization architecture for SDN that relies on a proxy-based approach. The NVP (Network Virtualization Proxy) is a virtualization proxy that intercepts messages exchanged between controllers and switches SDN enabling network virtualization. An implementation of the proposal was developed as a proof of concept and load testing was performed showing that the solution can provide network virtualization in a scalable manner, using less than 2.5 MB of memory to manage 100 switches performing simultaneous requests, whereas FlowVisor requires more then 200 MB.
Keywords: SDN, virtualization, NVP, FlowVisor.

1 Introduction

The Internet was originally designed to provide network services to a closed community, and has today become an undeniable success worldwide, with users of various types of services everywhere on the planet.

Specific adaptations have historically been proposed and implemented at the emergence of new demands. This approach, despite having attended to momentary needs, has generated increasing complexity and cost of maintaining the Internet. Moreover, the higher the number of these adjustments, the greater is the complexity of the resulting architecture, making it even more difficult to overcome future challenges, in a situation commonly referenced as Internet "ossification", increasingly resistant to structural changes [1].

In this context, Software Defined Networking (SDN) is today one of the most relevant solutions for Future Internet environment, and the OpenFlow protocol implementation is the best-known method [2]. Along with SDN, the field of Network Function Virtualization (NFV) has grown so as to allow resources to be shared and dynamic topologies to be created [3].

The main concept for working with network virtualization is the division into slices, to optimize the use of their resources (nodes or links) and to separate it into different logical instances. For example, this approach has been used in the FIBRE project, to create a common space between Brazil and the EU for future experimental Internet research into network infrastructure and distributed applications with more then 40 OpenFlow nodes [4].

The partitioning of the network enables the actions taken in one of the network slices, to not interfere with others, even if they are sharing the same physical infrastructure. In traditional architectures, the network is sliced through VLAN's technique, but, with the diversity of network models, the structure of VLANs makes the experiments with others protocols rather difficult to manage [1].

Currently, FlowVisor [5] is the leading virtualization solution available for OpenFlow networks. It acts as a layer of virtualization located between OpenFlow switches and the network controller allowing resources to be shared, but maintaining the isolation of a virtual network from others. A major problem with this solution is the scalability since the recommended requirements for operating the FlowVisor are 4 processor cores and 4 GB Java heap. Depending on the size and use of the network, these requirements can increase [6].

This article proposes the Network Virtualization Proxy (NVP), a new model of network virtualization that improves the use of computational resources in the virtualization process, through an innovative architecture for greater scalability. To prove the effectiveness of the proposal, an implementation has been developed, and load tests were performed comparing NVP with FlowVisor.

This article is structured as follows: Section 2 presents SDN virtualization related works. In Section 3, the NVP is detailed. In Section 4, the tests performed and their results are discussed. Finally, Section 5 presents the conclusions and future works.

2 Related Work

FlowVisor is a well-known networks virtualization solution for SDN OpenFlow environment [5]. It is proposed as a special controller that acts as a transparent proxy, located between the OpenFlow switch and the network controller. By using FlowVisor, it is possible divide the switches and have their resources controlled by more than one controller at the same time, thus enabling the creation of virtual networks with logical isolation between them.

The FlowVisor adopts an hierarchical architecture that allows multiple FlowVisor networks to be interlinked making virtualization of an already virtualized resource possible. In order to function seamlessly, it acts as a controller for the switches and as an OpenFlow switch for the controllers. Thus, it must store the information of the switches and controllers to enable the routing of messages between them. However, its architecture generates an overhead, because the same entity responsible for managing the virtualized network's information is responsible for forwarding the generated messages, including the packet_in. These are packets coming through the network and sent to the controller for review, which can consume a lot of resources to be forwarded between FlowVisors to reach the controllers destination.

The Prefix-based Layer 2 Network Virtualization (L2PNV) [7] is an extension of FlowVisor, with the main objective of providing a level 2 virtualization engine without using VLAN, instead basing the virtual networks created in Media Access Control (MAC) on the address of origin and destination. However, it was necessary to modify FlowVisor, the switch firmware used to support a modified version of OpenFlow and the host since it was necessary to enable MAC masking for these elements. Despite being discussed in the article that a test environment was created using the proposed solution and the necessary changes in the above-mentioned elements fit the demands of the proposal, no results related to scalability of the solution or comparison with other existing solutions were presented. In fact, no evaluation was submitted.

Aiming to overcome FlowVisor's major limitation, the fact that virtual topologies that may be created with FlowVisor are restricted to a subset of the physical topology, the Advisor [8] was proposed. This solution leverages the VLAN tag to differentiate between virtual links and the virtual network, making it possible to create virtual links by joining different physical links. However, the solution that the authors validate necessitates the manual configuration of network devices and the sending of dpctl commands. Furthermore, the solution limits the use of the VLAN header, leaving the less transparent solution for the user. In addition, tests have shown an increase in terms of latency when compared it to FlowVisor. Again, load tests with a large network, such as the FIBRE network, showing the scalability of the solution were not performed.

To solve the problem of virtual links, Vertigo [9] was proposed. An extension of FlowVisor, it basically adds a layer of intelligence which enables the creation of virtual topologies over the physical topology. In this case, it creates virtual links interconnecting physical links. Moreover, it may provide a complete virtual structure, since it is possible to virtualize the network nodes together with the links. The proposal was implemented in the testbed OFELIA, where it was possible to prove that the solution can, in fact, provide virtual links. It is possible to verify the data taken from the article itself, whereby the solution shows an increase of 44.70 % in overhead when compared with FlowVisor, a fact that makes the scalability of the proposal questionable.

The FlowVisorQoS proposed [10] solves the problem of ensuring bandwidth usage per slice in FlowVisor. Thus, it is possible to define minimum requirements for Quality of Service (QoS) that will be respected in the switches, ensuring that each flow does not exceed the specified limits. For the implementation of the solution, changes in the firmware of the switches were performed. However, despite achieving the solution's objectives, tests to show the solution behavior in a large-scale environment were not performed.

OpenVirteX [11] builds on the design of FlowVisor, and functions as an OpenFlow controller proxy , but, differently of FlowVisor, OpenVirtex provides Virtual Links and slices isolation. The hardware requirements for both FlowVisor and OpenVirtex are the same and they requires 4 core processors and 2GB RAM [12].

The Flow-N [13] is, to our knowledge, the first work on network virtualization that addresses scalability problems. It was proposed as an extension of the NOX controller. It enables virtualization-based containers and uses relational databases to map between the physical and virtual network topologies. The scalability tests presented in the study show an almost stable latency with 100 virtual networks created, while FlowVisor starts with a low value but increases to almost equalize the value of Flow-N. Unfortunately, only one chart is presented, and the proposal can not be evaluated further while details about the operation of the solution are not provided.

As discussed in the papers presented in this section, the virtualization solution for SDN must provide isolation, virtual links, and be prepared to support a large quantity of equipment, because all other services will be running virtualized over the physical equipments

Table 1 summarizes the main features of the proposed virtualization in this section. It was concluded that none of the protocols can fully meet all the requirements cited above in order to provide a reliable and scalable communication that might require an SDN for the virtualization.

Table 1: Virtualization Solutions Comparison

Proposal	Scalability	Virtual Links	Transparent	Isolation
FlowVisor	No	No	Yes	Partial
L2PNV	No	No	Yes	Partial
ADVisor	No	Yes	No	Partial
VeRTIGO	No	Yes	Yes	Partial
FlowVisorQoS	No	No	Partial	Yes
OpenVirtex	No	Yes	Yes	Yes
Flow-N	Partial	Yes	Yes	Partial

Finally, is important to emphasize that, despite the clear importance of scalability for virtualization solutions in the SDN environment, only one proposal attempts to address this issue. However, it does not provide the information necessary for a more satisfactory evaluation, such as the comparative numbers of supported switches, number of controllers, and number of virtual networks.

3 Network Virtualization Proxy (NVP)

As presented in Section 2, the fundamental requirements for virtualization in SDN are virtual links to enable a greater variety of topologies and scalability, aiming to cover a larger number of devices in the physical substrate. Such features expected for this technology could actually be used as a basis for production networks.

A key feature of the FlowVisor architecture is to enable its use hierarchically. This feature brings high flexibility regarding different possible topological configurations. However, this feature imposes an important limitation for network scalability, since it introduces more elements between the controller and the switch, as the hierarchical level increases.

The NVP enables virtualization scalability in an efficient way. Thus, the main contributions of our proposal are the following:

- Allow resources of OpenFlow switches to be shared between different controllers;
- Increase the network scalability, allowing the virtualization layer to support a high number of switches and controllers without generating a big network overhead;
- Provide a global network abstraction, in which all available resources are not separated hierarchically, i.e., increasing the number of network devices does not increase the number of elements between switches and controllers;
- Enable a formal modeling of virtualized resources.

In order to better structure the display and use of NVP, an CIM extension (Common Information Model) was developed to allow modeling of SDN using UML (Unified Modeling Language) [14].

3.1 NVP Architecture

The NVP is composed of two elements: the Proxy Flow Switch (FPS) and the Flow Proxy Manager (FPM). Its design was inspired in OpenFlow itself, in which the complexity of control is the removal of switches and passed to an external control entity. In this case, the FPS acts as a forwarder and FPM concentrates all of the system virtualization's information and intelligence. Its architecture is shown in Figure 1.

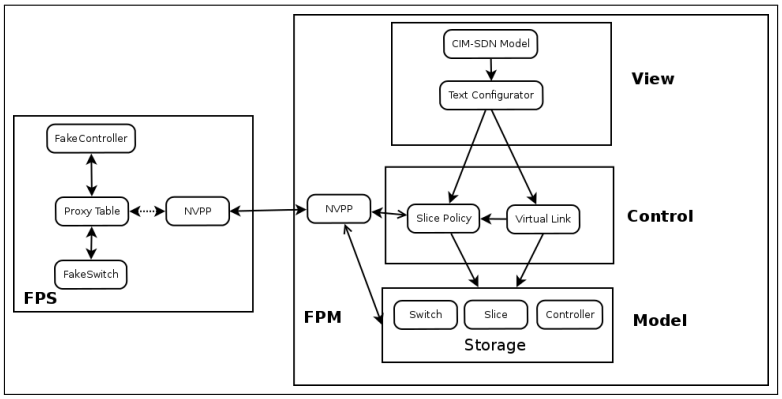

Figure 1: NVP Architecture

Flow Proxy Switch (FPS)

It is the entity responsible for forwarding the information between switches and controllers. It will exchange messages with OpenFlow switches and controllers and pass them on to the FPM.

After the network start up, FPS use is dedicated to consulting its routing table and deciding to which controller/switch the messages should be forwarded. It is formed of the components: FakeController, FakeSwitch, ProxyTable, and Network Virtualization Proxy Protocol - (NVPP).

- **FakeController:** This is an entity that acts as an OpenFlow controller, passing the idea on to the OpenFlow switch that is connected to the network controller. It is responsible for ensuring the transparency from the switches side and use NVPP to send the information obtained from the switches to the FPM;

- **FakeSwitch:** Like FakeController, it is responsible for ensuring transparency from the side of the controllers and providing information to those obtained about the resources that each controller will access (with the FPM through NVPP). It is an entity that acts as an OpenFlow controller, communicating the idea to the OpenFlow switch that is connected to the network controller;

- **Network Virtualization Proxy Protocol (NVPP):** It is a binary protocol, similar to OpenFlow, developed to enable communication between FPSs and FPM. Because of the need to maintain FPS as simple as possible, we chose to develop a binary protocol that can meet the need for communication between entities, generating as little computational overhead possible. The data types used in the NVP are similar to those used in OpenFlow protocol, and its use follows the same logic defined in the OpenFlow protocol specifications. [15];

- **Proxy Table:** It is a table that stores which resources of a given switch can be used by a particular controller. It is composed of the fields ctr _addr and ctr _port, which uniquely identify the network controller, the field datapath_id which identifies to which switch this flow is related, and the fields in_port and dl_vlan that identify the port and the vlan associated with the virtual network.

  Table 2: Proxy Table

ctr_addr	ctr_port	datapath_id	in_port	dl_vlan
192.168.1.2	6633	2	1	2
192.168.1.1	6633	2	1	1

  In the example of Table 2, an action of the flow type_mod arrival of a controller with ip 192.168.1.2 and running on port 6633 will be forwarded exclusively to the switch with the datapath_id 2 on port 1 and vlan 2. If one of the fields differ, the packet is discarded.

Flow Proxy Manager (FPM)

It is the element that performs network virtualization's effective control. It will contain a database with information about the switches, controllers, and the network slices. All the slices changes must pass through it, and it should embed the rules in FPS. A FPM will be used in each domain- there may be several FPS associated with it- allowing the network to be scalable, since the actual load generated in the network through the packet_in, and these will be handled only by the PFSs. Its architecture follows the pattern Model-view-controlller (MVC) and is described next.

- **Storage:** It is the component responsible for storing the switches' information, controllers, and the network slices. The data stored here will be used by the Slice Policy to feed the FPS;

- **Slice Policy:** Responsible for the slices creation, allowing the creation of policies and associating resources to controllers required by the administrator. It should use the information from switches and policies present in the Storage and create slices in FlowTable;
- **Virtual Link:** This element is responsible for mapping the physical links and enabling the creation of virtual links by setting up forwarding rules in the switches. Thus it is possible to interconnect continuous physical links and provide the abstraction of a virtual link directly connecting two ports of the switches;
- **Text Configurator:** It is the NVP configuration interface. It is similar to the configuration file used by FlowVisor to facilitate the adoption of NVP and uses JSON (JavaScript Object Notation) syntax;
- **CIM-SDN Model:** This is an XMI (XML Metadata Interchange) file that models the entire network to be virtualized and the virtual networks themselves. It uses the CIM-SDN [14], which is a CIM extension that allows the representation of SDN elements in a UML diagram, ensuring the consistency the network. It also maintains an updated documentation for easy understanding.

The NVP has its architecture divided into two main elements: the FPS and the FPM, aiming to provide, at the same time, scalability and a global network view. Scalability is the result of multiple FPSs that can be used in the network in order to provide the best use of the resources of the switches and controllers. The global view is available at FPM, which contains all the network information and can provide easy integration to other networks through interconnection with other FPMs from other networks.

3.2 Applying the NVP

Typically, NVP is located between the switches and the network controller. It is possible to see in Figure 2 as the components of NVP relate with other network components. One FPS can suit various switches and controllers, and, to enable network scalability, the number of FPSs can be increased to suit more switches and controllers. The FPM is unique to the network and is responsible for providing a global network view.

In Figure 3, the FPS and the MPF activity diagrams are presented. In the case of FPS, actions are started by the controllers and switches. The information of switches and controllers is collected, and subsequently, ProxyTable is used to determine the forwarding of packets. In FPM, the administrator starts activities, providing the CIM-SDN model as input to generate the creation of slices. It is worth noting that a packet is never forwarded to the MPF; only the FPS handles packets and does it using only ProxyTable as a decision resource.

The use of NVP is similar to FlowVisor plus the CIM-SDN. However, it is possible to directly use the configuration file, a fact that enables an easy integration with other tools that already have FlowVisor as the NFV.

4 Proposal Evaluation

An implementation to prove the concept of NVP was developed and its performance was compared with FlowVisor. The metrics used in the evaluation were the number of requests and cpu loads and memory usage.

In order to ensure the most efficient proposal implementation, the development of the NVP prototype was performed in C++ using the BOOST::ASIO [1]. In this version, FakeController

[1] http://www.boost.org/library

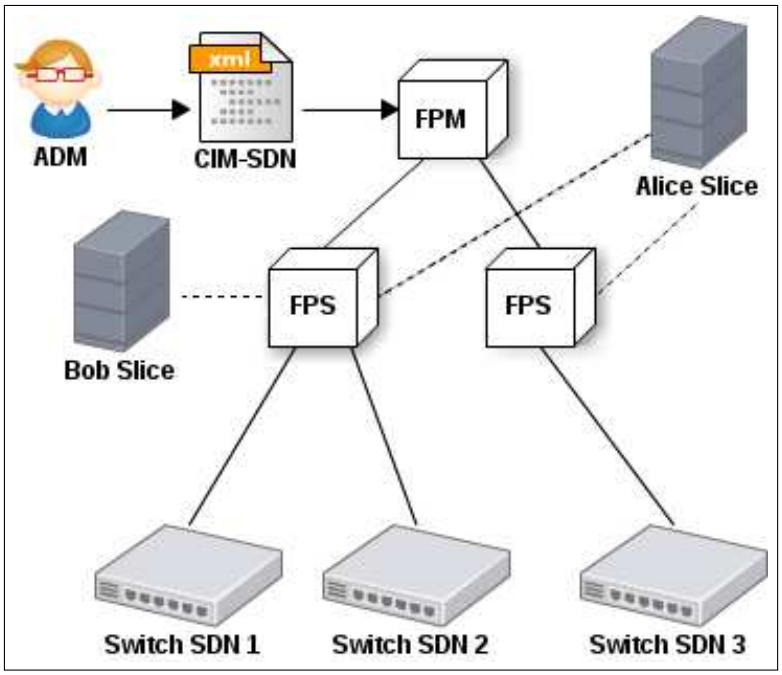

Figure 2: Applying the NVP

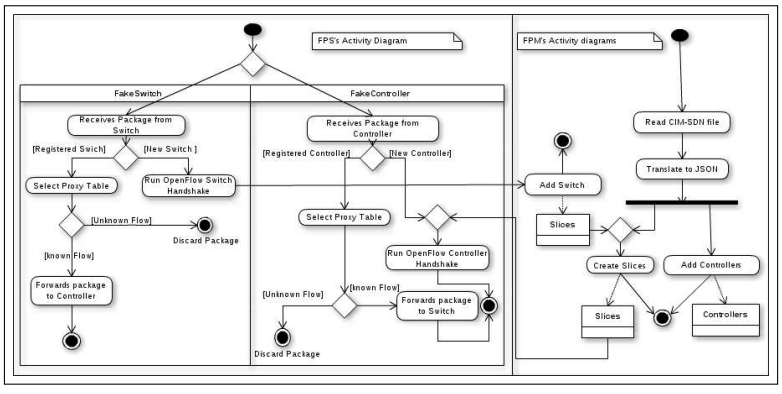

Figure 3: NVP Activity Diagrams

and FakeSwitch components were implemented in their entirety, as well as a short version of ProxyTable.

The only external library used was a file defining the types of data available in OpenFlow itself, to enable communication between the switches and controllers. The current implementation of FPS allows it to act as a proxy virtualization, although it may not include all elements of the proposal, since the FPM has not been fully developed.

4.1 Test Methodology

The methodology for evaluation and validation of NVP is based on the application execution in a real environment, but, with tools that emulate OpenFlow switches and allow the creation of a large number of elements for the experiment, the use of real OpenFlow switches is not necessary [16].

The tool used to emulate OpenFlow switches was CBENCH, which is part of the framework oflops [2]. Using the tool, it is possible to define the number of switches to be emulated and indicate to which network controller it must connect.

The controller used in the experiments was the POX, having switches emulated by CBENCH as clients. The experiments were performed on the same machine so that network traffic would not influence the response time of the components. The machine is a CPU Intel core 2 quad 2.5GHz with 4GB of RAM and uses Debian Wheezy.

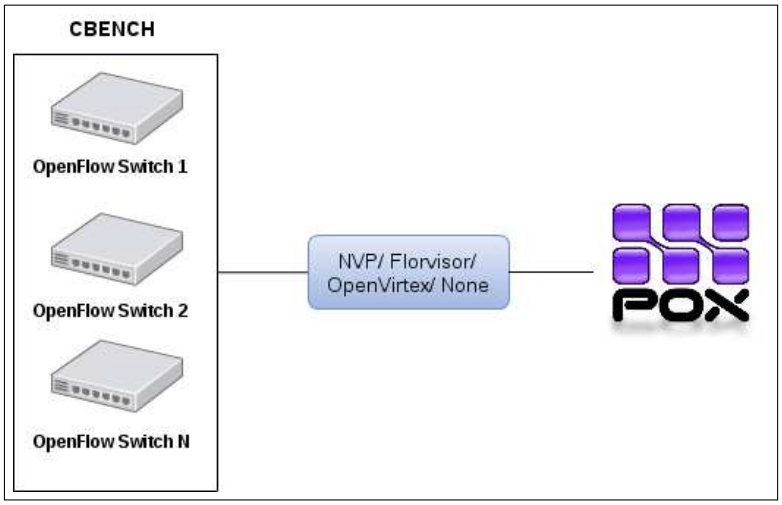

Figure 4: Experiments topology

The experiments used the POX controller [3] to handle the requests from the switches created with the CBENCH following this topology in Figure 4. Three experiments were performed, the first with the NVP between the switches and the controller, the second with FlowVisor taking the place of NVP, and the last experiment without any virtualization tool. Ten replicates were performed for each experiment using the number 1, 5, 10, 20, 40 and 100 switches to generate requests simultaneously.

4.2 Results Analysis

The goal of these experiments was to validate the NVP, demonstrating load tests with it to verify its behavior and compare it with the FlowVisor. The POX is presented, not for the

[2] http://archive.openflow.org/wk/index.php/Oflops
[3] http://www.noxrepo.org/pox/about-pox/

purpose of direct comparison, because it perform different tasks on the network, but to demonstrate the extent to which NVP, FlowVisor and OpenVirtex introduce overhead when acting as virtualization proxies.

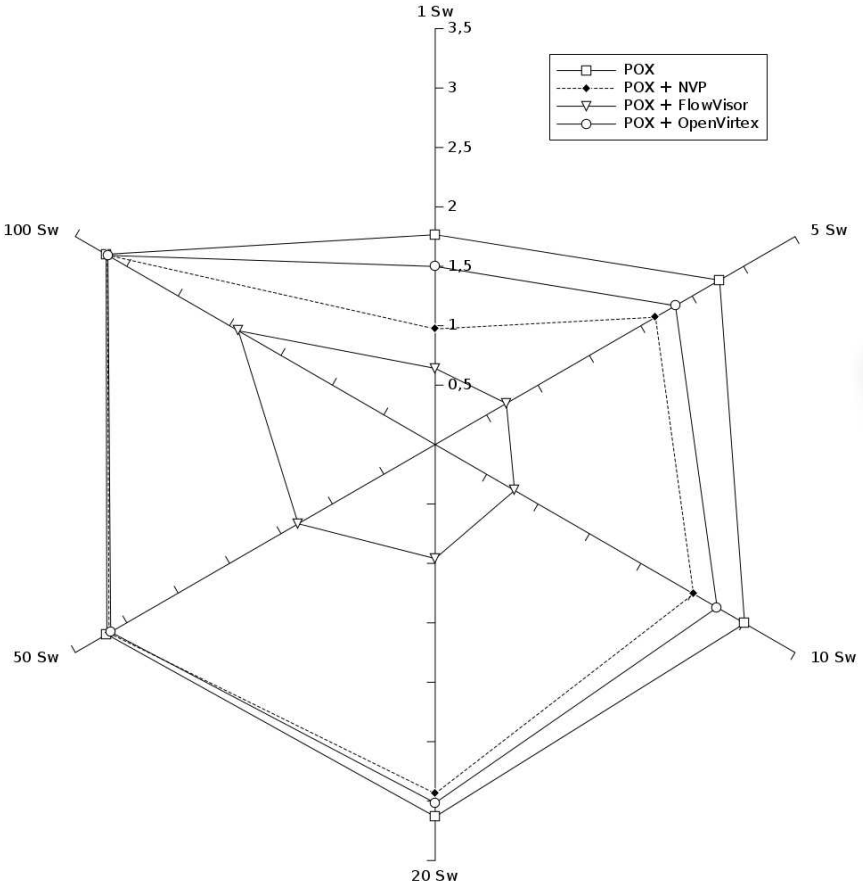

Figure 5: Reply per milisecond X Number of Switches

Figure 5 shows the number of responses that the controller can produce per millisecond. The direct comparison with FlowVisor shows a huge difference between the number of requests answered for each virtualization proxy. For one switch, the NVP is 53.68% better than FlowVisor, and, when the number of switches achieves 100, the NVP results are 89.83% better, showing a great increase in performance. When the NVP is compared with OpenVirtex their results are getting almost the same according to the increase of the number of switches, but for a small number of equipment the OpenVirtex has a better result.

Also, it is possible to see, when compared with POX, that the NVP shows fewer responses, as expected, since the message must be sent to the POX anyway. However, as the number of switches increases, it is possible to notice a reduction in the difference in the environment both with and without NVP. For one switch, the performance loss is 44.90 %, but it will decrease to 22.53 % with five switches until arriving at 1.10 % for 100 switches, showing a better performance when the number of switches is elevated.

Figure 6 shows the cpu load percentage of NVP, FlowVisor and OpenVirtex during the experiments. It is possible to observe that, even with requests for 100 switches at the same time, the CPU usage by NVP was less than 12% while FlowVisor gets, for the same number of switches, 107% of CPU, i.e., more than one CPU core is needed to handle the requests. The OpenVirtex shows a better result than FlowVisor, but uses more than 3 times the amount of memory when compared with NVP.

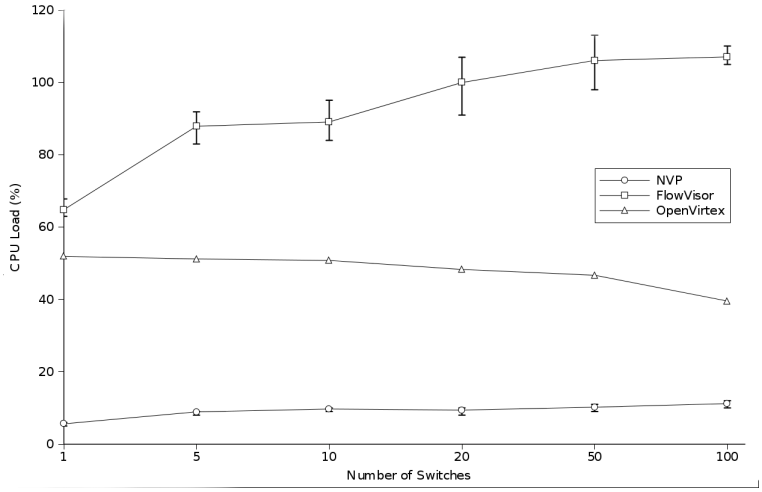

Figure 6: Cpu load time(%) X Number of Switches

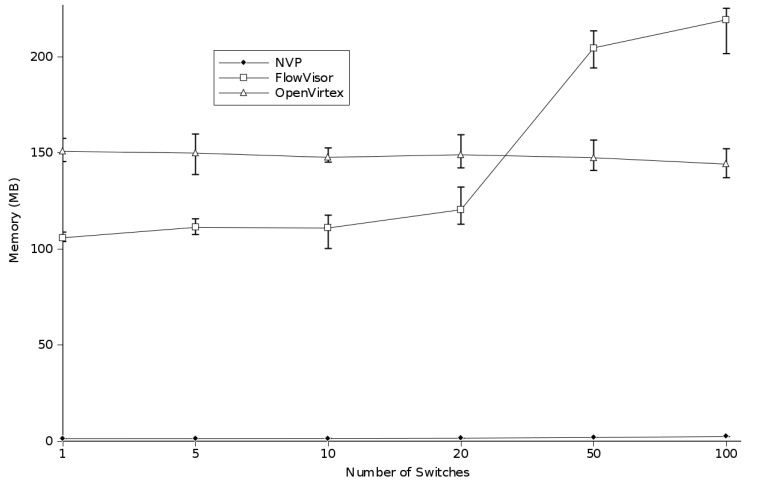

Figure 7: Memory Usage (MB) X Number of Switches

Figure 7 presents the memory consumption of NVP and FlowVisor during the experiments. The values presented are RSS (Resident Set Size), which is the physical memory the process currently uses. Again, even with 100 switches, total memory usage did not exceed 2.5 MB, showing that the solution exhibits a good memory usage. NVP would therefore be more attractive to clients, as opposed to FlowVisor, which uses more then 200 MB to handle the 100 switch requests. The memory used by OpenVirtex stays almost constant in 150 MB, overcoming in 60 times the memory used by NVP.

5 Conclusions and Future Work

This article proposes a framework for SDN virtualization, named Network Virtualization Proxy (NVP). The purpose of NVP is to provide a mechanism for scalable virtualization with isolation between virtual networks by creating and enabling the creation of virtual links. The innovative aspect of this work is that the proposed solution combines scalability and global network view.

The results presented in the experiments to allow for a validation of the proposal for the use of machine resources that will host the virtualization solution. Thus, NVP has demonstrated that it can act as a virtualization proxy without using many host resources, specifically, consuming, in our experiments, fewer than 2.5 MB of memory to manage connections originating from 100 different outfits. Also, all the comparisons with FlowVisor show a better results for the NVP proposal.

As future work, we intend to verify the individual limits of FPS and FPM, as well as examine a more detailed comparison with other virtualization proposals.

Bibliography

[1] Alcober, J. et al. (2013);Internet future architectures for network and media independent services and protocols, *15th International Conference Transparent Optical Networks, (ICTON)*, 1-4.

[2] Open Networking Foundation. Software-Defined Networking: The New Norm for Networks. White paper, Open Networking Foundation, Palo Alto, CA, USA (April 2012).

[3] King, D., Ford, C.(2013); A critical survey of Network Functions Virtualization (NFV), https://www.ietf.org/proceedings/86/slides/slides-86-sdnrg-3.pdf, 1-8.

[4] Sallent, S. et al. (2012); Fibre project: Brazil and europe unite forces and testbeds for the internet of the future, In: *Korakis, T., Zink, M., Ott, M. (eds.) TRIDENTCOM. Lecture Notes of the Institute for Computer Sciences, Social Informatics and Telecommunications Engineering*, Springer, 44: 372-372.

[5] Sherwood, R. et al. (2009 ; *Flowvisor: A network virtualization layer. OpenFlow Switch Consortium*, Tech. Rep.

[6] Bastin, N. (2011); Flowvisor System Requirements, https://openflow.stanford.edu/display/DOCS/System+Requirements. Accessed: 2014-06-09.

[7] Matias, J., et al. (2012); Implementing layer 2 network virtualization using openflow: Challenges and solutions. *Software Defined Networking (EWSDN), 2012 European Workshop On*, 30-35.

[8] Salvadori, E., Corin, R.D., Broglio, A., Gerola, M. (2011); Generalizing virtual network topologies in openflow-based networks, *Global Telecommunications Conference (GLOBECOM 2011)*, IEEE, 1-6.

[9] Corin, R.D. et al.(2012), Vertigo: Network virtualization and beyond. In: Software Defined Networking (EWSDN), *2012 European Workshop On*, 24-29.

[10] Gomes, V.S. et al. (2013); Flowvisorqos: Aperfeicoando o flowvisor para aprovisionamento de recursos em redes virtuais definidas por software, *IV Workshop de Pesquisa Experimental da Internet do Futuro-Simposio Brasileiro de Redes de Computadores e Sistemas Distribuidos (SBRC 2013)*, Brasilia, 35-41.

[11] Al-Shabibi, A. et al. (2014); Openvirtex: Make your virtual sdns programmable. In: Proceedings of the Third Workshop on Hot Topics in Software Defined Networking, *HotSDN'14*, ACM, New York, NY, USA , 25-30.

[12] OnLab; OpenVirtex System Requirements. http://ovx.onlab.us/getting-started/installation/. Accessed: 2015-07-14.

[13] Drutskoy, D., Keller, E. (2013), Rexford, J.; Scalable network virtualization in software-defined networks, *Internet Computing*, IEEE, 17(2): 20-27

[14] Pinheiro, B., Chaves, R., Cerqueira, E., Abelem, A. (2013); Cim-sdn: A common information model extension for software-defined networking, *Globecom Workshops (GC Wkshps), 2013 IEEE*, 836-841.

[15] ONF; OpenFlow Switch Specification. https://www.opennetworking.org/images/stories/downloads/sdn- resources/onf-specifications/openflow/openflow-spec-v1.0.0.pdf. Accessed: 2015-07-14 (2009).

[16] Jarschel, M. et al.(2011); Modeling and performance evaluation of an openflow architecture, *Proceedings of the 23rd International Teletraffic Congress. ITC'11*, 1-7.

INTERNATIONAL JOURNAL OF COMPUTERS COMMUNICATIONS & CONTROL
ISSN 1841-9836, 11(5):709-720, October 2016.

Fuzzy H_2 Guaranteed Cost Sampled-Data Control of Nonlinear Time-Varying Delay Systems

Z.-F. Qu, Z.-B. Du

Zifang Qu
Shandong Institute of Business and Technology
Yantai, Shandong, 264005, China
quzifang@163.com

Zhenbin Du*
Yantai University
Yantai, Shandong, 264005, China
*Corresponding author: zhenbindu@126.com

Abstract: We present and study a delay-dependent fuzzy H_2 guaranteed cost sampled-data control problem for nonlinear time-varying delay systems, which is formed by fuzzy Takagi-Sugeno (T-S) system and a sampled-data fuzzy controller connected in a closed loop. Applying the input delay approach and stability theorem of Lyapunov-Krasovskii functional with Leibniz-Newton formula, the H_2 guaranteed cost control performance is achieved in the sense that the closed-loop system is asymptotically stable. A new sufficient condition for the existence of fuzzy sampled-data controller is given in terms of linear matrix inequalities (LMIs). Truck-trailer system is given to illustrate the effectiveness and feasibility of H_2 guaranteed cost sampled-data control design.
Keywords: fuzzy T-S system; sampled-data; nonlinear systems; time-varying delay; H_2 guaranteed cost control

1 Introduction

Fuzzy Takagi–Sugeno(T-S)models [1] are used to describe nonlinear systems by a set of IF–THEN rules which gives a local linear representation. Since the work of Tanaka and Sugeno [2] on stability analysis and stabilization being published, many efforts have been made in developing systematic theory for such systems.

Because of the fast development of the digital circuit technology, using computers to design controller to reduce the implementation cost and time is more and more popular. The system of control is a sampled-data system. In sampling period,its control signals are constant. The overall control system becomes a sampled-data system, where the control signals are kept constant during the sampling period. It's a popular trend to study the analysis and synthesis of fuzzy sampled-data systems in many papers, see, for instance, [3–12] and the references therein. Of these works, stability analysis [3], stabilization [11], H_∞ control [4,6,7,9], H_2 GC control [8,10], fault-tolerant control [12] and tracking control [5] are researched, respectively.

Stability and robust stability theory was adopted in sampled-data time-delay systems [3, 4, 7, 9]. In industrial systems and information networks, it's popular to use time-delay systems. So, we should study time-delay systems and design some controllers for them. There have two ways for the stability analysis and synthesis of time-delay fuzzy T–S systems, i.e. delay-independent and delay-dependent approaches. With no respective of the size of the delay, we use delay-independent approach to assure stable conditions. The delay-dependent approach, contrast with the delay-independent approach, is complex in design procedure. So, it always have more conservative results. The delay-dependent approach supplies an upper bound of the time-delay.

It deals with the size of the time-delay, as a consequence, it usually provides less conservative results.

Among these works [3, 4, 7, 9], [7] is delay-independent and [3, 4, 9] are delay-dependent, where time delay is assumed to be constant. However, in practical engineering systems, the occurrence of time delay phenomena is often time-varying. Thus, fuzzy sampled-data control for time-varying delay systems is more appealing. In fuzzy sampled-datacontrol, there is no report aboutH_2 guaranteed cost controlproblem for the nonlinear time-varying delay systems.

In this paper, we consider the delay-dependent sampled-data H_2 guaranteed costperformance problem of the nonlinear time-varying delay system represented by a fuzzy T-S model. A Lyapunov-Krasovskii functional with Leibniz-Newton formula is employed to obtain new sufficient conditions in terms of linear matrix inequalities (LMIs) to the fuzzy H_2 guaranteed cost control performance. Based on the stability condition, the guaranteed cost control is minimized for the closed-loop system. We use truck-trailer system to prove the effectiveness and the feasibility of the proposed method.

The main contributions and advantages of the present paper are summarized as follows: (i) The H_2 design via fuzzy sampled-data control for nonlinear systems with time-varying delay is first obtained. (ii) Fuzzy sampled-data control algorithm is less conservative. Comparing with the existing works, the dimension of the LMIs in this paper is simplified, which adds the existence of feedback gains and lowers the implementation time. Experimental results illustrate that the fuzzy sampled-data controller has a larger sampling interval.

Notations: Throughout this paper, if not explicitly stated, we assumed that matrices have compatible dimensions. The notation $P>0(<0)$ is used to denote a positive (negative) definite matrix. The transpose of a matrix $P$is denoted by P^T. The symbol $*$ stands for the transposed element in symmetric positions.

2 Problem formulation

Consider the following nonlinear time-varying delay system:

$$\dot{x}(t) = f(x(t), x(t - d(t)), u(t)), \tag{1}$$

where $x(t) \in R^n$ is the state vector, $u(t) \in R^m$ is the control input vector, f is a nonlinear function, and $d(t)$ is time-varying delay.

The following fuzzy T-S model with time-varying delay described by IF–THEN rules is used to represent nonlinear time-varying delay system:

$$\text{IF } \xi_1(t) \text{ is } M_{i1} \text{ and } \cdot \quad \cdot \quad \cdot \text{ and } \xi_p(t) \text{ is } M_{ip}, \text{ THEN}$$

$$\dot{x}(t) = A_i x(t) + A_{id} x(t - d(t)) + B_i u(t), i = 1, \cdots, L, \tag{2}$$

where A_i, B_i and A_{id} are constant matrices of appropriate dimensions. L is the number of IF–THEN rules, M_{ij} are fuzzy sets and $\xi_1, \ldots, \xi_p$ are premise variables, $\xi(t) = [\xi_1 \ldots \xi_p]^T$, and $\xi(t)$ is assumed to be given or a measurable function vector. We consider the following two cases for the time-varying delay.

Case 1: $d(t)$ is a differentiable function satisfying for all $t \geq 0$:

$$0 \leq d(t) \leq d_M \text{ and } \dot{d}(t) \leq d_D,$$

where d_M and d_D are constants.

Case 2: $d(t)$ is a continuous function satisfying for all $t \geq 0$:

$$0 \leq d(t) \leq d_M,$$

where d_M is a constant.

By fuzzy blending, the overall fuzzy model is inferred as follows:

$$\dot{x}(t) = \sum_{i=1}^{L} \lambda_i(\xi(t))[A_i x(t) + A_{id} x(t - d(t)) + B_i u(t)], \tag{3}$$

where $\lambda_i(\xi(t)) = \frac{\beta_i(\xi(t))}{\sum_{i=1}^{L} \beta_i(\xi(t))}, \beta_i(\xi(t)) = \prod_{j=1}^{p} M_{ij}(\xi_j(t))$ and $M_{ij}(.)$ is the grade of the membership function of M_{ij}. $\beta_i(\xi(t)) \geq 0$, $i = 1, 2, \ldots, L$, $\sum_{i=1}^{L} \beta_i(\xi(t)) > 0$ for any $\xi(t)$, $\lambda_i(\xi(t)) \geq 0$, $i = 1, 2, \ldots, L$, $\sum_{i=1}^{L} \lambda_i(\xi(t)) = 1$.

We design the following fuzzy sampled-data controller for (3):

$$\text{IF } \xi_1(t_k) \text{ is } M_{j1} \text{ and } \cdot \quad \cdot \quad \cdot \text{ and } \xi_p(t_k) \text{ is } M_{jp}, \text{ THEN}$$

$$u(t) = K_j x(t_k), \quad j = 1, 2, \ldots, L,$$

where K_j is the sate feedback gain, the time t_k is the sampling instant satisfying $0 < t_1 < t_2 < \cdots < t_k < \cdots$, and sampling interval is a constant, i.e. $t_{k+1} - t_k = h_k = h$. The overall fuzzy sampled-data controller is as follows:

$$u(t) = \sum_{j=1}^{L} \lambda_j(\xi(t_k)) K_j x(t_k). \tag{4}$$

By using input delay approach, (4) is equivalent to (5)

$$u(t) = \sum_{j=1}^{L} \lambda_j(\xi(t_k)) K_j x(t - \tau(t)). \tag{5}$$

The closed-loop system (3) with (5) is given by

$$\dot{x}(t) = \sum_{i=1}^{L} \sum_{j=1}^{L} \lambda_i(\xi(t)) \lambda_j(\xi(t_k))[A_i x(t) + A_{id} x(t - d(t)) + B_i K_j x(t - \tau(t))]. \tag{6}$$

The following H_2 guaranteed costcontrol performance

$$J = \int_0^{\infty} (x^T(t) Q x(t) + u^T(t) R u(t)) dt. \tag{7}$$

must be minimized, where the weighting positive-definite matrices Q and R are specified beforehand according to the design purpose.

Determine a sampled-data state feedback controller such that the closed-loop system (6) is asymptotically stable and the upper bound of H_2 guaranteed cost function is minimized.

Lemma 2.1 (Gu et al. [13]). *For any positive definite symmetric constant matrix $M \in R^{n \times n}$, scalars r_1, r_2 satisfying $r_1 \leq r_2$, if $\varpi : [r_1, r_2] \to R^n$ is a vector function such that the integrations concerned are well defined, then*

$$\left(\int_{r_1}^{r_2} \varpi(s) ds \right)^T M \left(\int_{r_1}^{r_2} \varpi(s) ds \right) \leq (r_2 - r_1) \int_{r_1}^{r_2} \varpi^T(s) M \varpi(s) ds. \tag{8}$$

Remark 1: The premise variables $\xi_1, \ldots, \xi_p$ can be function of measurable state variables $x(t)$ and $x(t-d)$, or combination of measurable state variables. The limitation of design of fuzzy T–S approach is that some state variables must be measurable to construct fuzzy controller.
Remark 2: It should be noted that the control signal $u(t)$ holds constant during the period of $t_k \le t \le t_{k+1}$.

3 Fuzzy H_2 Guaranteed Cost Sampled-Data Control

In this section, we present a H_2 guaranteed cost sampled-data control scheme of the fuzzy system and minimization of the upper bound of (7).

Here, we give some sufficient conditions for the stability of the closed-loop system (6) in terms of LMIs.

Theorem 1. Suppose that, under case 1, for given matrices $Q > 0$, $R > 0$, scalars $h > 0$, $d_M > 0$, $d_D > 0$, $\mu > 0$,there exist matrices $\overline{P} > 0$, $\overline{R_1} > 0$, $\overline{R_2} > 0$, $\overline{R_3} > 0$, such that the following LMIs hold for all $i, j = 1, 2, \cdots, L$,

$$\Sigma_{ij} = \begin{bmatrix} \Sigma_{ij11} & \Sigma_{ij12} & \Sigma_{ij13} & 0 & \Sigma_{ij15} & \Sigma_{ij16} \\ * & \Sigma_{ij22} & 0 & 0 & 0 & 0 \\ * & * & \Sigma_{ij33} & \Sigma_{ij34} & \Sigma_{ij35} & 0 \\ * & * & * & \Sigma_{ij44} & 0 & 0 \\ * & * & * & * & \Sigma_{ij55} & \Sigma_{ij56} \\ * & * & * & * & * & \Sigma_{ij66} \end{bmatrix} < 0, \tag{9}$$

where

$$\begin{aligned} \Sigma_{ij11} &= A_i\overline{P} + \overline{P}A_i^T + \overline{R}_1 - \overline{R}_2 - \overline{R}_3, \Sigma_{ij12} = \overline{P}, \Sigma_{ij13} = B_i\overline{K_j} + \overline{R}_2, \Sigma_{ij15} = \mu\overline{P}A_i^T, \\ \Sigma_{ij16} &= A_{id}\overline{P} + \overline{R}_3, \Sigma_{ij22} = -Q^{-1}, \Sigma_{ij33} = -\overline{R}_2, \Sigma_{ij34} = \overline{K}_j^T, \Sigma_{ij35} = \mu\overline{K}_j^T B_i^T, \\ \Sigma_{ij44} &= -R^{-1}, \Sigma_{ij55} = -2\mu\overline{P} + h^2\overline{R}_2 + d_M^2\overline{R}_3, \Sigma_{ij56} = A_{id}\overline{P}, \\ \Sigma_{ij66} &= -(1-d_D)\overline{R}_1 - \overline{R}_3. \end{aligned}$$

Then there exists a sampled-data controller (4) with $K_j = \overline{K_jP}^{-1}(j = 1, 2, \cdots, L)$ such that H_2 guaranteed cost control performance (7) is minimized in the sense that the closed-loop system (6) is asymptotically stable.

Proof. Choose the Lyapunov-Krasovskii functional:

$$V(x_t) = V_1(x) + V_2(x_t) + V_3(x_t) + V_4(x_t), \tag{10}$$

where

$$V_1(x) = x^T(t)Px(t), \quad V_2(x_t) = \int_{t-d(t)}^{t} x^T(s)R_1x(s)ds,$$

$$V_3(x_t) = h\int_{-h}^{0}\int_{t+\theta}^{t} \dot{x}^T(s)R_2\dot{x}(s)dsd\theta, V_4(x_t) = d_M\int_{-d_M}^{0}\int_{t+\theta}^{t} \dot{x}^T(s)R_3\dot{x}(s)dsd\theta$$

and $P > 0$, $R_1 > 0$, $R_2 > 0$,$R_3 > 0$.

The derivative of Valong the trajectories of the system (6) is computed as follows:

$$\begin{aligned}\dot{V}_1(x) &= \dot{x}^T(t)Px(t) + x^T(t)P\dot{x}(t)\\ &= \sum_{i=1}^{L}\sum_{j=1}^{L}\lambda_i(\xi(t))\lambda_j(\xi(t_k))[x^T(t)A_i^TPx(t) + x^T(t-d(t))A_{id}^TPx(t)\\ &\quad +x^T(t-\tau(t))K_j^TB_i^TPx(t) + x^T(t)PAix(t) + x^T(t)PAidx(t-d(t))\\ &\quad +x^T(t)PB_iK_jx(t-\tau(t)). \end{aligned} \tag{11}$$

$$\begin{aligned}\dot{V}_2(x_t) &= x^T(t)R_1x(t) - (1-\dot{d}(t))x^T(t-d(t))R_1x(t-d(t))\\ &\le x^T(t)R_1x(t) - (1-d_D)x^T(t-d(t))R_1x(t-d(t)). \end{aligned} \tag{12}$$

By using Lemma 2.1, we have

$$-h\int_{t-h}^{t}\dot{x}^T(s)R_2\dot{x}(s)ds \le -\tau(t)\int_{t-\tau(t)}^{t}\dot{x}^T(s)R_2\dot{x}(s)ds \le -\left(\int_{t-\tau(t)}^{t}\dot{x}(s)ds\right)^T R_2\left(\int_{t-\tau(t)}^{t}\dot{x}(s)ds\right). \tag{13}$$

Leibniz-Newton formula is

$$\int_{t-h}^{t}\dot{x}(s)ds = x(t) - x(t-h). \tag{14}$$

Applying (13) and Leibniz-Newton formula, we have

$$\begin{aligned}\dot{V}_3(x_t) &= h^2\dot{x}^T(t)R_2\dot{x}(t) - h\int_{t-h}^{t}\dot{x}^T(s)R_2\dot{x}(s)ds\\ &\le h^2\dot{x}(t)^TR_2\dot{x}(t) - (x(t)-x(t-\tau(t)))^TR_2(x(t)-x(t-\tau(t)))^T\\ &= h^2\dot{x}^T(t)R_2\dot{x}(t) - x^T(t)R_2x(t) + x^T(t-\tau(t))R_2x(t) + x^T(t)R_2x(t-\tau(t))\\ &\quad -x^T(t-\tau(t))R_2x(t-\tau(t)). \end{aligned} \tag{15}$$

Similarly, by Lemma 2.1 and Leibniz-Newton formula, we have

$$\begin{aligned}\dot{V}_4(x_t) &\le d_M^2\dot{x}^T(t)R_3\dot{x}(t) - x^T(t)R_3x(t) + x^T(t-d(t))R_3x(t)\\ &\quad +x^T(t)R_3x(t-d(t)) - x^T(t-d(t))R_3x(t-d(t)). \end{aligned} \tag{16}$$

From (6), for a given $\mu > 0$,

$$\begin{aligned}0 &= -2\mu\dot{x}^T(t)P\dot{x}(t) + \mu\dot{x}^T(t)P\{\sum_{i=1}^{L}\sum_{j=1}^{L}\lambda_i(\xi(t))\lambda_j(\xi(t_k))[A_ix(t) + A_{id}x(t-d(t))\\ &\quad +B_iK_jx(t-\tau(t))]\} + \mu\{\sum_{i=1}^{L}\sum_{j=1}^{L}\lambda_i(\xi(t))\lambda_j(\xi(t_k))[A_ix(t) + A_{id}x(t-d(t))\\ &\quad +B_iK_jx(t-\tau(t))]\}^TP\dot{x}(t)\\ &= -2\mu\dot{x}^T(t)P\dot{x}(t) + \sum_{i=1}^{L}\sum_{j=1}^{L}\lambda_i(\xi(t))\lambda_j(\xi(t_k))[\mu\dot{x}^T(t)PA_ix(t)\\ &\quad +\mu\dot{x}^T(t)PA_{id}x(t-d(t)) + u\dot{x}^T(t)PBiKjx(t-\tau(t)) + ux^T(t)Ai^TP\dot{x}(t)\\ &\quad +\mu x^T(t-d(t))A_{id}^TP\dot{x}(t) + \mu x^T(t-\tau(t))K_j^TB_i^TP\dot{x}(t)]. \end{aligned} \tag{17}$$

From (11-12) and (15-17), we obtain

$$\dot{V}(x_t) + x^T(t)Qx(t) + u^T(t)Ru(t) \leq \sum_{i=1}^{L}\sum_{j=1}^{L} \lambda_i(\xi(t))\lambda_j(\xi(t_k))\tilde{x}^T(t)S\imath_{ij}\tilde{x}(t) \tag{18}$$

where

$$\tilde{x}(t) = [\ x^T(t) \quad x^T(t-\tau(t)) \quad \dot{x}^T(t) \quad x^T(t-d(t)\ ]^T,$$

$$S\imath_{ij} = \begin{bmatrix} S\imath_{ij11} & S\imath_{ij12} & S\imath_{ij13} & S\imath_{ij14} \\ * & S\imath_{ij22} & S\imath_{ij23} & 0 \\ * & * & S\imath_{ij33} & S\imath_{ij34} \\ * & * & * & S\imath_{ij44} \end{bmatrix} \tag{19}$$

with

$$\begin{aligned} S\imath_{ij11} &= A_i^T P + PA_i + R_1 - R_2 - R_3 + Q, S\imath_{ij12} = PB_iK_j + R_2, S\imath_{ij13} = \mu A_i^T P, \\ S\imath_{ij14} &= PA_{id} + R_3, S\imath_{ij22} = -R_2 + K_j^T R K_j, S\imath_{ij23} = \mu K_j^T B_i^T P, \\ S\imath_{ij33} &= -2\mu P + h^2 R_2 + d_M^2 R_3, S\imath_{ij34} = PA_{id}, \quad S\imath_{ij44} = -(1-d_D)R_1 - R_3. \end{aligned}$$

Pre- and post-multiplying the matrix $S\imath_{ij}$ in (19) by $diag\begin{bmatrix} P^{-1} & P^{-1} & P^{-1} & P^{-1} \end{bmatrix}$ with$\overline{P} = P^{-1}$,$\overline{R_1} = P^{-1}R_1P^{-1}$,$\overline{R_2} = P^{-1}R_2P^{-1}$,$\overline{R_3} = P^{-1}R_3P^{-1}$,$\bar{Q} = P^{-1}QP^{-1}$,$\bar{K}_j = K_jP^{-1}$ ($j = 1, 2, \cdots, L$), we have

$$S_{ij} = \begin{bmatrix} \sum_{ij11} + \bar{Q} & \sum_{ij13} & \sum_{ij15} & \sum_{ij16} \\ * & \sum_{ij33} + \bar{K}_j^T R \bar{K}_j & \sum_{ij35} & 0 \\ * & * & \sum_{ij55} & \sum_{ij56} \\ * & * & * & \sum_{ij66} \end{bmatrix}. \tag{20}$$

If (9) is satisfied, then $\Sigma_{ij} < 0$ is equivalent to $S_{ij} < 0$ in (20) by using the Schur complement. And, $S_{ij} < 0$ in (20) is equivalent to $S\imath_{ij} < 0$ in (19). Thus,

$$\dot{V}(x_t) + x^T(t)Qx(t) + u^T(t)Ru(t) < 0. \tag{21}$$

Integrating both sides of (21) from t= 0 to$t = \infty$, we obtain

$$V(x_t(\infty)) - V(x_t(0)) + \int_0^\infty (x^T(t)Qx(t) + u^T(t)Ru(t))dt < 0. \tag{22}$$

Thus, we have

$$J < V(x_t(0)) = x^T(0)Px(0). \tag{23}$$

Now, we provide a stability condition for the fuzzy T–S system (6) under case 2.

Theorem 2. Suppose that, under case 2, for given matrices $Q > 0$, $R > 0$, scalars $h > 0$, $d_M > 0$, $\mu > 0$, there exist matrices $\overline{P} > 0$, $\overline{R_1} > 0$, $\overline{R_2} > 0$such that the following LMIs hold

for all $i, j = 1, 2, \cdots, L$

$$\bar{\Sigma}_{ij} = \begin{bmatrix} \bar{\Sigma}_{ij11} & \bar{\Sigma}_{ij12} & \bar{\Sigma}_{ij13} & 0 & \bar{\Sigma}_{ij15} & \bar{\Sigma}_{ij16} \\ * & \bar{\Sigma}_{ij22} & 0 & 0 & 0 & 0 \\ * & * & \bar{\Sigma}_{ij33} & \bar{\Sigma}_{ij34} & \bar{\Sigma}_{ij35} & 0 \\ * & * & * & \bar{\Sigma}_{ij44} & 0 & 0 \\ * & * & * & * & \bar{\Sigma}_{ij55} & \bar{\Sigma}_{ij56} \\ * & * & * & * & * & \bar{\Sigma}_{ij66} \end{bmatrix} < 0, \tag{24}$$

where

$$\begin{aligned} \bar{\Sigma}_{ij11} &= A_i\overline{P} + \overline{P}A_i^T - \overline{R}_1 - \overline{R}_2, \bar{\Sigma}_{ij12} = \overline{P}, \bar{\Sigma}_{ij13} = B_i\overline{K_j} + \overline{R}_1, \bar{\Sigma}_{ij15} = \mu\overline{P}A_i^T, \\ \bar{\Sigma}_{ij16} &= A_{id}\overline{P} + \overline{R}_2, \bar{\Sigma}_{ij22} = -Q^{-1}, \quad \bar{\Sigma}_{ij33} = -\overline{R}_1, \quad \bar{\Sigma}_{ij34} = \overline{K}_j^T, \quad \bar{\Sigma}_{ij35} = \mu\overline{K}_j^T B_i^T, \\ \bar{\Sigma}_{ij44} &= -R^{-1}, \quad \bar{\Sigma}_{ij55} = -2\mu\overline{P} + h^2\overline{R}_1 + d_M^2\overline{R}_2, \bar{\Sigma}_{ij56} = A_{id}\overline{P}, \bar{\Sigma}_{ij66} = -\overline{R}_2. \end{aligned}$$

Then there exists a sampled-data controller (4) with $K_j = \overline{K_jP}^{-1}(j = 1, 2, \cdots, L)$ such that H_2 guaranteed cost control performance (7) is minimized in the sense that the closed-loop system (6) is asymptotically stable.

Proof. Choose the following Lyapunov-Krasovskii functional:

$$V(x_t) = V_1(x) + V_2(x_t) + V_3(x_t), \tag{25}$$

where

$$V_1(x) = x^T(t)Px(t), V_2(x_t) = h\int_{-h}^{0}\int_{t+\theta}^{t}\dot{x}^T(s)R_1\dot{x}(s)dsd\theta,$$

$$V_3(x_t) = d_M\int_{-d_M}^{0}\int_{t+\theta}^{t}\dot{x}^T(s)R_2\dot{x}(s)dsd\theta$$

and $P > 0$, $R_1 > 0$, $R_2 > 0$ are to be determined. Then following the similar line in Theorem 1, we can obtain Theorem 2.

If there is no time delay, then we have the following Corollary 1.

Corollary 1. Suppose that, for given matrices $Q > 0$, $R > 0$, scalars $h > 0$, $\mu > 0$, there exist matrices $\overline{P} > 0$, $\overline{R_1} > 0$, such that the following LMIs hold for all $i, j = 1, 2, \cdots, L$

$$\bar{\bar{\Sigma}}_{ij} = \begin{bmatrix} \bar{\bar{\Sigma}}_{ij11} & \bar{\bar{\Sigma}}_{ij12} & \bar{\bar{\Sigma}}_{ij13} & 0 & \bar{\bar{\Sigma}}_{ij15} \\ * & \bar{\bar{\Sigma}}_{ij22} & 0 & 0 & 0 \\ * & * & \bar{\bar{\Sigma}}_{ij33} & \bar{\bar{\Sigma}}_{ij34} & \bar{\bar{\Sigma}}_{ij35} \\ * & * & * & \bar{\bar{\Sigma}}_{ij44} & 0 \\ * & * & * & * & \bar{\bar{\Sigma}}_{ij55} \end{bmatrix} < 0, \tag{26}$$

where

$$\begin{aligned} \bar{\bar{\Sigma}}_{ij11} &= A_i\overline{P} + \overline{P}A_i^T - \overline{R}_1, \bar{\bar{\Sigma}}_{ij12} = \overline{P}, \bar{\bar{\Sigma}}_{ij13} = B_i\overline{K_j} + \overline{R}_1, \bar{\bar{\Sigma}}_{ij15} = \mu\overline{P}A_i^T, \bar{\bar{\Sigma}}_{ij22} = -Q^{-1}, \\ \bar{\bar{\Sigma}}_{ij33} &= -\overline{R}_1, \quad \bar{\bar{\Sigma}}_{ij34} = \overline{K}_j^T, \quad \bar{\bar{\Sigma}}_{ij35} = \mu\overline{K}_j^T B_i^T, \bar{\bar{\Sigma}}_{ij44} = -R^{-1}, \quad \bar{\bar{\Sigma}}_{ij55} = -2\mu\overline{P} + h^2\overline{R}_1. \end{aligned}$$

Then there exists a sampled-data controller (4) with $K_j = \overline{K_jP}^{-1}(j = 1, 2, \cdots, L)$ such that H_2 guaranteed cost control performance (7) is minimized in the sense that the closed-loop system (6) is asymptotically stable.

In the following, we give the design procedure of fuzzy sampled-data controller.

The H_2 guaranteed cost sampled-data fuzzy control problem can be formulated as the following optimization problem:

$$\min_{\bar{P}} Trace(J)$$

$$s.t.(9) and \begin{bmatrix} J & x^T(0) \\ * & \bar{P} \end{bmatrix} > 0. \tag{27}$$

Design Procedure: The delay-dependentH_2 guaranteed cost sampled-datacontrol for fuzzy time-varying delay system is summarized as follows.

Step 1: Select membership functions and fuzzy rules in (1).

Step 2: Give the upper bound of sampling interval $h > 0$ and a scalar $\mu > 0$.

Step 3: Solve the LMIs (27) to obtain $\overline{K_j}(j = 1, 2, \cdots, L)$ and $\overline{P}$.Thus,$K_j = \overline{K_j P}^{-1}$ $(j = 1, 2, \cdots, L)$ can also be obtained.

Step 4: Increase$h$, and repeat Step 3 until $\overline{K_j}(j = 1, 2, \cdots, L)$ and $\overline{P}$ can not be found.

Step 5: Confirm fuzzy H_2 guaranteed costsampled-datacontrol and stability of the closed-loop system, substitute P,$K_j(j = 1, 2, \cdots, L)$, μ and h into (19) and verify $S_{ij} < 0$.

Step 6: Construct the fuzzy sampled-data controller (4).

4 Simulation example

To test the effectiveness and feasibility of the proposed method, we consider the following truck-trailer system [14]

$$\begin{aligned} \dot{x}_1(t) &= -a\tfrac{v\bar{t}}{Lt_0}x_1(t) - (1-a)\tfrac{v\bar{t}}{Lt_0}x_1(t-t_d) + \tfrac{v\bar{t}}{lt_0}u(t) \\ \dot{x}_2(t) &= a\tfrac{v\bar{t}}{Lt_0}x_1(t) + (1-a)\tfrac{v\bar{t}}{Lt_0}x_1(t-t_d) \\ \dot{x}_3(t) &= \tfrac{v\bar{t}}{Lt_0}\sin(x_2(t) + a(v\bar{t}/2L)x_1(t) + (1-a)(v\bar{t}/2L)x_1(t-t_d)), \end{aligned} \tag{28}$$

where $l = 2.8 \quad L = 5.5$, $v = -1.0$, $a = 0.7$, $\bar{t} = 2.0$, $t_0 = 0.5$. $\quad x_1(t) \in [-\pi/2, \quad \pi/2]$,

$\dot{x}_1(t) \in [-3, \quad 3], x_2(t) \in [-\pi/2, \quad \pi/2], \dot{x}_2(t) \in [-2, \quad 2].x(t) = [x_1(t) \quad x_2(t) \quad x_3(t)]^T$,

$[x_1(0) \quad x_2(0) \quad x_3(0)] = \begin{bmatrix} 1.5 & -2 & 5 \end{bmatrix}$.

The nonlinear truck-trailer system is modeled by two-rule fuzzy T-S system.

Rule 1: IF $\theta(t) = x_2(t) + a(v\bar{t}/2L)x_1(t) + (1-a)(v\bar{t}/2L)x_1(t-t_d)$ is about 0,

$$Then \dot{x}(t) = A_1 x(t) + A_{d1}x(t-\tau_d) + B_1 u(t). \tag{29}$$

Rule 2: IF $\theta(t) = x_2(t) + a(v\bar{t}/2L)x_1(t) + (1-a)(v\bar{t}/2L)x_1(t-t_d)$ is about π or $-\pi$,

$$Then \dot{x}(t) = A_2 x(t) + A_{d2}x(t-\tau_d) + B_2 u(t). \tag{30}$$

where

$$A_1 = \begin{bmatrix} -a\frac{v\bar{t}}{Lt_0} & 0 & 0 \\ a\frac{v\bar{t}}{Lt_0} & 0 & 0 \\ a\frac{v^2\bar{t}^2}{2Lt_0} & \frac{v\bar{t}}{t_0} & 0 \end{bmatrix}, A_{d1} = \begin{bmatrix} -(1-a)\frac{v\bar{t}}{Lt_0} & 0 & 0 \\ (1-a)\frac{v\bar{t}}{Lt_0} & 0 & 0 \\ (1-a)\frac{v^2\bar{t}^2}{2Lt_0} & 0 & 0 \end{bmatrix}, B_1 = \begin{bmatrix} \frac{v\bar{t}}{lt_0} \\ 0 \\ 0 \end{bmatrix},$$

$$A_2 = \begin{bmatrix} -a\frac{v\bar{t}}{Lt_0} & 0 & 0 \\ a\frac{v\bar{t}}{Lt_0} & 0 & 0 \\ a\frac{dv^2\bar{t}^2}{2Lt_0} & \frac{dv\bar{t}}{t_0} & 0 \end{bmatrix}, A_{d2} = \begin{bmatrix} -(1-a)\frac{v\bar{t}}{Lt_0} & 0 & 0 \\ (1-a)\frac{v\bar{t}}{Lt_0} & 0 & 0 \\ (1-a)\frac{dv^2\bar{t}^2}{2Lt_0} & 0 & 0 \end{bmatrix}, B_2 = \begin{bmatrix} \frac{v\bar{t}}{lt_0} \\ 0 \\ 0 \end{bmatrix},$$

and $d = 10t_0/\pi$.

The membership functions are defined as

$$\begin{aligned} \lambda_1(\theta(t)) &= \left(1 - \frac{1}{1+\exp(-3(\theta(t)-0.5\pi))}\right) \times \left(\frac{1}{1+\exp(-3(\theta(t)+0.5\pi))}\right), \\ \lambda_2(\theta(t)) &= 1 - \lambda_1(\theta(t)). \end{aligned}$$

A two-rule sampled-data fuzzy controller is employed to stabilize the truck trailer system. The sampled-data fuzzy controller is designed as follows:

$$u(t) = \sum_{j=1}^{2} \lambda_j(\theta(t_k)) K_j x(t_k).$$

First, we assume that time delay $d(t) = 0$. Applying various methods of [8] (H_2 control), [10] (H_2 control) and Corollary 1, the dimensions of the LMIs are given in Table 1. It is seen from Table 1 that the dimension of the LMIs is greatly simplified in the proposed method of this paper.

Table 1: The comparison for the dimensions of LMIs (Corolarry 1)

Method	[8]	[10]	Corollary 1
Dimension	25	28	13

Next, we assume that the delay is time-invariant, i.e. $d_D = 0$. By using various the methods of [3](H_2 control) and Theorem2, the dimensions of the LMIs are given in Table 2. It is seen from Table 2 that the dimension of the LMIs is simplified in the proposed method of this paper, which adds the existence of feedback gains and lowers the implementation time.

Table 2: The comparison for the dimensions of LMIs (Theorem 2)

Method	[3]	Theorem 2
Dimension	20	16

By using various methods of [3] and Theorem 2, the maximum allowable upper bounds of sampling interval are given in Table 3, which show that Theorem 2 of this paper can get a larger sampling interval. This implies that the proposed method achieves a better performance.

Table 3: The maximum allowable upper bounds of sampling interval

Method	[3]	Theorem 2
$h_{\max}(t_d = 0.5)$	0.374	0.562
$h_{\max}(t_d = 1)$	0.315	0.471
$h_{\max}(t_d = 2)$	0.251	0.283

Finally, we consider the control design for time-varying delay $t_d = 1 + \sin t$. The maximum allowable upper bound of sampling interval that is obtained by Theorem 1 is 0.295.When the design parameters are given by $\mu = 1$, $d_M = 2$, $d_D = 1$ with the sampling interval $h = 0.295$,Theorem 1 gives the fuzzy state feedback control gains

$$K_1 = [1.0319\ \text{-}0.1019\ 0.0009], \quad K_2 = [1.0319\ \text{-}0.1019\ 0.0009].$$

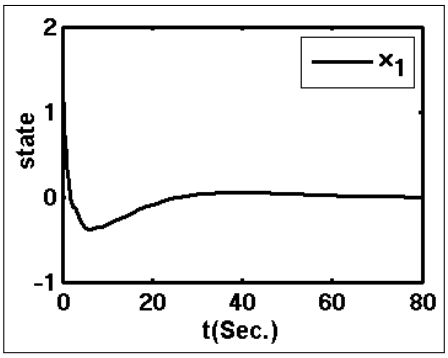

Figure 1: State response x_1

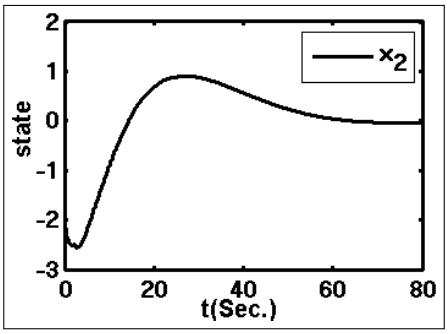

Figure 2: State response x_2

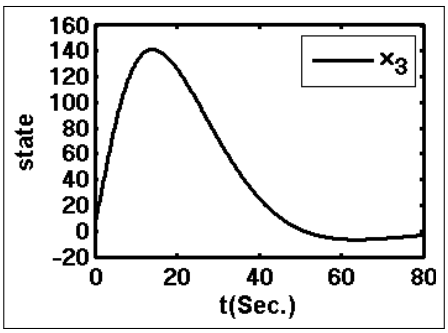

Figure 3: State response x_3

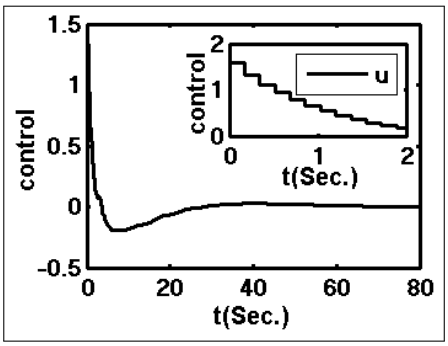

Figure 4: State response x_4

When time-varying delay t_d is $1.5 + 1.5 \sin t$, Theorem 1 gives the maximum allowable upper bound of sampling interval 0.172.With the design parameters $h = 0.172$, $\mu = 1.5$, $d_M = 3$, $d_D = 1.5$, $Q = diag\{\ 1 \quad 10 \quad 0.1\ \} \times 10^{-6}$,$R = 10^{-5}$, Theorem 1 gives the fuzzy state feedback control gains

$$K_1 = [0.9656\ \text{-}0.0657\ 0.0006]\,, \quad K_2 = [0.9656\ \text{-}0.0657\ 0.0006]\,.$$

The sampled-data fuzzy controller with the above control gains is applied to the truck trailer system, the results on the state responses$x_1,\ x_2,\ x_3$ and control law$u$are shown in Figures 1- 4.

Simulation results illustrate the fuzzy H_2 guaranteed cost sampled-data control design is effective and feasible. Figs. 1-3 show the system stability, and Fig.4 shows the sampled-data control signal for the system (28).

5 Conclusion

This work considers the fuzzyH_2 GC sampled-data control problem for nonlinear systems with time-varying delay. It should be pointed that this problem is more complicated and harder to deal with due to the coexistence of feedback delay and sampled-data control. A new sufficient condition for the existence of fuzzy sampled-data controller is given in terms of LMIs.

To better demonstrate our results, a truck-trailer system with sampled-data control is given. Simulation results show the effectiveness and feasibility of sampled-data control design. Furthermore, this method could be extended to H_∞ control.

Acknowledgment

This work was supported by the National Natural Science Foundation of China(61203320) and Shandong Natural Science Foundation (ZR2014FL023).

Bibliography

[1] T. Takagi; M. Sugeno. (1985); Fuzzy identification of systems and its applications to modeling and control, *IEEE Transactions on Systems, Man, and Cybernetics*, ISSN 0018-9472, SMC, 15(1):116-132.

[2] K.Tanaka; M.Sugeno.(1992); Stability analysis and design of fuzzy control systems, *Fuzzy Sets and Systems*, ISSN 0165-0114, 45(2):135-156.

[3] H. K. Lam;F. H. Leung. (2007); Sampled-data fuzzy controller for time-delay nonlinear systems: fuzzy-model-based LMI approach, *IEEE Transactions on Systems, Man, and Cybernetics-Part B: Cybernetics*, ISSN 1083-4419, 37(3): 617-629.

[4] D. -Y. Yang ; K. -Y. Cai. (2008); Reliable H∞ non-uniform sampling fuzzy control for nonlinear systems with time delay, *IEEE Transactions on Systems, Man, and Cybernetics-Part B: Cybernetics*, ISSN 1083-4419, 38(6): 1606–1613.

[5] H. K. Lam ;L. D. Seneviratne. (2009); Tracking control of sampled-data fuzzy-model-based control systems, *IET Control Theory & Applications*, ISSN 1751-8644, 3(1):56-57.

[6] J. Yoneyama. (2010); Robust H8 control of uncertain fuzzy systems under time-varying sampling, *Fuzzy Sets and Systems*, ISSN 0165-0114, 161(6): 859-871.

[7] C.-H. Lien;K.-W. Yu;C.-T. Huang;P.-Y. Chou;L.-Y. Chung ;J. -D. Chen. (2010); Robust H∞ control for uncertain T-S fuzzy time-delay systems with sampled-data input and nonlinear perturbations, *Nonlinear Analysis: Hybrid Systems*, ISSN 1751-570X, 4(3) : 550-556.

[8] J. Yoneyama. (2011); Robust guaranteed cost control of uncertain fuzzy systems under time-varying sampling, *Applied Soft Computing*, ISSN 1568-4946, 11(1): 225-249.

[9] P. Chen; Q. -L. Han;D. Yue ; E.-G. Tian. (2011); Sampled-data robust H8 control for T–S fuzzy systems with time delay and uncertainties, *Fuzzy Sets and Systems*, ISSN 0165-0114, 179(11):20-33.

[10] G.B.Koo;J.B.Park;Y.H.Joo. (2013); Guaranteed cost sampled-data fuzzy control for nonlinear systems: a continuous-time Lyapunov approach, *IET Control Theory & Applications*, ISSN 1751-8644, 7(13):1745-1752.

[11] F.-S.Yang;H.-G. Zhang;Y.-C.Wang. (2014); An enhanced input-delay approach to sampled-data stabilization of T–S fuzzy systems via mixed convex combination, *Nonlinear Dynamics*, ISSN 0924-090X,75(3):501-512.

[12] H.-Y.Li; X.-J.Sun;P.Shi ; H.K.Lam. (2015); Control design of interval type-2 fuzzy systems with actuator falut: sampled-data control approach, *Information Sciences*, ISSN 0020-0255, 302(1): 1-13.

[13] K. Gu;V.L. Kharitonov;J. Chen. (2003); *Stability of time-delay system*, Boston: Birkhauser, ISBN 0817642129.

[14] Y.-Y.Cao;P.M.Frank. (2001); Stability analysis and synthesis of nonlinear time-delay systems via linear Takagi-Sugeno fuzzy models, *Fuzzy Sets and Systems*, ISSN 0165-0114, 124(2):213-229.

INTERNATIONAL JOURNAL OF COMPUTERS COMMUNICATIONS & CONTROL
ISSN 1841-9836, 11(5):721-734, October 2016.

Continuous Distribution Approximation and Thresholds Optimization in Serial Multi-Modal Biometric Systems

M. Stanojević, I. Milenković , D. Starčević, B. Stanojević

Milan Stanojević, Ivan Milenković, Dušan Starčević
Faculty of Organizational Sciences,
University of Belgrade,
Jove Ilića 154, 11000 Belgrade, Serbia
(milans, ivan.milenkovic, starcev)@fon.bg.ac.rs

Bogdana Stanojević*
Mathematical Institute of the
Serbian Academy of Sciences and Arts,
Kneza Mihaila 36, 11000 Belgrade, Serbia,
*Corresponding author: bgdnpop@mi.sanu.ac.rs

Abstract: Multi-modal biometric verification systems use information from several biometric modalities to verify an identity of a person. The false acceptance rate (FAR) and false rejection rate (FRR) are metrics generally used to measure the performance of such systems.

In this paper, we first approximate the score distributions of both genuine users and impostors by continuous distributions. Then we incorporate the exact expressions of the distributions in the formulas for the expected values of both FAR and FRR for each matcher. In order to determine the upper and lower acceptance thresholds in the sequential multi-modal biometric matching, we further minimize the expected values of FAR and FRR for the entire processing chain. We propose a non-linear bi-objective programming problem whose objective functions are the two error probabilities. We analyze the efficient set of the bi-objective problem, and derive an efficient solution as a best compromise between the error probabilities. Replacing the least squares approximation of the score distributions by a continuous distribution approximation, this approach modifies the method presented in Stanojević et al. [15] (doi: 10.1109/ICCCC.2016.7496752)[a].

The results of our experiments showed a good performance of the sequential multiple biometric matching system based on continuous distribution approximation and optimized thresholds.

Keywords: multi-modal biometrics, sequential fusion, multi-criteria optimization, continuous distribution approximation.

1 Introduction

This paper is an extension of [15] (doi: 10.1109/ICCCC.2016.7496752). The mathematical model introduced in [15], that derives optimized thresholds for bi-modal biometric systems, is here formulated generally, for N-modal biometric systems. In addition, the linear approximation of the biometric scores, based on the least squares method, is here replaced by a non-linear continuous distribution approximation. We report our new computation results and compare them with previous results.

Biometrics is the automated recognition of individuals based on their behavioral and biological characteristics [11]. Biometric recognition is used for many purposes including criminal

identification, secure access control, forensics and so forth. It was intensively researched and widely applied in the last decade [18]. A number of biometric technologies have been developed and several of them are being used in a variety of applications [7]. The most commonly used modalities are fingerprints, face, iris, speech, and hand geometry. Due to their strengths and weaknesses, the choice of one or another modality is strictly dependent on the application requirements.

In his book [5], Kaklauskas presented different methods for analyzing the body language (movement, position, use of personal space, silences, pauses and tone, the eyes, pupil dilation or constriction, smiles, body temperature and the like) for better understanding people's needs and actions, including biometric data gathering and reading. Filip [3], briefly reviewed the book, and emphasized that it addressed two modern research domains: intelligent and integrated decision support systems and biometrics-based human-computer interface.

An analysis of a multi-modal biometric system based on level of fusion was presented in [10]. The authors discussed the biometric systems, the limitations of individual biometric, and various fusion levels and methods of multi-modal systems.

The parallel fusion mode was first introduced in 1998 [4]. Fingerprint and face modalities were simultaneously used for identification. Serial fusion of multiple matchers is a good trade-off between the widely adopted parallel fusion and the use of a mono-modal verification system [12]. An alternative to parallel fusion of biometric data is the use of serial fusion.

Kumar and Kumar [6] presented a new approach for the adaptive management of multi-modal biometrics. They employed the ant colony optimization for the selection of the key parameters like decision threshold and fusion rule, to ensure the optimal performance in meeting varying security requirements during the deployment of multi-modal biometrics systems.

Zhang et al. [18] proposed a novel framework for serial multi-modal biometric systems based on semi-supervised learning techniques. They have promoted the discriminating power of the weaker but more user convenient traits over the use of the stronger but less user convenient traits. In this way, they proposed an alternative to other existing serial multi-modal biometric systems that suggest optimized orderings of the traits deployed and parameterizations of the corresponding matchers but ignore the most important requirements of common applications. Their experiments on two prototype systems demonstrated the advantages of their methodology.

Marcialis et al. [8] proposed a theoretical framework for the assessment of performance of serial fusion multi-modal systems, theoretically evaluated the benefits in terms of performance, and estimated the errors in the model parameters computation. They analyzed the model from the point of view of its pros and cons, and performed preliminary experiments on a benchmark found in the literature.

The importance of the use of multi-modal biometrics in the area of secure person authentication is highlighted in a recent study [13]. That study provided a different perception on how to use biometrics on the highest level of the network security with the fusion of multiple biometric modalities.

Snelick et al. [14] studied the performance of the multi-modal biometric authentication systems using the state-of-the-art commercial off-the-shelf (COTS) fingerprint and face biometric systems on a large-scale population. They also proposed new methods of normalization and fusion that improved the accuracy of the biometric systems.

The remainder of the paper is organized as follows. In Section 2 we formulate the problem that we wish to solve. Two solving methods are presented in Section 3: the linear approximation method is briefly presented in Section 3.1, and our novel approach is introduced in Section 3.2. Our computational results on random generated instances are given in Section 4.1, and the numerical results on NIST-BSSR1 and NIST-BSSR2 databases are reported in Section 4.2. The conclusions and some directions for future work are included in Section 5.

2 The Formulation of the Problem

Multi-modal biometric verification systems use information from several biometric modalities to verify an identity of a person. The false acceptance rate (FAR) and false rejection rate (FRR) are metrics generally used to measure the performance of such systems. The FAR is the probability that the system incorrectly matches the input pattern to a non-matching template in the database. It measures the percent of invalid inputs which are incorrectly accepted. In case of similarity scale, if the person is an impostor in reality, but the matching score is higher than the threshold, then he is treated as genuine. The FAR depends on the threshold value: the FAR increases as the threshold decreases. The FRR is the probability that the system fails to detect a match between the input pattern and a matching template in the database. It measures the percent of valid inputs which are incorrectly rejected. It also depends on the threshold value: the FRR increases as the threshold value increases. The visual characterization of the trade-off between the FAR and FRR is generally given by a graphic representation of the genuine acceptance rate (GAR=1-FRR) with respect to the false acceptance rate.

In general, a matching algorithm performs a decision based on a threshold. The threshold determines how close to a template the input needs to be for it to be considered a match. If the threshold is reduced, there will be fewer false non-matches but more false accepts. Conversely, a higher threshold will reduce the FAR but increase the FRR. Our goal is to find the system's thresholds that assure a good compromise between the minimizations of the false acceptance rate and false rejection rate.

Pato and Millett, in their book [11], emphasized that the biometric recognition systems are inherently probabilistic. In their opinion, the biometric recognition involves matching, within a tolerance of approximation, of observed biometric traits against previously collected data for a subject. The approximate matching is required due to the variations in biological attributes and behaviors both within and between persons.

Let us assume that the multi-modal biometric system consists of N matchings. After any of the first $N-1$ matchings (indexed in the formulas from 2 to N), one of the following three decisions will be made: accept the person as genuine, reject the person as impostor, or demand another matching. Naturally, after the last matching (that uses the index 1 in formulas), only two decisions will be possible: to accept, or to reject the person.

For each modality in the system, we collect data from n persons. For each person we take m samples, and construct an $m \times n$ matrix M of input information. For real-life databases the components of matrix M are vectors derived by using classic protocols, that extract biometric features from the real data collected (images, videos, speeches).

In the beginning we restrict our attention to one of the first $N-1$ matchings. Using the matrix M we compute the distances between each two collected samples, and derive the distributions for the genuine users and impostors. The distribution of the genuine users is constructed using the distances between each two components of the same column of the matrix M. The distribution of the impostors uses the distances between each component of matrix M and each component of matrix M that lies on different columns. Two samples obtained from the same person are highly expected to have a small distance between them. Thus, the genuine distribution will generally have a range of smaller values than the impostor distribution. A graphical representation of such distributions is shown in Figure 2 (top) using normalized histograms.

Since the number of distances computed for the genuine distribution is significantly less then the number of distances computed for the impostor distribution, and the number of intervals used to construct the histograms is the same for both distributions, the height of the genuine distribution is significantly greater than the height of the impostor distribution.

Let A_k and B_k denote the minimal distance in the impostors distribution and the maximal

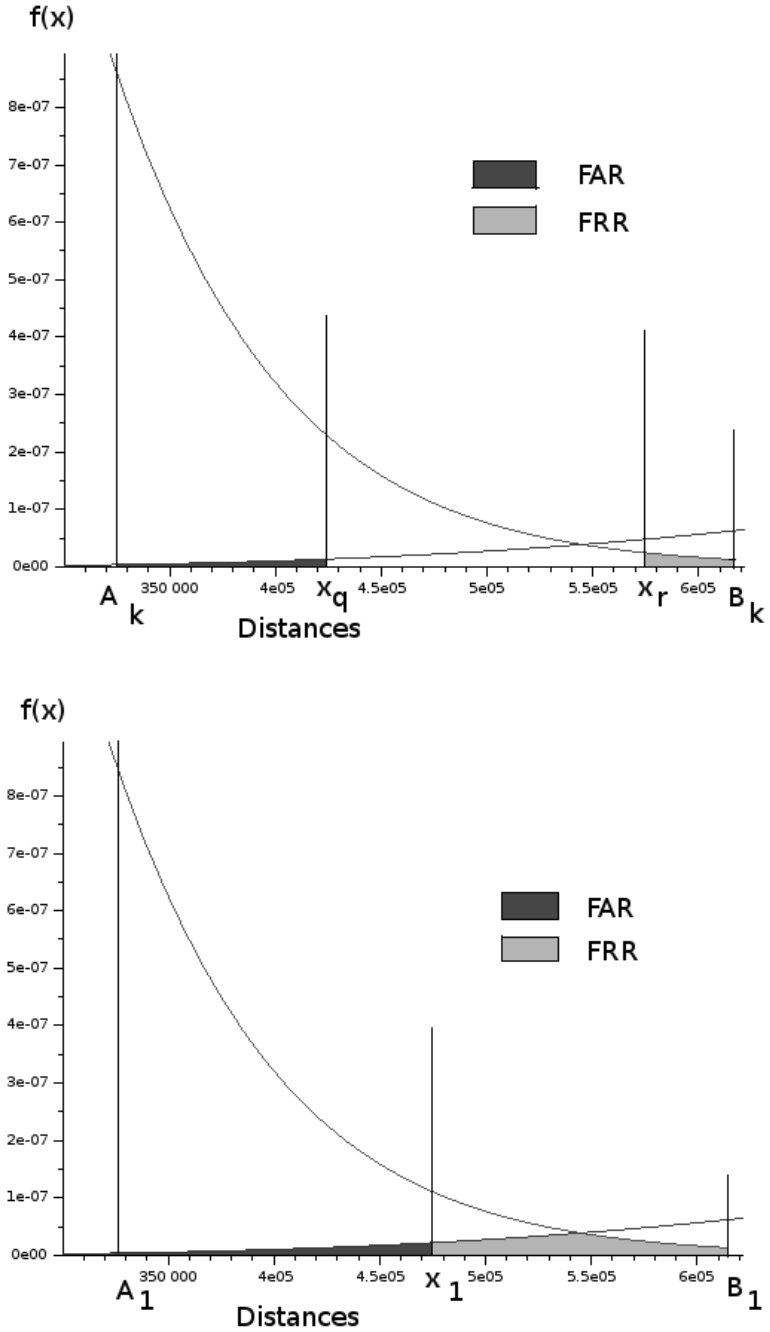

Figure 1: The areas involved in computing the FAR and FRR on the first $N-1$ match levels (top), and on the last match (bottom)

distance in the genuine distribution, respectively, for the k-th matching (we assume that $A_k < B_k$, otherwise the decision is trivial, and the system is error-free). When one of the first $N-1$ matchings of the biometric system is used to verify a person, a decision is made according to two thresholds $x_q, x_r \in [A_k, B_k]$, $q = 2k-2$, $r = 2k-1$ as follows: if the distance between the given sample and the sample in the database is less than x_q the person is accepted as genuine; if it is greater than x_r the person is rejected as impostor; but if the distance belongs to the uncertainty region $[x_q, x_r]$, the verification process demands another matching (see Figure 1, top).

For the last matching in the sequence, the distributions of both genuine users and impostors are constructed in the same way; two values A_1 and B_1 are specified, with the same meaning as A_k and B_k, $k = 2, \ldots, N$ from the first matchings; but the decision is based on a single threshold denoted by x_1, that lies between A_1 and B_1 as follows: if the distance is less than x_1 the identity of the verified person is accepted as a genuine user, otherwise it is rejected as impostor (see Figure 1, bottom).

The main problem is to find proper values for the thresholds involved in the given sequence of matchings. Our goal is to provide optimized values for these thresholds, in sense of minimizing both false acceptance and false rejection errors, FAR and FRR, respectively.

3 Solving Methods

We first have to evaluate the false acceptance and false rejection errors with respect to the thresholds x_k, $k = 1, \ldots, 2N-1$. Having a graphical representation of the score distributions of both genuine users and impostors, let $a_k(x_q)$, $q = k-2$ denote the area under the impostor distribution bounded to the right by the vertical line that passes through x_q; and let $b_k(x_r)$, $r = 2k-1$ denote the area under the genuine distribution bounded to the left by the vertical line that passes through x_r – for the k-th matching (see Figure 1, top). Similarly, let $a_1(x_1)$ denote the area under the impostor distribution bounded to the right by the vertical line that passes through x_1; and $b_1(x_1)$ denote the area under the genuine distribution bounded to the left by the vertical line that passes through x_1 – for the last matching (see Figure 1, bottom).

The probability of a false match error based on the k-th matching is $a_k(x_q)$, and it is $a_1(x_1)$ for the last matching. Similarly, the probability of a false non-match error based on the k-th matching is $b_k(x_r)$, and it is $b_1(x_1)$ for the last matching.

The function FAR_N, that describes the probability of a false match error in the general case of a biometric system with N modalities is computed using the recurrent formula

$$FAR_k(x_1, ..., x_{2k-1}) = a_k(x_q) + [a_k(x_r) - a_k(x_q)]\, FAR_{k-1}(x_1, ..., x_{2k-3}), \tag{1}$$

where $q = 2k-2$, $r = 2k-1$, $FAR_1(x_1) = a_1(x_1)$.

Similarly, the function FRR_N, that describes the probability of a false non-match error in the general case of a biometric system with N modalities is computed using the recurrent formula

$$FRR_k(x_1, ..., x_{2k-1}) = b_k(x_q) + [b_k(x_q) - b_k(x_r)]\, FRR_{k-1}(x_1, ..., x_{2k-3}), \tag{2}$$

where $q = 2k-2$, $r = 2k-1$, $FRR_1(x_1) = b_1(x_1)$.

In order to find proper bounds to the uncertainty regions involved in the verification process, we minimize both probabilities of error. Since a low false match error means a high false non-match error and reverse, we have to search for a good compromise between the two errors. Such

compromise is achieved by solving the bi-objective programming problem

$$\begin{aligned} \min \quad & FAR_N(x_1, ..., x_{2N-1}), \\ \min \quad & FRR_N(x_1, ..., x_{2N-1}), \\ \text{s.t.} \quad & A_k \leq x_{2k-2} \leq x_{2k-1} \leq B_k, k = 2, \ldots, N \\ & A_1 \leq x_1 \leq B_1. \end{aligned} \tag{3}$$

Model (3) is the generalization of Model (2) given in [15].

3.1 Local Linearization Approximation

In this section we briefly present the local linearization approach used in [15] to approximate the areas involved in Formulas (1) and (2). The discrete score distributions of both genuine users and impostors were approximated using the least squares method. A graphical representation of the discrete distributions (points) and their linear approximations (the straight lines) may be seen in Figure 4. The scores for genuine users are on the left, and the scores for the impostors are on the right. The representation is restricted to the region significant to the decision, i.e. to the intersection of the distributions.

In [15] the theoretical presentation of the approach was restricted to bi-modal systems, and quadratic expressions with respect to the thresholds x_1, x_2 and x_3, were derived. Combining them, a polynomial expressions of degree 4 were obtained, for the objective functions of the optimization model. The bi-objective optimization problem formulated in [15] is a particular case of Model (3), obtained for $N = 2$. For a general multi-modal matching system with N modalities, the expressions of the objective functions obtained by the linear approximation are polynomials of degree $2N$.

3.2 Continuous Distribution Approximation

In this section we propose a new way to approximate the discrete score distributions of both genuine users and impostors. In the previous approach, the discrete data collected from the users was grouped in intervals, relative frequencies were computed, and the discrete set of pairs *(frequency, midpoints of the intervals)* was continuously and linearly approximated using the least squares method.

We now propose to use a continuous distribution that approximate the initial discrete collection of data. We need to compute the mean and the variance of the data, separately for each modality, genuine users and impostors, and try to identify a continuous distributions that best fit the distance frequencies.

Figure 2 shows how the continuous distributions approximate the original score distributions for both genuine users and impostors, for one modality. In this representation the Gamma distribution was used for the genuine scores and the normal distribution for the impostors. For the same data set – representing the genuine users scores distribution – we performed a fit distribution test, that identified as best fit distributions the Gamma, Generalized Gamma (4P), and Johnson SB. The goodness of fit was performed for 61 well-known distributions. Among those distributions, the Kolmogorov-Smirnov test identified the Generalized Gamma (4P) distribution as the best fit, the Anderson-Darling test identified Johnson SB distribution as the best fit, while the Chi-squared test identified the Gamma distribution as the best fit.

Figure 3 graphically shows how the input data (with all values grouped in a histogram) may be approximated by Gamma, Normal, and Beta probability density functions. We were restricted to choose among Gamma, Normal, Beta, Erlang, and Chi-square distributions due

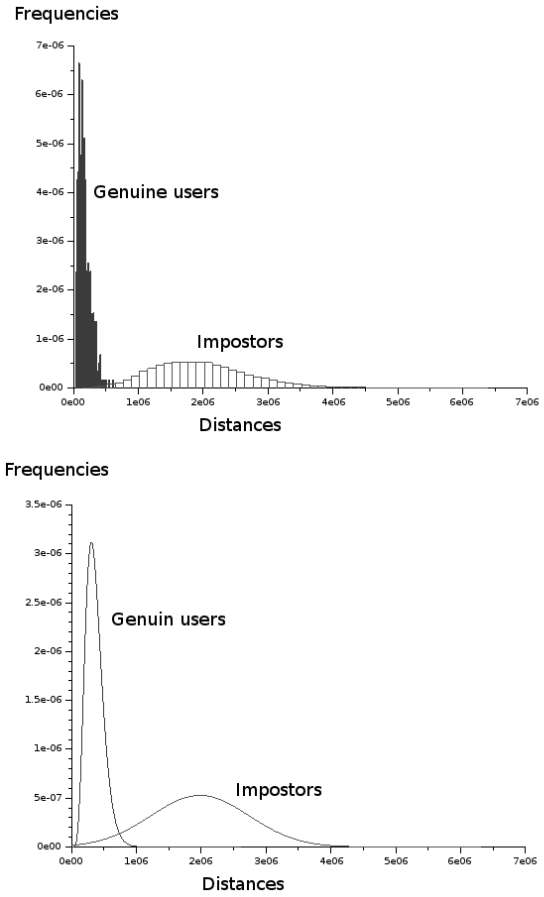

Figure 2: The approximation based on Gamma distribution for the genuine scores, and on normal distribution for the impostors scores versus the original (discrete) score distributions

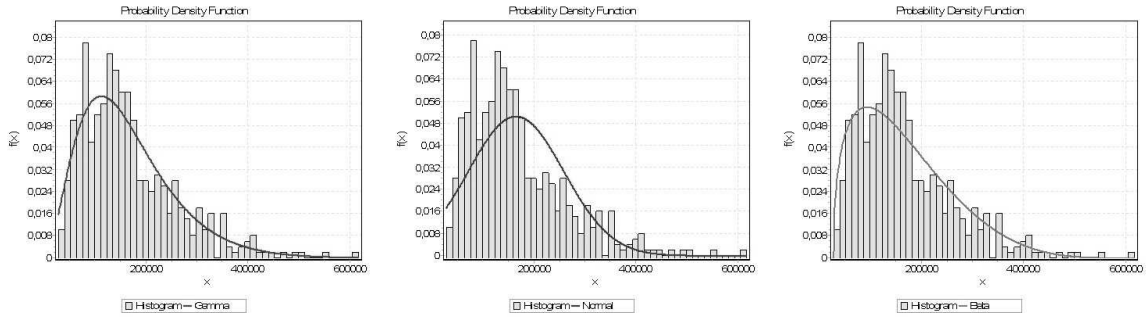

Figure 3: Probability density functions for the continuous approximations using Gamma, Normal, and Beta distributions. The characteristics of the distributions are given in Table 1

Table 1: Fitting results for the probability density functions of the Gamma, Normal, and Beta distributions presented in Figure 3

Distribution	Parameters
Gamma	$\alpha = 3.1919; \beta = 52049$
Normal	$\sigma = 92990; \mu = 166130$
Beta	$\alpha_1 = 1.4696; \alpha_2 = 4.7366; a = 29877; b = 616440$

Table 2: The goodness of fit for the Gamma, Normal, and Beta distributions (presented in Figure 3), using Kolmogorov-Smirnov, Anderson-Darling and Chi-squared statistics tests. The rank is given out of 61

Distribution	Kolmogorov-Smirnov statistic / rank	Anderson-Darling statistic / rank	Chi-squared statistic / rank
Gamma	0.04247 / 15	1.26490 / 19	6.4661 / 1
Normal	0.11578 / 37	11.63 / 36	50.698 / 38
Beta	0.06484 / 25	4.3973 / 27	22.072 / 25

to the toolbox of the programming language we used for the optimization. Despite the fact that these distributions are not the best fit, they behave well during experiments since they approximate relatively well the initial score distributions in along the intervals relevant to the optimization. We used *EasyFit 5.6 Standard* software (http://www.mathwave.com) for goodness fitting distribution.

Table 1 reports the parameters that describe the fitting results. These parameters were computed with respect to the mean and variance of the original score distribution. Table 2 shows the results for the statistic tests Kolmogorov-Smirnov, Anderson-Darling and Chi-squared applied to the data graphically represented in Figure 3. It also includes the ranks of the chosen distributions in the ranking list of 61 well-known distributions.

Figure 4 shows that the probability density function of the continuous distribution (the non-linear graph) better approximates the original set of data than the linear function (the straight line) obtained by the least squares method presented in the previous section. On the top side of the figure the approximations for the genuine users scores is given. For the impostors scores the approximations are given on the bottom side.

According to the new proposed approximation method, we use the cumulative density functions (*cdf*) to express the probabilities a_k and b_k, $k = 1, \ldots, N$, in Model (3). Thus, $a_k(x) = cdf_k^I(x)$, $k = 1, \ldots, N$ in FAR (1) for impostors, and $b_k(x) = 1 - cdf_k^G(x)$, $k = 1, \ldots, N$ in FRR (2) for genuine users. Model (3) is a nonlinear bi-objective problem independent on the approximation used. One way to solve Problem (3) is to aggregate the two objective functions, and optimize the obtained function. We propose the weighted sum method, with the initial weights $(1, 1)$, to aggregate the objectives. In this way we optimize the total error rate (TER), that is one parameter used in analyzing the performance of an biometric system.

By changing the set of weights, we favor one or another type of error. In order to chose certain weights to aggregate the FAR and FRR, the analyst must know/model the cost functions for false rejections and false acceptances. There are more system specific factors that may influence the priorities in favoring one or another of the error rates. Analyzing such characteristics is beyond the scope of this work. Our approach provides optimized thresholds from the point of view of minimizing the total error rate.

We solved the single objective optimization problem

$$\begin{aligned} \min \quad & FAR_N(x_1, ..., x_{2N-1}) + FRR_N(x_1, ..., x_{2N-1}), \\ \text{s.t.} \quad & A_k \leq x_{2k-2} \leq x_{2k-1} \leq B_k, k = 2, \ldots, N \\ & A_1 \leq x_1 \leq B_1. \end{aligned} \tag{4}$$

numerically. A starting point was chosen by taking the midpoint of the feasible interval for the threshold x_1, the point that is at one third from the left bound of the feasible interval for the x_{2k-2}, and the point that is at one third from the right bound of the feasible interval for the threshold x_{2k-1}, $k = 2, \ldots, N$. We optimized one variable at a time, fixing others to either their

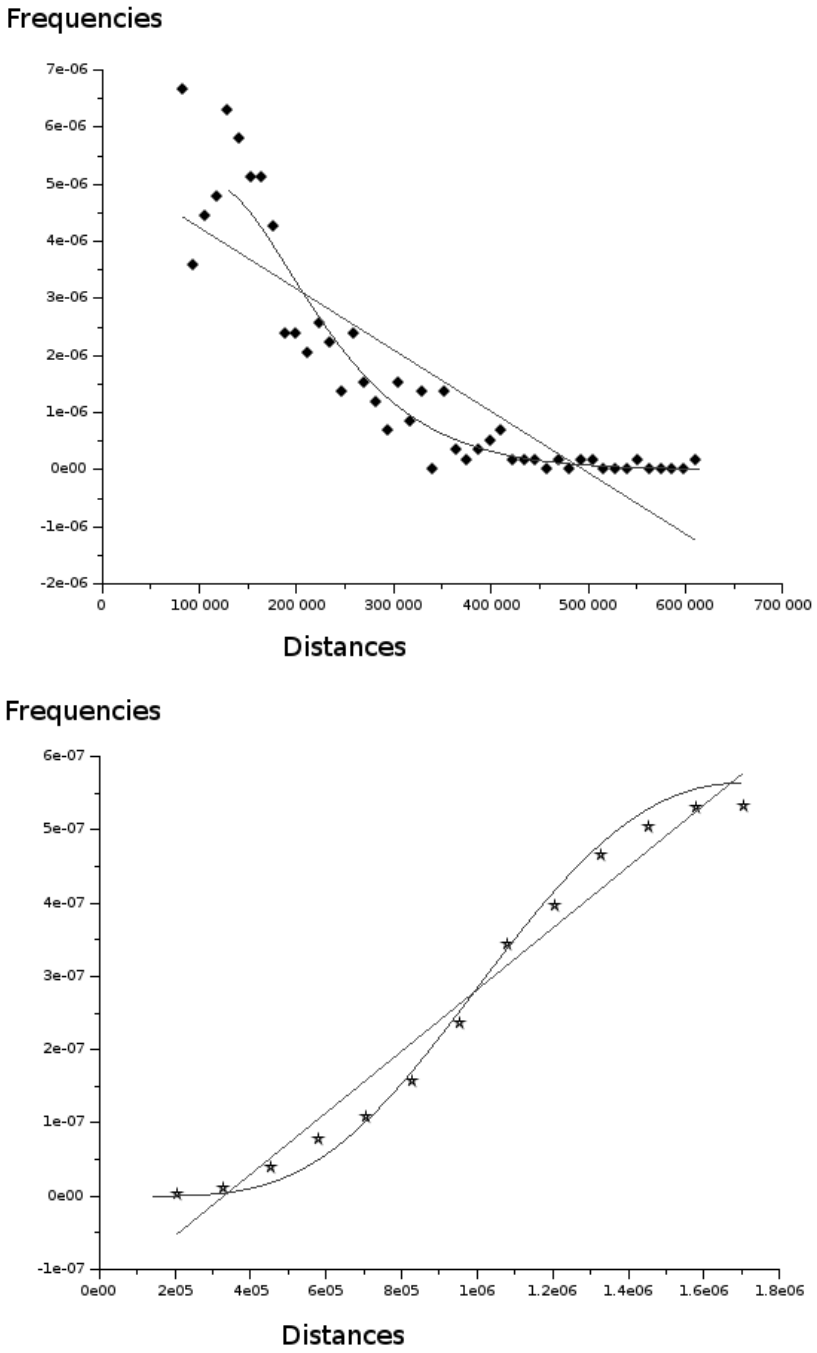

Figure 4: The approximation based on the least square method versus the approximation based on continuous distributions for both genuine users and impostors

initial values or previously obtained optimal values. The optimization process was stopped when the distance between two consecutive solutions dropped under a given threshold.

The advantage of finding optimized thresholds, to be used by the decision-maker in constructing the sequential multi-modal system, resides in yielding the needed information in the a priori stage of the decision. Generally, the trade-off between two conflicting objectives, and particularly the trade-off between FAR and FRR, may be a subject of a wider discussion. The usefulness of a priori, a posteriori, and interactive methods in multiple objective optimization are highly emphasized in the literature (see for instance [1]). A visualization technique for accessing the solution pool in the interactive methods of multiple objective optimization can be found in [2].

We used *GNU-Octave* (https://www.gnu.org/software/octave/) for the optimization step.

4 Computation Results

4.1 Experiments Using Random Generated Instances

In order to test the performance of our method we organized the experiments, as in [15].

First, the input data, necessary to construct the score distributions, were randomly generated according to the rules that made them proper data for biometric tests. More precisely, we have generated a set of vectors with l real positive components. Each of these vectors simulates the essential information that in real situations is extracted from the taken pictures of a person during a biometric measurement. The first sample of each user is generated as a vector of uniformly distributed random numbers. The mean and standard deviation were varied through instances. Each subsequent sample of the same user is generated as a vector of random numbers with normal distribution, keeping the same mean and variance as for its corresponding first sample. In this way we provided that the samples of one person are more similar to each other than when compared to samples of another person.

We computed the Euclidean distances between each two generated vectors, and split them in two categories to be used for the construction of the genuine and impostor distributions. For the continuous distribution approximations we used the Gamma distribution for the genuine users and the Normal distribution for the impostors. We computed the bounds A_k, B_k, $k = 1, 2$; used the approximations to evaluate the errors of false acceptance and false rejection; and constructed the bi-objective optimization model. In order to find the optimized thresholds we added the two error functions, and minimized the total error.

Each triple (x_1, x_2, x_3), including the triple of optimized thresholds, defines a bi-modal biometric system, whose performance will be evaluated.

In order to estimate the FAR and FRR of each system using the same data as in constructing the genuine and impostor distributions, we successively collected the answers of the system, obtained when each person $i = 1, \ldots, n$ claims that he/she is the person $k = 1, \ldots, n$, and he/she is verified with all samples $j = 1, \ldots, m$ of the person k, according to the specific thresholds of the system. Each time when the system accepts a person i as being the person k, the numerator of the ratio FAR increases with 1 unit. Similarly, each time when the system rejects a person i when he/she claims that he/she is person i the numerator of the ratio FRR increases with 1 unit. The nominator of FAR is $n(n-1)m^2$, while the nominator of FRR is $m(m-1)n/2$. Finally, we compute the genuine acceptance rate (GAR) as 1-FRR. When biometric samples of a control group are available, we collect the system's answers obtained by checking the control samples instead of the initial samples.

The numerical results are grouped in two tables. Table 3 contains the results obtained by both methods LS (based on least square approximation), and CD (based on continuous distribution approximation). Comparing the two methods we note that, considering the total error rate, CD

Table 3: Comparison of LS and CD for certain instances with given characteristics

Instances characteristics	FAR		GAR		TER	
	LS	CD	LS	CD	LS	CD
$n = 100, \quad m = 5, \quad l = 3$	9.4%	0.52%	99.6%	98.5%	9.80%	2.03%
$n = 100, \quad m = 5, \quad l = 5$	2.2%	0.77%	100%	99.5%	2.20%	1.26%
$n = 100, \quad m = 5, \quad l = 10$	0.05%	0.19%	99.2%	99.8%	0.85%	0.35%
$n = 200, \quad m = 5, \quad l = 10$	0.001%	0.05%	99.5%	99.9%	0.50%	0.15%

Table 4: The numerical results obtained by running CD on more instances with given characteristics

Instances characteristics	FAR		GAR		TER	
	$l = 5$	$l = 10$	$l = 5$	$l = 10$	$l = 5$	$l = 10$
$n = 100, \quad m = 10$	0.91%	0.08%	99.6%	99.94%	1.31%	0.14%
$n = 200, \quad m = 10$	0.96%	0.08%	99.7%	99.97%	1.31%	0.11%
$n = 500, \quad m = 10$	0.92%	0.08%	99.6%	99.98%	1.34%	0.10%

performs better than LS in all cases. Analyzing separately the values of the false acceptance rate and genuine acceptance rate, CD is better for two sets of instances, and LS is better for other two sets of data.

The results reported in Table 4 were obtained by running the CD method on instances with 100, 200 and 500 users. For each user 10 different samples were available. The samples were described by vectors of length 5 and of length 10. It is obvious that the number of genuine users used to train the system does not influence the error rates. Contrary, the length of the vectors used to describe the individuals is very important, as expected, since the error rates are much smaller in the case of $l = 10$ than in the case of $l = 5$. More precisely, when the length of the vectors is greater, more biometric information is enclosed in them, thus a more clear separation between individuals exists. Consequently, the score distributions of genuine users and impostors are less overlapped, the uncertain regions are smaller, and the total error rate is smaller. Contrary, a small vector length correspond to a wide overlapping of the score distribution, and to a biometric system with greater error rates.

4.2 Experiments Using the NIST-BSSR Matching Score Sets

The NIST BSSR1 multi-modal database contains scores from 517 users. For each user, the database contains one score set from the comparison of two right index fingerprints, one score set from the comparison of two left index fingerprints, and two score sets (from two separate matchers) from the comparison of two frontal faces. The score sets from the left (right) indexes are referred as "Li" ("Ri"). Each matching set contains 517 genuine scores and $266,772$ (i.e. 516×517) impostor scores. We transformed the given scores into distances, i.e. a great (small) score representing a similarity (non-similarity) between two collected samples is transformed to a small (great) distance between the same two samples. As a part of our experiments we derived the optimized thresholds for the bi-modal systems developed from the BSSR1 database; and considered the Li-Ri and Ri-Li 2-matcher combinations.

The NIST BSSR2 multi-modal database contains scores from 6000 users. For each user, the database contains one score set from the comparison of two right index fingerprints, and one score

Table 5: Computation results for NIST-BSSR1 instances

match		LS			CD Gamma-Normal			CD Gamma-Gamma		
1^{st}	2^{nd}	FAR	GAR	TER	FAR	GAR	TER	FAR	GAR	TER
Li	Ri	0.15%	94.59%	5.57%	0.62%	94.39%	6.23%	0.69%	95.36%	5.33%
Ri	Li	0.11%	93.82%	6.30%	0.35%	94.78%	5.58%	0.73%	95.30%	5.37%

Table 6: Computation results for NIST-BSSR2 instances

match		LS			CD Gamma-Normal			CD Gamma-Gamma		
1^{st}	2^{nd}	FAR	GAR	TER	FAR	GAR	TER	FAR	GAR	TER
Li	Ri	0.96%	95.87%	5.09%	1.03%	94.59%	6.46%	0.61%	95.42%	5.19%
Ri	Li	1.55%	96.12%	5.4%	0.75%	94.44%	6.40%	0.62%	95.44%	5.19%

set from the comparison of two left index fingerprints. The score set from the left (right) indexes are referred as "Li" ("Ri"). Each matching set contains 6000 genuine scores and 35,994,000 (i.e 5999×6000) impostor scores. As for the BSSR1 dataset, we transformed the similarity scores into distances; derived the optimized thresholds; and considered both possible combinations.

Tables 5 and 6 report the numerical results obtained by running CD on NIST-BSSR1 and NIST-BSSR2. In these tables we include the results obtained by running LS in order to compare the performances, and the results obtained by two versions of the CD. The first version used Gamma distribution for both genuine users and impostors, while the second version used Gamma distribution for the genuine users and the Normal distribution for the impostors. According to these experiments, it is better to choose the continuous distribution Gamma for both genuine users and impostors. For BSSR1 instances, the total error rate for CD Gamma-Gamma is considerably smaller than the total error rate obtained by LS method. For BSSR2 instances the total error rate obtained with CD Gamma-Gamma is better then the one obtained by LS, in the case when checking the left fingerprint is the first modality, and checking the right fingerprint is the second modality in the biometric system.

Many papers referred to the same matching score dataset (see for instance [6], [9], [16], and [17]). Searching for papers that report experimental results to compare with, we faced two main issues. First issue is related to the fact that there is no consistent way to deal with this database. For example, some authors randomly selected the scores for the system training, and used the rest for evaluation, thus making impossible to repeat their experiments; and/or discarded some scores due to apparent template acquisition errors, but without explaining which scores were discarded [16]. The second one is related to the fact that we propose a set of thresholds to be used in the multi-modal system; but we do not generate a ROC curve, thus the Equal Error Rate (EER) cannot be employed straightforward to validate our approach.

5 Conclusions and Future Works

In this paper we proposed a novel approach to determine the upper and lower acceptance thresholds in sequential multi-modal biometric matching systems. The new approach uses continuous distribution for the score distributions approximations of both genuine users and impostors. It improved the results obtained by the least square approximation approach. In the present paper we introduced the general mathematical model that may be used to minimize the total error function, and derive the thresholds in a general multi-modal system with N modalities. We solved the non-linear optimization problem numerically. The paper is an extension of [15], where the linear approximation of the biometric scores based on the least squares method was

introduced, and the optimization model was given biometric systems with 2 modalities.

One of the advantages of the new approach is the fact that it relays on less input parameters than the previous method. The method based on the least square approximation included the computation of the frequencies needed for constructing the histograms for the score distributions. The number of the intervals for the histogram is theoretically uncertain for guaranteeing the best results.

Generally, the optimization of the thresholds for a serial multi-modal system serves the a priori need of the decision maker when building a convenient multi-modal biometric system. Our method that provides optimized thresholds for a multi-modal biometric system is fast, and relatively simple to implement. For a biometric system that works in real time, the existence of multiple matchings, and the possibility that the unproblematic genuine users pass the system after the first match with a low false rejection rate, offers the advantage of an increased speed of the matching process. Moreover, if the first match is based on a face image, or a video record that may be taken even without user's will, then the process is even faster.

The numerical results of our experiments were reported in the paper. For the majority of our experiments on random generated instances, the pair (FAR, GAR), obtained by our method, dominates at least one pair (FAR, GAR) from the set of the final results obtained by the fusion based method. The experiments showed a good performance of the sequential bi-modal biometric matching system based on optimized thresholds and continuous approximation of the distribution scores.

Our numerical results on real life datasets were also included in the paper. We referred to the NIST-BSSR1 and BSSR2 data sets, and intend to extend our experiments to more benchmark data from the literature. We performed some experiments with multi-modal biometric systems with more than two matchings, but the instances were not yet statistically relevant. The research may advance by refining the approximation step needed for obtaining the expressions for the false acceptance and false rejection rates to be used for finding the optimized thresholds. One direction is to search for the fitting distributions that approximate well the initial score distributions just along the uncertain region. It is also possible to involve other metrics, instead of the Euclidean distance, to compare the samples vectors.

Acknowledgment

This research was partially supported by the Ministry of Education and Science, Republic of Serbia, Project numbers TR32013 and TR36006.

Bibliography

[1] Ehrgott, M. *;* (2000); *Multicriteria Optimization*, Berlin, Germany: Springer-Verlag, ISBN 3-540-21398-8.

[2] Filatovas, E.; Podkopaev, D.; Kurasova, O.; (2015), A Visualization Technique for Accessing Solution Pool in Interactive Methods of Multiobjective Optimization, *International Journal of Computers Communications & Control*, ISSN 1841-9836, 10:508-519.

[3] Filip, F.G.; (2015); Book Review: "Biometric and Intelligent Decision Making Support", *International Journal of Computers Communications and Control*, ISSN 1841-9836, 10(6):952-953.

[4] Hong, L.; Jain, A.; (1998), Integrating faces and fingerprints for personal identification, *IEEE Trans. Pattern Anal. Mach. Intell.*, ISSN: 0162-8828, 20(12):1295-1307.

[5] Kaklauskas, A.; (2015), *Biometric and Intelligent Decision Making Support*, Springer-Verlag, ISBN 978-3-319-13659-2.

[6] Kumar, A. ; Kumar, A.; (016), Adaptive management of multimodal biometrics fusion using ant colony optimization, *Information Fusion*, ISSN: 1566-2535, 32:49-63.

[7] Maltoni, D.; Maio, D.; Jain, A.K.; Prabhakar, S.; (2003); *Handbook of Fingerprint Recognition*, New York: Springer-Verlag, ISBN 978-1-84882-254-2.

[8] Marcialis, G.L.; Mastinu, P.; Roli, F. (2010), Serial fusion of multi-modal biometric systems. In: *Biometric Measurements and Systems for Security and Medical Applications (BIOMS)*, IEEE Workshop on, ISBN: 978-1-4244-6302-2, 1-7.

[9] Mehrotra, H.; . Singh, R; Vatsa, M.; Majhi, B.; (2016), Incremental Granular Relevance Vector Machine: A Case Study in Multimodal Biometrics, *Pattern Recognition*, ISSN: 0031-3203, 56:63-76.

[10] Pathak, M.; Srinivasu, N.; (2015), Analysis of multimodal biometric system based on level of fusion, *International Journal of Inventive Engineering and Sciences*, ISSN: 2319-9598, 3:8-11.

[11] Pato, J.N.; Millett, L.I. (eds); (2010); *Biometric Recognition – Challenges and Opportunities*, The National Academies Press, ISBN: 978-0-309-14207-6.

[12] Ross, A. ; Nandakumar, K.; Jain, A.K.*;* (2006); *Handbook of multibiometrics*, Springer, ISBN: 978-0-387-33123-2.

[13] Sheena, S.; Sheena, M.; (2014), A study of multimodal biometric systems, *International Journal of Research in Engineering and Technology*, ISSN: 2321-7308, 3:93-98.

[14] Snelick, R.; Uludag, U.; Mink,A.; Indovina, M.; Jain, A.; (2005), Large-scale evaluation of multimodal biometric authentication using state-of-the-art systems, *Pattern Analysis and Machine Intelligence, IEEE Transactions on*, ISSN: 0162-8828, 27:450-455.

[15] Stanojević, M. ; Milenković, I.; Starčević, D.; Stanojević, B.; (2016), Optimization of thresholds in serial multimodal biometric systems, 2016 6th International Conference on Computers Communications and Control (ICCCC), ISBN: 978-1-5090-1735-5, 140-146.

[16] Tulyakov, S. ; Li, J.; Govindaraju, V.; (2008), Enrolled Template Specific Decisions and Combinations in Verification Systems, *Biometrics: Theory, Applications and Systems, 2008. BTAS 2008.* 2nd IEEE International Conference on, Arlington, VA, 2008, ISBN: 978-1-4244-2729-1, 1-7.

[17] Villegas, M.; Paredes, R.; (2009), Score Fusion by Maximizing the Area under the ROC Curve", *Pattern Recognition and Image Analysis*, LNCS 5524, ISSN: 1054-6618, 473-480.

[18] Zhang, Q.; Yin, Y.; Zhan, D.-C.; Peng, J.; (2014), A Novel Serial Multimodal Biometrics Framework Based on Semisupervised Learning Techniques, *IEEE Transactions on Information Forensics and Security*, ISSN: 1556-6013, 9:1681-1694.

INTERNATIONAL JOURNAL OF COMPUTERS COMMUNICATIONS & CONTROL
ISSN 1841-9836, 11(5):735-747, October 2016.

A Momentum Theory for Hot Topic Life-cycle: A Case Study of Hot Hashtag Emerging in Twitter

L. Wang, X. Li, L.J. Liao, L. Liu

Liu Wang, Xin Li, Le-Jian Liao*, Li Liu
School of Computer Science
Beijing Institute of Technology
No. 5 South Zhongguancun Street
Beijing, 100081, China
wangliu2000@163.com, xinli@bit.edu.cn,
liaolj@bit.edu.cn, liuli0407@hotmail.com
*Corresponding author: liaolj@bit.edu.cn

Abstract:
The existing work on mining of hot topics is mainly based on topic multiplicity and attention from users in unit time. With the advent of social networking, the weight has been put on the hot topics which can effectively describe the importance and hotness of a topic. However, the researches on the influence exerted by the accumulation of attention towards hot topics and the alternation between hot topics and outdated ones are still relatively weak. In this paper, a novel algorithm for calculating the hotness of topics is proposed based on momentum. The number of the participants, but also the long tail effect of the historical accumulation on the topic is taken into consideration. Through this algorithm, we can accurately build a model for the hot topics on their emerging growing period and effectively describe the whole life circle of the topic. Additionally, the change between hot topics and old ones can be distinguished efficiently. Our experiments show that the process of a topic growing into a hot topic can be detected explicitly. Potential hot topics can be explored and the overdue ones can be rejected respectively.
Keywords: hashtag, hot topic, aging theory.

1 Introduction

In modern times social networking has become an important resource of real-time news updates. As smart phones and other mobile devices spread, there is a growing tendency that people use social networks such as Twitter and Weibo to obtain the hot issues happening across the world. Detecting the hot topics out from the large-scale of information posted online simultaneously is of significant interest for many reasons. For one, it shortens the time for users to obtain the hot topic, which may play an important role in decision-making. Also from the hot topics detected, one can easily have an understanding of current social dynamics.

Most of the social network systems may provide a ranking list of hot topics through the search or post count of keywords. While this approach fails to take the temporal relations of hot topics into account. Current hot topic detection solutions are mostly based on the topic multiplicity and attention from users in unit time, whereas they neglect the digestion of the hot topics. Also they aim to establish the topics from a clustering of keywords from the content layer, which overlooked the functions of a social network. From the point of view of research methods analysis, physics methods are applied in many fields, such as: Newton's theorem was applied to the [6, 18], the gravity was applied to manufacturing modeling [21], the application of the theorem of momentum was used in [26,34], [15] combined with momentum method to launch the stock prediction. They carried out the research of modeling by physics methods. From the social networking features, in addition to the security and network mining research [11, 28, 31, 35], also, many scholars are

still studying hashtags' other functions [27, 40], in [1, 37], Xiao and Aldhelaan were using social network to do the research on hot topic discovery and recommendation, Chen [13] combined with evolution model to achieve the topic prediction. The accumulation of topics in social networks and the integration of the topic have strong physics characteristics, so we try to find a way to use physics methods to model the topic in social networks and combine the momentum theorem with hashtags.

In this paper, we aim to detect those emerging hot topics according to the momentum theory with the use of hashtags. The momentum of hashtags can reveal the mechanism of dynamics from the temporal characteristics and quantity characteristics and discover the ideal life cycle of topics. This will result in using momentum theory to dig out hot topics more accurately and effectively. In this paper, the proposed algorithm does not need to collect and store a large number of historical data. Therefore, it is suitable for data streams real-time calculation. Moreover, the nested loops in the algorithm are few and the time complexity is approximate to O(n). Due to high computational efficiency, this algorithm is suitable for large data analysis as well.

The rest of the paper is organized as follows: In Section 2, we give a review of related works. In Section 3, we propose the definition of hot topics. Section 4 describes the theoretical model of topic hotness. In Section 5, we discuss the results of the experiments run. Finally, in Section 6, we present our conclusions and some future research directions.

2 Related Work

Topic Detection and Tracking (TDT) [2] has long been a foundation of the research related to hot topic detection. However, different from the traditional sources of information such as Web pages, texts, etc., information in social networks is often very short and sparse, also spreading rapidly. Under the background of the new era of social media, a series of work have been completed towards those characters. You et al. [7] utilized frequent item set mining algorithm SaM [8] to find out hot topics denoted by combinations of keywords. Thus, detecting the hot topics is comparable to mining frequent patterns from news streams. Similar to that, a recent work by Kim et al. [22] also took geographic elements into consideration, which provides a simple but useful approach to analyze real-time streaming data and finds geographic communities. According to FP-growth [20], Giannella et al. [19] proposed the FP-stream time window and the digestion concept of the support parameters. This new algorithm can let the outdated items expired and accumulate the importance of items based on the timeline as well. However, the algorithm is more complicated. Guo et al. [24] improved the tree structure in the Frequent Pattern stream mining algorithm (FP-stream) [19] and used the new algorithm to detect hot topics from twitter streams, which can lead to time-sensitive results. Lee et al. [17] developed an algorithm for ranking topics, using topic energy to represent the significance of a given topic at each time point within a time period. The strategy in determining topic energy value considers factors such as popularity, burstiness and informativeness, which suits the character of information on social network better. In [29], the key entity significance is computed through traditional "tf-idf" evaluation method [33] in the information retrieval literature. Then, clustering entities are used to generate significant events. Bun et al. [25] computed the value of a term by using tf*idf and clustered terms into a sentence. Yang et al. [39] applied the VSM to the task of news TDT and used a time window with a decaying function (TW-DF) to model the temporal relations between documents and events. Unfortunately however, the strategies above did not consider the temporal relations thoroughly. The newly generated hot topics cannot be distinguished from the outdated ones accurately.

Chen et al. [12, 16] proposed an aging theory to model life cycles of news events. For all user

messages generated from the topic time interval, the aging theory calculates their nutrition and convert the nutrition value to the energy value, and then add into the cumulative energy value of the topic. It also applies energy decaying strategy on the topic. As time goes by, the energy decays gradually. If the increase of the energy is less than the reduction of the energy, the topic will show a trend of attenuation. If the energy value is less than a given threshold, this topic is set to "death" state and is removed from the hot topics list. The aging algorithm defines α as the nutrition transferred factor and β as the nutrition decayed factor, $0 < \alpha < 1$, $0 < \beta < 1$, α decides the increase of nutrition from an input news document and β decides the nutrition loss in a period. Zheng et al. [41] utilized aging theory on candidate topics discovered by a clustering method in each time slot in BBS. With energy values updated at the end of each time slot according to the three functions of aging theory, hot topics in each time slot can be easily found. Chen et al. [14] combined aging theory with a term weighting scheme to extract genuine hot terms. Based on the extracted hot terms, key sentences are then identified and grouped into clusters that represent hot topics by using multidimensional sentence vectors. Cataldi et al. [10] improved the nutrition formula by using "idf" and formalized the keyword life cycle leveraging a novel aging theory intended to mine terms that frequently occur in the specified time interval which are relatively rare in the past. Wang et al. [36] took media focus and user attention into the classical aging theory and proved the importance of these two factors. In comparison with these approaches, our solution extracts hot topics based on hashtags according to the functions of a social network instead of the content aspect. The hot topic emerging theory based on momentum can explicitly distinguish new hot topics from outdated ones.

The methods mentioned emphasized topic extraction from a cluster of sentences or the frequency pattern of topics, but ignore the topic life cycle. The aging theory [12, 16, 41] discovers the life cycle of topic but does not deal with the older topic elimination mechanism very well. Chen et al. [23] proposed a similar idea to our model, defining hot velocity and hot acceleration to recognize hot topics but did not reveal the dynamic characteristics. Different from that model, we define hot topic emerging theory based on momentum. The utilization of momentum theory can successfully describe the whole life circle of a topic, thus sift out the newly emerged hot topics from the old ones more effectively.

3 Definition of Hot Topic

Hot topics in real microblogging systems have three characteristics: 1) the number of posts related to this topic would exceed a threshold; 2) the amount of users concerned should be large, especially those key persons; 3) a hot topic would occur at a short time [23]. In [14], the characteristics of hot topics are concluded based on [25] as those appear on many news channels and go through a life cycle of birth, growth, maturity, and death. In this paper, hot topics are defined as the topics which are both influential and latest. Four characteristics are summarized as follows:

i Timeliness. The hot topic refers to the people and things that have happened recently. Those topics which have been under discussion for more than seven days or one month cannot be regarded as hot topics.

ii Development. Due to the dynamics while topics are propagated, the influence of public opinion will spread as time goes by. The hot topics diffract backwards.

iii Accumulation. The more people are involved into the discussion of the topic, the hotter the topic is. However with more and more attention drawn on a certain topic, it becomes less possible to be hot topic again.

iv Digestion. As time goes on, the influence of a topic will unavoidably be watered-down. Thus hot topics have the character of obliviousness.

4 Kinetic Model of Topic Hotness

The topic under a certain time point can be regarded as a set of large number of synonymous terms. In other words, to describe this concept from the perspective of physics, we can assume each term as a particle which owns weight and velocity. Besides, the activeness of the particle represents its energy and the activeness of a topic is the reflection of the particles inside the set. As time goes on, the set is dynamically changing with terms increasing, thus the energy of the particles are changing too. In time $t-1$, the topic set is represented as $Topic_{n(t-1)}$. In time t, the additional subset $Topic_{n\Delta t}$ will join into $Topic_{n(t-1)}$ as the new set $Topic_{nt}$. This process can be regarded as two kinetic physical objects collided and fused into one kinetic physical object with the exchange of energy. In this paper, we adopt conservation of momentum to illustrate this process.

In this paper, we propose to use momentum to represent the physical characters in thermodynamics and dynamics of hot topic. Negative acceleration is imported to represent the digestion of hotness according to the attenuation of the hot topics while propagated. We use momentum equation to present the active momentum of topics which is aroused by discussion.

A topic is consists of many synonymous terms. In social networks, a post can be seen as a term, and similar terms constitute a topic. The topic set is varying all the time and the variation composes a time sequence. For a topic n, the topic set can be expressed as:

$$Topic_n := \{Topic_{n1}, Topic_{n2}, ..., Topic_{nt}\}$$

All kinds of topics are formed as the whole topic set:

$$Topic := \{Topic_1, Topic_2, ..., Topic_n\}$$

The current topic set is the combination of the former set and the subset increased during the interval, as:

$$Topic_{nt} := Topic_{n(t-1)} \cup Topic_{n\Delta t}$$

$$Topic_{n\Delta t} := \{term_{n1}, term_{n2}, ..., term_{nm}\}$$

We can also say that the topic under a specific time spot is the set of all the terms emerged before, as:

$$Topic_{nt} := \{term_{n1}, term_{n2}, term_{n3}, ..., term_{nt}\}$$

4.1 Momentum Modelling

In this paper, we use the equations below to represent the variation when a topic becomes hotter. The topic in $t-1$ can be seen as a physical entity m_{t-1} with weight and velocity. The increased terms inunder that topic can be regarded as another entity $m_{term_{\Delta t}}$. Thus the topic in t as an entity m_t is the combination of $m_{term_{\Delta t}}$ and m_{t-1} after a collision with the velocity of $v_{term_{\Delta t}}$.

The increased momentum of topic entity $m_{term_{\Delta t}}$ is the sum of the momentum of each term added. We can calculate the momentum of each topic as follows:

$$\overrightarrow{M}_{term_{\Delta t}} = \sum_{\Delta t=1}^{m} (m_{term_{\Delta t}} \times \vec{v}_{term_{\Delta t}}) \tag{1}$$

The momentum of the M_t equals to the sum of the momentum of m_{t-1} and $M_{term_{\Delta t}}$. The total momentum is invariable before and after the collision. $\vec{v}_{t-1} + \vec{g}\Delta t$ represents the final velocity after Δt. The development and digestion of topic can be expressed clearly by this equation:

$$\overrightarrow{M}_t = m_{t-1} \times (\vec{v}_{t-1} + \vec{g}\Delta t) + \overrightarrow{M}_{term_{\Delta t}} \tag{2}$$

The weight of the topic in time t is the sum of the weight of itself before collision and the weight of the topic added, which shows the accumulation of topic. The more the topic is discussed, the heavier the topic is.

$$m_t = m_{t-1} + \sum_{\Delta t=1}^{m} m_{term_{\Delta t}} \tag{3}$$

In time t, the velocity of the topic is the quotient of total momentum and total weight.

$$\vec{v}_t = \overrightarrow{M}_t / m_t \tag{4}$$

The topic reaches a height in a certain velocity after being represented in physics. In this paper we define this height as the hotness of the topic in that time spot.

$$\overrightarrow{H}_t = \vec{v}_{t-1} \times t \tag{5}$$

The height is not able to keep growing according to the digestion of the topic. Under this circumstance we use acceleration of gravity g to lower the height (hotness). The equation is modified as follows:

$$\overrightarrow{H}_t = \vec{v}_{t-1} \times t_0 + \frac{1}{2} \times \vec{g}\Delta t^2 \tag{6}$$

4.2 Modelling Solution

In social networks, Hashtag (#) is used extensively to determine the topic, which is convenient to aggregate and classify vast amounts of information and let people who follow a certain topic get the relevant information more easily. Twitter showed its significant value in information propagation almost before every emergency and important activity due to the aggregation of using hashtags. We can draw a safe conclusion that hashtag reflects the true tendency of topics and has great potential in the reconstruction and compilation of information. In this paper we use hashtag for identification modeling of topics. A topic under a specific time spot is defined as a set with synonymous hashtags.

$$Topic_{nt} := \{hashtag_{n1}, hashtag_{n2}, hashtag_{n3}, ..., hashtag_{nt}\}$$

At a specified time, more similar hashtags means the topic is more active. In a specific period of time, topic is a sequence of sets. In this Section we use m for the weight of hashtag, v for the velocity of hashtag, and M for the momentum of hashtag. The topic hotness modeling algorithm is as follows:

5 Experiment Analysis And Result

5.1 Data Corpus and Parameter Settings

In this paper we adopt the historical(2009/6/11-2009/12/31) data from Twitter as corpus. We extracted 460,496 twitter terms and 22,063 hashtags in total, neglecting those topics which lasted

Algorithm 1 Topic Hotness Modeling

Input: The set of hashtags which emerged during a certain period of time
Output: The topics list ranked by hotness in each time spot t

1: **for** $t = t_0$ **do**
2: Process the data we collected and aggregate into topic set $Topic$.
3: **for** each topic $Topic_n$ from $Topic$ **do**
4: Obtain the set $\{term_{n1}, ..., term_{nt}\}$ of the $Topic_{nt}$
5: Calculate the hotness of $Topic_{nt}$ by $\overrightarrow{H}_t = \vec{v}_{t-1} \times t_0 + \frac{1}{2} \times \vec{g}\Delta t^2$
6: **end for**
7: output the topic list ordered by H_t
8: $t = t + 1$
9: **end for**

Table 1: Parameter Setting

Parameter	Value
Hashtag Initial Velocity v	10
Hashtag Weight m	1
Acceleration g	-3
Interval t (day)	1

less than 3 days or contained less than 2 posts, the coverage can meet the needs of simulation experiments. The main parameters of the computer for this modelling are as follows: CPU is Intel(R) Core(TM)2 Duo, Main Frequency is 2.0GHz, Memory Frequency is 777MHz, Memory Capacity is 1.96GB, Running Environment is WINDOWS XP. The rest parameters are set as the Table 1.

5.2 Comparison of Hot Topic detection

In this experiment, our momentum theory (M) is compared to two proposed methods. The baseline method (A) [12, 16] is a basic aging method. Cataldi et al. [10] improved a method (A-TF) which enhanced the aging method by using an augmented normalized term frequency. As a result, top 3 and top 10 generated hot topics from each method are evaluated using official TDT measures including: precision (p), recall (r) and F1-measure ($F1$).

In Table 2, the best score for each item is represented in bold. In the top 3 comparison, our momentum theory achieves both highest precision and recall which results in the best $F1$ score, while the aging method achieves both reasonable precision and recall. In the top 10 comparison, the precision of our momentum theory is still the highest in the first 10 hot hashtags but loses

Table 2: Comparison of Three Methods

	Method	p	r	$F1$
Top 3	A	0.67	**0.67**	0.67
	M	**1.00**	**0.67**	**0.80**
	A-TF	0.50	0.50	0.50
Top 10	A	0.63	0.71	0.67
	M	**0.88**	0.78	**0.82**
	A-TF	0.56	**0.83**	0.67

Table 3: Top 3 Hashtags Changing Circumstances in A Week in Three Methods

	2009/7/6	2009/7/7	2009/7/8	2009/7/9	2009/7/10	2009/7/11
M	mileycyrus 140army 140mafia	mileycyrus 140army 140mafia	mileycyrus 140army gorillapenis	140army mileycyrus gorillapenis	140army zyngapirates urumqi	zyngapirates hottest100 ashes
A	livestrong iranelection 140mafia	moonfruit nothingpersonal iranelection	turnon turnoff iranelection	notagoodlook iranelection 140mafia	ff followfriday iranelection	unacceptable iranelection ff
A-TF	livestrong iranelection musicmonday	moonfruit iranelection livestrong	turnon turnoff iranelection	iranelection 140mafia notagoodlook	ff followfriday iranelection	unacceptable iranelection ff

recall. We believe that is due to the fact that the momentum mechanism likes to remove the old topics. The recall of A-TF is the best, because it improves the aging algorithm which will be sensitive of hot topics and enlarge its coverage, but there is a reduction in the precision. In the *F1* item, the momentum theory has maintained the highest standards. In conclusion, the comprehensive performance of momentum theory is better than the other two algorithms.

5.3 Comparison of Hot Topic Trending

Due to space limitations, Table 3 represents the top 3 hashtags from 2009/7/6 to 2009/7/11 in the momentum theory (M), the aging algorithm (A) and the improved aging algorithm (A-TF) . These results show that the topic trending in M is relatively stable. Hashtag #mileycyrus, #140army and#zyngapirates are stable up to first place in turn. In the last two algorithms, #iranelection is ranked in the top 3 places. However, according to the historical data checking, this hashtag appeared over 20,000 times a day in June and was already ranked as hottest topic at that time in all three algorithms. Clearly, in July #iranelection should not be a hot topic again. Hashtag #140mafia's overall performance is good, the repeating number is higher and the potential of impacting as hottest topic is great, so it is ranked as top 3 in the three algorithms. Although it is stable in M, it is unstable in A and A-TF.

Table 4 presents the top 10 hashtags in two days (2009/7/6-2009/7/7) in three algorithms. Hashtag #mileycyrus remains first place in M in two days, ranks 7th in A, falls out of the top 10 in A-TF and only ranks 17th as 0.635 energy value. It is because there are a lot of old hot topics which interfere with these two days of ranking, while these old hashtags already were the hot topics in an earlier time. #140army is in second place in M, but ranks 13th and 11th in A and A-TF separately, falling out of top 10. #flip2009 is captured only by M, while it gets its highest times in 5th July and 6th July. But due to relatively lower times, it is abandoned by two aging algorithms. As we mentioned before, #140mafia is captured in all three methods. #tcot, #spymaster and #tweetmyjobs had more than thousands of times per day from 2009/6/12 and were listed as hot topics in momentum theory at that time. These are not hot news yet, but these hashtags are still ranked as top 10 hashtags in A and A-TF. #mj is a standard hot hashtag which arise sharply in 7th July as 1,077 times occur, however, it is replaced by #tcot in A and A-TF due to the shortcoming of lower discrimination degree of the aging theory.

Because of the large amount of data and limited space, we take hashtag #mileysycyrus as an example to analyze the trending of different algorithms. Figure 1 Shows the times, hotness and energy value six months profiles of hashtag #mileysycyrus, which is the hottest topic of 6th July in momentum theory.

In Figure 1 A, this hashtag began to appear in 12th June. After that, it did not reproduce for about a week. Later, it appeared sometime in a lower rate. On 5th July, it shot up suddenly

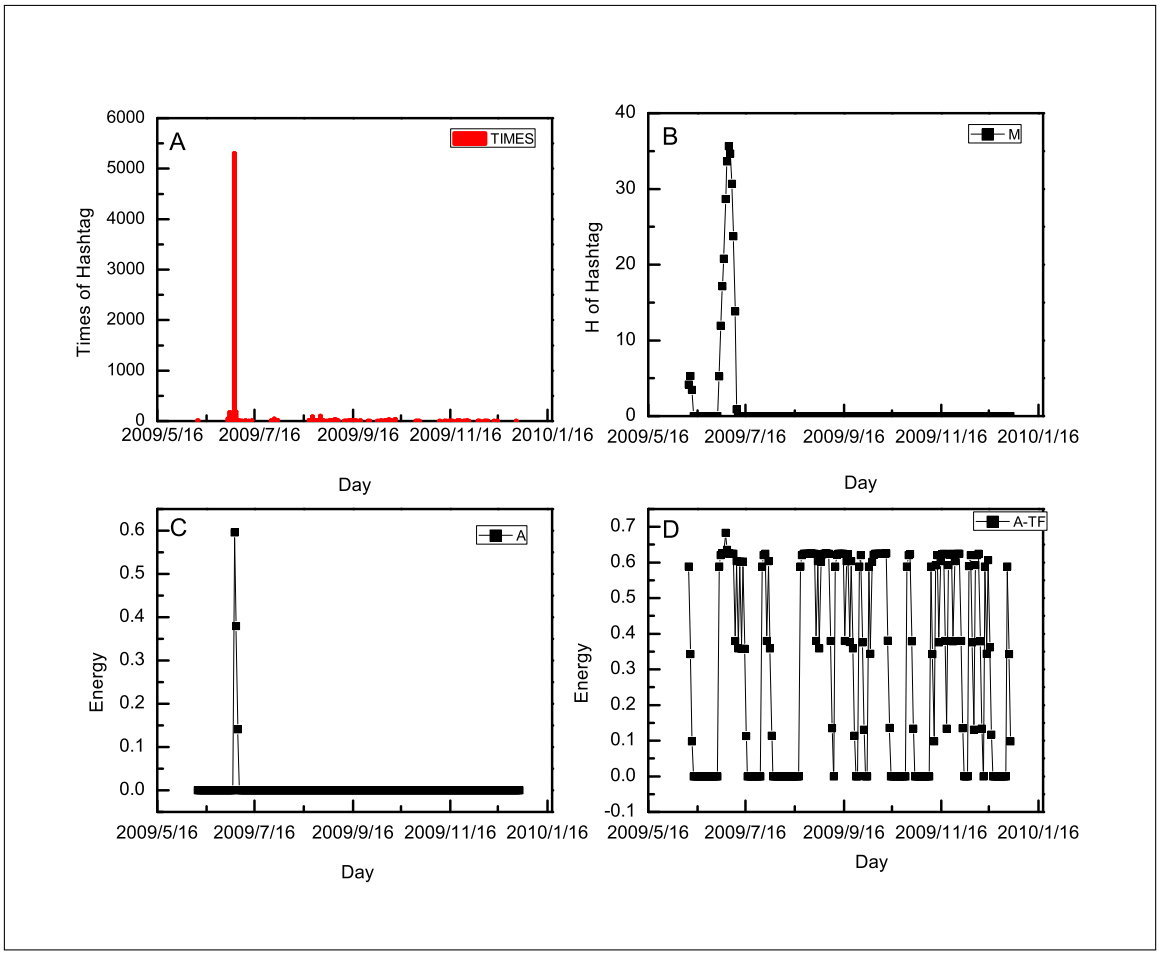

Figure 1: Comparison of #mileysycyrus (A:occurrence number of hashtag per day, B:hotness of hashtag per day in momentum theory, C:energy value of hashtag per day in aging method, D:energy value of hashtag per day in A-TF method)

Table 4: Top 10 Hashtags in Two Days in Three Methods

	Hashtag	M	Times	Hashtag	A	Times	Hashtag	A-TF	Times
7-6	mileycyrus	33.63	187	livestrong	0.56	4026	livestrong	0.67	4026
	140army	27.93	781	iranelection	0.55	2640	iranelection	0.66	2640
	140mafia	27.68	2316	140mafia	0.53	2316	musicmonday	0.66	2966
	moonfruit	26.23	2124	moonfruit	0.51	2124	140mafia	0.66	2316
	gorillapenis	24.98	984	musicmonday	0.50	2966	moonfruit	0.66	2124
	flip2009	21.19	12	spymaster	0.47	1616	spymaster	0.65	1616
	mj	20.86	288	tcot	0.40	1206	tcot	0.65	1206
	rw09	20.64	16	gorillapenis	0.39	984	gorillapenis	0.64	984
	katemcrae	19.36	10	mileycyrus	0.38	187	militarymon	0.64	933
	cmonbrazil	19.11	140	honduras	0.30	676	jobs	0.64	827
7-7	mileycyrus	35.64	18	moonfruit	0.62	5147	moonfruit	0.64	5147
	140army	30.88	461	nothingpersonal	0.54	3670	iranelection	0.63	1902
	140mafia	29.23	1644	iranelection	0.51	1902	livestrong	0.63	1228
	gorillapenis	29.09	559	140mafia	0.49	1644	140mafia	0.63	1644
	moonfruit	25.65	5147	livestrong	0.47	1228	musicmonday	0.63	1423
	cmonbrazil	20.13	47	musicmonday	0.46	1423	spymaster	0.63	936
	urumqi	19.61	153	spymaster	0.40	936	tcot	0.63	839
	mj	19.27	1075	tcot	0.36	839	tweetmyjobs	0.63	1013
	crocmint	19.27	6	tweetmyjobs	0.34	1013	gorillapenis	0.63	559
	xinjiang	19.05	110	threadless	0.30	1192	jobs	0.63	642

and reached 5,302 times, then declined rapidly. Although it repeated a few dozens or hundreds times later, but never rose again sharply. In Figure 1 B, momentum theory captures the hotness rising rapidly on 5th, 6th, 7th July and declining dramatically quickly. This hotness is higher than other hashtags, so it is ranked in first place. The aging theory also finds this change but does not list this hashtag in a higher position (only the 9th place) due to a relative lower energy value compared with other hashtags. The A-TF method almost gets every higher repeat rate moments, but it cannot distinguish the highest point from all higher points clearly. So, it is not able to choose this hashtag from the data corpus efficiently. As a result, it falls out of the top 10 hashtags. In Figure 1, momentum theory presents a higher sensitivity and better ability to discriminate the hottest hashtags from others than the other two algorithms.

Extrapolating the results from the experiment, we can obtain the hottest topics during the period of time we captured by the algorithm we proposed, and compared with the hot hashtags that are extracted by the rank of occurrence.

From the comparison of Table 5, we can explicitly observe that the occurrence of the hashtag may mislead to the generation of a hot topic, such as #followfriday, #ff and #1. Those topics own little valid information, however are regarded as hot according to the high frequency of occurrence. By the algorithm we proposed, the topics which lack realistic meaning will be eliminated by the momentum equation. The topics which survive will be the active ones with realistic meaning.

6 Conclusion and Future Work

In this paper we propose a novel algorithm for hot topic detection based on momentum theory using hashtags for defining a topic. The main contributions of the paper are as follows.

Table 5: Hottest Hashtags in Half A Year

	Momentum Theory		Occurrence		
	Hashtag	Hotness	Hashtag	Days	Times
1	tehran	44.73	ff	113	417802
2	nomaschavez	44.19	iranelection	116	368519
3	happybirthdaymikey	43.13	tcot	120	288091
4	nem	43	jobs	115	243586
5	iranelection	41.14	mobsterworld	85	203445
6	zain	38.93	followfriday	113	188664
7	happybirthdaypink	38.2	1	114	166260
8	teenisland	38.15	musicmonday	109	t164399
9	blackbery	37.94	140mafia	105	149078

First we analyze the characteristics of hot topics and conclude into four points:1) Timeliness. 2) Development. 3) Accumulation. 4) Digestion. Then we build a hot topic detection model with momentum theory. The experiments show that our model can identify those emerging hot topics effectively and accurately.

In the future, we hope to filter the posts under each topic to provide the users with a purer source of information without the distraction from irrelevant posts. Our algorithm standardizes the topic life cycle into a very stable curve which makes the topic prediction possible. Some artificial intelligence techniques have been applied in mathematical modeling [4, 32, 38], and some achievements have been obtained in the prediction of data modeling [3, 5, 9, 30]. We will try to use these techniques to predict the hot topics in the next step.

Acknowledgment

The authors would like to thank the anonymous reviewers for their insightful comments. The authors also thank Yanmei Zhai and Xu Han for their help with data preparation and experiments. This work has been partially supported by National Program on Key Basic Research Project under Grant No. 2013CB329605, NSFC under Grant No. 61300178 and Natural Science Foundation of Beijing under Grant No. 4092037.

Bibliography

[1] Aldhelaan, M.; Alhawasi, H. (2015); Graph Summarization for Hashtag Recommendation, *2015 3rd International Conference on Future Internet of Things and Cloud (FiCloud)*, 698-702.

[2] Allan, J.; Carbonell, J.; Doddington, G., et al. (1998); Topic Detection and Tracking Pilot Study Final Report, *Proceedings of the DARPA Broadcast News Transcription and Understanding Workshop*, 194-218.

[3] Asadi, S.; Hadavandi, E.; Mehmanpazir, F., et al. (2012); Hybridization of evolutionary Levenberg-Marquardt neural networks and data pre-processing for stock market prediction, *Knowledge-Based Systems*, 35(15): 245-258.

[4] Aydemir, E.; Koruca, H.I. (2015); A New Production Scheduling Module Using Priority-Rule Based Genetic Algorithm, *International Journal of Simulation Modelling*, ISBN 1726-4529, 14(3): 450-462.

[5] Bas, E.; Egrioglu, E.; Aladag, C.H., et al. (2015); Fuzzy-time-series network used to forecast linear and nonlinear time series, *Applied Intelligence*, 43(2): 1-13.

[6] Blekas, K.; Lagaris, I.E. (2013); A Spectral Clustering Approach Based on Newton's Equations of Motion, *International Journal of Intelligent Systems*, 28(4): 394-410.

[7] Bo, Y.; Ming, L.; Bing-Quan, L., et al. (2012); Detecting hot topics in technology news streams, *Machine Learning and Cybernetics (ICMLC), 2012 International Conference on*, ISBN 2160-133X, 5:1968-1974.

[8] Borgelt, C. (2010); Simple Algorithms for Frequent Item Set Mining, *Advances in Machine Learning II*, ISBN 978-3-642-05178-4, 263(16):351-369.

[9] Caldeira, J.F.; Moura, G.V.; Santos, A.A.P. (2016); Predicting the yield curve using forecast combinations, *Computational Statistics & Data Analysis*, 100: 79-98.

[10] Cataldi, M.; Caro, L.D.; Schifanella, C. (2010); Emerging topic detection on Twitter based on temporal and social terms evaluation, *Proceedings of the Tenth International Workshop on Multimedia Data Mining*, 1-10.

[11] Chang, M.K.; Cheung, W.; Tang, M. (2013); Building trust online: Interactions among trust building mechanisms, *Information & Management*, 50(7): 439-445.

[12] Chen, C.; Chen, Y.-T.; Sun, Y., et al. (2003); Life Cycle Modeling of News Events Using Aging Theory, *Machine Learning: ECML 2003*, ISBN 978-3-540-20121-2, 2837(7):47-59.

[13] Chen, J.; Yu, J.; Shen, Y. (2012); Towards Topic Trend Prediction on a Topic Evolution Model with Social Connection, *The Ieee/wic/acm International Joint Conferences on Web Intelligence & Intelligent Agent Technology*, 153-157.

[14] Chen, K.Y.; Luesukprasert, L.; Chou, S.c.T. (2007); Hot Topic Extraction Based on Timeline Analysis and Multidimensional Sentence Modeling, *IEEE Transactions on Knowledge and Data Engineering*, ISBN 1041-4347, 19(8): 1016-1025.

[15] Chen, T.L. (2012); Forecasting the Taiwan Stock Market with a Novel Momentum-based Fuzzy Time-series, *Review of Economics & Finance*, 2:38-50.

[16] Chien Chin, C.; Yao-Tsung, C.; Meng Chang, C. (2007); An Aging Theory for Event Life-Cycle Modeling, *Systems, Man and Cybernetics, Part A: Systems and Humans, IEEE Transactions on*, ISBN 1083-4427, 37(2): 237-248.

[17] Chung-Hong, L.; Tzan-Feng, C.; Hsin-Chang, Y. (2011); An automatic topic ranking approach for event detection on microblogging messages, *Systems, Man and Cybernetics (SMC), 2011 IEEE International Conference on*, ISBN 1062-922X, 1358-1363

[18] Galperin, E.A. (2011); Information transmittal, Newton's law of gravitation, and tensor approach to general relativity, *Computers & Mathematics with Applications*, 62(2): 709-724.

[19] Giannella, C.; Han, J.; Pei, J., et al. (2003); Mining Frequent Patterns in Data Streams at Multiple Time Granularities, *Data Mining Next Generation Challenges & Future Directions.*

[20] Han, J.; Pei, J.; Yin, Y. (2000); Mining frequent patterns without candidate generation, *SIGMOD Rec.*, ISBN 0163-5808, 29(2): 1-12.

[21] Hrelja, M.; Klancnik, S.; Balic, J., et al. (2014); Modelling of a turning process using the gravitational search algorithm, *International Journal of Simulation Modelling*, ISBN 1726-4529, 13(1): 30-41.

[22] Hwi-Gang, K.; Seongjoo, L.; Sunghyon, K. (2013); Discovering hot topics using Twitter streaming data social topic detection and geographic clustering, *Advances in Social Networks Analysis and Mining (ASONAM), 2013 IEEE/ACM International Conference on*, 1215-1220.

[23] Jiangfeng, C.; Jianjun, Y.; Yi, S. (2012); Towards Topic Trend Prediction on a Topic Evolution Model with Social Connection, *Web Intelligence and Intelligent Agent Technology (WI-IAT), 2012 IEEE/WIC/ACM International Conferences on*, 1:153-157.

[24] Jing, G.; Peng, Z.; Tanb, J., et al. (2012); Mining Hot Topics from Twitter Streams, *Procedia Computer Science*, 9(11): 2008-2011.

[25] Khoo Khyou, B.; Ishizuka, M. (2002); Topic extraction from news archive using TF*PDF algorithm, *Web Information Systems Engineering, 2002. WISE 2002. Proceedings of the Third International Conference on*, 73-82.

[26] Khulief, Y.A. (2010); Numerical Modelling of Impulsive Events in Mechanical Systems, *International Journal of Modelling & Simulation*, 30: 80-86.

[27] Kotsakos, D.; Sakkos, P.; Katakis, I., et al. (2015); Language agnostic meme-filtering for hashtag-based social network analysis, *Social Network Analysis & Mining*, 5(1): 1-14.

[28] Li, M.; Tang, M. (2013); Information Security Engineering: a Framework for Research and Practices, *International Journal of Computers Communications & Control*, 8(4): 578-587.

[29] Liu, M.; Liu, Y.; Xiang, L., et al. (2008); Extracting Key Entities and Significant Events from Online Daily News, *Intelligent Data Engineering and Automated Learning-IDEAL 2008*, ISBN 978-3-540-88905-2, 5326(26):201-209.

[30] Liu, C.H.; Xiong, W. (2015); Modelling and Simulation of Quality Risk Forecasting in a Supply Chain, *International Journal of Simulation Modelling*, ISBN 1726-4529, 14(2): 359-370.

[31] Ma, H.; Lu, Z.; Li, D., et al. (2014); Mining hidden links in social networks to achieve equilibrium Ąî, *Theoretical Computer Science*, 556:13-24.

[32] Ramesh Kumar, L.; Padmanaban, K.; Balamurugan, C. (2016); Optimal Tolerance Allocation in a Complex Assembly Using Evolutionary Algorithms, *International Journal of Simulation Modelling*, ISBN 1726-4529, 15(1): 121-132.

[33] Salton, G. (1989); *Automatic text processing: the transformation, analysis, and retrieval of information by computer*, ISBN 0-201-12227-8.

[34] Ternik, P.; Rudolf, R. (2013); Laminar Natural Convection of Non-Newtonian Nanofluids in a Square Enclosure with Differentially Heated Side Walls, *International Journal of Simulation Modelling*, 12(1): 5-16.

[35] Tran, D.H.; Nguyen, H.L.; Zhao, W., et al. (2011); Towards security in sharing data on cloud-based social networks, *Information, Communications and Signal Processing (ICICS) 2011 8th International Conference on*, 1-5.

[36] Wang, C.; Zhang, M.; Ru, L., et al. (2008); Automatic online news topic ranking using media focus and user attention based on aging theory, *Proceedings of the 17th ACM conference on Information and knowledge management*, 1033-1042.

[37] Xiao, Z. (2014); A SOCIAL NETWORK-ORIENTED MINING ALGORITHM FOR HOT TOPIC DATA, *Computer Applications & Software*

[38] Yang, K.W.; Zhang, P.L.; Ge, B.F., et al. (2015); A Variables Clustering Based Differential Evolution Algorithm to Solve Production Planning Problem, *International Journal of Simulation Modelling*, ISBN 1726-4529, 14: 525-538.

[39] Yang, Y.; Pierce, T.; Carbonell, J. (1998); A study of retrospective and on-line event detection, *Proceedings of the 21st annual international ACM SIGIR conference on Research and development in information retrieval*, 28-36.

[40] Zangerle, E.; Gassler, W.; Specht, G. (2013); On the impact of text similarity functions on hashtag recommendations in microblogging environments, *Social Network Analysis & Mining*, 3(4): 889-898.

[41] Zheng, D.; Li, F. (2009); Hot Topic Detection on BBS Using Aging Theory, *Web Information Systems and Mining*, ISBN 978-3-642-05249-1, 5854(14): 129-138.

Author index